Department of Electrical and Information Engineering
Electrical and Information Engineering
Ph.D. Program
SSD: ING-INF/03– TELECOMMUNICATIONS

Final Dissertation

Integration of Terrestrial and Non-Terrestrial Technologies in IoT Networks

---

by
Antonio Petrosino

Supervisors:

Prof. Luigi Alfredo Grieco
Prof. Gennaro Boggia
Dott. Lorenzini Marco

Coordinator of Ph.D. Program:
Prof. Mario Carpentieri

Course n°36, 01/11/2020-31/10/2023

Politecnico di Bari

LIBERATORIA PER L'ARCHIVIAZIONE DELLA TESI DI DOTTORATO

Al Magnifico Rettore
del Politecnico di Bari

Il sottoscritto Antonio Petrosino nato a Bari (BA) il 20/09/1991 residente a Triggiano (BA) in via Sandro Pertini, 88 e-mail antonio.petrosino@outlook.com iscritto al 3° anno di Corso di Dottorato di Ricerca in Electrical and Information Engineering ciclo XXXVI ed essendo stato ammesso a sostenere l'esame finale con la prevista discussione della tesi dal titolo:

"Integration of Terrestrial and Non-Terrestrial Technologies in IoT Networks"

DICHIARA

1) di essere consapevole che, ai sensi del D.P.R. n. 445 del 28.12.2000, le dichiarazioni mendaci, la falsità negli atti e l'uso di atti falsi sono puniti ai sensi del codice penale e delle Leggi speciali in materia, e che nel caso ricorressero dette ipotesi, decade fin dall'inizio e senza necessità di nessuna formalità dai benefici conseguenti al provvedimento emanato sulla base di tali dichiarazioni;
2) di essere iscritto al Corso di Dottorato di ricerca Electrical and Information Engineering ciclo XXXV, corso attivato ai sensi del "*Regolamento dei Corsi di Dottorato di ricerca del Politecnico di Bari"*, emanato con D.R. n.286 del 01.07.2013;
3) di essere pienamente a conoscenza delle disposizioni contenute nel predetto Regolamento in merito alla procedura di deposito, pubblicazione e autoarchiviazione della tesi di dottorato nell'Archivio Istituzionale ad accesso aperto alla letteratura scientifica;
4) di essere consapevole che attraverso l'autoarchiviazione delle tesi nell'Archivio Istituzionale ad accesso aperto alla letteratura scientifica del Politecnico di Bari (IRIS-POLIBA), l'Ateneo archivierà e renderà consultabile in rete (nel rispetto della Policy di Ateneo di cui al D.R. 642 del 13.11.2015) il testo completo della tesi di dottorato, fatta salva la possibilità di sottoscrizione di apposite licenze per le relative condizioni di utilizzo (di cui al sito http://www.creativecommons.it/Licenze), e fatte salve, altresì, le eventuali esigenze di "embargo", legate a strette considerazioni sulla tutelabilità e sfruttamento industriale/commerciale dei contenuti della tesi, da rappresentarsi mediante compilazione e sottoscrizione del modulo in calce (Richiesta di embargo);
5) che la tesi da depositare in IRIS-POLIBA, in formato digitale (PDF/A) sarà del tutto identica a quelle **consegnate**/inviate/da inviarsi ai componenti della commissione per l'esame finale e a qualsiasi altra copia depositata presso gli Uffici del Politecnico di Bari in forma cartacea o digitale, ovvero a quella da discutere in sede di esame finale, a quella da depositare, a cura dell'Ateneo, presso le Biblioteche Nazionali Centrali di Roma e Firenze e presso tutti gli Uffici competenti per legge al momento del deposito stesso, e che di conseguenza va esclusa qualsiasi responsabilità del Politecnico di Bari per quanto riguarda eventuali errori, imprecisioni o omissioni nei contenuti della tesi;
6) che il contenuto e l'organizzazione della tesi è opera originale realizzata dal sottoscritto e non compromette in alcun modo i diritti di terzi, ivi compresi quelli relativi alla sicurezza dei dati personali; che pertanto il Politecnico di Bari ed i suoi funzionari sono in ogni caso esenti da responsabilità di qualsivoglia natura: civile, amministrativa e penale e saranno dal sottoscritto tenuti indenni da qualsiasi richiesta o rivendicazione da parte di terzi;
7) che il contenuto della tesi non infrange in alcun modo il diritto d'Autore né gli obblighi connessi alla salvaguardia di diritti morali od economici di altri autori o di altri aventi diritto, sia per testi, immagini, foto, tabelle, o altre parti di cui la tesi è composta.

Bari, 23/08/2023 Firma Antonio Petrosino

Il/La sottoscritto, con l'autoarchiviazione della propria tesi di dottorato nell'Archivio Istituzionale ad accesso aperto del Politecnico di Bari (POLIBA-IRIS), pur mantenendo su di essa tutti i diritti d'autore, morali ed economici, ai sensi della normativa vigente (Legge 633/1941 e ss.mm.ii.),

CONCEDE

- al Politecnico di Bari il permesso di trasferire l'opera su qualsiasi supporto e di convertirla in qualsiasi formato al fine di una corretta conservazione nel tempo. Il Politecnico di Bari garantisce che non verrà effettuata alcuna modifica al contenuto e alla struttura dell'opera.
- al Politecnico di Bari la possibilità di riprodurre l'opera in più di una copia per fini di sicurezza, back-up e conservazione.

Bari, 23/08/2023 Firma Antonio Petrosino

Politecnico di Bari

Department of Electrical and Information Engineering
Electrical and Information Engineering
Ph.D. Program
SSD: ING-INF/03– TELECOMMUNICATIONS

Final Dissertation

Integration of Terrestrial and Non-Terrestrial Technologies in IoT Networks

---

by
Antonio Petrosino

Referees:
Prof. Simone Morosi
Prof. Ernestina Cianca

Supervisors:
Prof. Luigi Alfredo Grieco
Prof. Gennaro Boggia
Dott. Lorenzini Marco

Coordinator of Ph.D. Program:
Prof. Mario Carpentieri

Course n°36, 01/11/2020-31/10/2023

«I don't know half of you half as well as I should like; and I like less than half of you half as well as you deserve.»

The Fellowship of the Ring by Bilbo Baggins

POLITECNICO DI BARI

Abstract

Department of Electrical and Information Engineering

Doctor of Philosophy

Integration of Terrestrial and Non-Terrestrial Technologies in IoT Networks

by Antonio Petrosino

In the rapidly evolving landscape of technological progress in next-generation telecommunication networks, the integration of space-based innovations with terrestrial networks has emerged as a central focus of research and development within the scientific community. While the introduction of the Fifth Generation (5G) technology has brought massive improvements in term of latency and data rate, the evolving challenges within the domain of the Internet of Things (IoT) require for an in-depth exploration of cutting-edge solutions to cope with the digital divide problem and the need for ubiquitous connectivity even in harsh region. To bridge this gap, this work delves into the groundbreaking potential of Non-Terrestrial Network (NTN), by emphasizing the indispensable role played by the Low Earth Orbit (LEO) CubeSats. Furthermore, it also investigates terrestrial advancements in resource virtualization and emerging communication technologies, such as Light Fidelity (LiFi), for their pivotal contributions to the evolution of IoT. Finally, it showcases the immense potential of the integration between non-terrestrial and terrestrial technologies within the IoT domain, highlighting their capacity to serve as primary drivers of innovation.

Contents

List of Figures

List of Tables

List of Acronyms

3GPP 3rd Generation Partnership Project

5G Fifth Generation

5G&B 5G & Beyond

AES Advanced Encryption Standard

AP Access Point

AWGN Additive White Gaussian Noise

BER Bit Error Ratio

BLER BLock Error Ratio

CDF Cumulative Distribution Function

CFO Carrier Frequency Offset

C-IoT Cellular Internet of Things

CLOR Co-Location Object Relationship

CoAP Constrained Application Protocol

COTS Commercial-Off-The-Shelf

CRC Cyclic Redundancy Check

C-SGN Cellular IoT – Serving Gateway Node

CSI Channel State Information

CSK Color-Shift Keying

CWM Continuous Wave Modulation

CWOR Co-Work Object Relationship

DHT Discrete Hartley Transform

DL DownLink

ECDF Empirical Cumulative Distribution Function

EDT Early Data Transmission

eNB Evolved Node-B

EPS Evolved Packet System

ESA European Space Agency

FBMC Filter Bank Multi-Carrier

FDMA Frequency Division Multiple Access

FoV Field of View

GEO Geostationary Earth Orbit

GLS Genetic Local Search

GN Ground Node

GNSS Global Navigation Satellite System

GR Greedy Algorithm

HARQ Hybrid Automatic Repeat Request

HPA High Power Amplifier

HPBW Half Power Beam Width

HSS Home Subscriber Server

IIoT Industrial Internet of Things

ILP Integer Linear Programming

IMR Intelligent Metasurface Reflector

IoT Internet of Things

IPS Indoor Positioning System

IRS Intelligent Reflecting Surface

ISL Inter-Satellite Link

ITU International Telecommunication Union

KPI Key Performance Indicator

L2S Link-To-System

LBO Local Break-Out

LED Light-Emitting Diode

LEO Low Earth Orbit

LiFi Light Fidelity

LLS Linear Least Square

LoS Line-of-Sight

LP-WAN Low Power Wide Area Network

LTE Long Term Evolution

M2M Machine-to-Machine

MAC Media Access Control

MCL Maximum Coupling Loss

MCS Modulation and Coding Scheme

MILP Mixed-Integer Linear Programming

MIMO Multiple-Input Multiple-Output

MINLP Mixed-Integer Non-Linear Programming

MISO Multiple-Input Single-Output

ML Machine Learning

MME Mobility Management Entity

MQTT Message Queue Telemetry Transport

MTC Machine Type Communication

NAS Non Access Stratum

NB-IoT NarrowBand IoT

NFV Network Function Virtualization

NIDD Non-IP Data Delivery

NLoS Non-Line-of-Sight

NOMA Non-Orthogonal Multiple Access

NPBCH Narrowband Physical Broadcast Channel

NPDCCH Narrowband Physical Downlink Control Channel

NPDSCH Narrowband Physical Downlink Shared Channel

NPRACH Narrowband Physical Random Access Channel

NPUSCH Narrowband Physical Uplink Shared Channel

NRU Number of Resource Unit

NTN Non-Terrestrial Network

OFDM Orthogonal Frequency Division Multiplexing

OFDMA Orthogonal Frequency Division Multiple Access

OMA Orthogonal Multiple Access

OOK On-Off Keying

OOR Ownership Object Relationship

OWC Optical Wireless Communication

PAM Pulse Amplitude Modulation

PAPR Peak to Average Power Ratio

PBM Pulse-Based Modulation

PD PhotoDetector

PDCP Packet Data Convergence Protocol

PDU Protocol Data Unit

PGW Packet Gateway

PHY Physical

POR Parental Object Relationship

PPM Pulse Position Modulation

PWM Pulse Width Modulation

QAM Quadrature Amplitude Modulation

QoE Quality of Experience

QoS Quality of Service

RAO Random Access Opportunity

RF Radio Frequency

RIS Reconfigurable Intelligent Surface

RLC Radio Link Control

RMSE Root Mean Squared Error

RRC Radio Resource Control

RSS Received Signal Strength

RTD Round Trip Delay

RU Resource Unit

SA Simulated Annealing

SatCom Satellite Communication

SCA Successive Convex Approximation

SCEF Service Capability Exposure Function

SDN Software-Defined Networking

SGW Serving Gateway

SIoT Social Internet of Things

SISO Single-Input Single-Output

SNR Signal to Noise Ratio

TA Timing Advance

TBS Transport Block Size

TDMA Time Division Multiple Access

TMS Trust Management System

TS Tabu Search

TTI Transmission Time Interval

UAV Unmanned Aerial Vehicle

UE User Equipment

UFMC Universal Filtered Multi-Carrier

UL UpLink

UPA Uniform Planar Array

VIM Virtualised Infrastructure Manager

VLC Visible Light Communication

VNF Virtualized Network Function

WDM Wavelength Division Multiplexing

Wi-Fi Wireless Fidelity

WPT Wireless Power Transfer

Personal Scientific Contributions

All the scientific contributions produced during the doctoral course are listed below.

International Journals:

- Giovanni Iacovelli, Giovanni Grieco, **Antonio Petrosino**, Luigi Alfredo Grieco, Gennaro Boggia. *"Fair Energy and Data Rate Maximization in UAV-Powered IoT-Satellite Integrated Networks"* in **IEEE Transactions on Communications**, 2023, DOI: 10.1109/TCOMM.2023.3343417.

- **Antonio Petrosino**, Giuseppe Piro, Luigi Alfredo Grieco, Gennaro Boggia. *"On the Optimal Deployment of Virtual Network Functions in Non-Terrestrial Segments"* in **IEEE Transactions on Network and Service Management**, 2023, DOI: 10.1109/TNSM.2023.3275248.

- **Antonio Petrosino**, Domenico Striccoli, Oleksandr Romanov, Gennaro Boggia, Luigi Alfredo Grieco. *"Light Fidelity for Internet of Things: A Survey"* in **Optical Switching and Networking**, volume 48, page 100732, 2023, DOI: 10.1016/j.osn.2023.100732

- Giancarlo Sciddurlo, **Antonio Petrosino**, Mattia Quadrini, Cesare Roseti, Domenico Striccoli, Francesco Zampognaro, Michele Luglio, Stefano Perticaroli, Antonio Mosca, Francesco Lombardi, Ivan Micheli, Antonio Ornatelli, Vincenzo Schena, Alessandro Di Mezza, Alessio Mattioni, Daniele Morbidelli, Gennaro Boggia, Giuseppe Piro. *"Looking at NB-IoT over LEO Satellite Systems: Design and Evaluation of a Service-Oriented Solution,"* in **IEEE Internet of Things Journal**, vol. 9, no. 16, pp. 14952-14964, 15 Aug.15, 2022, DOI: 10.1109/JIOT.2021.3135060.

International Conferences:

- **Antonio Petrosino**, Giuseppe Piro, Luigi Alfredo Grieco, Gennaro Boggia. *"An Optimal Allocation Framework of Security Virtual Network Functions in 6G Satellite Deployments"* in Proc. of **2022 IEEE 19th Annual Consumer Communications & Networking Conference (CCNC)**, pages 917–920, 2022, DOI: 10.1109/CCNC49033.2022.9700728.

- Luigi Alfredo Grieco, Giuseppe Piro, **Antonio Petrosino**, Simone Morosi, Alessandro Guidotti, Daniele Tarchi, Alessandro Vanelli-Coralli, Ernestina Cianca, Marina Ruggieri, Pierpaolo Salvo, Francesco Matera, Valeria Petrini, Simona Valbonesi. *"Integration of terrestrial and Non-Terrestrial networks for automotive: challenges and perspectives within the S11 RESTART project"* in Proc. of **2023 AEIT International Conference on Electrical and Electronic Technologies for Automotive (AEIT AUTOMOTIVE)**, Modena, Italy, 2023, DOI: 10.23919/AEITAUTOMOTIVE58986.2023.10217255.

- Giancarlo Sciddurlo, **Antonio Petrosino**, Domenico Striccoli, Giuseppe Piro, Luigi Alfredo Grieco, Gennaro Boggia. *"Boosting Service Provisioning in SIoT by Exploiting Trust and Capability Levels of Social Objects"* in Proc. of **2022 IEEE International Conference on Smart Computing (SMARTCOMP)"**, pages 1–6, 2022, DOI: 10.1109/SMARTCOMP55677.2022.00077.

- **Antonio Petrosino**, Giancarlo Sciddurlo, Sergio Martiradonna, Domenico Striccoli, Giuseppe Piro, Gennaro Boggia. *"WIP: An open-source tool for evaluating system-level performance of NB-IoT non-terrestrial networks"* In Proc. of **2021 IEEE 22nd International Symposium on a World of Wireless, Mobile and Multimedia Networks (WoWMoM)**, pages 236–239, 2021, DOI: 10.1109/WoWMoM51794.2021.00042.

Under Review:

- **Antonio Petrosino**, Giovanni Iacovelli, Domenico Striccoli, Oleksandr Romanov, Luigi Alfredo Grieco, Gennaro Boggia. *"A Primer on Visible Light Indoor Positioning System via Intelligent Metasurface Reflectors"* in **IEEE Internet of Things Journal**.

Project Involvement

My research work is framed on the topic of "IoT Technologies for Secure Transport Management Systems" and is funded by Istituto Italiano Ricerca e Sviluppo - (ISIRES). It focuses on the development and analysis of innovative methodologies for Internet of Things (IoT) network security in Transport Management Systems. Throughout the duration of this project, alongside my Ph.D. research activities, I have also conducted research following the strategic agenda of a prestigious company, known as Elettric80. Specifically, the primary goal of this work is to develop a complete framework able to guarantee secure connectivity to vehicle fleets equipped with IoT sensors, even in remote areas of the planet where the construction and installation of traditional terrestrial network infrastructure would not be economically feasible. Indeed, one of the objectives of future mobile networks is to use the so-called Non-Terrestrial Network (NTN) to support such connectivity, which can also be utilized for Transport Management Systems. To begin with, it has been necessary to study all the enabling technologies in the vast domain of IoT technologies. Furthermore, the performance of each reference technology has been investigated based on three fundamental indicators: coverage area, data rate, and latency. On the one hand, considering Fifth Generation (5G), due to its high data rate and low latency, it is suitable for any type of service, even critical applications. On the other hand, the coverage of this technology is not yet ubiquitous and may never be, especially in rural scenarios where it would be an economically unviable investment. Indeed, in a scenario where the terrestrial coverage is lacking, it can be useful to opt for something diametrically opposite (i.e., low data rate and high latency), such as NTN NarrowBand IoT (NB-IoT).

Once a subset of suitable IoT radio access technologies have been chosen, the work has been improved with a preliminary analysis of the Transport Management System. It is a key service that enables companies to optimize logistics by facilitating the coordinated physical movement of goods from suppliers to consumers. Specifically, a Transport Management System is often integrated into a much more complex system with various functionalities called supply chain management. Indeed, the main objectives can be summarized in three categories, as follows:

- Planning, that is the part that manages the shipment methods, aiming to minimize costs associated with routes based on performance parameters such as distance and costs generated.
- Execution, on the other hand, manages the interaction between various entities in the entire chain, including carriers, distributors, warehouses, and most importantly, customers. The goal is to provide all necessary information in an automated manner to expedite procedures.
- Optimization is the process that gathers all the data necessary to measure specific performance indicators and potentially display them in reports or detailed analyses. This process facilitates overall management for the company, often leading to increased customer satisfaction and, inevitably, increased sales.

Market evolution has driven an increasing demand for real-time information from customers. Delivery in a few days is no longer sufficient, and there is even a demand for deliveries

within hours of placing an order. To achieve real-time updates, one of the challenges to address is the integration of Transport Management Systems with other technologies. Given the enormous amount of data, this integration certainly cannot rely on manual processes throughout the entire chain.

To this aim, the most significant and compelling integration within the Transport Management Systems is undoubtedly the IoT. Specifically, the utilization of various devices, including sensors, plays a pivotal role in monitoring critical factors. A paramount use case involves the real-time monitoring of fleet vehicles, offering the benefits as previously discussed. These sensors encompass a range of functionalities, from assessing the livability of the driver's cabin, to GPS for location tracking. Additionally, sensors for monitoring fuel and radiator liquid levels, tire pressure, and vehicle battery voltage are essential components. Lastly, load cells are employed to measure the quantity of goods being transported and contribute to optimizing weight distribution, thereby enhancing overall stability. While most of these sensors exhibit minimal power consumption, it's worth noting that gas detection sensors require efficient management to prevent significant energy depletion. Finally, in situations where terrestrial coverage is unavailable, the NB-IoT module can be leveraged to establish communication with satellites in orbit, enabling the continued transmission of data to the central system.

In this context, it's important to note that alternative energy sources from the vehicle itself or support from solar panels can also be considered, always taking into account the average power output, which can vary depending on the weather conditions in the areas where it will be used. In addition, it has been decided that separate development boards with different functionalities will be installed for the cabin and the semi-trailer. The cabin board will be capable of acquiring data from the onboard diagnostic interface if necessary. Additionally, a camera will be added inside the cabin for audio/video capture for traffic control, pointing towards the road, or for emergency situations, pointing inside. In contrast, the semi-trailer board will exclude the gas detection sensors, as they are not necessary for optimal energy consumption. In the final application, it will be possible to associate these two boards to allow them to collaborate.

In conclusion, studies have been conducted on the potential implementation of onboard intelligence within the edge of the network to process sensor data, and various real-world testbeds have been created using the following technologies: Arduino, Raspberry Pi, OpenmoteB, LoPy, Mosquitto, NodeRed, InfluxDB, and containers/docker.

Introduction

Nowadays, in an era characterized by rapid technological evolution, the integration of space-based technologies into terrestrial networks has emerged as a focal point of research and development within the scientific community [1]. Although the advent of Fifth Generation (5G) technology has brought about substantial enhancements in data rate and latency, it has also given rise to new challenges and requirements. In particular, Internet of Things (IoT) networks, facilitating the interconnection of smart devices, assume a pivotal role in shaping the future of telecommunication and connectivity. In fact, the widespread use of such devices, which includes everyday items embedded with sensors and connectivity, along with the rising demand for seamless global connectivity, jointly propels the pursuit of the next-generation network requirements [2]. As a result, 5G & Beyond (5G&B) networks are seen as a responsive solution to society's evolving telecommunication needs [3].

To address this gap, one of the most significant aspects of 5G&B is its emphasis on global coverage, moving away from an exclusive focus on high-speed connections. Unfortunately, closing the digital divide through terrestrial infrastructure alone is not economically feasible in remote and uninhabited regions. In these areas, for instance, the use of IoT smart devices can be essential, allowing for the monitoring of critical phenomena such as weather and climate change. Utilizing satellite networks is a promising solution. Satellites have the exceptional ability to reach remote and inaccessible areas, making them a crucial component in overcoming the limitations of terrestrial infrastructure [4]. In the realm of IoT, establishing even minimal connectivity in remote and harsh environments with low data transmission requirements and high latencies is still an extreme challenge [5]. In this context, Low Earth Orbit (LEO) CubeSats have gained significant traction, driven by cost reductions in both launch and manufacturing processes. These reductions have largely been facilitated by standardization efforts and pioneering aerospace companies like SpaceX. Consequently, this research aims to investigate the integration of space-based technologies, especially LEO CubeSats, into terrestrial telecommunication architectures. The primary focus is on exploring the applications, advantages, and disadvantages of Non-Terrestrial Network (NTN), with an emphasis on bridging the digital divide and enabling widespread connectivity [6].

Furthermore, while enhancing network coverage is a primary objective of 5G&B, it's essential to maintain research efforts in cutting-edge technologies for the IoT, essential to meet the demands of the ever-increasing number of users and requests. These technologies encompass resource virtualization for both terrestrial and NTN networks and the use of light for data transmission to address limitations in the electromagnetic spectrum bandwidth, especially in indoor settings. Resource virtualization is a key aspect that can significantly impact network development. For instance, the introduction of the Digital Twin as an enabling technology aims to create digital representations of physical entities or resources, blurring the line between the virtual and physical worlds. This concept opens up novel opportunities for human-machine interaction and the integration of intelligent services into daily life [7].

Moreover, due to the limited availability of the Radio Frequency (RF) spectrum, Visible Light Communication (VLC) technology has emerged as an innovative solution for wireless data transmission, with standardization under IEEE 802.11bb [8]. VLC, using Light-Emitting Diode (LED) technology, has the potential to provide high-speed broadband internet services while utilizing existing lighting infrastructure in various applications. This approach not only

reduces deployment costs but also enhances energy efficiency, thanks to the extended lifespan and reduced power consumption of LED lamps. Furthermore, VLC-based Indoor Positioning Systems (IPSs) have gained attention due to their immunity to multipath phenomena and inter-room interference, setting them apart from traditional RF technologies like Bluetooth and WiFi. As a result, the development of VLC-based positioning algorithms has become a focal point in both academic research and industry applications [9].

Finally, a concise overview of the thesis chapters is presented below. Chapter 1 provides a comprehensive examination of both terrestrial and non-terrestrial technologies suitable for the IoT domain. Furthermore, Chapter 2 delves into the adaptation of traditional communication at the physical and link levels to enable satellite communication effectively. Moreover, Chapter 3 introduces an open-source tool designed to assess NTN system-level performance. Chapter 4 addresses space resource virtualization and their optimized allocation through heuristic methods. Hence, Chapter 5 presents an integrated IoT-Satellite and Unmanned Aerial Vehicle (UAV) network that ensures fair energy distribution among network sensors while maintaining fairness in data transmission rates. In addition, Chapter 6 offers an innovative perspective on terrestrial resource virtualization by introducing the concept of Social Internet of Things (SIoT). Chapter 7 provides an extensive overview of VLC capabilities closely related to the IoT domain. Then, Chapter 8 proposes a novel IPS system using visible light technology and Intelligent Metasurface Reflector (IMR). Finally, the last Chapter summarizes the work and outlines potential directions for future investigation.

Chapter 1

Introduction to Terrestrial and Non-Terrestrial Technologies in IoT Networks

In an era marked by rapid technological advancement, the integration of space-based technologies into terrestrial networks has become a focal point of extensive research and development. Despite significant progress brought about by 5G technology, new challenges and requirements have arisen, particularly in the context of the IoT. The proliferation of IoT smart devices and the growing demand for seamless global connectivity are driving the quest for the next-generation network. Addressing the digital divide, especially in remote areas, requires innovative solutions, including NTN, with low-latency, coverage, and accessibility advantages. The resurgence of LEO CubeSats, driven by standardization and cost reductions, further enhances space-based technology integration for ubiquitous connectivity. Additionally, terrestrial advancements like resource virtualization and VLC play a crucial role in IoT evolution. VLC, standardized by IEEE 802.11bb and commonly referred to as Light Fidelity (LiFi), offers high-speed data transmission through LED technology while utilizing existing lighting infrastructure. This approach reduces deployment costs, enhances energy efficiency, and provides immunity to interference, making it valuable for IoT and IPS.

1.1 5G & Beyond: Innovation and Challenges

The advent of 5G mobile technology has brought revolutionary shifts beneath established wireless networks. These shifts are primarily propelled by the escalating demand for mobile data traffic and the substantial proliferation of connected devices. Specifically, 5G represents a significant leap forward from its predecessor generation of mobile communication. It offers beyond comparison data speeds, low latency, massive device connectivity, and enhanced network reliability. The game-changing features that define 5G are [10]:

- **Enhanced Data Speeds**: 5G networks are expected to offer data speeds that are several times faster than 4G, potentially reaching up to 20 gigabits per second (Gbps). This capability will revolutionize how we consume data, enabling high-definition streaming, seamless virtual reality experiences, and more.
- **Ultra-Low Latency**: The reduced latency in 5G networks, as low as 1 millisecond, will enable real-time applications such as remote surgery, autonomous vehicles, and augmented reality, which rely on instantaneous data transmission.
- **Massive Device Connectivity**: 5G networks are designed to support a significantly higher number of connected devices per square kilometer, making the IoT a ubiquitous reality.

- **Improved Reliability**: Advanced technologies like network slicing and edge computing will ensure more robust and dependable network performance, even in high-density urban areas.

While the release of 5G technology promises tremendous advantages, its implementation faces an abundance of challenging issues. The deployment of 5G infrastructure necessitates significant financial investments, the installation of an extensive network of small cells, and the allocation of new frequency bands. It is unlikely to yield cost-efficiency in remote and challenging terrains such as forests, deserts, oceans, and other areas where establishing telecommunication infrastructure imposes substantial financial burdens on companies with constrained returns. The substantial capital required for infrastructure expansion, particularly in harsh regions, may dissuade certain areas from embracing 5G technology, thereby engendering an inequality in access to its advantages, thus deepening the existing digital divide [11].

To close this gap, the strategic pathway toward the realization of 5G&B signifies a collaborative endeavor aimed at tackling the challenges entailed in the adoption of 5G technology. A central emphasis of this endeavor lies in the resolution of issues such as the digital divide and the augmentation of global connectivity, achieved through the progression of both terrestrial and non-terrestrial technologies. This is achieved through the optimization of terrestrial networks and the exploration of satellite communication integration [12], [13].

1.2 Non-Terrestrial Technologies in the IoT domain

This Section discusses the pivotal concepts and technological advancements and adaptation within the realm of NTN technologies suitable for the IoT domain. First, it introduces the NarrowBand IoT (NB-IoT) as a cutting-edge Low Power Wide Area Network (LP-WAN) technology meticulously engineered to facilitate efficient data transmission from a multitude of interconnected devices on the ground toward the satellite segment. Indeed, it helps the realization of the Ubiquitous Intelligent Mobile Society, underscored by the principles of scalability and on-demand access to connectivity and computational services.

However, the dynamic nature of NTN, influenced by satellite movements, necessitates advanced management strategies. While existing approaches for deploying Virtualized Network Function (VNF) at the edge of terrestrial networks fall short in addressing the challenges posed by satellite mobility and intermittent visibility, there is a need for specialized orchestration frameworks to effectively deploy VNFs across satellites in response to service requests.

Finally, drones play a vital role in the IoT by providing essential connectivity, especially in regions with limited conventional communication infrastructure. Indeed, the integration of satellite and UAV communications into the IoT enables real-time monitoring, autonomous operations, and innovative solutions, creating a holistic ecosystem that advances connectivity and intelligence in society.

1.2.1 Radio Access Technologies

NB-IoT is an LP-WAN radio communication technology designed to serve a large number of devices, optimized for services characterized by small and infrequent data transmissions. A single NB-IoT carrier requires a 180 kHz bandwidth for downlink and uplink [14]. In addition, multiple carriers can be used to extend the link capacity. In general, these carriers may be deployed inside an Long Term Evolution (LTE) channel (in-band), within the guard-bands of the LTE bandwidth (guard-band), or mapped onto GSM carriers of 200 kHz (stand-alone).

At the physical layer, NB-IoT is based on Orthogonal Frequency Division Multiplexing (OFDM). In the downlink, it entirely acquires the LTE numerology, Specifically, the Evolved

Node-B (eNB) operates on the whole bandwidth of 180 kHz (which is subdivided into 12 subcarriers with a spacing Δf = 15 kHz) and across 1 ms long Transmission Time Intervals (TTIs). On the other hand, the uplink may adopt an additional subcarrier spacing Δf = 3.75 kHz, leading to 48 subcarriers in a single NB-IoT carrier. Moreover, it supports both Single-Tone and Multi-Tone transmissions, the latter with Δf = 15 kHz only. In Single-Tone a specific subcarrier is allocated to a particular user only, while Multi-Tone allows to schedule 3, 6, or 12 subcarriers to a single user. According to the transmission configuration, a different Resource Unit (RU) size is used, as reported in Table 1.1. An RU is the smallest unit to map a transport block [15].

TABLE 1.1: RU sizes

Transmission	Subcarriers	Δf	BW	Slots	TTI
Single-Tone	1	3.75 kHz	3.75 kHz	16	32 ms
	1	15 kHz	15 kHz	16	8 ms
Multi-Tone	3	15 kHz	45 kHz	8	4 ms
	6	15 kHz	90 kHz	4	2 ms
	12	15 kHz	180 kHz	2	1 ms

In general, NB-IoT reuses the existing LTE physical channels, including Narrowband Physical Downlink Shared Channel (NPDSCH), Narrowband Physical Downlink Control Channel (NPDCCH) and Narrowband Physical Broadcast Channel (NPBCH) for the downlink and Narrowband Physical Uplink Shared Channel (NPUSCH) for the uplink, while properly adjusting them to suit the narrow bandwidth. Moreover, it defines a new Narrowband Physical Random Access Channel (NPRACH) which uses the Single-Tone configuration with Δf = 3.75 kHz in order to provide more capacity during the Random Access Procedure [16].

Finally, repetition of transmissions is a key enabler for achieving a coverage enhancement in NB-IoT. Essentially, each transmission may be repeated a configurable number of times in order to improve the probability of a successful reception. However, the coverage is extended at the expense of higher transmission rates. All NB-IoT channels can benefit from repetition, hence properly achieving coverage requirements.

NB-IoT has been standardized by the 3rd Generation Partnership Project (3GPP) in Release-13 for serving IoT devices through the mobile network infrastructure [17]. The widespread growth of IoT applications is currently embracing some challenging scenarios, including those concerning devices deployed in geographical areas where terrestrial networks are not present or hard to reach (for instance deserts, oceans, or forests). Here, service continuity and fast service deployment can be successfully achieved only by leveraging disruptive methodologies that go beyond the boundaries imposed by current terrestrial networks.

Recently, the scientific literature and the 3GPP standardization body considered as viable the integration of NB-IoT in satellite-based architectures. Without any doubt, the design of the space segment is not easy. A number of state of the art contributions already tackled the related operational technical challenges, while focusing on feasibility studies at both physical and link levels [18]–[27], satellite constellation [21], [25], and Random Access procedure [19], [26], [27]. However, aside from the important findings they report, detailed selection of physical (and standards-compliant) transmission settings, protocol stack configuration, and a significant system-level evaluation of the overall communication architecture are still unexplored topics. Also, the discussion started by the 3GPP in RAN2 technical meetings (see [28] and [29]) is still in its embryonic stage and no turnkey solutions have been standardized yet.

To bridge this gap, the work presented herein addresses the design of a fully functional NB-IoT over satellite service, compliant with 3GPP specifications, and aiming to face the

most critical issues arising from the employment of NB-IoT over NTNs into a real application scenario*.

Differently from the current scientific literature, it follows a service-oriented methodology that:

- illustrates application requirements and technological constraints that characterize a reference use case (taken from the smart agriculture domain);
- configures the whole protocol stack for ensuring the transmission of tens of bytes generated at the application layer within a single data packet, even in the absence of a feeder link;
- identifies low-level adaptations for counteracting the issues that affect the satellite communication during the random access procedure, Doppler shift, and frequency carrier offset;
- conducts an accurate link-level investigation to retrieve physical settings that guarantee an effective ground-satellite communication;
- defines a satellite constellation offering a realistic service operating in Europe;
- investigates the performance of the conceived architecture through system-level simulations.

Obtained results demonstrate that a constellation of 24 LEO satellites, grouped into 8 different orbits and moving at an altitude of 500 km ensures communication latencies ranging from 16 minutes to 75 minutes, depending on the served number of terminals and the physical transmission settings. At the same time, the adoption of the Early Data Transmission scheme can reduce communication latencies up to 40%. By reducing the number of satellites per orbit (from 3 to 2), it is still possible to drain all the generated data, but at the cost of a much higher average communication latency.

1.2.2 NTN Architectures

Satellite Communication (SatCom) is expected to have a primary role in 5G&B networks [12]. Thanks to its ubiquity capabilities and the robustness against natural disasters, SatCom fosters network spread in a cost-effective way, by either delivering connectivity where telecommunication infrastructures are lacking or upgrading low-quality terrestrial networks (i.e., oceans, forests, and deserts). Such a cutting-edge connectivity model can naturally provide backup links in case of network failures. Moreover, it offers additional connections to offload terrestrial networks, while preserving the performance of specific loss or delay-sensitive applications. At the same time, it strongly promotes the scalability of mobile networks, since satellites easing allow possible future further expansions of current 5G deployments, as shown in Figure 1.1.

For these reasons, SatCom results particularly effective for Machine Type Communication (MTC) scenarios, envisaged for IMT-2020 and beyond [30], especially when a huge number of low cost devices need connectivity in large areas not covered by terrestrial networks. Here, the main challenge is to allow connectivity to a massive number of devices which can have some design constraints or conflicting KPIs, including extended battery lifetime and long transmission range.

*This work is the result of research activities carried out by different academic and industrial partners, collaborating as a partnership in the context of the project "3GPP Narrow-Band Internet-of-Things (NB-IoT) User Sensor Integration into Satellite" funded by the European Space Agency (ESA) under contract no. 4000129810/20/NL/CLP, https://artes.esa.int/projects/nbiot4space

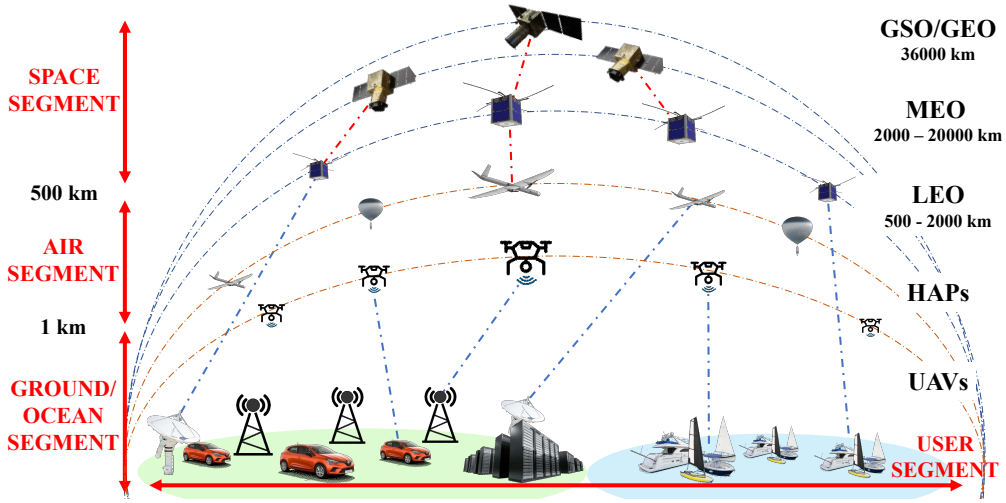

FIGURE 1.1: Integration of Terrestrial and Non-Terrestrial technologies.

NB-IoT, is already regarded as a candidate LP-WAN addressing the requirements of the future 5G developments for MTC [31]. A number of recent studies also considered NB-IoT as a promising technology for 5G satellite MTC [19], [22], [24]–[26], [32]–[36]. Furthermore, the scientific literature is mainly focusing the attention on physical and link-level analysis only. To overcome this issue, the availability of a system-level simulator to support the research activities represent a mandatory requirement. In fact, simulation tools aiming to effectively support both the design and the analysis of this emerging field while reducing costs related to real-world prototypes are extremely important.

Starting from these premises, the work presented herein also provides a twofolded contribution. First, it presents a novel simulation tool, conceived as a new module for the open-source 5G-air-simulator, modeling NB-IoT satellite-based communication systems. Specifically, the existing code has been properly updated to support the system-level analysis of an NB-IoT satellite-based communication system, implementing several link-to-system abstraction models, the cell selection procedure, and a configurable satellite constellation. In particular, the blind repetitions are now managed during the scheduling and transmission procedures. Furthermore, the radio channel model for satellite NB-IoT has been implemented, thus improving the accuracy of the results. Finally, a new mobility model is defined for simulating the movement of a variable number of satellites belonging to the configured constellation. All these features have been coherently integrated within the rest of the 5G-air-simulator tool, hence offering the opportunity to test flexible network deployments. Second, to demonstrate the actual effectiveness of the developed tool, this work presents a preliminary performance evaluation of a NB-IoT satellite-based communication system. Specifically, it considers reference monitoring scenarios where a configurable number of users are positioned either uniformly over the simulated area or in several smaller clusters. Then, the number of NPRACH Preamble Collision and the end-to-end delay are statistically analyzed. Finally, the average packet delivery ratio is investigated for further completeness of the performance evaluation. Results show the crucial trade-off between the number of satellites per orbit and overall network performances.

1.2.3 Resource Virtualization

While the 5G of mobile communication systems are being deployed in many parts of the World, recent research interests are moving towards the 5G&B of mobile networks [37]. At the time of this writing, there already exists a common consensus that 5G&B networks will

target the very ambitious goal to realize a Ubiquitous Intelligent Mobile Society, based on scalable and effective fruition of connectivity and computing services on demand, and wherever needed [11], [38], [39]. To this end, NTN entities will cooperate with conventional terrestrial networks to provide three-dimensional wireless connectivity, also covering deserts, forests, and oceans [40], [41].

The global coverage capabilities will enable a range of innovative 5G&B-oriented use cases and the potential for customized, on-demand services through the use of the spatial segment [42]–[45]. However, the on-demand deployment of customized services raises the need for the dynamic management of the NTN. Indeed, the dynamic deployment of services and applications at the edge of the terrestrial networks is a research topic widely investigated in the current state-of-the-art. Specifically, Software-Defined Networking (SDN) and Network Function Virtualization (NFV) principles can be used to separate the data and control planes in NTNs and configure their functionalities according to service requests [46], [47].

Valuable contributions, for example, propose optimal approaches able to minimize latency and energy consumption [48]–[51], or to maximize the user throughput [52]. Unfortunately, these solutions cannot be applied to the considered 5G&B satellite infrastructure. In fact, they do not consider the movement of satellites and the intermittent connectivity among NTN terminals, satellites, and core network. Also, a recent survey confirms that the optimal provisioning of security services in 5G&B satellite deployment still represents an unexplored research topic [39].

Specifically, the network dynamism provoked by satellites' movement invites considering the usage of effective orchestration frameworks willing to deploy specialized VNFs across satellites, on demand[53], [54]. Unfortunately, conventional strategies conceived for the VNF deployment at the edge of terrestrial networks, like [43]- [63], appear inadequate for this purpose, because of the motion of satellites and the resulting intermittent visibility they grant to the terminals on the Earth's surface. Still, the contributions explicitly focusing on NTNs, such as [64]–[81], just concentrate on quasi-static scenarios, thus ignoring the challenging issues (i.e., intermittent visibility and dynamic network configuration) introduced by satellites' movement and communication protocols enabling the integration of terrestrial space network elements.

Based on these premises [82], the work presented herein intends to extend the current state of the art by successfully addressing the aforementioned open research challenges and providing the following main scientific contributions:

1. Definition of a novel network architecture able to collect service requests and related quality of service constraints, implement a service orchestration function, and effectively deploy the corresponding VNFs across satellites over time. The resulting approach is general and may support any kind of service. Specifically, a new communication protocol has been conceived to enable the interaction among terrestrial and space network entities (distributed among User, Edge, and Cloud layers) during three different operating phases, namely service request, configuration, and provisioning;

2. Design of a system model able to catch the network configuration (i.e., groups of terminals on the Earth's surface, satellites' constellation, orbits and consecutive visibility time windows, allocation of VNFs over time, and so on) and quantify the deployment delay experienced by the end-users;

3. Formulation of an optimization problem willing to dynamically allocate VNFs among satellites over a looking-ahead time horizon, based on service requests, computational capabilities of involved satellites, visibility matrices, and expected deployment delay bounds;

4. Development of three different strategies based on meta heuristic approaches (i.e., Tabu Search (TS) [83], Simulated Annealing (SA) [84], and Genetic Local Search (GLS) [85]), able to solve the aforementioned optimization problem.

Computer simulations have been carried out to demonstrate the effectiveness of the proposed approach, in terms of average deployment delay, resource consumption, and processing time, by varying parameter settings. The study demonstrates that the three heuristic approaches can produce outcomes that are similar to the optimal solution, as well as better performance with respect to a benchmark technique, namely Greedy Algorithm (GR) algorithm. Among the others, the SA-based strategy emerges as the best solution that can guarantee better performance in terms of service deployment delays, resource consumption, and processing time.

1.2.4 Drones and Satellites

The growth of the number of users, as well as the diversity of services, has been enabled primarily by the expansion of traditional terrestrial wireless communication systems [86]. At the same time, emerging applications impose challenging requirements that must be addressed through the technological advancement of innovative telecommunication facilities [87]. In this context, 5G&B mobile system [88] promises an ubiquitous coverage across Earth that leverages an integrated access backhaul that unifies space, aerial, and ground infrastructures [42]. In this regard, the integration of terrestrial and non-terrestrial technologies

[89] represent a flexible solution to provide wireless access services with high data rate and reliability, which are key enablers for a variety of both civil and military applications, including Earth observation and mapping, intelligent transportation systems, and disaster rescue. Furthermore, recent 3GPP standardization efforts [28], [90]–[92] identified NTNs [40], [93] as a solution to grant connectivity where traditional terrestrial infrastructure is not practical or cost-effective. On the one hand, Low Earth Orbit (LEO) satellite constellations are important to provide full-coverage broadband services for ground users through space-ground interconnection. Manufacturing and launching processes for these constellations have matured, enabling the implementation and deployment of these systems at scale [6], [12]. On the other hand, Unmanned Aerial Vehicles (UAVs) [94], also known as drones, have received significant attention due to their flexibility and applicability in manifold scenarios. In particular, network architectures can benefit from their high mobility, easy deployment, and reusability [95].

Specifically, drones play a pivotal role in the realm of the IoT [96], representing an enabling technology to provide pervasive connectivity even where the classical communication infrastructure is not available. The IoT allows interconnection between the physical and digital realms, revolutionizing industries by offering disruptive prospects for automation, efficiency, and data-driven decision-making. Therefore, the integration of satellite and UAV communications in the IoT domain enables real-time monitoring, autonomous operations, and novel solutions across industries such as agriculture, transportation, and surveillance. This combination results in a full ecosystem, propelling progress toward a smarter and more connected society.

Despite the great advantages in terms of seamless and reliable connectivity, the energy lifetime of IoT devices represents a challenging aspect that is usually not taken into account, especially in harsh environments.

To this end, Wireless Power Transfer (WPT) [97] has been recognized as an effective solution to cope with this issue. In traditional WPT systems, specialized energy transmitters are installed at fixed locations to send RF signals to charge IoT nodes, especially low-power ones. However, the range of these systems is limited by the low efficiency of end-to-end power transmission over long distances. Therefore, fixed-location energy transmitters must

be densely deployed to wirelessly recharge a large number of low-power devices, which would significantly increase the cost and hinder large scale implementation.

To tackle this issue, the majority of the scientific literature focuses on the combination of WPT and UAVs as a solution to support an IoT network in terms of power delivery and information transmission. In particular, they focus on the optimization of different aspects, such as the movements of the UAV [98]–[105], power allocation [99], [101]–[103], [105], [106], energy harvesting time [100]–[103], [106], [107], and the beamforming vectors of the antenna [104], [105].

To the best of the authors' knowledge, however, the state of the art does not consider the potential of satellites, and their integration with drones and WPT, as a comprehensive solution for IoT networks in harsh conditions.

Starting from the discussion above, this work combines together the advantages of these technologies by investigating a UAV-powered IoT-satellite integrated network, where a drone wirelessly recharges a set of Ground Nodes (GNs), while a LEO CubeSat provides connectivity for data exchange. Specifically, the objective is to achieve a fair maximization in terms of harvested energy and transmitted data.

The main contributions of this work are as follows:

- An integrated NTN is designed to enable the uplink data transmission of GNs to a LEO CubeSat, within its visibility window. These IoT nodes are deployed in a specific area and are recharged by a UAV, equipped with an array antenna, that employs WPT. Accordingly, a mathematical model is developed to characterize the UAV-GN channel and CubeSat-GN communication link.

- Two Mixed-Integer Non-Linear Programming (MINLP) problems are formulated to fairly maximize (i) the harvested energy of the GNs by jointly optimizing the UAV kinematics and the array antenna beamforming vectors, and (ii) the total transmitted data by fine-tuning the transmission plan of the nodes communicating with a LEO CubeSat. Both problems are non-convex and hence intractable. Therefore, the first is divided into two sub-problems, which are alternatively solved by leveraging also the Successive Convex Approximation (SCA) technique, until convergence to a quasi-optimal solution is achieved. Following a similar strategy, also the second problem is solved by adopting the two aforementioned techniques.

- A lower-bound mathematical expression for the harvested energy is derived. The stochastic nature of the UAV-GN channel model represents a challenge, which is addressed by imposing a maximum out-of-service probability. This leads to a non-linear energy-harvesting model that can be employed also for system design and assessment.

- A simulation campaign is conducted to prove the effectiveness of the proposed solution. In particular, multiple scenarios are analyzed and discussed under different parameter configurations, which include transmission power, number of GNs, and array antenna size. The performance of the conceived algorithm is then compared with a baseline approach, where the drone follows a snake-like trajectory and periodically recharges the nearest node, while adopting an optimal transmission scheduling.

Numerical results demonstrate that the proposed strategy outperforms the baseline in terms of total transmitted data.

1.3 Cutting-Edge Terrestrial Technologies

This Section introduces the emergence of the SIoT [108] as a solution to address the escalating number of IoT devices within the terrestrial segment. Specifically, it presents a novel

paradigm where smart objects autonomously establish social networks, creating opportunities for enhanced resource visibility and service discovery [7]. This transition from smart objects to social entities unlocks various application scenarios, necessitating robust methodologies for service provisioning with an emphasis on trustworthiness. In this context, the Trust Management System (TMS) [109] assumes a pivotal role by evaluating the conduct of social objects and ensuring trustworthy interactions through the computation of trust levels, thereby discouraging malevolent or erroneous behaviors among nodes.

Furthermore, another noteworthy solution that addresses the challenges posed by the proliferation of IoT devices and the constrained RF spectrum is the emergence of VLC as a promising wireless data transmission technology [110]. Standardized as IEEE 802.11bb [8], VLC harnesses the potential of LED to deliver high-speed broadband internet services while leveraging existing lighting infrastructure, consequently reducing deployment expenses. Moreover, VLC exploits the extensive unlicensed bandwidth available in the visible light spectrum, spanning approximately 400 to 800 THz, to enable data rates of up to 10 Gbps, presenting an enticing alternative to conventional RF communication.

Lastly, IPS founded on VLC technology have garnered significant attention from both academia and industry due to their distinct advantages [111]. In contrast to RF technologies such as Bluetooth and WiFi, VLC-based IPS inherently mitigate issues related to multipath phenomena and inter-room interference by capitalizing on the characteristics of high propagation loss and limited wall penetration associated with visible light. RSS-based methods are widely adopted for VLC IPS, benefiting from the minimal noise levels inherent to VLC channels [112]. This is evident in studies examining channel estimation errors and real-world testbeds achieving centimeter-level accuracy. Furthermore, advancements in IPS precision involve techniques like random forest algorithms and spatial clustering to mitigate noise interference, particularly in challenging room corners [9].

1.3.1 From Social IoT to the Digital Twin

The promising integration of Social Networks in the IoT domain promoted the birth of the SIoT [7]. By leveraging autonomous interactions, smart objects can build social relationships composing a Social Network without human intervention. Thus, the transition from smart objects to social objects introduces additional opportunities to enhance network resource visibility and service discovery [108]. Reproducing the digital counterpart of the physical IoT devices strongly favors the network navigability and opens the opportunity to explore several new application scenarios (e.g., healthcare applications [113], and Vehicular Social Networks [114]). It requires the development of effective methodologies for service provisioning, where the trustworthiness of service providers must be guaranteed [115]. In this context, the TMS represents the key element for the evaluation of the behavior of social objects and their selection as a service provider. It facilitates trusted interactions between social objects by computing their trust level, thus penalizing nodes that adopt malicious or incorrect behaviors [116].

The research in this field explored many methodologies devoted to calculate and manage the trust levels of the service providers in SIoT environments (see [117]–[122] and the review of the state of the art in Section 6.1). However, to the best of the authors' knowledge, specific strategies accounting for the computing capabilities of social objects in the TMS to speed up and improve service provisioning are still an unexplored issue. Furthermore, available solutions are not fully applicable to real-world scenarios due to their computational complexity, being not easily manageable by most of the resource-constrained IoT devices.

In order to extend the scientific literature in this direction, this work proposes a novel resource capability-aware scheme for the TMS. Specifically, the additional functionalities introduced in this contribution jointly consider the trustworthiness, resource availability, and

the computational capabilities of the objects registered in the Social Network to speed up the trusted service provisioning. Furthermore, differently from other works, the proposed strategy exploits fog computing to implement all the TMS functionalities. It relieves the processing and storage efforts of the IoT nodes for the overall TMS procedure, including the construction of social relationships, thus making the strategy suitable for realistic scenarios.

Simulation results show the effectiveness of the proposed scheme in terms of latency in service provisioning (reduced up to 67% with respect to the baseline solutions) while guaranteeing fairness in the distribution of available resources among service providers. Furthermore, the new features of the TMS improve the responsiveness of the identification of malicious devices, promptly excluding them from the process of service provisioning.

1.3.2 Visible Light Communication

The prevailing scarcity of the RF spectrum has paved the way for the emergence of VLC as an innovative solution for wireless data transmission. This technology, recently standardized as IEEE 802.11bb [8], holds the potential to deliver high-speed broadband internet services through the utilization of LEDs. Given their widespread usage in residential, industrial, and urban applications, VLC technology can leverage the existing lighting infrastructure, resulting in diminished deployment costs. Furthermore, the employment of LED lamps can contribute to improve energy efficiency, capitalizing on the extended operational lifespan and reduced consumption. Further, the huge unlicensed bandwidth available for VLC allows to achieve data rates up to 10 Gbps. Indeed, the visible light spectrum is thousands of times greater than the entire RF spectrum, encompassing frequencies ranging from approximately 400 to 800 THz.

The fluctuation in light intensity directly pertains to the information contained in the transmitted message. In LiFi, there are several types of modulation, including single carrier, multiple carrier, and color modulation [123]. For example, the blinking of the LED (even at negligible frequencies for the human eye) can be used for the data transmission. In particular, if the LED is switched on it can be considered as a digital "1". On the contrary, if the LED is switched off, it is treated as a digital "0" [124]. Despite LiFi networks can be easily implemented as a bidirectional half-duplex system in VLC, some intriguing works make use of VLC for the DownLink (DL) and the infrared spectrum for the UpLink (UL) [125]. This is useful to avoid distracting human mobile users without affecting the lighting conditions of the room [126]. Moreover, it prevents interference between the UL and DL, by allowing simultaneous signal broadcasting [127], [128].

Since LEDs are already widely used in homes, factories, and streetlights, LiFi may take use of the existing lighting infrastructure by reducing the deployment fee. This holds true especially for massive IoT devices deployments, due to the capability of light-based communication to provide very large bandwidth and support high nodes density, which are important requirements for IoT environments [129]. Moreover, the adoption of LED lamps in LiFi can increase energy efficiency. In fact, as known, LED lamps are characterized by very long lifetimes and reduced energy consumption [130]. So, they can be effectively employed in LiFi systems by integrating data transfer and low-power illumination in a constrained scenario, such as IoT [129], [131], [132]. Even though it is clear that the amount of energy consumed depends on the various system components, the intrinsic low-power nature of LEDs, combined with additional techniques aiming to save energy (that will be discussed more in detail in Section 7.7), can greatly help to reduce the overall energy consumption in LiFi systems [130], [133]–[135].

The well-known IoT paradigm defines a network of smart interconnected objects that can sense real-world phenomena and transmit information over the Internet without the need for human interaction [136]. According to [137], in 2022 the IoT market reached around 15

billion active connections. In this context, wireless access is currently mostly accomplished with the aid of RF. However, radio technologies in access networks are already approaching their limit in terms of throughput and Quality of Service (QoS). Specifically, owing to the currently saturated RF spectrum, it is challenging to accommodate the ever-growing amount of devices to be handled in a IoT environment [138]. Furthermore, the application of the RF presents some relevant issues, including poor privacy due to radio waves freely penetrating walls, a huge amount of energy required for signal relaying and service equipment cooling, and limitations in its adoption in some environments like aircraft, hospitals, and specific factories. To cope with these issues, the implementation of LiFi may disclose disruptive services in the IoT domain.

Nevertheless, despite LiFi is still in its early stages and is not yet commonly accessible, numerous teams and researchers are working to create and deploy LiFi-based networking solutions [139]. Consequently, several review and survey papers are discussing the main functionalities of LiFi, but separately from the IoT environment. According to this, and to the best of the authors' knowledge, a thorough analysis of the state of the art in LiFi technology integrated into IoT environments is still missing. To fill this gap, the primary goal of this work is to comprehensively examine all areas in which academics are focusing their efforts on the suitability and potential of the LiFi applied to a highly dynamic environment such as the IoT. Then, based on this analysis, the main challenges and open issues are illustrated, to provide guidelines for future research directions on this theme.

1.3.3 Light-based Indoor Positioning System

IPSs based on VLC represent a promising application which has caught great interest from academia and industry, due to many pivotal features. Differently from RF technologies (e.g., Bluetooth, WiFi, and ZigBee), VLC-based IPSs provide inherent immunity to multi-path phenomena and inter-room interference, due to high propagation loss and light inability to penetrate walls. Therefore, the scientific community has acknowledged the importance to develop VLC-based positioning algorithms [9].

Specifically, the Received Signal Strength (RSS)-based methods represent the most used approach to develop an IPS that can achieve high accuracy thanks to the low level of noise characterizing the VLC channel. To prove that, the authors in [140] study the channel estimation error by considering the Line-of-Sight (LoS) path of the emitted light by multiple ceiling-mounted LEDs and the Additive White Gaussian Noise (AWGN) noise composed of thermal, shot, and background. Furthermore, the authors in [141] implement a real-world testbed to evaluate the performance of a 3D IPS by means of a deep learning method that obtains a centimeter accuracy. Another noteworthy contribution aims to improve the IPS accuracy, by involving a random forest algorithm and spatial clustering to mitigate the noise contribution in the corner of the room [142].

Recently, the scientific literature has considered the joint employment of VLC and Reconfigurable Intelligent Surface (RIS) [143] to enhance Signal to Noise Ratio (SNR) [144] by improving coverage on otherwise unreachable areas. In the context of VLC, a specific type of RIS is of particular importance, namely IMR [145] which can operate in reflective and absorption mode.

However, to the best of the authors' knowledge, there are no scientific contributions that consider the positioning capability of a VLC-based IMR-assisted IPS. In light of the above, the major contributions are summarized hereby.

- The IMR-assisted VLC channel gain, encompassing the LoS and Non-Line-of-Sight (NLoS) contributions, is investigated along with the corresponding noise model.

- A novel RSS-based IMR-assisted positioning algorithm is proposed, which leverages Linear Least Square (LLS)-based Trilateration through distances derived from averaged LED and IMR signal samples.
- A simulation campaign is carried out to validate the theoretical findings and to analyze the impact of the distance, the bandwidth, the optical power, the number of IMR, and the number of samples on the overall accuracy.

Numerical results demonstrate a remarkable estimation accuracy in terms of distance absolute error and position Root Mean Squared Error (RMSE).

Chapter 2

Looking at NB-IoT over LEO Satellite Systems: Design and Evaluation of a Service-Oriented Solution

The adoption of the NB-IoT technology in satellite communications intends to boost Internet of Things services beyond the boundaries imposed by the current terrestrial infrastructures. Apart from link-level studies in the scientific literature and preliminary 3GPP technical reports, the overall debate is still open. To provide a further step forward in this direction, the work presented herein pursues a novel service-oriented methodology to design an effective solution, meticulously stitched around application requirements and technological constraints. To this end, it conducts link-level and system-level investigations to tune physical transmissions, satellite constellation, and protocol architecture, while ensuring the expected system behavior. To offer a real smart agriculture service operating in Europe, the resulting solution exploits 24 Low Earth Orbit satellites, grouped into 8 different orbits, moving at an altitude of 500 km. The configured protocol stack supports the transmission of tens of bytes generated at the application layer, by also counteracting the issues introduced by the satellite link. Since each satellite has the whole protocol stack on-board, terminals can transmit data without the need for the feeder link. This ensures communication latencies ranging from 16 minutes to 75 minutes, depending on the served number of terminals and the physical transmission settings. Moreover, the usage of the Early Data Transmission scheme reduces communication latencies up to 40%. These results pave the way towards the deployment of an effective proof-of-concept, which drastically reduces the time-to-market imposed by the current state of the art.

2.1 State of the Art on NB-IoT over satellite systems

The review of the state of the art is organized as in what follows: first, the scientific contributions focusing on NB-IoT over satellite systems are discussed in Section 2.1.1; then, recent 3GPP activities on NTN networks are illustrated in Section 2.1.2. These two latter Sections also note the scientific and technical lacks covered by this work.

2.1.1 Related Works on NB-IoT over satellite links

The scientific literature investigated the possibility to use NB-IoT (with specific adaptations) in satellite-based communication systems. As summarized in Table 2.1, available studies focus the attention on the analysis and the selection of a suitable antenna type [18]–[20], the evaluation of the link budget [18]–[24], the design of a satellite constellation [21], [25], the study of link-level performance [18], [24], the evaluation of the Doppler shift [19], [20], [22], [24]–[27], and the management of the Random Access procedure [19], [26], [27]. Other interesting related works, such as [146] and [2], investigate Doppler shift and Random Access

TABLE 2.1: Review of Related Works

Features	[18]	[19]	[20]	[21]	[22]	[23]	[24]	[25]	[26]	[27]	[146]	[2]	This work
NB-IoT in satellite communications	✓	✓	✓	✓	✓	✓	✓	✓	✓	✓			✓
Antenna Selection	✓	✓	✓										✓
Link Budget Evaluation	✓	✓	✓	✓	✓	✓	✓						✓
Constellation Design				✓				✓					✓
Visibility Time													✓
BLER curves Analysis	✓						✓						✓
Doppler shift Evaluation		✓	✓		✓		✓	✓	✓	✓	✓	✓	✓
Random Access Procedure		✓							✓	✓	✓	✓	✓
Protocol Stack Configuration													✓
System-level Architectural Design													✓
System-level Performance Analysis													✓

procedure in satellite communication systems based on LTE and 5G, respectively. Focusing the attention on specific aspects of the system and in the absence of uniform assumptions, these studies appear isolated. Nevertheless, the effective deployment of NB-IoT over satellite links requires a service-oriented approach where protocols, architectural, physical, and functional aspects are accounted for altogether. In this sense, the main contribution of this work is to describe every aspect of interest, by reviewing, enhancing, redefining, modelling, and simulating it in the context of an exhaustive proof of the feasibility of the target solution, while endorsing the compelling capabilities allowed by regenerative satellites.

2.1.2 Recent 3GPP discussions

The 3GPP started the standardization of NTN in Release-15, addressing deployment scenarios, related system parameters (e.g., architecture, satellite altitude, orbit), and adapted channel models [90]. Available reports and specifications use the concept of narrow-band access (already introduced with NB-IoT) to characterize a service-link provided by a mobile satellite in the frequency band below 6 GHz. Moreover, they define two possible deployment scenarios. The *wide area IoT service* intends to provide a global continuity of service to a group of moving sensors in areas partially covered by terrestrial networks. The *local area IoT service*, instead, is conceived for a group of sensors able to collect data and report to a central point installed on a moving platform. In this case, the satellite has to guarantee the connectivity between the mobile core network and the base stations serving IoT devices. In both cases, 3GPP remarks the optional integration of the Inter-Satellite Link (ISL) and the possibility to consider either a satellite with bent-pipe payload or the implementation of the base station on-board the satellite.

More recently, with Release-17, 3GPP proposed new amendments from Physical (PHY) to Non Access Stratum (NAS) layers, aiming to improve performances of NTNs in terms of latency, coverage, and power consumption [147]. Particularly interesting is the discussion presented in [29], whose goal is to investigate the applicability of [28] in NTN deployments for explicit support of IoT services based on NB-IoT.

As anticipated in Section 1.2, 3GPP activities on NTN networks are not complete. Therefore, this work leverages all the guidelines proposed by preliminary 3GPP technical reports and pursues the ambitious goal to provide concrete answers to the open questions recently arisen from 3GPP.

2.2 The reference use case and related requirements

The reference use case taken into account in this work refers to the smart agriculture scenario, which represents one of the most promising application fields, where NB-IoT technology over satellite can be effectively employed.

As well-known, farms require constant and continuous connection and communication with monitoring systems employed for different purposes (i.e., harvest management, power consumption of machines and facilities, optimization of production processes, or environmental control for greenhouse and open field management) [148]–[150]. In this context, satellites play a key role to answer the challenges of future farming, especially for large customers that require hundreds or thousands of NB-IoT devices for precision farming in rural areas. This is testified by several companies that are leveraging LEO satellite-based connections to deliver seamless, real-time communications in 100% of the globe [151]. Currently, there are also initiatives aiming to help mobile operators to accelerate the process of deploying new NB-IoT devices and services connected through satellite-based systems in smart agriculture scenarios [152].

These motivations are also based on the project funded by the European Space Agency (ESA), mentioned in Section 1.2, which considers the smart agriculture scenario as one of the most interesting case studies.

Without loss of generality, this study assumes that clusters of IoT devices are distributed in the geographical area covered by the satellite. Each cluster is deployed in a rectangular crop field of size 30 hectares. This is about the maximum size of a crop field as present in some European countries [150]. A so large field size allows evaluating the system performance for a wide area covered by a high number of sensors. Sensor nodes are supposed to be placed uniformly in the whole field, with a 10 m inter-spacing. Therefore, a total number of 3000 nodes can be deployed in each cluster.

Like in the vast majority of smart agriculture scenarios, wireless sensor units deployed on-ground are characterized by four different types of components, i.e., the application-specific sensors, the processing unit, the radio transceiver, and the battery power [148]. The energy needed by each sensor is almost totally consumed by the radio transceiver when the node is active, so it depends on the time interval needed by the node to successfully transmit its generated measurement. Nevertheless, the node is active only during the Random Access procedures and the TB transmissions, each one taking not more than tens of milliseconds. Since a sensor node is active for a small fraction of time a day, monitoring sensors operated in smart agriculture can effectively exploit embedded rechargeable batteries powered by solar cells that are enough for the system to work properly, as testified by several works found in the literature [148], [153]–[157]. As a consequence, energy consumption is not a relevant issue in the considered application scenario, and its impact on the system performance can be neglected in this study.

In the use case under analysis, portable sensors are used to measures five different soil-related parameters for monitoring purposes: soil moisture, rain/water flow, soil temperature, conductivity, and salinity [148]. These sensed measurements are collected with a 2-byte precision each. In addition, 2 bytes of sensor ID (65536 different sensors can be addressed, which is enough for the depicted scenario) are included to identify the specific sensor data come from. Finally, 6 additional bytes of latitude/longitude coordinates from a GPS module are added to the generated message, to locate the position of the sensed data with high accuracy. The whole size of the message generated by each sensor is thus 18 bytes at the application layer.

To monitor the field efficiently, the sensed parameters do not need to be generated with a high frequency. So, it is supposed that all the five measurements are collected by each node 6 times per day, i.e., a measurement of each type is collected every 4 hours by each sensor node. Furthermore, this very low frequency of data generation can be easily manageable by the network since it allows each node to exploit the visibility time of more satellites (passing over the field) to transmit its own data. To this end, sensed data are collected by the node and buffered until the node enters the satellite visibility time. During this time interval, the node

attempts to send the content of the buffer to the base station on the satellite until its successful reception.

Regarding the system requirements, this works intends to fulfil the following challenging aspects:

- **NB-IoT compliance**: the adoption of standard 3GPP technology shall be endorsed as much as possible with the aim to support device interoperability, application extendability, and cost-efficiency. In particular, it is necessary to provide a solution with simplified hardware, which guarantees a long battery life.
- **Guarantee of a service area and timing compliant with application characteristics**: satellite coverage shall be ensured in the service area with an interval of a few hours, allowing the sensors to transmit data within this interval.
- **Need for a proper satellite configuration to cover the entire zone of interest**: the satellite system is designed to cover the European zone of interest, which is a portion of about 6700 km of the Earth surface of 60° longitude, starting from 20° west to 40° east.
- **Data transfer accomplishment within the visibility time**: the visibility time represents the period during which the NTN terminal can set up a radio bearer and perform the data transmission towards the satellite. A transmission round shall be shorter than the visibility time, which in turn is a function of the satellite orbit characteristics and the achieved link budget.
- **Satellite access latency shall not significantly shrink the time window for sensor data transmission**: the average amount of time required for finalizing the Random Access procedures is the first delay contribution that is inflated by the satellite Round Trip Delay (RTD). Such a setup delay shall be at least an order of magnitude lower than the overall visibility time, in order to not impair actual data transmission.
- **The satellite link shall support the reliable communication**: satellite provides a wireless channel significantly affected by several propagation impairments. Specifically, propagation losses on the ground-space link are due to different contributions, including absorption of the atmosphere, attenuation by rain, scintillation of troposphere and ionosphere, depolarization effects, and fog and atmospheric gas attenuation. All of these essential aspects should be taken into account to identify suitable physical layer settings and system configurations that guarantee reliable communication.
- **Doppler effect compensation**: because of the movement of the satellite, a shift in the frequency domain will occur. The Doppler shift requires adaptations at the physical layer.
- **Need for a communication infrastructure resilient to feeder-link unavailability**: the connection between the satellite and the rest of the NB-IoT network functional elements is not guaranteed over time. The feeder-link is set up when a gateway is under the satellite spot-beam and this might be time-shifted with respect to service-link availability. As a consequence, the whole architecture shall be designed in order to allow NTN terminals to exchange data with satellites, even in the temporary absence of the feeder-link.
- **Optimization of the satellite cost**: the decoupling of the satellite service and feeder-link poses the problem of how to guarantee an end-to-end service. Solutions can embrace the setup of a satellite constellation and the deployment of on-board processing.

2.3 Protocol architecture and low-level adaptations

In line with 3GPP standardization activities on NTN networks [90], the architecture considered in this work implements the *Local Area IoT Service* scenario.

As for the baseline satellite infrastructure, the reference architecture embraces NTN terminals, satellite, and NTN-Gateway. NTN terminals and satellite exchange data through the *service-link*. In particular, the NTN terminal can establish a connection with a single satellite of the constellation during its visibility period. Indeed, when a new satellite belonging to the same orbit passes over the area where the aforementioned NTN terminal is deployed, that device restarts the configuration procedures in a stateless way. On the other hand, satellite and NTN-Gateway interact with each other through the *feeder-link*. The NTN-Gateway could be located in a different geographical area, thus leading to a time-shifted contact over a feeder-link with the serving satellite.

In this work, the network architecture design is driven by the requirement of decoupling service-link and feeder-link. Therefore, since the feeder-link availability is not always guaranteed, data transmissions through the service-link can be still implemented asynchronously with respect to the data offload to the NTN-Gateway. To this end, the conceived solution assumes to install the full Evolved Packet System (EPS) protocol stack on-board the satellite. The overall service can be implemented through a satellite constellation without ISL. Indeed, possible configurations that exploit ISL and multiple gateways are not considered and the resulting solution ensures a significant reduction of both complexity and costs. Such an important technical choice has been initially considered by the Cellular Internet of Things (C-IoT) architecture [158]. But, at the time of this writing and to the best of the authors' knowledge, it has never been investigated from the system-level perspective, representing an attractive solution for international companies, like ESA, working on satellite systems.

Fig. 2.1 depicts the proposed network architecture and the resulting protocol stack. The satellite hosts different logical nodes, including eNB, Cellular IoT – Serving Gateway Node (C-SGN), and Local Break-Out (LBO). The eNB, that is the base station, implements the Uu interface offering the radio connectivity with NTN terminals. C-SGN implements the functionalities of the rest of the EPC protocol stack. For this reason, it includes:

- the Mobility Management Entity (MME) handles Control Plane communications by means of NAS signalling supported by Radio Resource Control (RRC) protocol;
- the Serving Gateway (SGW) and the Packet Gateway (PGW) handle User Plane communications supported by IP at a higher layer;
- the Home Subscriber Server (HSS) is in charge of the NTN terminal network registration and authentication.

To support the asynchronous data delivery, messages delivered by NTN terminals through service-link are temporarily stored on-board the satellite, by leveraging a local application implemented through the LBO. Collected data can be offloaded to a remote NTN-Gateway (on the ground) as soon as it will be in the line of sight with the satellite. To embrace multiple possibilities at the same time, the feeder-link can be implemented by using non-3GPP technologies, offering data rates comparable or higher than those registered in the uplink direction.

Starting from the afore described high-level protocol architecture, some specific adaptations must be integrated into different levels of the communication stack for properly counteracting the issues introduced by the satellite communication link.

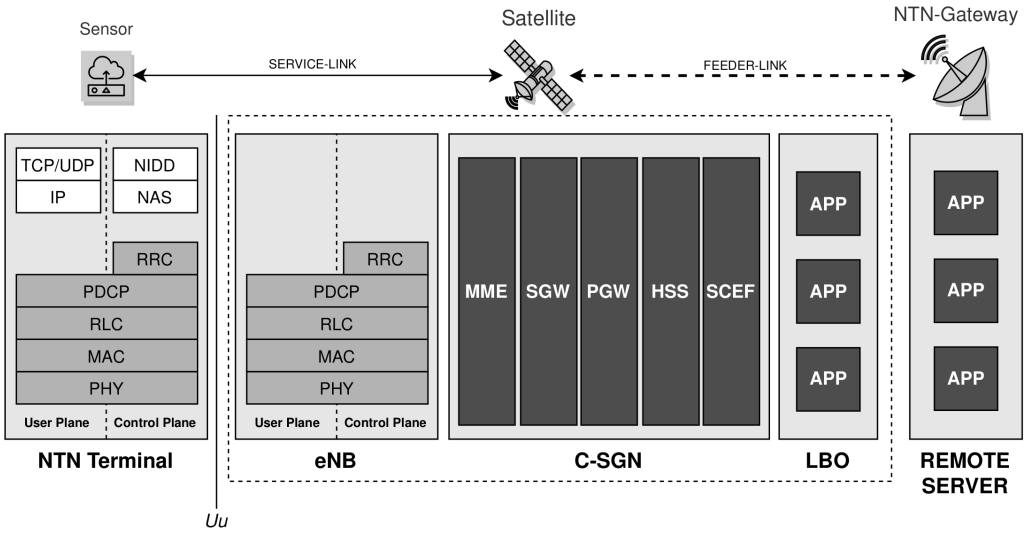

FIGURE 2.1: The proposed network architecture and the protocol stack of the NTN terminal and satellite.

2.3.1 Selected adaptations for the Uu interface

Regarding the Uu interface, adaptations are required for both Control Plane and User Plane [159]. A new method for uplink transmission, called Non-IP Data Delivery (NIDD), is available and allows to encapsulate user data in NAS messages of the Control Plane, involving both MME and Service Capability Exposure Function (SCEF) components, as an alternative to IP-based data transport. NIDD introduces an overhead of 6 bytes due to the header size of the NAS message. Furthermore, new RRC procedures available since Release-15 allow suspending and (then) quickly resume the RRC connection, which is very useful considering the limited visibility intervals.

As specified in Section 2.2, the total size of each message coming from a sensor node is equal to 18 bytes. At the application layer, the Constrained Application Protocol (CoAP) protocol is chosen [160], introducing an associated 4 bytes of overhead. It is a web-based protocol that relies upon the request-response (or client-server) paradigm and asynchronous data exchange. These two features are both suitable for the considered scenario, where sensors exchange data on-demand and with a low frequency. NIDD is selected at the transport layer as an alternative to the canonical UDP/IP solution. In fact, CoAP is compatible with NIDD, leading to an overhead reduction from 28 bytes of the UDP/IP solution to 6 bytes, as described above.

At lower layers, Packet Data Convergence Protocol (PDCP), Radio Link Control (RLC) and Media Access Control (MAC) protocols have been properly configured to meet NTN NB-IoT constraints and associated requirements. To this end, data retransmissions have been demanded to the MAC layer only, i.e., enabling the Hybrid Automatic Repeat Request (HARQ) process, disabling retransmission and feedback-based procedures at PDCP and RLC layers. Furthermore, Protocol Data Unit (PDU) segmentation at the RLC layer has been disabled. This in turn translates into the possibility to use PDUs with an extremely simplified header for all the three layers [161]–[163], adding a minimum of 4 bytes of overhead.

In conclusion, with the proposed configuration, account is taken for 18 bytes for data, 4 bytes for application, 6 bytes for NIDD and a total of 4 bytes for all lower layers (i.e., PDCP, RLC and MAC). Consequently, the smallest transport block that fits one of the possible options for the Transport Block Size (TBS), enabling the opportunity to exploit the Early Data Transmission (EDT) protocol in the proposed solution, is equal to 41 bytes (328 bits),

as specified in [164].

2.3.2 Selected adaptations for the Random Access procedure

The Random Access procedure is exploited by NTN terminals to acquire the uplink resources needed for data transmission.

First of all, the network needs to know which Random Access Opportunity (RAO) a preamble belongs to, in order to determine the correct Timing Advance (TA) for the synchronization of the uplink transmission.

If the periodicity of the RAO is not large enough, the preamble receiving windows of two consecutive RAOs could overlap each other, creating ambiguity on the RAO a preamble belongs to. An excellent solution to avoid this issue, investigated in [28], is to extend the interval between two RAOs to an amount greater than two times the maximum delay difference experienced by two NTN terminals within the same cell.

Enhancements to the Timing Advance are required as well. The TA command exceeds the maximum value allowed by the standard, which covers a distance of at most 100 km between the NTN terminal and the satellite [27]. To cope with this issue, the most promising solutions consider an autonomous TA calculation by the NTN terminal. It exploits the Global Navigation Satellite System (GNSS) to derive its position and the satellite ephemeris provided by the network to estimate the propagation delay through geometric formulas [165]. An alternative solution to GNSS is to broadcast a common TA offset related to a reference point located at the center of the beam (Nadir). The differential part of the TA, evaluated for the NTN terminal with respect to the reference point, can be compensated by the TA command without introducing any modification to the standard since it falls in the 100 km range also in the worst case of an NTN terminal at the cell edge.

Even if the majority of these solutions must be better investigated through experimental testbeds, these adaptations have been selected as the most appropriate choices for the scenario under analysis.

2.3.3 Selected adaptations for Doppler Shift and Carrier Frequency Offset

In satellite communication, two undesirable effects emerge in the frequency domain: the Doppler shift and the Carrier Frequency Offset (CFO). The former is caused by the relative movement between the NTN terminal and the satellite. Since in the selected scenario the NTN terminals are fixed on the ground, it is exclusively due to the satellite movement. The latter, instead, describes the frequency shift given by the inaccuracy of the receiver local oscillators. These two effects produce a frequency shift that causes interference in adjacent subcarriers in the uplink, thus posing a relevant issue for signal reception.

According to [2], a maximum Doppler shift of 950 Hz can be tolerated by the LTE physical layer. Nevertheless, by following the model presented in [146] and the indications provided in [28], the scenario considered in this work will experience a Doppler shift from -30 kHz to 30 kHz. Because these values are much more above the tolerated limit of 950 Hz, additional methodologies must be integrated into the adapted Uu interface to achieve Doppler compensation. Also for the CFO, it is necessary to introduce compensation techniques. Following 3GPP specifications, in fact, where an NTN terminal crystal accuracy can be 10 ppm, a CFO of about 20 kHz is derived at the carrier frequency chosen in the reference scenario [28].

The Uu interface conceived in this work may integrate two suitable solutions for the Doppler shift compensation. The first is based on the standard recommendations and makes use of GNSS capable devices with the knowledge of the satellite ephemeris so that the position of the satellite and the relative distance from it can be estimated autonomously by NTN terminals.

The second solution refers to not GNSS-enabled devices. It starts from the study carried out in [25], which aims to jointly compensate the Doppler shift and the CFO. If compared to the Doppler shift, the CFO has a constant value during the whole satellite visibility. Given the absence of any positioning information, an estimator can be used, based on the prior knowledge of the expected Doppler Shift, which is always contained within the maximum deviation range computed for the selected scenario. To perform a correct initial Doppler shift estimation and compensation, the filter bandwidth is widened by a frequency range that includes the maximum Doppler shift and the CFO, so that it can always contain the modulated signal affected by the total frequency shift. Then the Doppler shift estimation is updated periodically through a first-order differential system. It is able to track and compensate the Doppler variations in time, with a periodicity that allows the inclusion of shift variation into the 950 Hz value. Accordingly, an 80 ms periodicity is sufficient to satisfy the Doppler compensation rate during all the satellite visibility periods.

2.4 Link-level analysis and satellite constellation

The design of an effective communication architecture that leverages the NB-IoT technology over a satellite-link grounds its roots on a deep investigation of link-level features.

2.4.1 Antenna Selection

Regarding the NTN terminal, the antenna must be easily deployable, at a low cost. For this reason, the solution considered in this work adopts a monopole antenna with linear polarization, installed horizontally-oriented. Such an antenna type is already available as a Commercial-Off-The-Shelf (COTS) product [166].

Regarding the satellite, it is important to keep the best trade-off between the amount of power radiated by the antenna and the High Power Amplifier (HPA), which is responsible to generate such power. Small satellites cannot host a large HPA. But, to counteract the reduced power resource offered by a small HPA, it is possible to increase the radiated power by working on the antenna gain. However, it is not possible to overstate in this direction because a high antenna gain translates to an increased volume, mass, and deployment complexity. Based on these aspects, this work considers a tile circular patch antenna for the satellite, whose deployment must be managed by taking into account the possible dynamical steady states of the satellite orbit. Moreover, the signal generated by a monopole antenna, with linear polarization, experiences a polarization rotation when propagating through the Earth's ionosphere (because of the impact of the Earth's magnetic field). Consequently, the satellite may receive a signal with a polarization different from the one expected by its receiving antenna. This generally worsens communication performance. An antenna with circular polarization at the satellite side, however, partially mitigates this effect. In this context, the worst case of misalignment between circular and linear polarization, equal to 45°, produces a penalty of 3 dB. Note that the tile circular patch antenna offers good performance regarding the coverage of the satellite beam. The Half Power Beam Width (HPBW) factor represents the angle in which the relative power is higher than the 50% of the peak power of the main lobe reported in the effective radiated field of the antenna. The main lobe of the selected antenna ensures $\pm$ 56° HPBW, thus resulting in a very suitable choice for the scenario under study.

In both cases, the selected antennas offer a not negligible gain, equal to 5.19 dB for the one installed on the NTN terminal and 6.97 dB for the antenna patch hosted by the satellite. Please note that these values have been calculated by considering the analytical formulation presented in [166] and by leveraging (for the satellite only) a linear approximation in the frequency range spanning from 1900 MHz to 2200 MHz.

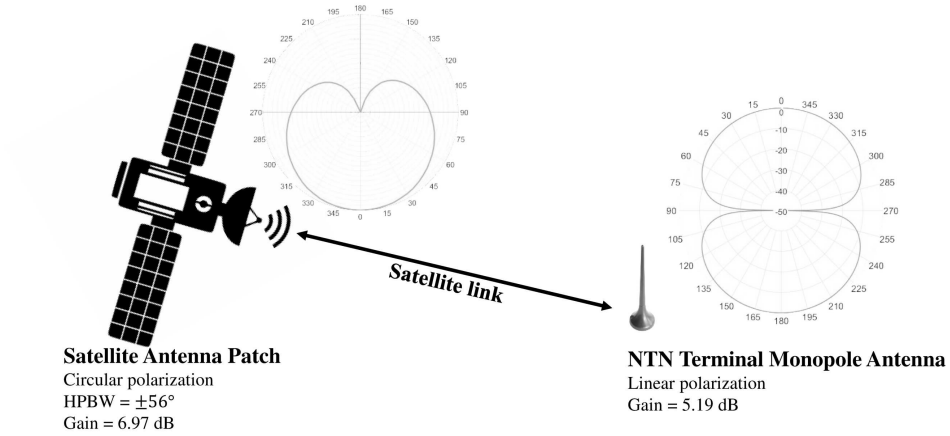

FIGURE 2.2: Proposed antennas types and related radiation diagrams.

To conclude, Fig. 2.2 shows additional details on the selected antenna types, also reporting the related radiation diagrams.

2.4.2 Link Budget Analysis

Given the power gain offered by the selected antennas, the transmission power imposed by the NB-IoT technology, and the propagation losses, the link budget analysis allows obtaining the satellite antenna altitude and the range of elevation angles at which the radio link could be established. The link budget evaluation is based on the analysis carried out in [167] for satellite communications systems. The design of the satellite system is based on theoretical formulas that accurately model real phenomena that impair the signal propagation in both uplink and downlink directions. Therefore, according to the analytical description of the satellite link carried out in [167], the link budget is expressed in dB as a function of both frequency carrier f_c and elevation angle θ_{el}:

$$LB(\theta_{el}, f_c) = P + G_{ANT}(f_c) - FSPL(\theta_{el}, f_c) - L_{imp}(\theta_{el}, f_c) + DCF(\theta_{el}, f_c), \quad (2.1)$$

where P represents the signal power, G_{ANT} is the sum of the base station and NTN terminal antenna gains (reported in Section 2.4.1), $FSPL$ describes the free space path loss, L_{imp} provides additional losses due to the propagation, and DCF is the sum, expressed in dB, of the diagram correction factors of transmitting and receiving antennas. Note that Eq. (2.1) does not consider multi-path fading models because the paths due to obstacles on Earth are negligible if compared to the one reaching the satellite. The amount of impairments L_{imp}, instead, is calculated by considering the air attenuation that takes into account the dry air absorption [168], the rainfall attenuation that estimates the droplet absorption, as described in [169], [170], the scintillation attenuation that takes into account the fluctuations of the amplitude and the phase of a radio wave [166], the polarization attenuation that considers the difference between the polarization of both receiving antenna and incoming radio wave [167], and the fog and atmospheric gas absorption [171], [172]. The models used to evaluate the attenuation due to air, rainfall, scintillation and atmospheric gas absorption are predictive models, based on estimates defined analytically in the most recent updates of the ITU-R recommendations cited above.

Fig. 2.3 reports the link budget evaluated as a function of the elevation angle and the satellite altitude. Without loss of generality, it is considered an NTN terminal deployed in the European field of view.

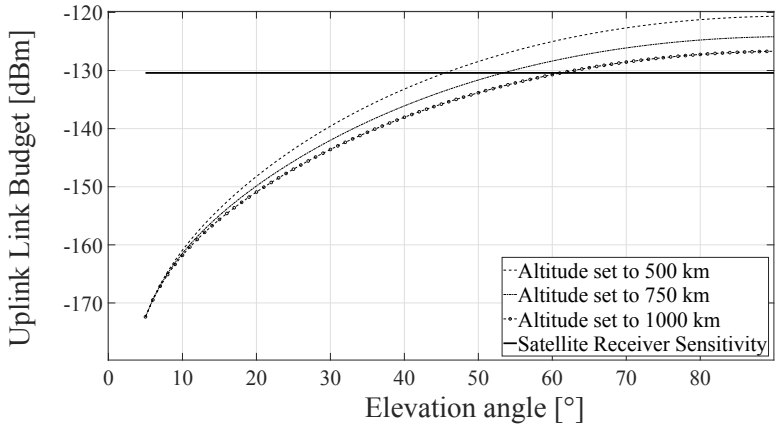

(A) Uplink

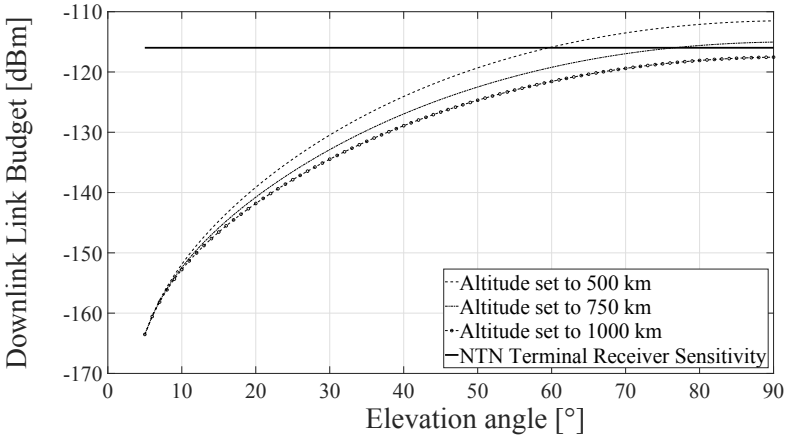

(B) Downlink

FIGURE 2.3: Link Budget in the function of Elevation Angle for different orbital altitudes.

In line with NB-IoT specifications [90], the carrier frequency and the transmission power have been set to f_c=1995 MHz and P=23 dBm, respectively, for the uplink. In the downlink, instead, they have been set to f_c=2185 MHz and P=33 dBm, respectively. Overall, the link budget strongly depends on the user-satellite elevation angle: it increases when the elevation angle progressively approaches 90°. At the same time, the link quality decreases with the satellite altitude. In both uplink and downlink, the receiver antenna captures the attenuated signal and the noise power. Therefore, it is important to understand in which conditions the power of the received signal is higher than the receiver sensitivity. Now, according to [167], the receiver sensitivity represents the noise power of the link expressed by the Nyquist formula reported in Eq. (2.2):

$$RS|_{dBm} = 30 + 10log_{10}(k_B T_{sys} BW), \tag{2.2}$$

where k_B is Boltzmann constant, T_{sys} is the equivalent system noise temperature accounting for both antenna and receiver noise, and BW is the NB-IoT subcarrier bandwidth. According to [173], $T_{sys} = 150$ °K for the uplink and $T_{sys} = 290$ °K for the downlink. On the other hand, instead, BW depends on the chosen transmission configuration.

To conclude, Fig. 2.3 also reports the calculated receiver sensitivity. Obtained results invite to select the lowest satellite altitude (i.e., 500 km) to reach a suitable link budget for

smaller elevation angles. An altitude of 500 km provides the best trade-off between elevation angle (which determines coverage area) and connectivity (expressed in terms of power level perceived by the receiver).

Given the link budget and the receiver sensitivity, it is possible to calculate the expected value of SNR:

$$SNR = LB(\theta_{el}, f_c) - RS. \tag{2.3}$$

Fig. 2.4 depicts the SNR curves as a function of the elevation angle for different transmission modes in the uplink. NB-IoT technology allows using subcarriers individually in order to ensure a greater concentration of power on a narrower band. This results in increasing the coverage range and power gain. The marked improvement in the single-tone configuration (almost 10.8 dB if compared to multi-tone) makes this solution more attractive for the conceived architecture. As shown in Fig. 2.4, the single-tone configuration achieves good SNR values for lower elevation angles with respect to multi-tone. As explained in Section 2.1.1, even if the adoption of a single-tone configuration with a subcarrier of 3.75 kHz would further increase the SNR, this comes at a cost of a longer subframe duration. Therefore, the intermediate configuration (single-tone with a subcarrier of 15 kHz bandwidth) is selected as the best trade-off between SNR performance and time resources employment. In fact, it guarantees higher SNR with the same elevation angle if compared to multi-tone configuration.

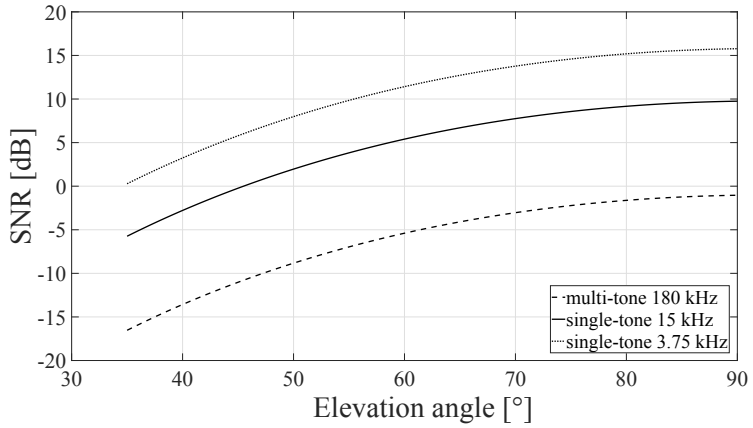

FIGURE 2.4: SNR in different transmission mode configurations for the uplink.

In line with these considerations, BW is set to 15 kHz for the uplink and 180 kHz for the downlink. The receiver sensitivity differs for uplink and downlink configurations. In fact, considering a subcarrier bandwidth of 15 kHz, the uplink communication experiences a lower receiver sensitivity compared to the downlink one, calculated for a subcarrier bandwidth of 180 kHz, resulting in -130 dBm and -117 dBm, respectively.

Note that the intersections between the link budget curves and the receiver sensitivity, shown in Fig. 2.3, identifies the elevation angle after which the SNR is greater than zero. Nevertheless, the radio link could be established even at negative SNRs under certain configurations, resulting in lower elevation angles. The practical feasibility of the connection is determined by the investigation of the communication success probability defined by the study of the BLock Error Ratio (BLER) curves, as reported in Section 2.5.2.

2.4.3 Satellite Constellation

The employment of a single satellite per orbit for the chosen 500 km altitude results in very short periods of visibility. On the contrary, considering a constellation of multiple satellites, NTN terminals may have more occasions to transmit their data, thus reducing the periods during which they remain without satellite coverage. This would also lower the amount of data stored and forwarded by each NTN terminal while simplifying the satellite hardware and reducing the NTN terminals energy consumption (which is an important requirement for the IoT technology).

The satellite platform of interest for this study must adopt cheaper solutions, able to satisfy the cost optimization requirement. From this point of view, this work assumes to adopt either small or nano-satellites, providing an effective and low-cost solution with several simplifications in the system design and deployment. Taking this aspect into account, the choice fell on a 12U CubeSat in a 2x2x3 configuration [174]. This platform is composed of several units that can be assembled in a fully scalable and flexible fashion to reach the needed performance.

A LEO Cubesat operating at the altitude of 500 km (corresponding to an orbital radius equal to 6878.14 km) presents a flying speed needed to maintain the satellite in orbit equal to 7612.6 m/s.

Accordingly, the orbital period is equal to 1 hour and 34 minutes. The number of satellites per orbit must be properly selected to jointly achieve cost and service requirements. A lower number of satellites is surely preferable from the cost perspective. At the same time, however, it is also necessary to consider the low variability of the frequency of sensed data transmission, as well as the battery life of NTN terminals. Thus, to achieve a suitable trade-off between the two aforementioned constraints, the proposed architecture integrates 2 or 3 satellites per orbit. In the first case, an NTN terminal can see a satellite every 47 minutes and 18 seconds, even if the 500 km orbital period for a single satellite is of 1 hour and 34 minutes. In the latter case, instead, an NTN terminal can see a satellite every 31 minutes and 32 seconds.

The well-known System Tool Kit [175] is used to evaluate the satellite spot-beam diameter. Specifically, according to the goal to cover about 6700 km of longitude corresponding to the European field, the performed investigation highlighted that about 8 circular orbits (i.e., with a 0° eccentricity) and sun-synchronous (i.e., with a 97°/98° orbital inclination) are required to ensure the continuous service requirement. In this way, the whole satellite constellation should involve 24 satellites.

Fig. 2.5 reports the covered geographical area and shows a snapshot of beam coverage and satellite orbits. It is important to note that the areas covered by the satellite beams that belong to adjacent orbits present an overlap. Nevertheless, in order to avoid interference among satellite transmissions on NTN terminals, the solution proposed herein assumes that satellites of different orbits are spatially shifted (as depicted in Fig. 2.5).

2.5 System-level performance of NB-IoT over satellite

The isolated knowledge of the link budget is not sufficient to evaluate the feasibility of the resulting satellite architecture. For this reason, this Section proves the effectiveness of the proposed architecture through system-level simulations. In particular, the presented analysis evaluates how physical and system configurations influence (1) the ability of the overall communication architecture to disseminate data through the service-link and (2) the resulting communication latencies.

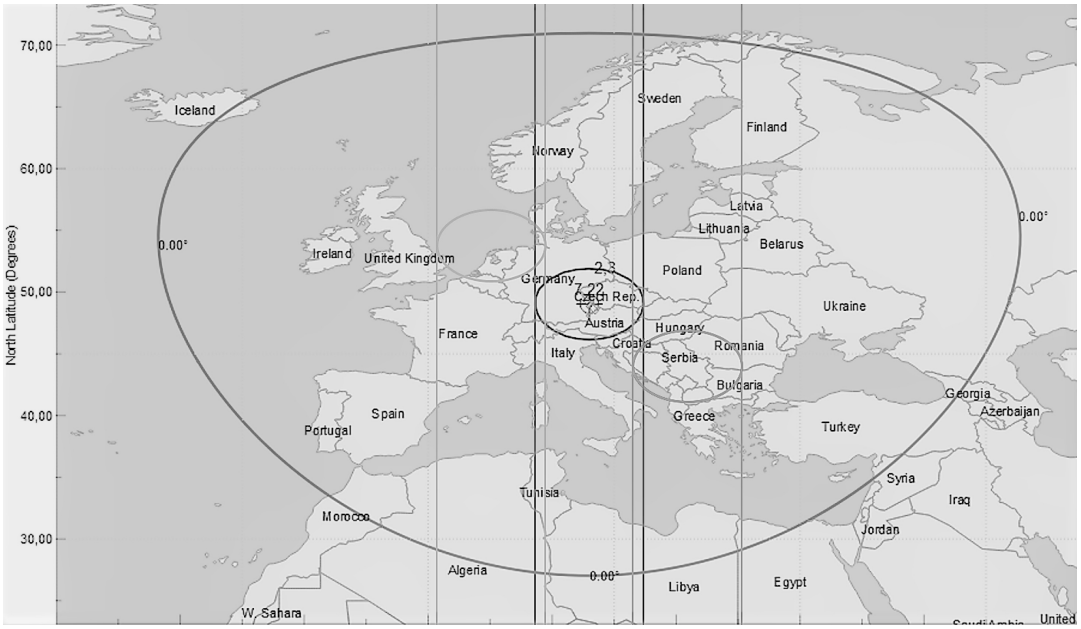

FIGURE 2.5: European field of view and satellite beam coverage.

2.5.1 System-level tool and parameter settings

System-level simulations are conducted through the 5G-air-simulator [176] [177]. It represents a well-known system-level simulator, supporting NB-IoT. Among the implemented functionalities, it is important to remark that the model for the Random Access procedure available in 5G-air-simulator has been already validated from an analytical point of view in [178]. This ensures the trustworthiness of the results discussed below. Furthermore, the tool has been properly enhanced to embrace the implementation of the conceived NTN scenario [179].

Regarding the physical layer, the transmitted power and the configurated bandwidth used in this study have been already declared in Section 2.4. Other parameters to be configured include: Modulation and Coding Scheme (MCS), TBS, and Number of Resource Unit (NRU). The MCS is set to QPSK, since it guarantees a higher spectral efficiency with respect to BPSK. The TBS represents the amount of data passed through the physical layer which will be mapped into the NPUSCH channel. Its value is set to 328 bits, according to the configuration of the protocol stack discussed in Section 2.3.1. Given the TBS, a data packet can be transmitted by using different NRUs. In line with [180], NRU can be set to 2, 3, 4, 5, or 6. On the one hand, higher values of NRU correspond to a higher data protection level at the physical layer. From another hand, instead, the higher the NRU, the longer-lasting the physical transmission of a data packet. According to the high distances of the considered satellite scenario and the resulting latencies, the upper bound of the number of HARQ retransmissions has been set to 4.

Regarding the Random Access procedure, the number of the available preambles is set to 48, the periodicity of the RAO is set to 80 ms, and the backoff window is set to 65536 ms.

To evaluate the impact of the traffic load, a different number of clusters of NTN terminals are considered. As already anticipated in Section 2.2, each cluster contains 3000 NTN terminals deployed in a single crop field with an area of 30 hectares. Each NTN terminal generates data every 4 hours. Moreover, every 4 hours, all the available NTN terminals generate their data within a time slot of 1 minute. In this way, it is possible to investigate how the designed approach reacts in critical bursty traffic conditions.

The satellite allocates radio resources to NTN terminals that won the access procedure according to the round-robin scheduler.

Finally, computer simulations are conducted to observe 48 hours of network activity. Such an amount of time embraces a large number of satellite visibility cycles and allows obtaining stable average results.

2.5.2 Link-to-system model

A link-to-system model represents the first step towards an accurate system-level study. In fact, it is able to describe the quality of the communication achieved under specific parameter settings, while ensuring an abstraction of transmission, propagation, and reception aspects. In this context, the 5G-air-simulator tool has been extended to implement the propagation model, link budget, and SNR model, as discussed in Section 2.4. Then, BLER curves have been integrated as well, in order to simulate the quality of the communication link as a function of the measured SNR. To this end, MATLAB LTE Toolbox has used to generate BLER curves. Given the setting of physical parameters, the BLER has been computed as the ratio between the total number of received blocks for which the control of the Cyclic Redundancy Check (CRC) fails and the total number of transmitted blocks. Furthermore, to achieve a fine-grained BLER evaluation, SNRs values have been chosen in the range spanning from -10 dB to 10 dB. The total number of transmitted blocks has been set to 1000.

Fig. 2.6 shows the obtained BLER curves as a function of NRU and SNR. Results highlight that higher NRU values provide a better protection of data transmitted at the physical layer. At the same time, higher SNRs values are associated with better link conditions. Thus, bases on these premises, it is possible to conclude that the BLER reduces with both NRU and SNR.

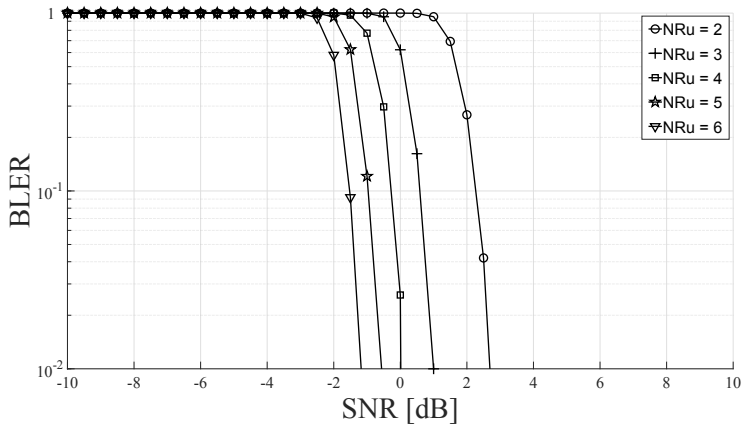

FIGURE 2.6: BLER curves

2.5.3 Satellite attach procedure and visibility time

Each NTN terminal starts the attachment procedure when the receiver power of the reference signal transmitted by the satellite experiences a coupling loss lower than the Maximum Coupling Loss (MCL) threshold, set to 154 dB. Based on the selected parameter settings and the aforementioned MCL threshold, the average SNR value (measured in the downlink direction) is equal to -4.9 dB. Moreover, according to the study reported in Section 2.4.2, this SNR value is obtained for elevation angles equal to 46.3° for the downlink. Such a condition determines the beginning of the visibility time.

Now, considering the satellite altitude of 500 km, a trigonometrical analysis allows calculating the diameter of the effective satellite footprint. Considering the slant range (that is the distance from the NTN terminal and the satellite, calculated as a function of the conceived elevation angle), the diameter of the effective footprint approximately results in 890 km. Indeed, by exploiting the relative speed (i.e., with respect to the Earth) of the LEO satellite equal to 7059 m/s and the aforementioned effective footprint, definitively it is possible to determine the visibility time, approximately equal to 125 s.

2.5.4 Communication latencies over the service-link

The communication latency represents the amount of time required by a packet to be successfully received by one of the satellites of the constellation, with respect to its generation time instant. Fig. 2.7 and Fig. 2.8 show the communication latency measured when the EDT transmission scheme is disabled and enabled, respectively. Reported curves describe the impact of different physical configurations and different network loads. In this case, each orbit hosts 3 satellites.

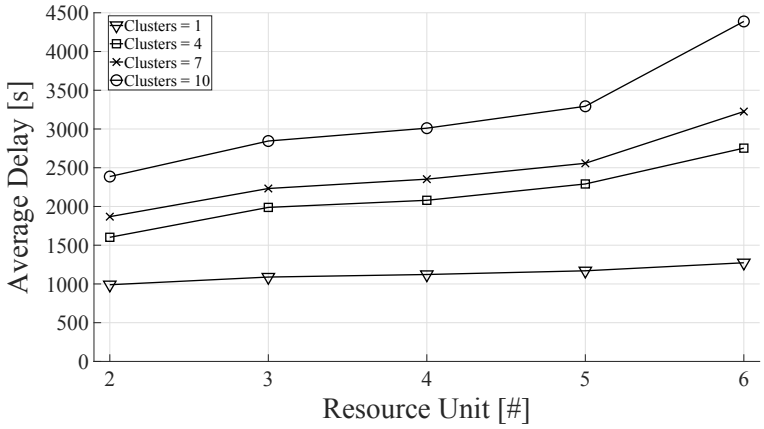

FIGURE 2.7: Average end-to-end delay with EDT disabled.

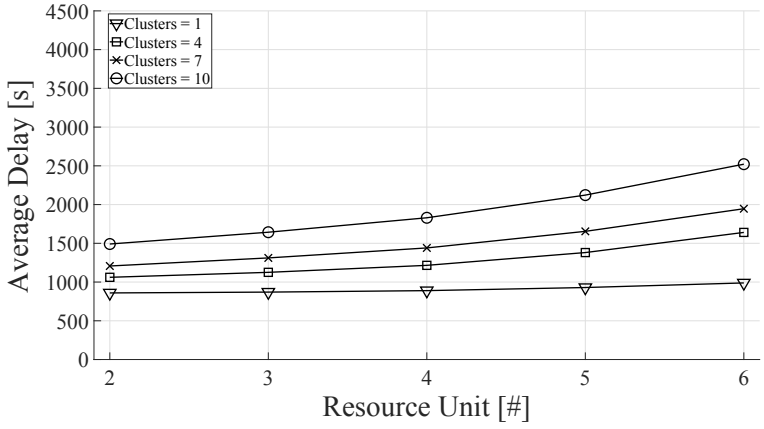

FIGURE 2.8: Average end-to-end delay with EDT enabled.

First of all, the communication latency depends on the probability to win a Random Access procedure. As expected, a higher number of clusters determines the growth of NTN

terminals aiming to access the network and, in turn, the collision probability during the Random Access procedure. This justifies the increment of the communication latency with the number of clusters served by the configured satellite architecture.

Furthermore, also the NRU assigned to each NTN terminal strictly affects the average end-to-end delay. Although a transport block distributed into many RUs guarantees high protection, it results in a longer transmission time, impacting considerably on end-to-end delay.

On the contrary, the EDT scheme ensures the reduction of the communication latency up to 40%, thanks to its ability to delivery of the data packet along with the Msg3 of the Random Access procedure.

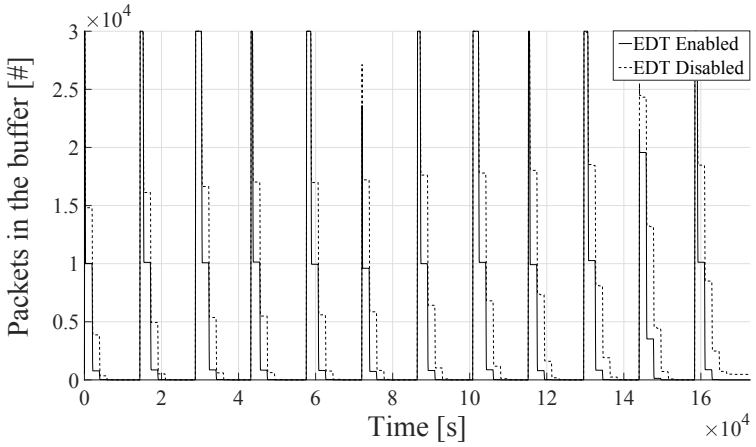

FIGURE 2.9: Number of packets in the buffer with 10 clusters.

TABLE 2.2: Average communication latency measured under different constellation designs.

RACH Configuration	Satellites per orbit	Average end-to-end delay [s]			
		$n_C = 1$	$n_C = 4$	$n_C = 7$	$n_C = 10$
EDT disabled	3	969	1602	1869	2386
	2	1816	2739	3124	3895
EDT enabled	3	859	1061	1207	1491
	2	1646	1909	2128	2546

2.5.5 Ability of the system to drain buffered data through the service-link

The analysis of the aggregate number of packets stored in all the NTN terminals allows verifying whether the designed satellite architecture is able to successfully support the offered service. If this value quickly grows, it means that the network cannot satisfy all the requests made by the NTN terminals. Consequently, the generated messages will overload the network. On the contrary, if packets in the buffer do not accumulate very fast, the network can absorb the traffic generated by the NTN terminals.

Fig 2.9 demonstrates the effective ability of the designed approach to drain buffered data through the service-link, considering a constellation of 24 satellites (i.e., 3 satellites per orbit). Without loss of generality, results only refer to the highest loaded scenario (10 clusters of NTN terminals, i.e., 30000 nodes), where NRU is set to 2. Reported curves highlight that NTN terminals need more than one visibility time to transmit their data. The dissemination of the whole packet burst generated by the NTN terminals is faster when EDT is enabled.

2.5.6 Impact of the number of satellites per orbit

To provide further insight, Tab. 2.2 reports the average communication latency measured when a different number of satellites per orbit is taken into account. As for the previous analysis, the study is conducted by considering NRU equal to 2. As expected, communication latency increases with the number of clusters (n_C). Moreover, EDT always ensures better results. Nevertheless, a constellation with 2 satellites per orbit is still able to drain all the generated data but at the cost of higher communication latency.

Chapter 3

An Open-Source tool for Evaluating System-Level Performance of NB-IoT Non-Terrestrial Networks

SatCom is expected to play a leading role in 5G&B networks. Thanks to its ubiquity capabilities, in fact, it promises to enable Machine-Type Communication services also in large areas not covered by terrestrial networks (i.e., oceans, forests, and deserts). In this context, worldwide research is investigating the possibility to use NB-IoT as a key enabling communication technology for upcoming Non-Terrestrial Networks. Current studies, however, focus the attention on physical and link-level aspects, while ignoring to evaluate system-level performance. To make matter worse, no system-level simulators are currently available to support and boost research activities in this direction. To bridge this gap, the contribution of this work is twofold. First, it presents a novel simulation tool, conceived as a new module for the open-source 5G-air-simulator, modeling NB-IoT satellite-based communication systems. Specifically, it implements several link-to-system abstraction models (embracing transmission, propagation, and reception mechanisms), the cell selection procedure, and a configurable satellite constellation. Furthermore, these essential features are successfully integrated within the rest of the 5G-air-simulator, thus offering the opportunity to test flexible network deployments (e.g., by varying the number and the distribution of users) under different application statistics. Second, to demonstrate the actual effectiveness of the developed tool, this work also presents a preliminary performance assessment of a NB-IoT satellite-based communication system enabling reference monitoring scenarios. The conducted system-level study highlights how network and satellite configurations significantly impact system performance in terms of communication latency and service reliability.

3.1 An Overview on Satellite Nb-IoT

3.1.1 State of the Art on Non Terrestrial Networks and NB-IoT

The role of satellite technologies to extend the terrestrial network is of fundamental importance for LP-WAN services. Indeed, satellite IoT systems are able to provide efficient solutions in remote areas where terrestrial technologies fail or do not exist. The uniqueness of the NTNs in this aspect allows to guarantee service continuity of the Machine-to-Machine (M2M) and IoT devices even in critical situations or for emergency services, in particular in the maritime and aeronautical fields, promising countless advantages thanks to an enormously more extensive coverage and improvement in terms of scalability and availability [3]. In [181] important issues on the satellite technology are discussed, such as interoperability of heterogeneous networks and QoS management. In addition, it is explained that there is no real awareness of the potential advantages deriving from the use of satellites in such communication scenarios, inviting to continue research in this direction.

The fact that the integration of terrestrial and non-terrestrial networks is a key aspect of new communication technologies is highlighted in [182]. Therein, LoRA, SigFox, and 5G alternatives such as NB-IoT, are considered and evaluated for this purpose. Despite the generalized use of IoT, satellite systems typically target a few special use-cases and different architectures and technologies for distinct use-cases and requirements are proposed and evaluated. The paper [32] studies the integration of satellite communication into 5G networks, also using NB-IoT technology. Specifically, it shows that 5G devices can communicate at low bit rates through satellites, alongside the terrestrial infrastructure. Moreover, it provides the study on the sizing of the system and the modeling of the channel, thanks to calculations on link budget by analyzing the performance required by the communication. The work in [33] focuses on extending NB-IoT and LTE-M technology for NTN, complementing the existing terrestrial deployment. The authors describe how the design of the terrestrial architecture must be modified to support satellite communication, while identifying adaptations at the physical level and proposing signaling schemes to support the new features. The importance of extending NB-IoT coverage and services to a scenario using LEO satellite is highlighted in [34]. Here, new coding and modulation schemes are proposed to improve the performance of LEO satellite networks. A LEO satellite constellation is studied in [19] to provide NB-IoT radio service. This technology holds promise for encouraging applications such as sensor reporting around the globe. Authors of [25] present an NB-IoT architectural solution based on a LEO satellite to discuss the impact of the large Doppler shift. Also papers [24], [35] propose an NB-IoT satellite architecture on LEO, analyzing the advantages of communication carried out with this system. Specifically, these works propose an uplink scheduling technique able to mitigate the differential Doppler shift up to a value tolerable by the standard. The work in [26] considers an NB-IoT over satellite system, identifying various deployment options based on satellite orbit, payload and cell type. A customized configuration for NPRACH is also proposed, to reduce the negative impact of typical satellite channel impairments on the NB-IoT Random Access procedure. The work [22] studies the design of an NB-IoT system using a constellation of LEO satellites and proposes an algorithm to analyze the best configuration to reduce the impact of the satellite channel, from a link-level point of view. In [36] the Bit Error Ratio (BER) is evaluated to determine the number of collisions and their impact on a satellite NB-IoT system, to accommodate the maximum number of devices in the proposed communication scenario.

The majority of the aforementioned papers employ link-level simulators and focus the attention on a single communication link. At the same time, recent works suggest that there is a growing demand for flexible tools for designing and testing new algorithms and protocols for NB-IoT-based satellite scenarios. Nonetheless, at the time of this writing, and to the best of authors knowledge, there are no system-level simulators available to the research community that specifically address the considered scenario.

In this context, the open-source simulation framework 5G-air-simulator [176] appears as a solid instrument to carry out system-level analyses of a number of technical components already standardized by the 3GPP. Indeed, 5G-air-simulator already provides support for a variety of NB-IoT features. However, the available version of the simulator does not support the NB-IoT technology in a satellite scenario. For these reasons, the work presented herein proposes an open-source implementation of an NB-IoT satellite-based communication system, built upon the 5G-air-simulator tool. Moreover, it is important to emphasize that there exists some preliminary research work already using the baseline version of 5G-air-simulator [183], [184], confirming that the simulation tool has recently gained currency also in SatCom.

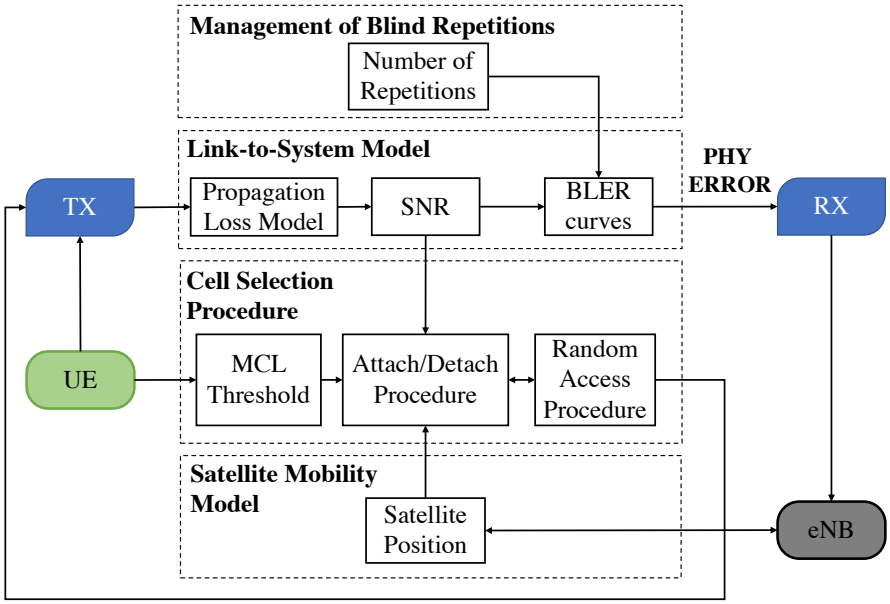

FIGURE 3.1: Overall vision of the interaction between the implemented simulator features.

3.2 The Proposed Simulation Module

The proposed module has been developed for the well known 5G-air-simulator tool, which already provides the support to baseline NB-IoT features [176]. Starting from the initial assumptions formulated for the reference network deployment, this Section describes the main features of the proposed tool, including Link-To-System (L2S) model, management of blind repetitions and their impact on BLER curves, cell selection, and mobility models for a constellation of satellites. From one hand, the proposed L2S model perfectly integrates channel and communication models widely accepted in the current state of the art. From another hand, the rest of implemented features offers the opportunity to test new (because beyond the current studies presented in the literature) SATCOM configurations, while satisfying the reference 3GPP specifications. Figure 3.1 shows a general overview of the implemented module and remarks the interaction between different building blocks, presented below.

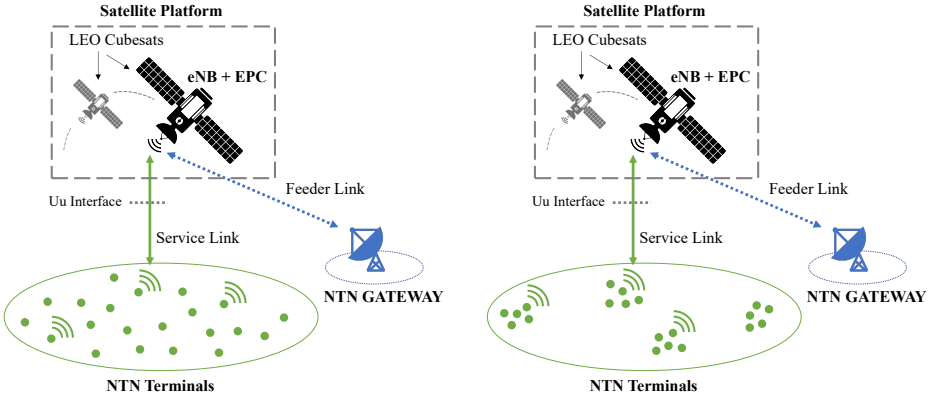

(A) Uniform Distribution (B) Cluster Distribution

FIGURE 3.2: The reference network architecture.

3.2.1 Initial assumption on the Architecture

Fig. 3.2 depicts the NB-IoT Satellite-Based architecture considered in this work. The figure points out two possible configurations regarding the distribution of the device on the ground. A configurable number of fixed NTN terminals may be positioned randomly on the simulated area, either following a uniform distribution or in many smaller clusters. This latter case allows to simulate different use cases where NTN terminals are tightly deployed only in specific areas.

Coverage and traffic profiles are other important aspects that have a major impact on the choice of an effective satellite network architecture. First of all, it is critical to allow NTN terminals to transmit data when needed, preventing the congestion of transmission buffers as much as possible. For this reason, a satellite should have a relatively low orbital time to avoid users remaining for too long without service. As expected, satellite communications present serious propagation impairments, due to the long distance. In line with 3GPP guidelines [28], this work assumes to use LEO satellites for guaranteeing feasible communication links with a satisfactory levels of SNRs.

However, a single LEO satellite may not be able to run across its entire orbit at the aforementioned rate. Therefore, it is necessary to consider several satellites per orbit, forming a constellation, to drastically reduce the time periods during which ground-based devices remain without satellite coverage [21]. In this context, the Cubesats [185] are a solution that provides low costs and several simplifications in the system deployments for the satellite constellation. These small satellites composing the Satellite Platform can be assembled in a fully scalable and flexible way in order to address the required performance, while keeping device costs low. In this regard, the tool allows the possibility to configure the number of Cubesats per orbit to ensure greater deployment flexibility.

Each NTN terminal is a 3GPP NB-IoT User Equipment (UE) able to use a direct satellite access, thanks to an adapted Uu interface. The NB-IoT technology is used to implement the service link, established between the NTN terminal and the remote satellite.

The feeder link is the radio link between the NTN Gateways and the Satellite Platform. It is preferable to have a limited number of gateways in order to dramatically reduce system costs, even though this leads to relatively longer periods of time of service unavailability, i.e., satellites can only offload their data when the feeder link is active. However, this is not a problem since the targeted scenarios generally consider delay-tolerant applications.

According to this architecture, we assume that every satellite of the LEO constellation implements a Base Station. As a consequence, NTN terminals are expected to perform again the network attach procedure each time they are covered by a different satellite.

It is important to stress that during the creation of the NTN terminals in the configured scenario only uplink channels are considered, i.e., the downlink transmission is not modeled. Moreover, only Single-Tone transmissions are taken into account, in order to both achieve better performance due to the increased robustness over the service link and further exploit NB-IoT capabilities to manage a multitude of users thanks to its wise bandwidth management.

3.2.2 Management of Blind Repetitions

The first extension introduced in the 5G-air-simulator is the handling of the blind repetitions. It provides the transmission in a bundle of the same Transport Block, replicated for a specified number of times. This key-feature enables the communication even at low SNR values. Indeed, it is crucial to maximizing both the visibility time and the total throughput.

The number of total blind repetitions can be set for the NPUSCH transmissions via the `FrameManager::SetNRep` method. Then, this value is retrieved when performing the scheduling procedure. Specifically, now the methods `RUsAllocation` of both the implemented

scheduler classes (i.e., FIFO and Round Robin) take into account this parameter while assigning RUs to users and finalizing the scheduling procedure. In this way, the reception event happens after the correct amount of time, which depends on the number of repetitions and the actual slot duration, as well as on the number of RUs allocated to the UE.

It is important to highlight that also the L2S model uses the adopted number of repetitions to estimate a suitable BLER, as explained in what follows.

3.2.3 Link-to-System Model

In the context of non-terrestrial NB-IoT networks, one of the most important factors which determine architectural decisions is represented by the satellite link performance, that allows supporting direct connectivity between NTN terminals and satellite. Therefore the L2S model is of fundamental relevance since it offers a simplified (but still accurate) abstraction of transmission, propagation, and reception functionalities. It associates a link-level analysis to the system-level simulation tool. Indeed, in a system-level simulator, it is reasonable to provide a simplified channel model. Otherwise, it would result in excessive complexity and execution time. This model contains the SNR expressions for both downlink and uplink channels, and the BLER curves for each transmission mode.

The 5G-air-simulator did not originally model the radio channel for NB-IoT. Thus, a new propagation loss model is developed to evaluate the signal received by the satellite, considering the non-idealities of the channel in the satellite scenario.

Specifically, the SNR is analytically modeled by taking into account the power gains and losses due to the propagation over the radio channel. Given the elevation angle of the service link, i.e., θ_{el}, and the carrier frequency, f_c, the SNR SNR quantifying the link performance, evaluated in dB, can be modeled as in Equation 2.1 [166]:

where P represents the signal transmission power and G_{ANT} represents the sum of the antenna gains of satellite and NTN terminal (in dBi). PL is the free space path loss that accounts for the radiowave attenuation due to propagation, and L_{imp} represents additional losses due to all the impairments considered, such as:

- the air attenuation, which accounts for the dry air absorption [168];
- the fog attenuation, which predicts the attenuation due to clouds and fog on Earth-space paths [171];
- the attenuation due to atmospheric gas absorption, which estimates of gaseous attenuation [167], [168];
- the attenuation due to droplets and rain fall, which estimates the slant-path rain attenuation as described in [169];
- the polarization attenuation that accounts for the difference between the polarization of the receiving antenna and the polarization of the incoming (incident) wave [166];
- the attenuation due to scintillation, which accounts for small time-scale fluctuations (on the order of fractions of a second) of the amplitude and the phase of a radiowave [167].

In addition, DCF is the sum, in dB, of the diagram correction factors of transmitting and receiving antennas. These factors take into account the mismatch between theoretical and real antenna radiation diagrams, as a function of the elevation angle and the carrier frequency.

Finally, the noise power N can be evaluated by taking into account the system noise power at the receiving antenna, which is a function of the equivalent noise temperature at the satellite and the noise figure of the amplifiers at the receiver front end (for a detailed computation of the system noise power please refer to [167]).

The `PropagationLossModel::AddLossModel` method is properly extended to obtain the power value of the received signal by using the model described above.

For this purpose, a new header file is defined containing the results of the link-level analysis, such as the received power from the satellite at NTN terminal side and the received power from the NTN terminal at satellite side at different elevation angles, as well as the BLER curves for each transmission mode.

The new method `BLERvsSINR_nb-iot_SAT::GetRxPowerfromElAngle_SAT` evaluates the received power at the satellite side for each value of the elevation angle experienced by the NTN terminal. As a consequence, during the reception, the satellite retrieves an SNR value related to the uplink configuration used for the transmission, which reflects the quality of the channel. In essence, this SNR value is exploited to estimate the BLER for the received block using new SNR-BLER curves, which determines the probability that it has been correctly received. Specifically, this operation is performed in the method `nb-iotSimpleErrorModel::CheckForPhysicalError`.

To this end, the BLER is estimated by considering the chosen MCS, the number of used RUs, the number of NPUSCH blind repetitions, and the SNR experienced at the satellite during the reception. The BLER value is drawn by `BLERvsSINR_nb-iot_SAT::GetBLER_SAT`, using SNR-BLER curves stored into the header file and generated using the MATLAB LTE Toolbox [186].

As a representative example, Figure 3.3 depicts the BLER curves for a fixed TBS and four blind repetitions.

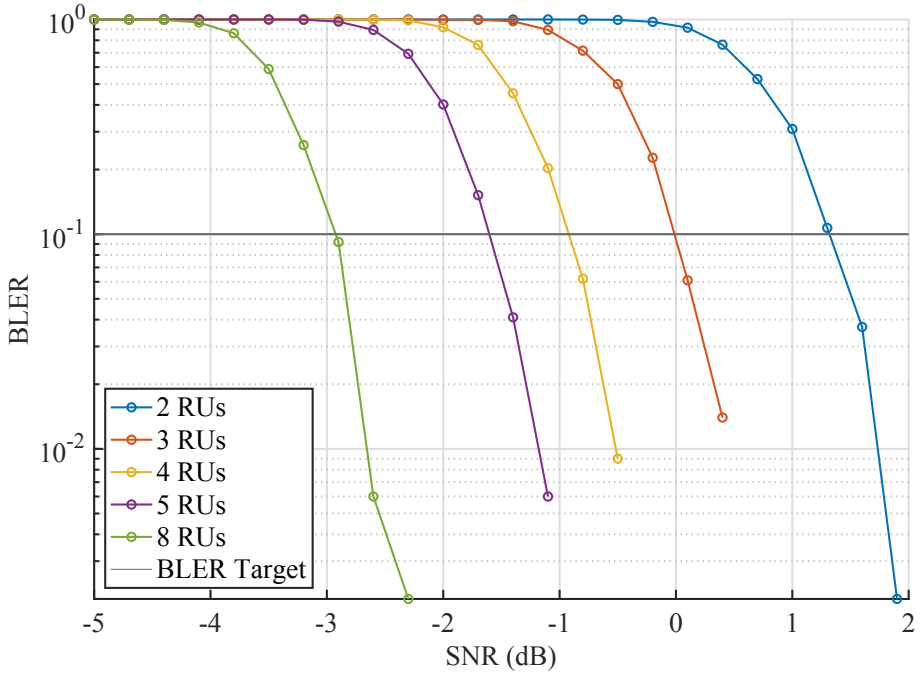

FIGURE 3.3: Example BLER curves for TBS of 256 bits and blind repetitions set to 4.

3.2.4 Satellite Mobility Model

A new mobility model, i.e., `SatelliteMovement` has been defined. It manages the movement of the satellites by defining their coordinates in the selected scenario. Figure 3.4 provides a general overview on the implemented mobility model. Specifically, `SatelliteMovement::GetSatPosition` tracks the position of the satellite. For the purposes of the simulation, and

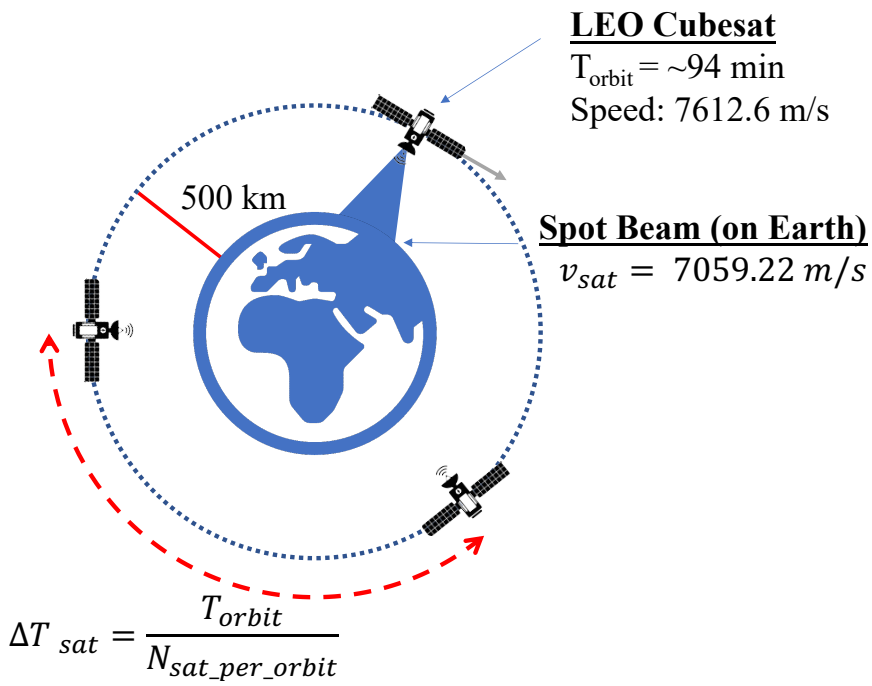

FIGURE 3.4: Key parameters of the implemented mobility model.

without loss of generality, satellites movement was considered exclusively in one direction on a reference axis of the Cartesian plane, i.e., the x-axis. The point value of the considered position refers to the centre of the beam that covers the area on the ground. Based on the number of satellites in the orbit and the time instant, this method provides the updated value of the position according to the following equation:

$$x_{Sat}(t) = x_{0,Sat} + v_{sat}(t \mod \Delta T_{sat}), \tag{3.1}$$

where $x_{0,Sat}$ corresponds to the initial position of the satellite, v_{sat} represents the relative speed of the satellite spot beam on the Earth, t represents the time instant considered and the modulo operation is needed to exploit the periodicity of the position function. Finally, ΔT_{sat} represents the elapsed time between two different satellites. It is given by T_{orbit}, that is the time taken by the satellite to make one complete revolution around the Earth, e.g., about 94 minutes, over $N_{sat\_per\_orbit}$, that is the number of the satellites in a single orbit. ΔT_{sat} may be expressed as:

$$\Delta T_{sat} = \frac{T_{orbit}}{N_{sat\_per\_orbit}}. \tag{3.2}$$

3.2.5 Cell Selection Procedure

The position of the satellites is useful for determining whether the entities involved in the communication, i.e., NTN terminals and the satellite, are actually in reciprocal visibility and therefore able to communicate or not. For this purpose, a new extension is introduced. This computation is performed within the `UserEquipment::UpdateUserPosition` method.

First, NTN terminals not having an empty transmission buffer measure the power of the downlink signal received from the satellite. To this end, an essential parameter to determine the maximum coverage the cellular system can support is defined by the MCL and expressed as follows:

$$MCL[dB] = P_{TX} - P_{RX}. \tag{3.3}$$

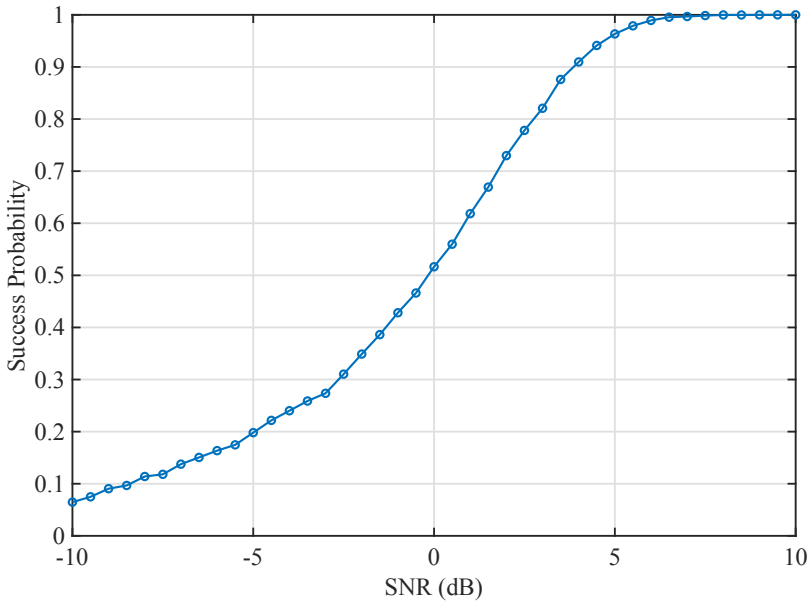

FIGURE 3.5: Cell Selection success probability at different SNR values.

P_{TX} is the transmitted signal power by the satellite and P_{RX} represents the received signal power on NTN terminal side. The former is equal to 33 dBm of the parabolic reflector antenna used for the simulation. The latter is estimated by the L2S model, specifically from the link model for downlink channel, starting from the elevation angle. It can be evaluated since the simulator knows both NTN terminal and satellite positions.

Once the MCL goes under a defined threshold, i.e. 164 dB, the NTN terminal starts the attach procedure to the satellite. For evaluation purpose, the MATLAB LTE Toolbox was used to estimate if the NTN terminal can retrieve the correct Cell Information from the downlink signal at different SNR values.

Figure 3.5 depicts the success probability of the cell selection procedure. The NTN terminal can start the Random Access Procedure after the attach procedure is successfully completed.

The NTN terminal continuously monitors the downlink power signal in order to maintain the connection with the satellite. Thanks to this approach, the simulator can model an error during the Msg2 and Msg4 reception of the Random Access Procedure. If so, the procedure has to be rescheduled again. On the other hand, the NTN terminal may fail the attach procedure even if it accomplishes the Random Access Procedure, breaking possibility to communicate.

3.3 Performance Evaluation

This section presents a preliminary performance assessment of an NB-IoT satellite-based communication system for reference monitoring scenarios. To demonstrate the actual effectiveness of the developed tool, the conducted system-level study highlights how network and satellite configuration significantly impact system performance.

3.3.1 Simulation Scenario

The reference scenario is called nb-Cell-sat and the command-line syntax to investigate it is:

```
./5G-air-simulator nbCell-Sat nS nU nC mcs nR  period boW spa (seed),
```

TABLE 3.1: Parameters of the Scenario

Parameter	Value
nS	4, 8 satellites
nU	1000, 3000, 5000, 10000 users [188]
mcl	164 dB
mcs	2, 4, 6, 8
nR	1, 2, 4
uplinkBand	1980-2000 MHz
uplinkConfig	Single-Tone
spa	3.75, 15 kHz
rachPreamble	48
rachPeriod	240 ms
backoff	2048 ms
ueAntennaPower	23 dBm
eNBAntennaPower	33 dBm
seed	1-50

where:

- nS is the number of satellites per orbit;
- nU is the number of users in the simulation area;
- mcs is theMCS to be used for the transmissions;
- nR is the number of NPUSCH and NPRACH repetitions;
- spa is the subcarrier spacing;
- seed is an optional seed to initialize random quantities to different, but reproducible, values in each simulation run.

For the simulation purpose, the fixed area on the Earth, that contains the NTN terminals, was chosen with a circular shape as the same size of the satellite spot beam.

At the application layer, the selected traffic model is the periodic uplink reporting [187]. In fact, monitoring is one of the most common use cases for MTC in NTNs [28]. The application payload size follows a Pareto distribution with shape parameter $\alpha = 2.5$, characterized by a minimum size of 20 bytes and a cut off of 200 bytes. The split of inter-arrival time periodicity is 1 day (40%), 2 hours (40%), 1 hour (15%), and 30 minutes (5%).

Regarding on the Random Access, the number of possible NPRACH preambles is the maximum allowed by the standard, i.e., 48. We chose 240 ms as the NPRACH periodicity while the Backoff Parameter is set to 2048 ms. In this way, the probability of collisions due to the preamble retransmissions may be mitigated. Moreover, it is important to emphasize that these values are also compatible with higher RTTs typical of NTNs [26]. The duration of the RAR window and the Contention Resolution Timer are set in accordance with the defined number of NPRACH repetitions.

The simulator also provides support to multiple coverage classes. However, in this case, only one coverage class has been considered since all the NTN terminals are supposed to experience the same level of coverage with respect to the satellite. In particular, we chose to use an MCL value of 164 dB. The chosen scheduling algorithm is the Round Robin, since it is proven to guarantee lower average delays with respect to FIFO and avoid the starvation problem [189]. The duration of the simulation has been chosen in order to allow a vision of

at least 8 cycles of visibility by the satellites on the area involved in the communication. We considered a 20 MHz bandwidth from 1980 MHz to 2000 MHz frequency and a single NB-IoT carrier. The main parameter settings considered in this study are summarized in Table 3.1.

This is strictly related also to the selected use case satellite scenario that reduces the transmission time only to the visibility time. Then, it is not recommended to let a single user to use the whole bandwidth, even if for a few milliseconds.

Different Key Performance Indicators (KPIs) have been measured by processing the output trace files. In particular, the number of NPRACH preamble collisions and the end-to-end delay are statistically analyzed. Finally, the average delivery ratio of the packets is investigated for further completeness of the performance evaluation.

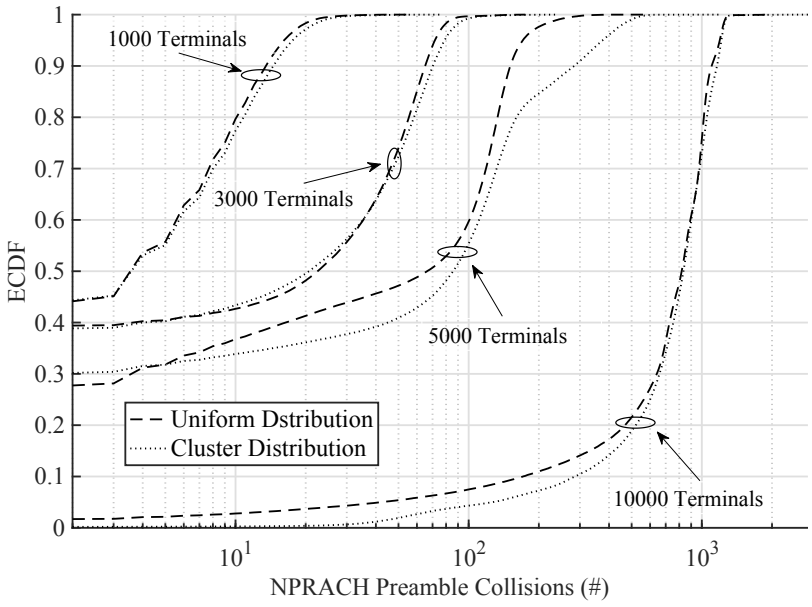

(A) 4 Cubesats

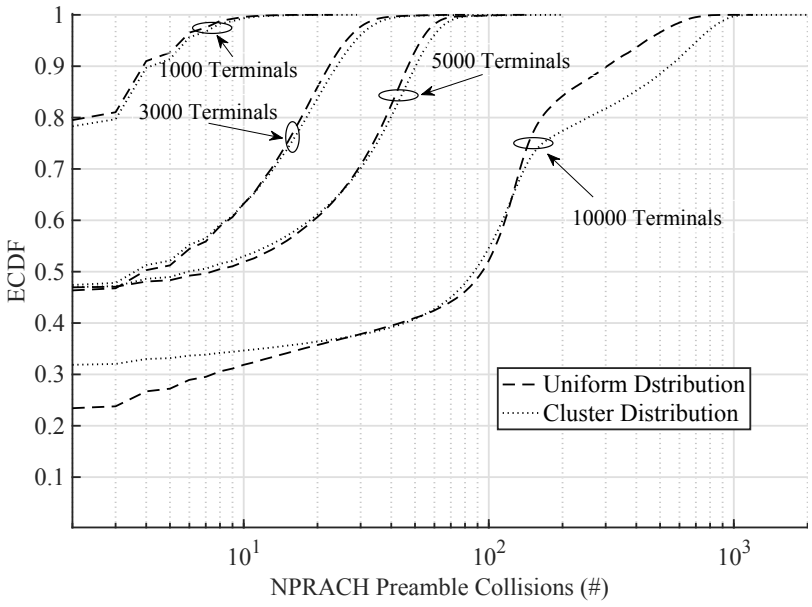

(B) 8 Cubesats

FIGURE 3.6: ECDF of the NPRACH Preamble collisions

3.3.2 NPRACH Preamble Collision

Figure 3.6 shows the number of NPRACH preamble collisions. First of all, the number of Cubesats in the Satellite Platform greatly impacts NPRACH performance. In fact, with fewer Cubesats, ground terminals remain without satellite coverage for longer periods. As soon as they return in visibility, a great burst of NPRACH preamble transmissions occurs, hence leading to several collisions.

Besides, also a greater number of NTN terminals leads to an overall higher number of preamble collisions, as expected. For instance, with 4 Cubesats and 10000 NTN terminals, the probability of having less than 100 collisions is below 10%. This demonstrates that NPRACH represents a bottleneck for dense network deployments.

Finally, it is important to highlight that the cluster distribution impacts negatively on the performance, and this is more true for a higher number of terminals. Indeed, according to the implemented mobility models, all the users of a cluster come back in coverage practically at the same time. In contrast, the attachment is more gradual when NTN terminals are uniformly distributed.

3.3.3 End-to-End Packet Delays

End-to-End packet delays are reported in Figure 3.7. They are computed by taking into account the influence of cell selection, random access procedure, scheduling decisions, and the actual physical transmission.

Following the previous NPRACH considerations, the most noticeable feature is that the constellation numerousness significantly affects the end-to-end packet delays. In particular, more Cubesats allow covering NTN terminals for more protracted periods, hence reducing end-to-end delays. Besides, the amount of time needed to complete the random access procedure increases with a higher number of NTN terminals. Indeed, when more users perform the random access procedure, the number of collisions rises. As a consequence, packet delays also grow with the number of NTN terminals.

It is important to mention that, for 3000 and 5000 NTN terminals, the difference in performance is barely noticeable. A considerably higher delay would be expected in the case of 5000 NTN terminals since the number of collisions is higher. Nonetheless, the scheduling delay is limited in such a case, precisely because fewer users successfully complete the random access procedure. The other way around happens with 3000 NTN terminals. As a consequence, performance is similar in both cases.

3.3.4 Delivery Ratio

To conclude, the packet delivery ratio (i.e., the ratio between correctly received packets and transmitted packets) is analyzed for all the sets of simulations. Specifically, Figure 3.8 shows the achieved average delivery ratio.

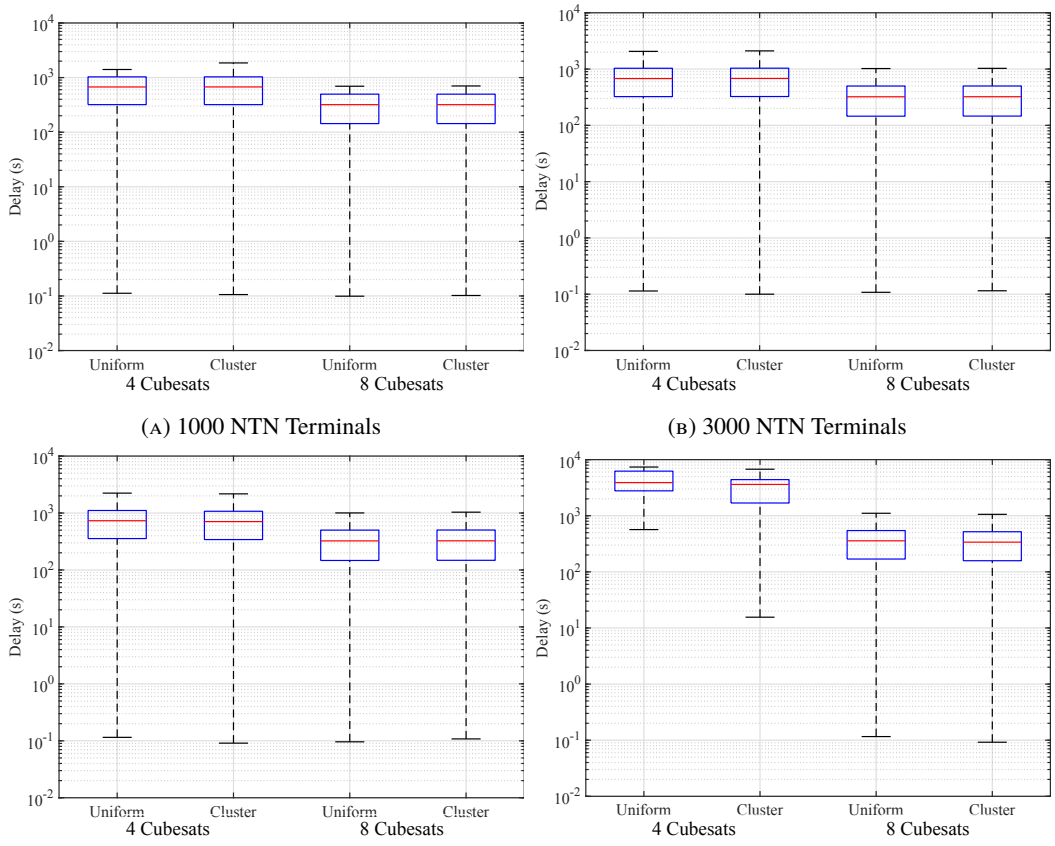

(A) 1000 NTN Terminals

(B) 3000 NTN Terminals

(C) 5000 NTN Terminals

(D) 10000 NTN Terminals

FIGURE 3.7: Box plots of the end-to-end packet delays. Each box plots identifies the median delay (i.e., the red line), the 25^{th} and the 75^{th} percentile (i.e., the bottom line and the top line of the blue rectangle), as well as the minimum and the maximum measured delay value (i.e., the edges of the vertical black line).

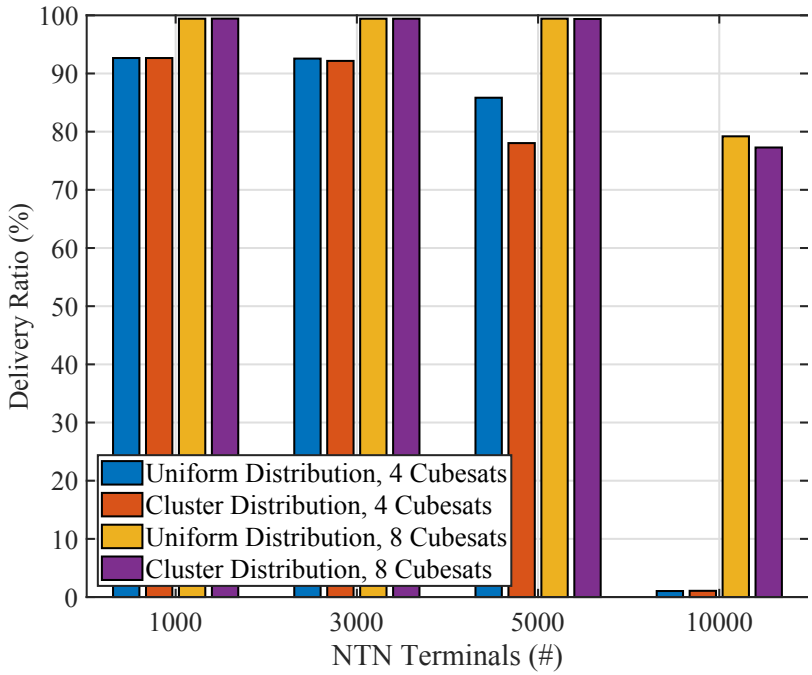

FIGURE 3.8: Delivery Ratio.

Evidently, 8 Cubesats constellations hold the greatest packet delivery ratios. Conversely, when a massive number of NTN terminals is deployed, performance is extremely reduced. Nonetheless, it is important to emphasize that fewer satellites provide decent performance (e.g., delivery ratios higher than 90%) for a reduced number of the NTN terminals. This also highlights the fact that proper constellation dimensioning is crucial.

Finally, the aforementioned considerations for NPRACH and delays reflect in the obtained delivery ratios, therefore proving the accuracy of the analysis.

Chapter 4

On the Optimal Deployment of Virtual Network Functions in Non-Terrestrial Segments

In the upcoming 5G&B of mobile communication systems, space network entities will cooperate with conventional terrestrial networks to provide three-dimensional wireless connectivity around the World. By considering the resulting massive amount of data to be managed into non-terrestrial segments, it will be necessary to dynamically configure functionalities across space network entities. Preliminary contributions in this context focus on quasi-static scenarios, while ignoring the challenging issues (i.e., intermittent visibility, dynamic network configuration, and communication delays) introduced by satellites' movement and communication protocols enabling the integration of terrestrial and non-terrestrial networks. To bridge this gap, this work presents a network architecture with novel orchestration capabilities of services into non-terrestrial segments. In the proposed approach, the interaction between terrestrial and non-terrestrial entities and the cloud has been detailed across service request, configuration, and provisioning phases. Then, starting from a system model describing the network configuration and the resulting deployment delays of services, an optimization problem has been formulated to dynamically allocate Virtual Network Functions (VNFs) among LEO CubeSats over a looking-ahead horizon, based on service requests, computational capabilities of the involved CubeSats, visibility matrices, and expected deployment delay bounds. Finally, the proposed optimization problem has been solved through three heuristic strategies. Computer simulations have been carried out to demonstrate the ability of the developed strategies to achieve results close to the optimal solution and to ensure better performance against a benchmark scheme.

4.1 Related Works

The dynamic provisioning of VNFs at the edge of the terrestrial networks has been widely investigated in the current scientific literature. Most noteworthy contributions addressed this topic by formulating optimization problems (quite often solved through heuristic techniques), willing to reduce energy consumption [55], improve resource allocation [56], or minimize the end-to-end delay [57]–[59]. Other works focused attention on the real-time provisioning of services via VNFs. In this context, the proposed approaches have been conceived to lower the migration cost of the VNFs [60], [61], maximize the security level of each VNF [62], reduce the energy consumption [63], or minimize the end-to-end delay [43].

The advent of 5G&B-oriented use cases brought a rapid increment of research efforts focusing on NTN [44]. Recent contributions also emphasize the use of computational resources onboard satellites for task offloading and advanced service provisioning to ground users [53]. However, the enticing solutions designed for the terrestrial network appear inadequate for the

NTN infrastructure due to the motion of the satellite and the intermittent visibility offered by a satellite constellation. In this context, the contributions discussed in [64]–[67], [69], [70] addressed the task offloading theme over the NTN segment, but without explicitly mentioning the usage of VNFs. These solutions have been conceived in order to improve the load balance in the network, by separating services into different network slices [64], manage the allocation of communication [65] or computational (i.e., processing and storage) [66] resources in order to maximize the number of accomplished requests, as well as minimize the end-to-end delay [67], [68]. Likewise, the strategy presented in [69] aims to lower energy consumption by optimizing the satellite resources according to the forecast number of ground users to be served. Furthermore, the solution proposed in [70] jointly minimizes the energy consumption and the end-to-end delay by handling the offloading and the resource allocation strategy with a game theory and Lagrange multiplier based methods.

Other contributions, such as [71]–[76], [78]–[80] tackled such an important research topic by leveraging the virtualization and quick reconfiguration capabilities provided by the NFV and SDN paradigms, respectively. Most contributions in this context aim to maximize the number of the accomplished request in each time interval [71]–[77] by solving the proposed optimization problem with meta-heuristic solutions. Furthermore, other works minimize the bandwidth usage with a greedy approach solution [78], minimize the end-to-end delay [79]–[81], or increase the link reliability [190].

Without a doubt, the current state of the art, as summarized in Table 4.1, provides preliminary (but very valuable) approaches to the task offloading problem in NTN. However, all of the reviewed solutions present some shortcomings that must be addressed in the ongoing research activities. To begin, they usually develop a system model by assuming a quasi-static scenario, willing to manage the task offloading process within the single upcoming time slot. Differently, the mobility of satellites belonging to a given constellation requires the definition of more complex and sophisticated schemes supporting, for example, a looking-ahead optimization. Furthermore, the communication protocol enabling the interaction and the configuration into NTN segments is quite often neglected. On the contrary, this work would extend the current state of the art by offering concrete answers to these challenging research issues.

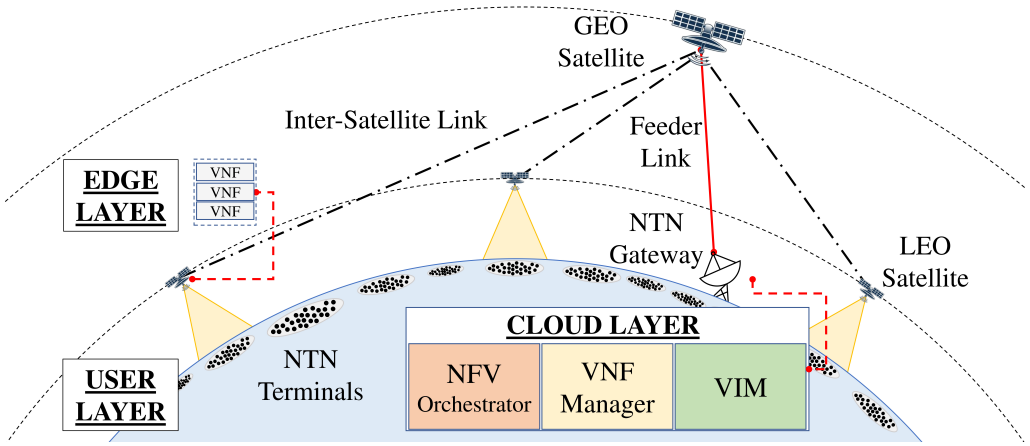

FIGURE 4.1: The reference network architecture.

4.2 The proposed approach

This Section describes the proposed network architecture and the related protocol interaction enabling the on-demand provisioning of customized services into NTN segments. Then, it presents a novel looking-ahead optimization problem, based on an accurate system model

TABLE 4.1: Review of Related Works.

References	Satellite Architecture Design	NTN Network	End-to-end Delay Optimization	Real time On-Demand VNF Deployment	Satellite visibility Constraints for LEO constellation	Looking Ahead Optimization	Protocol Stack Design
[55]				✓			
[56]				✓			
[57]			✓	✓			
[58]			✓	✓			
[59]			✓	✓			
[43]			✓	✓			
[62]				✓			
[61]				✓			
[63]				✓			
[60]				✓			
[64]		✓			✓		
[66]	✓	✓					
[65]	✓	✓			✓		
[69]		✓			✓		
[70]		✓	✓				
[67]		✓	✓				
[79]	✓	✓	✓		✓		
[68]		✓	✓				
[76]	✓	✓		✓			
[72]		✓		✓			
[78]		✓		✓			
[74]		✓		✓	✓		
[75]	✓	✓		✓	✓		
[80]	✓	✓	✓	✓	✓		
[81]	✓	✓	✓	✓			
[190]	✓	✓		✓			
[77]		✓		✓			
[73]	✓	✓		✓	✓		
[71]	✓	✓		✓	✓		
This work	✓	✓	✓	✓	✓	✓	✓

describing the expected delays for deploying services, according to the actual parameter settings.

4.2.1 The reference network architecture

This work focuses on a NTN-based architecture in accordance with the recommendations discussed beginning with Release 17 [10] and progressing to the5G&B scenarios [1], in which satellites host specific VNFs capable of processing the huge amount of data sent by heterogeneous NTN terminals deployed on the Earth's surface [191].

The resulting network architecture is composed of User, Edge, and Cloud Layers, as depicted in Fig. 4.1.

At the User Layer, NTN terminals sharing the same organization and geographic region and offering and/or offering the same service are grouped into the same cluster. In each cluster, the service provider deploys and configures a dedicated entity, namely master node, which is in charge of: i) realizing the need for a given cluster of NTN terminals to deliver data and use specific VNFs deployed onboard the satellite, ii) announcing the service request to the remote NFV Orchestrator hosted by the Cloud Layer, through space network elements belonging to the Edge Layer, iii) learning the outcome of the orchestration algorithm, and iv) announcing within the cluster of NTN terminals the presence of a satellite hosting a requested service. Without loss of generality, it is possible to assume that the interaction among NTN terminals and the master node is implemented through out-of-band communication, enabled (for example) by LoRaWAN or WiFi technologies.

The Edge Layer includes a constellation of LEO CubeSats, Geostationary Earth Orbit

(GEO) satellites, and NTN gateways. Today, the constellation of LEO CubeSats is considered as the widely used low-cost satellite platform because of its low overall infrastructure deployment cost. Therefore, it concretely offers a cost-effective deployment of NTN segments, thus fostering connectivity also in remote areas of the Earth [192]. In the proposed network architecture, a LEO CubeSat represents the first contact point for the master node of a cluster, issuing a service request. Such a request must be delivered to the remote NFV Orchestrator in the Cloud Layer. Nevertheless, the constant movement of a LEO CubeSat makes intermittent the connection with the NTN terminals on the ground. Specifically, they can establish a connection with a given LEO CubeSat for a short period, namely visibility window, as depicted in Fig. 4.2. Furthermore, even the connection with the NTN gateways spread on the Earth is intermittent [193]. Indeed, to overcome this issue, the constellation of LEO CubeSats exploits inter-satellite links with a group of GEO satellites, granting connectivity even with the lack of a persistent feeder link with NTN gateways. As a result, the multi-hop connectivity established at the Edge Layer easily allows the LEO CubeSat to forward service requests to the Cloud Layer. Additionally, once configured (i.e., through the protocol architecture and optimization algorithm proposed in this work), LEO CubeSat can establish a connection with NTN terminals and provide them with the required services.

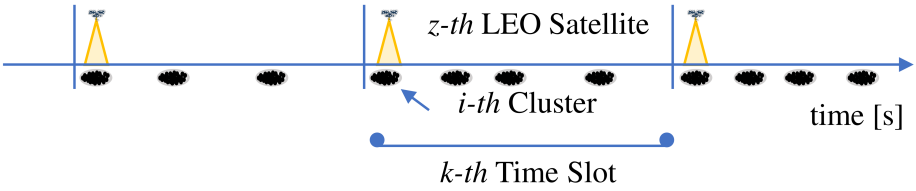

FIGURE 4.2: Intermittent connectivity between terminals on the Earth and the LEO satellite constellation.

Finally, the Cloud Layer includes the NFV Orchestrator, the VNF Manager, and the Virtualised Infrastructure Manager (VIM). The NFV Orchestrator elaborates the VNFs deployment instruction borne by the VNF Manager. The VIM provides an interface through the SDN facilities that support the implementation of the optimization outcome by exploiting its comprehensive knowledge of the network topology. Thus, the Cloud Layer exploits these entities for the implementation of the optimization outcome by dynamically deploying VNFs onboard the LEO CubeSats [194].

4.2.2 Protocol interaction

The protocol interaction between Terrestrial and non-Terrestrial entities belonging to User, Edge, and Cloud Layers is detailed in what follows across three consecutive phases, namely service request, configuration, and service provisioning (see Fig. 4.3).

Phase 1: Service Request. The master node realizes the need of a given cluster of NTN terminals to deliver data and use specific VNFs deployed onboard one of the available LEO CubeSat. As a consequence, the master node announces the service request to the first visible LEO CubeSat. Subsequently, the NTN gateway receives the forwarded request through the persistent feeder link ensured by the GEO satellite. Therefore, the NFV Orchestrator gathers all the received requests by the Edge Layer and collects them into a list of unaccomplished tasks.

Phase 2: Configuration. The Cloud Layer knows the set of unaccomplished tasks and their processing requirements, the network topology, and the computational resources available in LEO CubeSats. Based on these details, it implements an optimal allocation of VNFs (as discussed below), over the constellation of LEO CubeSats. Then, the NFV Orchestrator

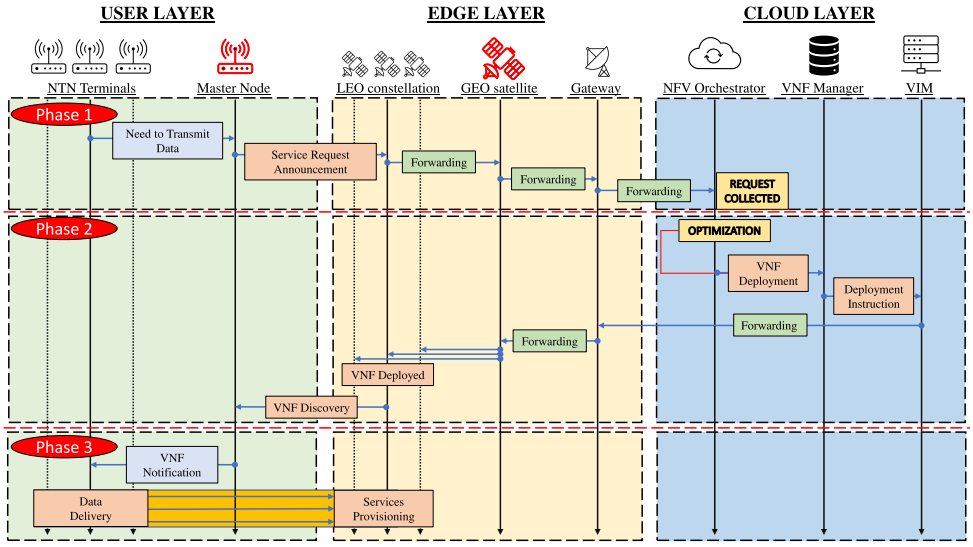

FIGURE 4.3: Interaction among network entities.

sends the optimization outcome to the VNF Manager, aiming at deploying the given VNFs in the constellation. Subsequently, the Virtualised Infrastructure Manager receives the deployment instruction forwarded by the VNF manager. Finally, the VNFs are deployed in the constellation through the feeder link ensured by the NTN gateways and the GEO satellites. The master node is finally informed about the deployment of the requested VNF onboard a specific LEO CubeSat.

Phase 3: Service Provisioning. At the beginning of the Service Provisioning phase, the master node notifies the cluster of NTN terminals about the presence of the given LEO CubeSat configured to receive and process (via dedicated VNFs) their data. As anticipated before, the communication between the master node and NTN terminals can be enabled through out-of-band communication, such as LoRaWAN or WiFi. Finally, the NTN terminals' communication can be supported by the requested services onboard that LEO CubeSat for the whole visibility window. Obviously, the set of unaccomplished tasks is updated by removing the services that are already deployed.

4.2.3 System model

Since the orbits of LEO CubeSats are independent of each other, the proposed system model considers a group of LEO CubeSats belonging to the same orbit of a constellation. This choice does not limit the generality of the presented methodology [193]. The main mathematical symbols used to formulate the system model are reported in Table 4.2.

Indeed, let $\mathbf{\Sigma} = \{\sigma_1, \ldots, \sigma_S\}$ be the set of evenly spaced LEO CubeSats in the considered orbit and $S = \|\mathbf{\Sigma}\|$ be the number of the LEO CubeSats in the considered orbit. Likewise, the processing and memory capabilities of the z-th LEO CubeSat are expressed with $c(\sigma_z)$ and $m(\sigma_z)$, respectively. Similarly, let $\mathbf{\Psi} = \{\psi_1, \ldots, \psi_L\}$ be the list of the master nodes belonging to the clusters served by the LEO CubeSats of the considered orbit, with $L = \|\mathbf{\Psi}\|$ denoting the number of clusters. Finally, let $\mathbf{\Pi} = \{\pi_1, \ldots, \pi_W\}$ be the list of the different types of services provided by the Cloud Layer.

As well known, the amount of time required by a given LEO CubeSat to complete a revolution around the Earth depends on the height of its orbit. The motion of the LEO CubeSat, as Newton's form of Kepler's third law, that is: $T_o = 2\pi\sqrt{\frac{R^3}{GM_e}}$, where T_o represents the revolution time of the LEO CubeSat, R is the average radius of the orbit estimated as the distance from the center of the Earth, G is the gravitational constant, and M_e is the mass of the

TABLE 4.2: List of main symbols.

Symbol	Description
$\mathbf{\Psi}$	List of clusters, $L = \|\mathbf{\Psi}\|$
$\mathbf{\Sigma}$	List of LEO CubeSats, $S = \|\mathbf{\Sigma}\|$
$\mathbf{\Pi}$	List of available services
ψ_i	Master node of the i-th cluster
σ_z	z-th LEO CubeSat
$\pi_{\mathbf{w}}$	w-th service
$c(\sigma_z)$	Processing capability of the z-th LEO CubeSat
$m(\sigma_z)$	Memory capability of the z-th LEO CubeSat
$t(r_{k,f})$	Time slot in which the request has been generated
$\psi_i(r_{k,f})$	Master node of the i-th cluster that generated the request
$\pi_w(r_{k,f})$	Requested service
$\tau(r_{k,f})$	Provisioning upper bound delay
$\xi(r_{k,f})$	Processing load associated with request
$\zeta(r_{k,f})$	Memory load associated with the request
λ_i	Number of requests generated in a day for the i-th cluster
$\mathbf{V}(k)$	LEO CubeSat visibility matrix for the k-th time slot
$\mathbf{B}(k)$	Services deployment matrix for the k-th time slot
$\mathbf{R}(k)$	Set of pending requests at the k-th time slot
T_p	Time slot duration
$T(k)$	Time horizon at the k-th time slot

Earth [195]. Accordingly, a given same satellite can periodically communicate with a specific cluster of NTN terminals every T_o. Anyway, since the LEO CubeSats in the considered orbit are evenly spaced, the elapsed time between two consecutive visibility windows is stated as: $T_p = \frac{T_o}{S} = \frac{2\pi}{S}\sqrt{\frac{R^3}{G \cdot M_e}}$.

Based on these premises, the proposed system model assumes to partition time into time slots, lasting T_p. Therefore, the consecutive steps belonging to the procedure described in Section 4.2.1 are implemented over consecutive time slots. Specifically, requests are collected by the NFV Orchestrator during the k-th time slot. Subsequently, the looking-ahead optimization problem (formally described in Section 4.2.4) is solved within the $(k+1)$-th time slot. Finally, according to the solution of the optimization problem, the VNFs will be deployed onboard satellites in the upcoming time slots, i.e., starting from the $(k+2)$-th time slot and within a specified deadline.

The list of pending requests at the k-th time slot is denoted with $\mathbf{R}(k)$. Each request $r_{k,f} \in \mathbf{R}(k)$, where $F_k = \|\mathbf{R}(k)\|$ and $f = 1, \ldots, F_k$, (delivered to the NFV Orchestrator) includes the following information:

- the master node belonging to the cluster that generated the request, $\psi_i(r_{k,f})$,
- the requested services, $\pi_w(r_{k,f})$,
- the time slot in which the request has been generated, $t(r_{k,f})$,
- the upper bound delay for the provisioning of the requested services, $\tau(r_{k,f})$,
- the processing load associated with the request, $\xi(r_{k,f})$,
- the memory load associated with the request, $\zeta(r_{k,f})$.

Without loss of generality, it is assumed that $\tau(r_{k,f})$ is defined as a multiple of the time slot, that is $\tau(r_{k,f}) = nTp$.

As anticipated, a cluster can establish a communication with only one LEO CubeSat during a time slot and only for a short visibility window. Indeed, the proposed system model introduces the $\mathbf{V}(k)$ matrix to represent the reciprocal visibility between LEO CubeSats and clusters on the ground during the k-th time slot. Therefore, $v_{i,z}(k) = 1$, with $v_{i,z}(k) \in \mathbf{V}(k)$, if the z-th LEO CubeSat can communicate with the i-th cluster in the k-th time slot. Otherwise, $v_{i,z}(k) = 0$. The values of the $\mathbf{V}(k)$ matrix depend on the deploying position of both clusters and satellites in the network.

Furthermore, the services deployment matrix $\mathbf{B}(k) = \big(b_{w,z}(k)\big) \in \{0,1\}^{L \times S \times T(k)}$ contains boolean flags denoting if the z-th satellite hosts the w-th VNFs when $b_{w,z}(k) = 1$, with $b_{w,z}(k) \in \mathbf{B}(k)$. Otherwise, $b_{w,z}(k) = 0$. In this case, it depends on the outcome of the optimization problem, as defined in Section 4.2.4.

4.2.4 Optimization problem

The goal of the optimization problem proposed in this work is to dynamically deploy VNFs onboard satellites while ensuring that:

- the deployment of the service must be performed within a strict deadline,
- for all the LEO CubeSats, the sum of the processing and memory requirements pertaining to the deployed VNFs, is never greater than their capabilities,
- the sum of all the experienced service provisioning delays is minimized.

As mentioned in Section 4.1, prior works solely consider a quasi-static scenario and neglect the movement of LEO CubeSat throughout the optimization process. Differently, this work formulates a novel optimization problem willing to dynamically deploy VNFs across LEO CubeSats, over a looking-ahead horizon.

Given the list of pending requests, that is $\mathbf{R}(k)$, and the set of the request's upper bound delay, that is $\mathcal{T}(k) = \{\tau(r_{k,1}), \ldots, \tau(r_{k,F_k})\}$, the proposed looking-ahead optimization algorithm considers an observation time interval $T(k)$ defined as:

$$T(k) = \max \mathcal{T}(k). \tag{4.1}$$

According to the proposed system model, $T(k)$ is a multiple of the duration of a single time slot T_p. In the k-th time slot, the partial service provisioning delay already accumulated by a generic request $r_{k,f}$ can be defined as the elapsed time between the generation and the current time slot, that is $k - t(r_{k,f})$. Such a delay may increase, slot by slot, till the actual VNFs provisioning onboard a given LEO CubeSat. Indeed, given the service deployment matrix for all the time slots available till the end of the observation time interval $T(k)$, the delay achieved by the service $r_{k,f}$ can be formally defined as:

$$\delta(k, r_{k,f}) = \sum_{\nu=1}^{T(k)} \sum_{\sigma_z \in \Sigma} \Big(b_{w,z}(\nu) \, [k + \nu - t(r_{k,f})] \Big), \tag{4.2}$$

while considering that $\sum_{\nu=1}^{T(k)} \sum_{\sigma_z \in \mathbf{\Sigma}} b_{w,z}(\nu) \geq 1, \ \forall r_{k,f} \in \mathbf{R}(k)$. Such an expression implicitly assumes that the request will be accomplished at least by a single LEO CubeSat within the time horizon $T(k)$.

It is important to note that messages exchanged among the involved entities experience communication delays. However, these delays can be safely considered much lower than the duration of the time slot (as discussed in detail in Section 4.3.5), which is used as the minimum time interval of interest for the conceived system model, the formulated optimization problem,

and the resulting service provisioning. As a consequence, by assuming to observe the overall system on a time-slot basis, the impact of both network architecture and interaction flow is intrinsically taken into account.

The objective function to be minimized can be formally defined as the sum of all the partial delays related to each pending request, as reported in what follows:

$$\begin{aligned} U(k) &= \sum_{r_{k,f} \in \mathbf{R}(k)} \delta(k, r_{k,f}) = \\ &= \sum_{r_{k,f} \in \mathbf{R}(k)} \left[\sum_{\nu=1}^{T(k)} \sum_{\sigma_z \in \mathbf{\Sigma}} \left(b_{w,z}(\nu) \left[k + \nu - t(r_{k,f}) \right] \right) \right]. \end{aligned} \tag{4.3}$$

Indeed, the dynamic allocation of VNFs across CubeSats, over a looking-ahead horizon, is formulated in this work through an Integer Linear Programming (ILP) problem:

$$P1 : \min_{\mathbf{R}\,\mathbf{\Sigma}} \sum_{r_{k,f} \in \mathbf{R}(k)} \left[\sum_{\nu=1}^{T(k)} \sum_{\sigma_z \in \mathbf{\Sigma}} \left(b_{w,z}(\nu) \left[k + \nu - t(r_{k,f}) \right] \right) \right]$$

$$\text{s.t.} \sum_{r_{k,f} \in \mathbf{R}(k)} b_{w,z}(\nu)\, \xi(r_{k,f}) \leq c(\sigma_z), \forall \sigma_z, \nu \tag{4.4a}$$

$$\sum_{r_{k,f} \in \mathbf{R}(k)} b_{w,z}(\nu)\, \zeta(r_{k,f}) \leq m(\sigma_z), \forall \sigma_z, \nu \tag{4.4b}$$

$$\sum_{\sigma_z \in \mathbf{\Sigma}} \sum_{\nu = t(r_{k,f})+2}^{\tau(r_{k,f})} b_{w,z}(\nu)\, v_{i,z}(\nu) = 1, \forall r_{k,f} \tag{4.4c}$$

$$b_{w,z}(\nu) \leq v_{i,z}(\nu), \forall \pi_w, \sigma_z, \nu, \tag{4.4d}$$

where (4.4a) specifies that the sum of the computing requirements of the VNFs deployed on a given LEO CubeSat cannot exceed the CPU processing capabilities of the considered satellite. Furthermore, (4.4b) states that the total amount of memory used by the allocated VNFs on a given LEO CubeSat in any time slot must not exceed its memory capability. Moreover, (4.4c) ensures that a VNF requested by a pending request is deployed, by the NFV Orchestrator, no later than its deadline, beginning at least two time slots after the request is generated (allowing for collection and optimization). Finally, (4.4d) mandates the NFV Orchestrator to deploy the VNFs only onboard specific LEO CubeSat capable of communicating with the cluster within the deadline, specifically during its visibility window.

4.3 Performance evaluation

This Section investigates the effectiveness of the proposed methodology in different scenarios and through computer simulations.

First of all, it is important to remark that the non-convex optimization problem formulated in Section 4.2.4 is NP-hard. Indeed, a brute force strategy can be hypothetically used to test all the binary combinations of the 3D matrix (i.e., $\mathbf{B}(k) = \left(b_{w,z}(k)\right) \in \{0,1\}^{L \times S \times T(k)}$), every time slot and for the overall observation time interval. Such an approach, however, is feasible only for simple scenarios (e.g., with few LEO CubeSats and few clusters on the ground). More in general, instead, the optimal solution cannot be retrieved in a polynomial time.

At the same time, conventional optimization frameworks like Gurobi, CVXR, or Casadi cannot be used in this context because they work with decision variables represented by 2D

matrices, whereas the proposed approach deals with decision variables in the form of a 3D matrix.

To bridge this gap and solve the formulated optimization problem three different heuristic strategies, inspired by well-known meta-heuristic approaches (such as TS [83], SA [84], and GLS [85]) have been properly developed and tested through a custom Python tool. More details about the implemented algorithms can be found in Appendix 4.4.

The behavior of the developed strategies has been also compared with respect to a benchmark scheme, namely GR algorithm. Specifically, it deploys the required VNFs on the first available LEO CubeSat with sufficient memory and processing power without utilizing any optimization methods.

4.3.1 Preliminary Results

In this Section, the single iteration of the whole optimization procedure is analyzed in depth, based on the work in [82]. In particular, the optimization problem formulated in Section 4.2.4 is solved by using a well-known meta-heuristic solution method, namely Tabu Search [83]. The system model, the optimization problem, and the aforementioned solution method have been implemented in Python. The conducted study considers a scenario where the computational capability of each satellite is set to $c(\sigma_z) = 3, \forall z$, and the computational requirement for each service request is set to $\xi(r_{k,f}) = 1, \forall r_{k,f}$. It also assumes that security VNFs must be provided within 10 time slots from the generation of the request. On the other hand, the number of the clusters served by the constellation is set to $L = 60$.

First of all, the impact of the number of pending requests on system performance is investigated. To this end, it is assumed that each cluster may have only 1 pending request. Moreover, service requests are generated in order to ensure an average number of pending requests, that is μ, ranging from 15 to 30. Instead, the number of satellites in the orbit is set to $S = 3$. Fig. 4.4a shows the Empirical Cumulative Distribution Function (ECDF) of the service provisioning delays experienced by all the clusters. As expected, the delays increase with the network load. A high number of requests in the same time slot, in fact, overloads the constellation. Consequently, the clusters may wait for more visibility times before being served by a satellite hosting the requested security VNF on board. In any case, however, the targeted upper bound (equal to 10 time slots) is always satisfied. As well known, the Tabu Search is able to find the optimal solution after a number of iterations, which strictly depends from the initial solution randomly chosen by the algorithm. Indeed, there is not a specific relation between the amount of iterations needed to solve the optimization problem and the traffic load. Results reported in Fig. 4.4b just show that Tabu Search employs from 19 to 36 iterations to minimize the objective function.

The second study discussed herein investigates the impact of the number of satellites on system performance, while setting the average number of pending request to $\mu = 15$. Fig. 4.5a confirms (once again) the ability of the optimization problem to satisfy the expected upper bound delay. At the same time, Fig. 4.5b highlights that the number of iterations needed to find the optimal solution generally increases with the number of satellites in the orbit. This is due to the higher size of matrices managed by the algorithm. The only exception is registered when $S = 6$. In that case, however, even if the number of iterations needed to solve the problem is lower, their duration is higher (as discussed below). Indeed, the higher number of satellites per orbit brings to an increment of the problem complexity. The complexity of the proposed optimization problem is measured on the host machine with 4-core 3.5 GHz CPU and 16 GB of RAM. The amount of time required by the Tabu Search algorithm to find the optimal solution is reported in Table 4.3, for all the scenarios discussed before. It is possible to observe that a simple machine, like the one adopted in the conducted study, is able to solve the optimization problem before the end of the current time slot only for low

number of satellites per orbit. On the contrary, in the case the number of satellites per orbit is higher than 4, the optimal solution is obtained after a higher amount of time. Definitively, it is possible to conclude that the computational complexity required to solve optimization problem increases with the number of satellites per orbit. At the same time, however, it is very important to remark that the feasibility of the proposed approach can be still reached by using machines with higher computing capabilities, as well as by exploiting other meta-heuristic solution methods.

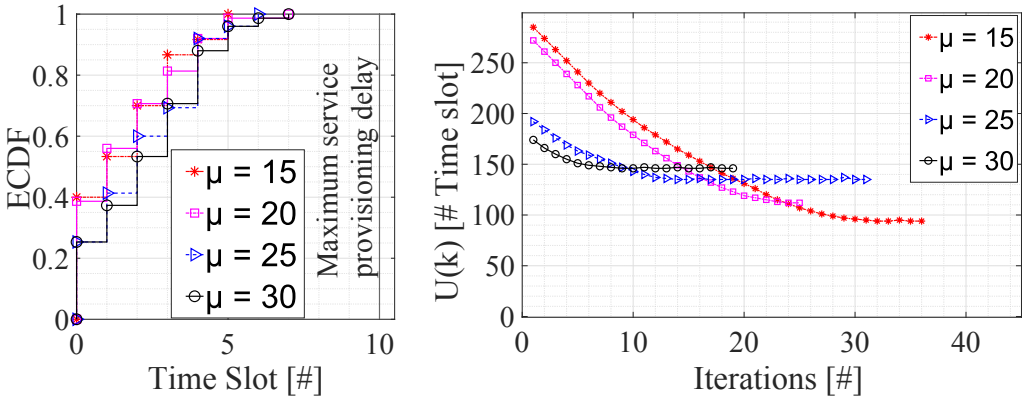

(A) Service provisioning delay.

(B) Objective function $U(k)$.

FIGURE 4.4: Impact of μ on network performance.

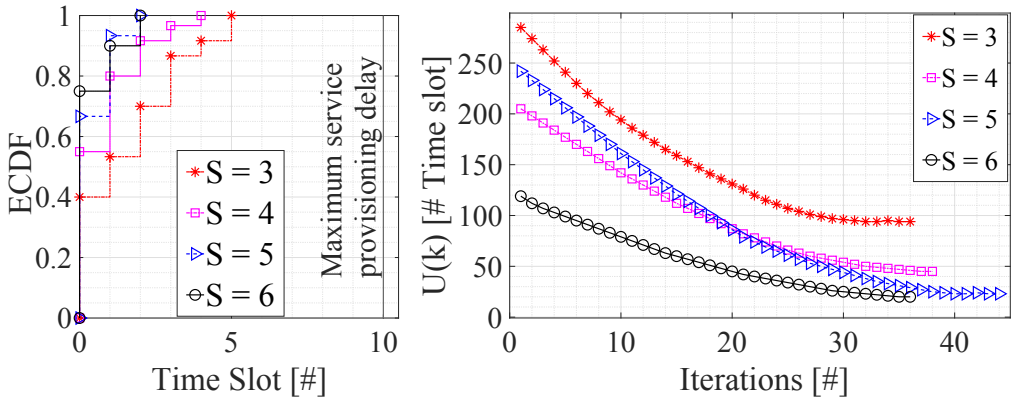

(A) Service provisioning delay.

(B) Objective function $U(k)$.

FIGURE 4.5: Impact of S on network performance.

4.3.2 The considered use case

The 3GPP, starting from Rel-15 [196], began exploring the potential of a new communication standard for NTNs, by examining various deployment scenarios and challenges. At the time of writing, Rel-17 [5], [10] is investigating key issues related to business roles, service, and network management when orchestrating services in the space segment [197]. The ease of deploying LEO CubeSats satellite constellations is driving the growth of tailored services for various companies [198], [199]. Indeed, since NTN segments are called to securely manage an ever-growing amount of data, connections, and services, it is extremely important to envisage novel methodologies for the dynamic and optimal deployment of VNFs properly devoted to security functionalities (including authentication, authorization, firewall, intrusion detection systems, intrusion prevention systems, and so on). Of course, given the limited amount of

Impact of μ with S = 3			**Impact of S with μ = 15**		
μ	T_p [min]	Solving Time	S	T_p [min]	Solving Time
15	31.53	0.25 T_p	3	31.53	0.26 T_p
20	31.53	0.17 T_p	4	23.65	0.65 T_p
25	31.53	0.21 T_p	5	18.91	1.40 T_p
30	31.53	0.11 T_p	6	15.76	1.89 T_p

TABLE 4.3: Solving time.

TABLE 4.4: Computational Capabilities Exposed by LEO CubeSats for the Considered Services [201].

Symbol	**Parameter**	**Value**
$m(\sigma_z)$	Memory capability	64 GB
$c(\sigma_z)$	CPU processing capability	128 Gigacycles/s
β^c	Maximum aggregated throughput	92 kbps

resources on the LEO CubeSats, these security services should only be activated as needed to conserve onboard resources [200]. To this aim, security VNFs are considered to demonstrate the effectiveness of the proposed approach in a realistic use case. It's worth noting that our scenario does not restrict the use of the proposed approach in other contexts.

4.3.3 Parameter setting

The study has been conducted by varying the number of clusters deployed on the Earth's surface, the number of LEO CubeSats in the orbit, and the average number of services issued in a day by each cluster.

The altitude of LEO CubeSats is set to 500 km. The corresponding orbit period is equal to $T_o = 5676$s. Moreover, the number of LEO CubeSats, that is S, in the orbit, is set to 3 and 5. Indeed, based on the number of satellites per orbit, T_p is equal to:

$$T_p = \begin{cases} 1892\ s, & \text{if } S = 3, \\ 1135\ s, & \text{if } S = 5. \end{cases} \tag{4.5}$$

Considering the time slot duration, the impact of processing and transmission time, in the order of milliseconds, can be negligible.

It is assumed that each LEO CubeSat is equipped with a PowerEdge R6515 with AMD EPYC 7702P, 2.00 GHz, 64 core, and 64 GB RAM [201], as indicated in Table 4.4.

In the considered scenario, the clusters are uniformly distributed on the Earth's surface covered by the considered orbit. In particular, the number of clusters L varies between 100 and 200. Let λ_i be the average number of requests generated by the $i-$th cluster in a day, set to 6 and 12 events per day. Accordingly, the average number of requests received by the Cloud Layer in a day is equal to $\lambda = \lambda_i L$. Data generated by terminals belonging to each cluster can be processed by means of services summarized in Table 4.5. The service is chosen randomly for each request. The expected computational capabilities of VNFs strictly depend on the amount of data generated by each cluster. The proposed study considers a worst-case scenario, in which each cluster exploits the overall available satellite bandwidth during the related visibility time to send data, denoted with β^c bps. Therefore, given the CPU

TABLE 4.5: Security Services Requirements for VNFs implementation.

Provider	**Service**	ξ^c **[cycles/bit]**	$\zeta(r_f)$ **[GB]**
Fortigate VM [202]	NGFW	9	4
	IPSec VPN	14.5	2
	Threat Prot.	11.3	4
Cisco ASAv [203]	Stateful IDS	4.2	4
	AES VPN	6.9	2
Juniper vSRX [204]	FW	2.3	2
	IPS	2.4	2
	APPMonitor	1.5	2
Others	Snort IDS/IPS [205]	9.5	2
	OpenVPN AES-NI [206]	31	4

cycles required to process one bit, that is ξ^c cycles/bit, the overall processing requirement of a service is equal to $\xi(r_f) = \xi^c \cdot \beta^c$ cycles/s [43]. The conducted study assumes that the radio access technology used in the link between LEO CubeSat and clusters is the NB-IoT. In this case, $\beta^c = 92$kbps [207].

4.3.4 KPIs

The evaluated KPIs include:

- **deployment delay of services**: it represents the amount of time (expressed as a multiple of the time slot) needed to deploy a VNF requested by a group of NTN terminals on a specific LEO CubeSat. In general, and according to the design principles at the basis of the conceived approach, it is expected the deployment delay ranges from a minimum of two time slots (one slot is required to deliver the request to the Cloud Layer during the Phase 1 and the other one is required to elaborate the deployment instructions during the Phase 2) to the expected upper bound delay,
- **percentage of computational resources (including RAM and CPU) consumed by LEO CubeSats for hosting the deployed VNFs**: it represents the amount of RAM and the processing capabilities utilized onboard each LEO CubeSat in relation to the total amount of resources hosted in the space segment,
- **average processing time of each heuristic algorithm in solving the optimization problem**: it represents the amount of time (expressed in seconds) spent by the Cloud Layer in evaluating the optimal deployment of VNFs requested by the pending services.

Computer simulations consider an observation period of 60000s, embracing multiple visible time intervals. Moreover, the analysis of deployment delay of requested services and the percentage of computational resources consumed onboard satellite has been organized into two parts. The former focuses the attention on a specific simulation run (e.g., network realization) and illustrates the considered KPI as a function of time. The latter, instead, reports minimum, average, and maximum values, as well as the 25th and 75th percentile of the measured KPI, obtained by considering numerous realizations.

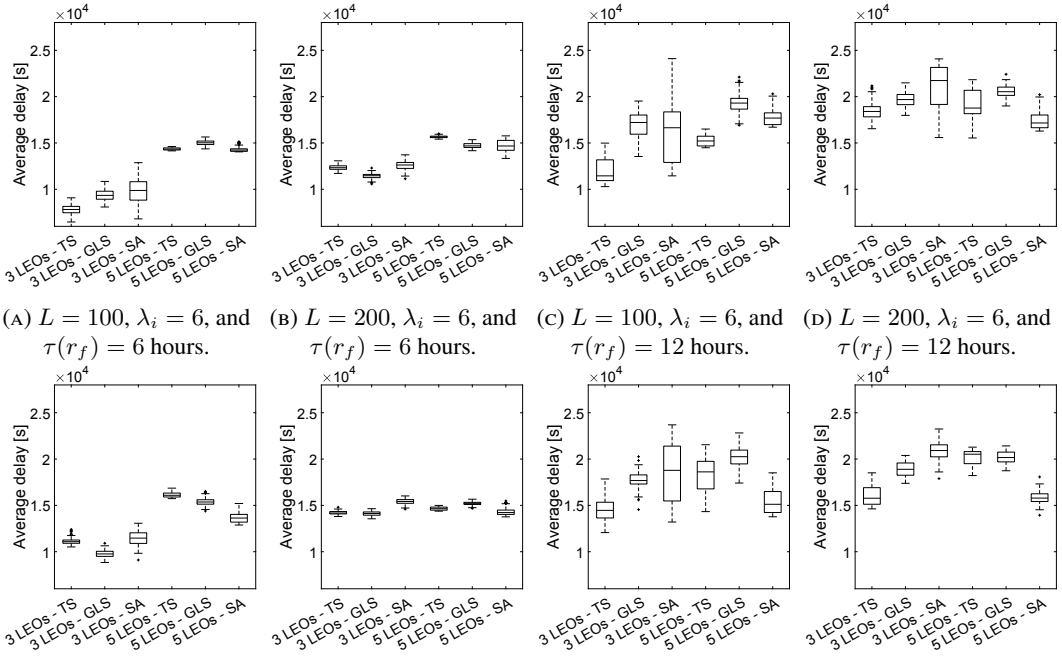

(A) $L = 100$, $\lambda_i = 6$, and $\tau(r_f) = 6$ hours. (B) $L = 200$, $\lambda_i = 6$, and $\tau(r_f) = 6$ hours. (C) $L = 100$, $\lambda_i = 6$, and $\tau(r_f) = 12$ hours. (D) $L = 200$, $\lambda_i = 6$, and $\tau(r_f) = 12$ hours.

(E) $L = 100$, $\lambda_i = 12$ and $\tau(r_f) = 6$ hours. (F) $L = 200$, $\lambda_i = 12$ and $\tau(r_f) = 6$ hours. (G) $L = 100$, $\lambda_i = 12$, and $\tau(r_f) = 12$ hours. (H) $L = 200$, $\lambda_i = 12$, and $\tau(r_f) = 12$ hours.

FIGURE 4.7: Confidence interval for the deployment delay of security services.

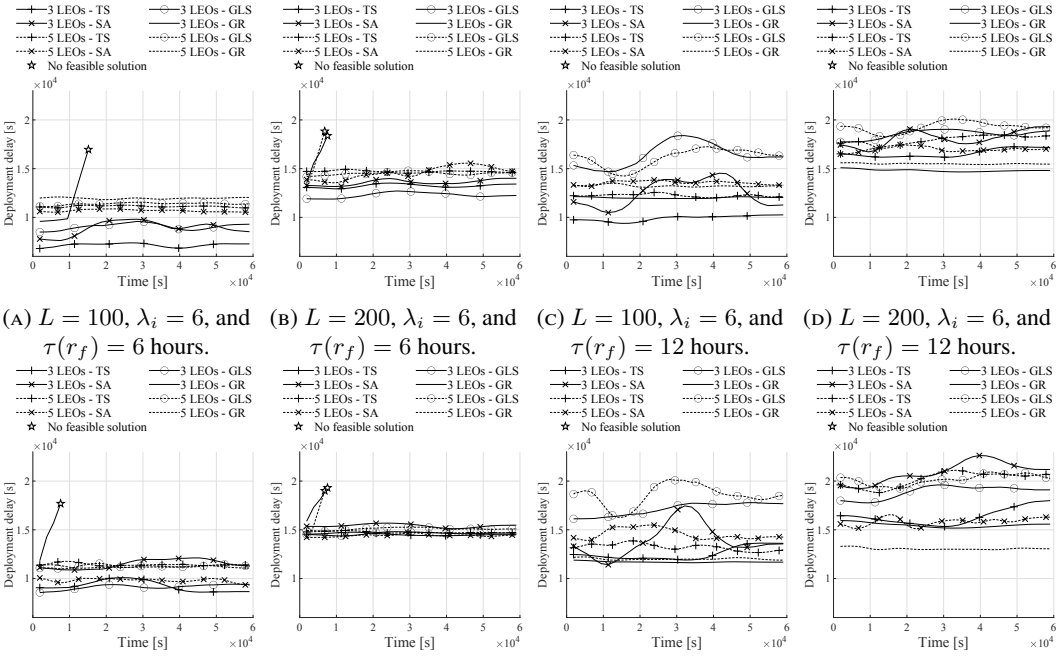

(A) $L = 100$, $\lambda_i = 6$, and $\tau(r_f) = 6$ hours. (B) $L = 200$, $\lambda_i = 6$, and $\tau(r_f) = 6$ hours. (C) $L = 100$, $\lambda_i = 6$, and $\tau(r_f) = 12$ hours. (D) $L = 200$, $\lambda_i = 6$, and $\tau(r_f) = 12$ hours.

(E) $L = 100$, $\lambda_i = 12$ and $\tau(r_f) = 6$ hours. (F) $L = 200$, $\lambda_i = 12$ and $\tau(r_f) = 6$ hours. (G) $L = 100$, $\lambda_i = 12$, and $\tau(r_f) = 12$ hours. (H) $L = 200$, $\lambda_i = 12$, and $\tau(r_f) = 12$ hours.

FIGURE 4.6: Deployment delay of security services.

4.3.5 Deployment delay of security services

Fig. 4.6 shows the deployment delay of the deployed security services, experienced for a single specific test. Moreover, reported results have been obtained by averaging the deployment

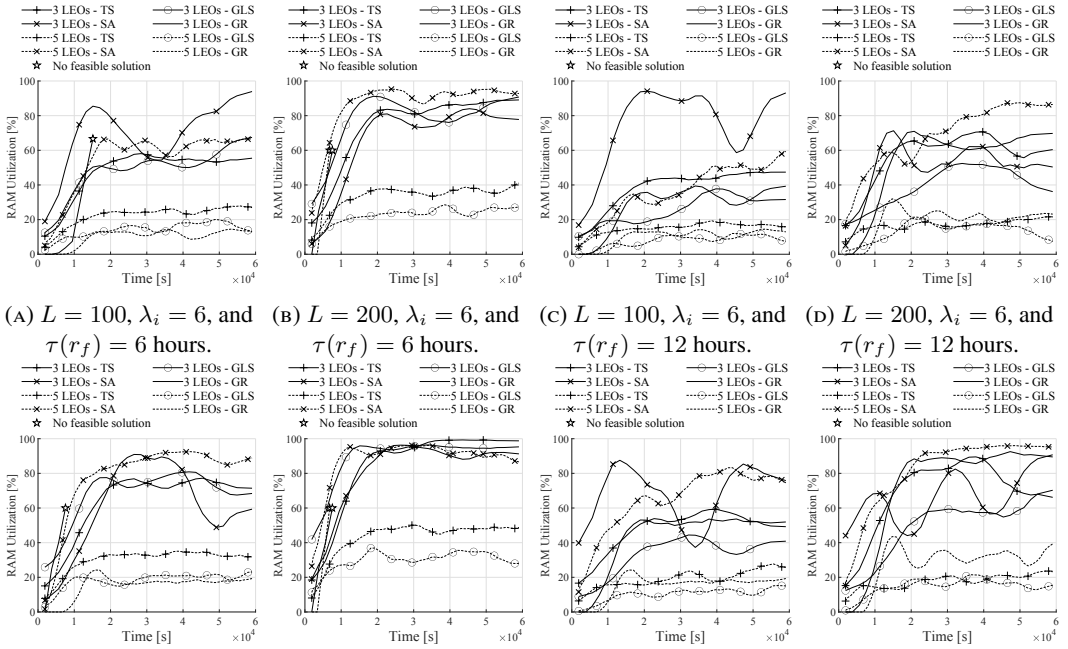

(A) $L = 100$, $\lambda_i = 6$, and $\tau(r_f) = 6$ hours. (B) $L = 200$, $\lambda_i = 6$, and $\tau(r_f) = 6$ hours. (C) $L = 100$, $\lambda_i = 6$, and $\tau(r_f) = 12$ hours. (D) $L = 200$, $\lambda_i = 6$, and $\tau(r_f) = 12$ hours.

(E) $L = 100$, $\lambda_i = 12$, and $\tau(r_f) = 6$ hours. (F) $L = 200$, $\lambda_i = 12$, and $\tau(r_f) = 6$ hours. (G) $L = 100$, $\lambda_i = 12$, and $\tau(r_f) = 12$ hours. (H) $L = 200$, $\lambda_i = 12$, and $\tau(r_f) = 12$ hours.

FIGURE 4.8: RAM utilization.

delays experienced by each service request across moving windows of 5 time slots each.

Looking at the behavior of the benchmark scheme, that is the GR algorithm, it is possible to observe that it cannot provide a feasible solution in several scenarios, including the one with 3 LEO CubeSats, 100 clusters on the ground, and an upper bound delay equal to $\tau(r_{k,f}) = 6$ hours, as well as the one with the same upper bound delay, 200 clusters on the ground, and 5 LEO CubeSats. All these negative results are achieved because the GR algorithm tends to overload LEO CubeSats thus being not able to accept further requests.

On the contrary, the proposed approach always guarantees feasible solutions, independently from the heuristic algorithm adopted to find a solution for the formulated optimization problem. More specifically, obtained results show that the deployment delay increases with the number of clusters. In fact, the more clusters interact with the NTN segment, the higher the number of pending requests to be handled by the NFV Orchestrator at each optimization round. In these conditions, the NFV Orchestrator may encounter a lack of available resources across the first visible LEO CubeSats. Therefore, it is obliged to delay the deploy the VNFs by considering other future time slots (according to the conceived looking-ahead time horizon logic). Indeed, a longer deadline introduces a higher extent of the solution space, bringing an increment of deployment delays. Furthermore, regardless of the number of LEO CubeSats in the orbit, the deployment delay remains almost the same in the majority of the investigated scenarios. It relies on the exploration strategy of the optimal solution in the solution space for each heuristic approach.

To provide a further insight, additional tests have been conducted to collect performance levels by considering multiple realizations. Indeed, Fig. 4.7 depicts minimum, average, and maximum values of the experienced deployment delays, together with both the 25th and 75th percentile. The analysis of the GR algorithm has been omitted in this case because the previous analysis already highlighted its inability to provide feasible solutions in the most of investigated scenarios.

Regarding the proposed approach, instead, all the obtained results confirm the analysis reported in Fig. 4.6. Moreover, it also shows that the greatest deviation from the average

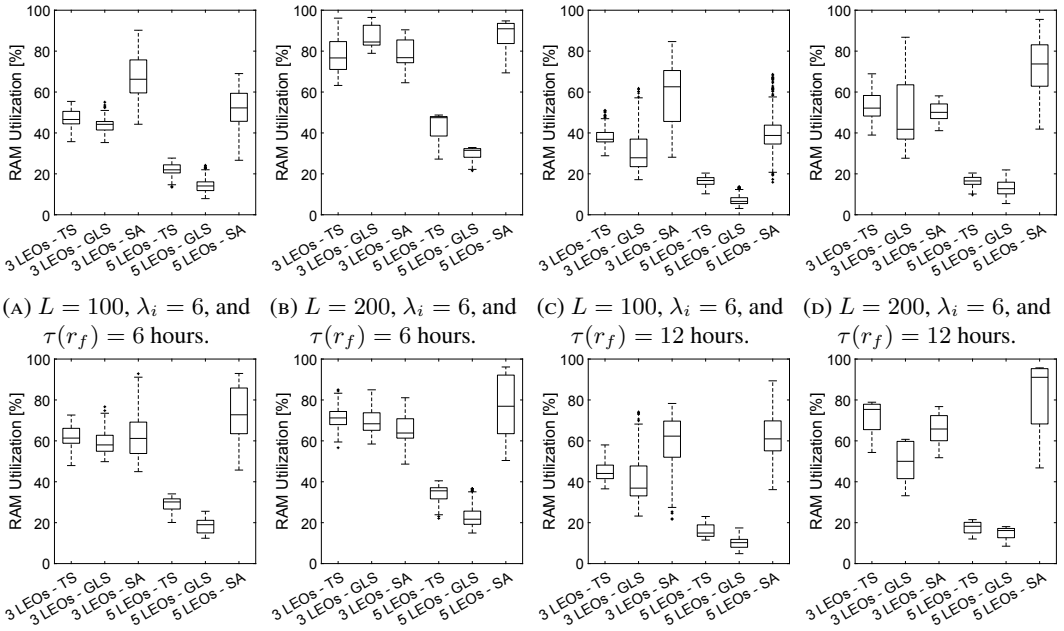

(A) $L = 100$, $\lambda_i = 6$, and $\tau(r_f) = 6$ hours. (B) $L = 200$, $\lambda_i = 6$, and $\tau(r_f) = 6$ hours. (C) $L = 100$, $\lambda_i = 6$, and $\tau(r_f) = 12$ hours. (D) $L = 200$, $\lambda_i = 6$, and $\tau(r_f) = 12$ hours.

(E) $L = 100$, $\lambda_i = 12$ and $\tau(r_f) = 6$ hours. (F) $L = 200$, $\lambda_i = 12$ and $\tau(r_f) = 6$ hours. (G) $L = 100$, $\lambda_i = 12$, and $\tau(r_f) = 12$ hours. (H) $L = 200$, $\lambda_i = 12$, and $\tau(r_f) = 12$ hours.

FIGURE 4.9: Confidence interval for the RAM utilization.

value (up to 30%) is registered in scenarios with 3 satellites and when the SA method is used. Conversely, with 5 satellites, the maximum deviation (up to 13%) is obtained with the TS method. In any case, obtained results always demonstrate the ability of the developed heuristic strategy to meet the expected quality of service constraint in all the considered scenarios.

To conclude, it has emerged that TS outperforms the other approaches in almost all scenarios with a low number of LEO CubeSats (i.e., 3) in the orbit, by reducing up to 25% the deployment delay of services. On the contrary, SA well suits scenarios with a higher number of LEO CubeSats (i.e., 5), for which it reduces up to 20% of the measured deployment delay.

4.3.6 Percentage of computational resources consumed by LEO CubeSats

Fig. 4.8 shows the percentage of RAM consumed by the deployed VNFs over time. Also in this case, reported curves have been generated by considering a single specific test and by averaging the measured KPI among all the satellites and across moving windows of 5 time slots each. It is important to remark that Fig. 4.8 depicts a specific realization that is a time-varying process and jointly influenced by the random number generator adopted by the simulation tool, the statistical generation of service requests (see, for instance, the variable λ_i of the i-th cluster), and the chosen optimization strategy. Peaks in Fig. 4.8 are registered when the network is handling a larger number of requests.

In line with the previous comments, the GR algorithm does not present feasible solutions for all the investigated scenarios. In those (few) configurations where it provides an effective deployment of VNFs, the percentage of consumed RAM is comparable with respect to results registered by the strategies proposed in this work.

As expected, the higher the number of served clusters, the higher the resulting memory consumption onboard the satellites. Furthermore, a wider deadline and higher number of LEO CubeSats in the considered orbit causes a higher extent of the set of feasible solutions to explore. As a result, the memory resources are allocated less efficiently by each heuristic algorithm. It is noteworthy to highlight that the SA-based strategy registers better allocation of memory resources in scenarios with a higher number of satellites.

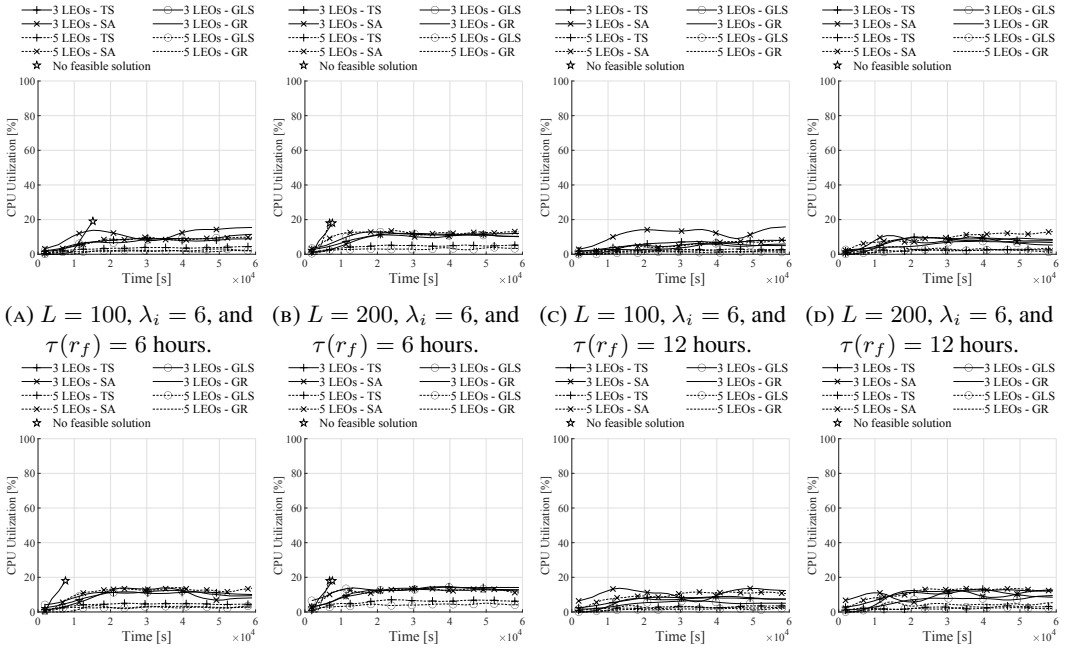

(A) $L = 100$, $\lambda_i = 6$, and $\tau(r_f) = 6$ hours. (B) $L = 200$, $\lambda_i = 6$, and $\tau(r_f) = 6$ hours. (C) $L = 100$, $\lambda_i = 6$, and $\tau(r_f) = 12$ hours. (D) $L = 200$, $\lambda_i = 6$, and $\tau(r_f) = 12$ hours.

(E) $L = 100$, $\lambda_i = 12$, and $\tau(r_f) = 6$ hours. (F) $L = 200$, $\lambda_i = 12$, and $\tau(r_f) = 6$ hours. (G) $L = 100$, $\lambda_i = 12$, and $\tau(r_f) = 12$ hours. (H) $L = 200$, $\lambda_i = 12$, and $\tau(r_f) = 12$ hours.

FIGURE 4.10: CPU utilization.

On the other hand, Fig. 4.10 shows the percentage of the CPU usage. Due to the low data rate of the considered radio access technology (i.e., NB-IoT), the processing capability never represents a blocking condition for the deployment of the VNFs.

With reference to parallel tests, Fig. 4.9 and Fig. 4.11 depict minimum, average, and maximum values, as well as the 25th and 75th percentile, of both RAM and CPU usage, respectively. Here, Fig. 4.9 highlights that the SA-based strategy exhibits the most significant deviations from the mean value, both for the configurations involving 3 LEO CubeSats and 5 LEO CubeSats. Notably, within the multiple realizations, the largest deviation recorded is up to 50% and 60% from the mean value, respectively. Fig. 4.11, instead, illustrates that the CPU usage remains consistently below 20%, with a negligible deviation from the mean value. Note that, also in this case, the analysis of the GR algorithm has been omitted because of its inability to provide feasible solutions for all the considered scenarios.

4.3.7 Processing time

The processing time emphasizes the computational burden required by each heuristic algorithm to find a solution to the optimization problem. It has been evaluated with a computer Intel(R) Xeon(R) Bronze 3106 CPU with 16 cores at 1.70GHz and 92 GB of RAM. In this case, the number of clusters deployed on the ground is set to 100, 150, and 200. Results are shown in Fig. 4.12.

The evaluation of the processing time for the GR algorithm is negligible because it just defines the VNFs allocation without implementing any time-consuming task.

Particularly important is the processing time for the proposed approach. The developed heuristic strategies, in fact, are called to provide an optimal and feasible solution within a threshold represented by the time slot duration. Only in this way, they will be able to trigger the deployment of VNFs onboard LEO CubeSats in time.

From the analysis of Fig. 4.12, it is possible to observe that only the TS-based strategy reaches a high value of processing time, very close to the threshold (i.e., the time slot duration).

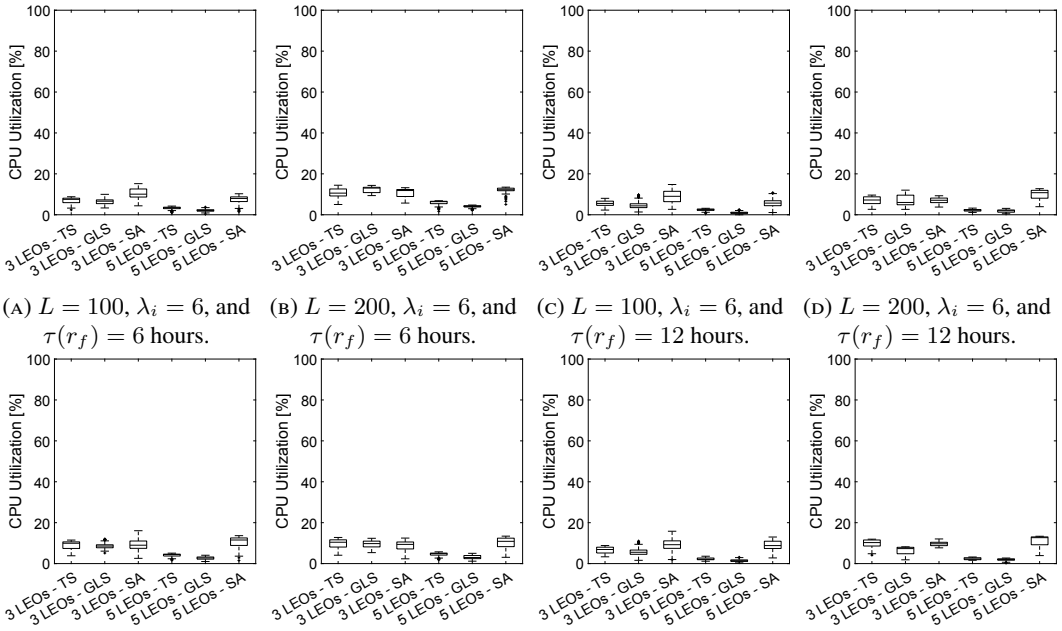

(A) $L = 100$, $\lambda_i = 6$, and $\tau(r_f) = 6$ hours. (B) $L = 200$, $\lambda_i = 6$, and $\tau(r_f) = 6$ hours. (C) $L = 100$, $\lambda_i = 6$, and $\tau(r_f) = 12$ hours. (D) $L = 200$, $\lambda_i = 6$, and $\tau(r_f) = 12$ hours.

(E) $L = 100$, $\lambda_i = 12$ and $\tau(r_f) = 6$ hours. (F) $L = 200$, $\lambda_i = 12$ and $\tau(r_f) = 6$ hours. (G) $L = 100$, $\lambda_i = 12$, and $\tau(r_f) = 12$ hours. (H) $L = 200$, $\lambda_i = 12$, and $\tau(r_f) = 12$ hours.

FIGURE 4.11: Confidence interval for the CPU utilization.

Indeed, it is the heaviest heuristic approach in terms of processing load for each considered scenario as demonstrated by the results. Nevertheless, by jointly taking into account all the considered KPIs, since the SA-based strategy is able to find an optimal solution in a lower time than other approaches, it represents the best choice for both processing time and deployment delay of services, by saving up 95% in processing time than TS.

4.3.8 Comparison with the optimal solution

In conclusion, to further demonstrate the effectiveness of the proposed approaches against the optimal solution, a comparison in smaller scenarios has been conducted. In detail, the number of clusters on the ground L is set to 5, the upper bound delay $\tau(r_f)$ is equal to 6 hours, λ_i is set to 1, and the number of LEO CubeSat S ranges from 2 to 5. Fig. 4.13 depicts how these heuristic schemes are able to produce results comparable to those expected by an optimal solution. Obtained results allow to trust the effectiveness of the heuristic strategies also in more complex scenarios.

4.4 Heuristic Implementation Details

The design and the implementation of the three heuristics are based on the following common methods:

- As a first step, it is introduced a way to estimate the utility function starting from a feasible solution, by exploiting the 3D matrix as input.
- Then, it has been implemented a method that helps to explore the neighbourhood of a given solution (i.e., swap move) by applying a little variation from the initial one and by checking its feasibility. For example, this is done by assuming to deploy a given VNF on another LEO CubeSat of the orbit, as well as by assuming to make available that VNF in a different time slot. It is worth noting that the parameters of each heuristic

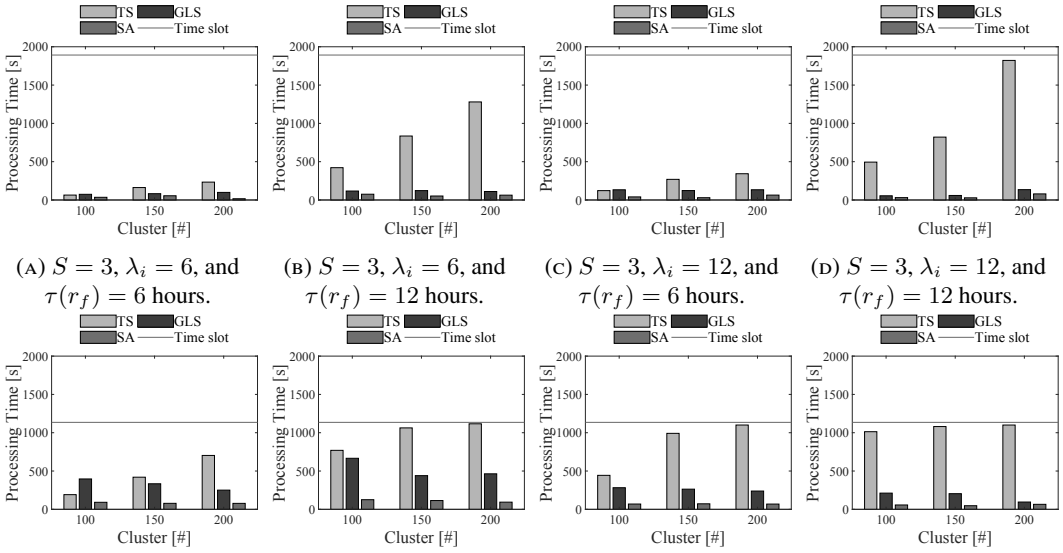

(A) $S = 3$, $\lambda_i = 6$, and $\tau(r_f) = 6$ hours.
(B) $S = 3$, $\lambda_i = 6$, and $\tau(r_f) = 12$ hours.
(C) $S = 3$, $\lambda_i = 12$, and $\tau(r_f) = 6$ hours.
(D) $S = 3$, $\lambda_i = 12$, and $\tau(r_f) = 12$ hours.
(E) $S = 5$, $\lambda_i = 6$, and $\tau(r_f) = 6$ hours.
(F) $S = 5$, $\lambda_i = 6$, and $\tau(r_f) = 12$ hours.
(G) $S = 5$, $\lambda_i = 12$, and $\tau(r_f) = 6$ hours.
(H) $S = 5$, $\lambda_i = 12$, and $\tau(r_f) = 12$ hours.

FIGURE 4.12: Processing time.

approach have been determined experimentally throughout the simulations to ensure the optimal performance for each method.

- The iteration ends upon reaching a specific criterion, which varies depending on the algorithm, as detailed below.

More specifically, the technique based on the TS meta-heuristic approach starts with an initial random solution and proceeds through a sequence of swap moves that lead to a new solution inside the neighbourhood of the current one, with the utility function assuming a value smaller than the selected value. To avoid the trap of local minimum, TS permits "worsening moves". However, it is possible to risk sliding back into the local minimum quickly after. To cope with this issue, it is crucial to make the last moves in the search path "forbidden", so that the algorithm cannot retrace its steps and fall back into the local minimum. Specifically, its stopping condition is verified when the same solution (i.e., $\mathbf{B}(k)$) is elected as the best solution on two different iterations in a row since exploring the same neighbourhood more than one time is pointless.

The technique based on the SA meta-heuristic approach begins with the generation of a random solution. After that, a new feasible one is generated by performing a swap move starting from the original. If the new solution's utility function is less than the initial one, it is accepted as the new solution. Otherwise, it can still be accepted with a decreasing likelihood as the search duration increases. If this probability is dropped too fast, the algorithm faces the risk of being stuck in a local minimum. On the other side, increasing the chance of adopting worsening solutions too slowly, lengthens the total search time. Specifically, to reach the equilibrium state in a sufficient time, the likelihood is imposed by the Metropolis Criterion, which is equal to $\min\{1, e^{-(\frac{U_2-U_1}{T})}\}$, where U_1 and U_2 express the value of the utility function of starting solution of the iteration and the newly generated one, respectively. T is the decreasing factor that drives the final equilibrium state. Finally, the maximum number of iterations is equal to 10000.

Furthermore, the technique based on the GLS meta-heuristic approach represents a search algorithm that generates solutions to problems by using strategies inspired by natural genetic populations. The basic idea is to create a population composed of random feasible solutions

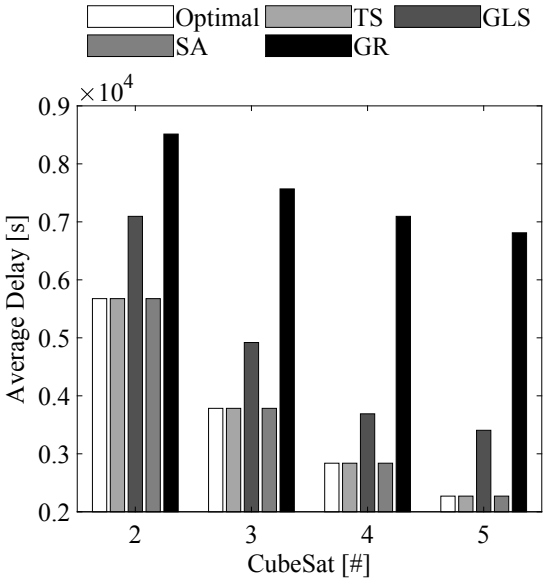

FIGURE 4.13: Comparison with the optimal solution with $L = 5$ and $\tau(r_f) = 6$ hours.

to a given problem. In particular, each element in the population can be utilized to generate new members of the population through crossover or mutation, specifically, by combining two alternative solutions to obtain another one. In detail, the optimal solution search starts with a population of 400 feasible solutions, which are then used to define a set of 200 parents. Finally, for each iteration, 80 new solutions are created by combining the others contained in the set of parents. The maximum number of iterations for this algorithm is set equal to 100.

Chapter 5

Fair Energy and Data Rate Maximization in UAV-Powered IoT-Satellite Integrated Networks

Non-Terrestrial Networks represent a valuable solution for providing connectivity to Internet of Things (IoT) devices in remote areas, where classical infrastructure is unavailable. Due to the low-power nature of IoT devices, an Unmanned Aerial Vehicle (UAV) can prevent the energy depletion of these Ground Nodes (GNs) by employing Wireless Power Transfer through an array antenna. Starting from the mathematical modeling of such a scenario, two Mixed-Integer Non-Linear Programming problems are formulated to fairly maximize (i) the energy distribution and (ii) the total amount of data transmitted to a Low Earth Orbit CubeSat. Therefore, it is necessary to optimize the drone kinematics, the transmission scheduling plan, and the beamforming vectors of the array antenna. To cope with their non-convexity, both problems are mathematically manipulated to reach a tractable form, for which two optimization algorithms are proposed and their complexity analyzed. To prove the effectiveness of the overall solution, a comprehensive simulation campaign is conducted under several parameter settings, such as number of GNs and UAV antenna elements with different transmission power levels. Finally, the proposal is compared with a baseline, which confirms the superiority of the proposal up to 7 times in terms of total transmitted data.

Notations: boldface lower case letters refer to vectors; $j = \sqrt{-1}$ is the imaginary unit; $\mathbf{x}^{\mathsf{T}}$ is the transpose of a generic vector $\mathbf{x}$; $\mathbf{x}^{\mathsf{H}}$ is the Hermitian of a generic vector $\mathbf{x}$; $\mathbf{x} \otimes \mathbf{y}$ denotes the Kronecker product between two generic vectors; $x \sim \mathcal{CN}(\mu, \sigma^2)$ define a circularly symmetric complex Gaussian distribution x with mean μ and variance σ^2; $\mathbf{I}_x$ represents the identity matrix of dimension x; $J_x(\cdot)$ denotes Bessel function of the first kind of order x; $\mathcal{O}(x)$ denotes the time-complexity of an algorithm of input size x, i.e, big O notation. The most significant parameters used in this work are summarized in Table 5.1.

5.1 Related Work

The scientific literature is currently focusing on enhancing traditional IoT networks by (i) expanding their coverage and (ii) improving the battery life of the devices.

Regarding the former, some intriguing contributions include the design of (i) communication and protocol schemes by adapting terrestrial technology to the space segment [193], (ii) resource allocation schemes able to improve energy efficiency [208], and (iii) more reliable LEO satellite-terrestrial communication techniques [209]. In this context, UAVs employed as mobile base station represent a valuable methodology to achieve ubiquitous connectivity.

For instance, the authors in [210] aim at improving the perceived network quality by the user and minimizing the communication outages, while enhancing the data rate and the fairness of the transmission. Most noteworthy scientific efforts placed a great emphasis on the

pairing of these two technologies by defining a hybrid network that leverages UAVs as relays to support satellite communications. In this context, the spectral efficiency and the outage probability are optimized in [211] by proposing a UAV relay selection and power allocation scheme. Other contributions design the transmission scheduling and the UAV trajectory to increase the system capacity [212] and energy efficiency [213].

For what concerns the battery life of the devices, WPT emerged as a disruptive technology for energy harvesting [214]. For instance, the authors in [215] propose a method that allows a node to first gather energy and then use it to transmit. Specifically, they investigate the optimal duration of a timeslot in a Time Division Multiple Access (TDMA) protocol, which maximizes the spectrum efficiency. Other approaches also consider the presence of a Intelligent Reflecting Surface (IRS) [216] to maximize the transferred power [217] and the throughput [218] of the users.

Moreover, cutting-edge approaches integrated the potential of WPT technology with the high mobility of the UAVs. A first setup is envisioned in [219] and [220], where energy-constrained nodes are optimally served by a UAV which acts as a base station, powered by WPT.

Recent works are also exploring the employment of UAV as a standalone WPT source. Clearly, one of the most critical aspects to be optimized is the UAV trajectory, which affects many facets of the mission, such as (i) the total amount of collected data [103], (ii) the age of information [107], (iii) the energy harvested by the GNs [98], [99], [102], [104], [105], (iv) the out-of-service probability [100], and (v) the UAV power consumption [101]. In particular, a novel scheme aided by an IRS, which simultaneously addresses WPT and information transmission for IoT sensors, is proposed in [103]. The protocol is divided into two phases: in the first one the drone recharges the devices while in the second one gathers the data. The objective is to maximize the total network sum-rate by optimally deriving the trajectory, the power allocation, the energy harvesting scheduling of the nodes, and the phase-shift matrix of the surface. Furthermore, the authors in[107] investigate a scenario in which a UAV recharges the GNs, collects data, and then transfers them to a data center. The aim is to minimize the average age of information by jointly optimizing the UAV trajectory and the time allocated for WPT. Moreover, the approach proposed in [98] intervenes by supplying power at GNs with limited battery capacities deployed at remote areas. Given that UAV is employed as a wireless power supplier and data collector, its overall energy consumption must be optimized subject to task collection and resource budget requirements. In [100], it is discussed the minimization of the energy depletion of GNs, and hence their outage probability. The latter is subject to the UAV elevation angle and the time slot allocation between the energy harvesting and the information transmission of each GN. Finally, the authors in [101] study a scenario in which a UAV is in charge of sustaining the devices of a network by periodically flying back and forth from a fixed position. Two approaches are proposed to minimize the average UAV power consumption by determining the trajectory, the duration of working periods, and the charging phase. The works above, however, consider a single antenna to perform WPT. To fill the gap, the approaches proposed in [104] and [105] investigate the impact of an antenna array to increase energy efficiency by taking advantage of beamforming.

To the best of the authors' knowledge, there is a lack of contributions that design and evaluate the performance of a UAV-powered IoT network that relies on a LEO CubeSat for information transmission. In this regard, this work proposes an optimization strategy to fairly distribute energy via WPT operation across GNs, while maximizing the transmitted sensed data.

Symbol	Description	Symbol	Description
N	Number of discrete timeslots for the transmission phase.	$\chi_{n,g}^{\text{SG}}$	Link budget for the link between the CubeSat and the GN.
K	Number of discrete timeslots for the charging phase.	$\Upsilon_{n,g}^{\text{SG}}$	Link noise power for the link between the CubeSat and the GN.
G	Number of GN.	$\Gamma_{n,g}^{\text{SG}}$	SNR of the link between the CubeSat and the GN.
δ	Duration of each timeslot, in seconds.	R_n^{SG}	Maximum achievable data rate of the CubeSat-GN link.
$\mathbf{q}_k^{\text{U}}$	Position of the UAV in cartesian coordinates.	B	GN-CubeSat channel bandwidth.
$\mathbf{v}_k^{\text{U}}$	Velocity of the UAV in meters per second.	MCL	MCL.
$\mathbf{q}_n^{\text{S}}$	Position of the CubeSat in cartesian coordinates.	$\Delta_{n,g}^{\text{SG}}$	Uplink coupling loss between the CubeSat and the g-th GN.
$d_{k,g}^{\text{UG}}$	Distance between the UAV and the g-th GN.	$\mathbf{v}^{\text{S}}$	Orbital speed of the CubeSat over Earth.
$d_{n,g}^{\text{SG}}$	Distance between the CubeSat and the g-th GN.	G^{E}	Earth's gravitational constant.
$\theta_{n,g}^{\text{SG}}$	Inclination angle between the CubeSat and the g-th GN.	M^{E}	Mass of the Earth, expressed in kilograms.
$\varphi_{n,g}^{\text{SG}}$	Azimuth angle between the CubeSat and the g-th GN.	v^{F}	CubeSat speed footprint over Earth in meters per second.
$\vartheta_{n,g}^{\text{SG}}$	Elevation angle between the CubeSat and the g-th GN.	F^{S}	CubeSat footprint diameter, expressed in meters.
r	Earth radius, expressed in meters.	T^{V}	CubeSat visibility time, expressed in seconds.
$\mathbf{\Lambda}$	Transmission scheduling plan.	$\theta_{k,g}^{\text{UG}}$	Inclination angle between the UAV and the g-th GN.
$\mathbf{\Omega}$	Recharge scheduling plan.	$\varphi_{k,g}^{\text{UG}}$	Azimuth angle between the UAV and the g-th GN.
$L_{n,g}^{I}$	Communication loss between the CubeSat and the g-th GN.	$\mathbf{h}_{k,g}$	Channel vector of the UAV-GN WPT link with Rician fading.
$G_{n,g}^{\text{S}}, G_{n,g}^{\text{G}}$	Antenna gain of LEO CubeSat and GN.	κ	Rician K-factor.
ζ	Free space phase constant.	$\gamma_{k,g}$	Channel gain of the UAV-GN WPT link.
ϱ	Effective radius of the CubeSat antenna.	$E_{k,g}$	Energy harvested by the g-th GN, expressed in Joules.
f^{SG}, f^{UG}	Carrier frequencies in Hertz.	$P, \overline{P}$	Transmission power of the UAV and the GNs in Watts.

TABLE 5.1: Main notations used in this work.

5.2 System Model

The entire mission, depicted in Figure 5.1, is divided into two phases. The first one considers a UAV wirelessly charging a set of G low-power GNs, while the second comprises the transmission of sensed data from the nodes to a LEO CubeSat.

The first phase is uniformly split into K timeslots of duration δ seconds each. The UAV flies at a fixed height z^{U} and follows a discretized trajectory, denoted by $\mathbf{q}_k^{\text{U}} = [x_k^{\text{U}}, y_k^{\text{U}}]^{\mathsf{T}} \in \mathbb{R}^2$, at a velocity of $\mathbf{v}_k^{\text{U}} \in \mathbb{R}^2$, with $k = 1, \ldots, K$. The GNs are uniformly deployed over an area of interest with a diameter equal to d^{A} and can be in either one of these three states: energy harvesting, data upload, and idle. Moreover, each one is placed at known coordinates denoted by $\mathbf{q}_g^{\text{G}} = \left[x_g^{\text{G}}, y_g^{\text{G}}\right]^{\mathsf{T}} \in \mathbb{R}^2$, with $g = 1, \ldots, G$. Therefore, it is possible to define the inclination and azimuth angles, i.e, $\theta_{k,g}^{\text{UG}}$ and $\varphi_{k,g}^{\text{UG}}$, between the g-th GN and the UAV as

$$\theta_{k,g}^{\text{UG}} = \arccos \frac{z^{\text{U}}}{d_{k,g}^{\text{UG}}}, \quad \varphi_{k,g}^{\text{UG}} = \arctan 2 \frac{y_k^{\text{U}} - y_g^{\text{G}}}{x_k^{\text{U}} - x_g^{\text{G}}}, \tag{5.1}$$

and corresponding distance as:

$$d_{k,g}^{\text{UG}} = \sqrt{\|\mathbf{q}_k^{\text{U}} - \mathbf{q}_g^{\text{G}}\|^2 + (z^{\text{U}})^2}. \tag{5.2}$$

Similarly to the former, also the second phase is split into N equal timeslots of duration δ seconds. The LEO CubeSat is assumed to be at constant altitude z^{S}, following a sun-synchronous circular orbit, denoted by $\mathbf{q}_n^{\text{S}} = [x_n^{\text{S}}, y_n^{\text{S}}]^{\mathsf{T}} \in \mathbb{R}^2$, with $n = 1, \ldots, N$, at steady speed $\mathbf{v}^{\text{S}} \in \mathbb{R}^2$.

Thus, the inclination $\theta_{n,g}^{\text{SG}}$ and azimuth $\varphi_{n,g}^{\text{SG}}$ angles, between the g-th GN and the LEO CubeSat read:

$$\theta_{n,g}^{\text{SG}} = \arccos \frac{z^{\text{S}}}{d_{n,g}^{\text{SG}}}, \quad \varphi_{n,g}^{\text{SG}} = \arctan 2 \frac{y_n^{\text{S}} - y_g^{\text{G}}}{x_n^{\text{S}} - x_g^{\text{G}}}, \tag{5.3}$$

where the CubeSat-GN distance $d_{n,g}^{\text{SG}}$, also known as slant range [221], can be expressed as

$$d_{n,g}^{\text{SG}} = \sqrt{r^2 \sin^2 \vartheta_{n,g}^{\text{SG}} + (z^{\text{S}})^2 + 2z^{\text{S}} r} - r \sin \vartheta_{n,g}^{\text{SG}}, \tag{5.4}$$

with r representing the Earth's radius and $\vartheta_{n,g}^{\text{SG}} = \frac{\pi}{2} - \theta_{n,g}^{\text{SG}}$ being the elevation angle. Note that, $0 \leq \vartheta_{n,g}^{\text{SG}} \leq \pi/2$ and specifically $\vartheta_{n,g}^{\text{SG}} = 0$ at the sunrise and the sunset, while $\vartheta_{n,g}^{\text{SG}} = \pi/2$

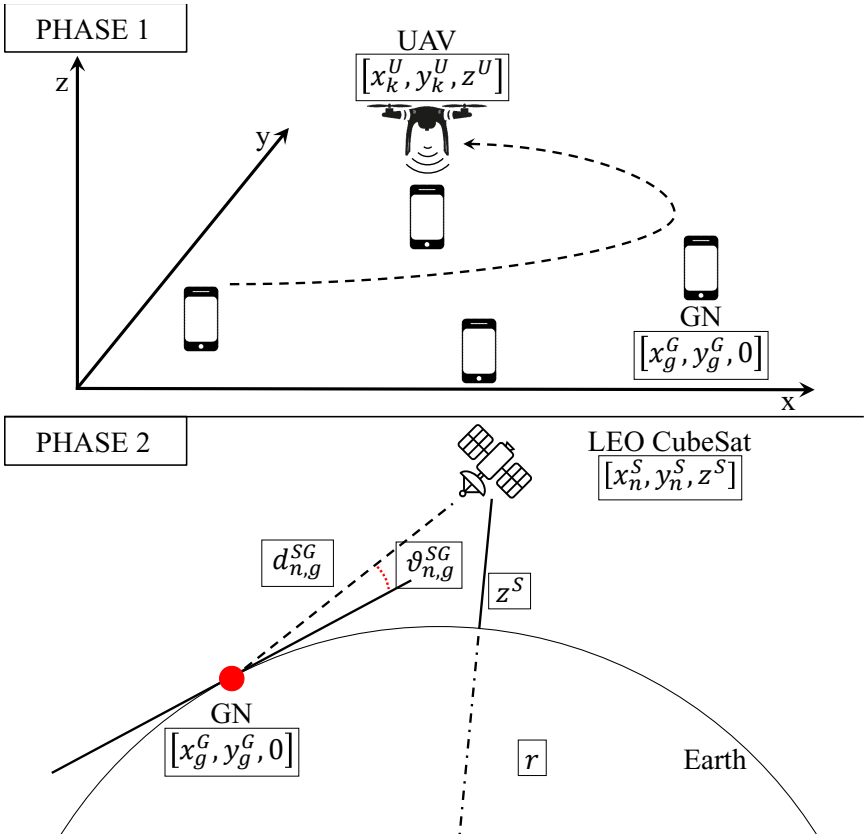

FIGURE 5.1: Reference scenario.

when the CubeSat is over the GNs. Since the altitude of the CubeSat is fixed, $d_{n,g}^{\text{SG}}$ depends only on the elevation angle. Finally, according to the scheduling plan $\mathbf{\Lambda} = (\lambda_{n,g}) \in \{0,1\}^{N \times G}$, if the energy harvested in the first phase is sufficient, then a GN can transmit the sensed data in the second one.

5.3 Drone Model

The UAV is equipped with an Uniform Planar Array (UPA), with $S = L \times W$ antenna elements, which works in one of the resonant frequencies of the GNs' monopole antenna. Beamforming is adopted in order to maximize the power transfer to the GN of interest. Typically, the air-to-ground links are characterized by a strong LoS component. However, the multi-path fading caused by reflections on the ground is not negligible. Therefore, the Rician distribution is adopted to capture both LoS and NLoS components [222], thus granting a realistic representation of the UAV-GN channel. Consequently, following Rician fading, the channel vector for the Multiple-Input Single-Output (MISO) link between the UAV and the g-th GN, characterized by the Rician K-factor κ, can be modeled as:

$$\mathbf{h}_{k,g} = \sqrt{\frac{\kappa}{\kappa+1}}\bar{\mathbf{h}}_{k,g} + \sqrt{\frac{1}{\kappa+1}}\tilde{\mathbf{h}}_{k,g} \in \mathbb{C}^{S \times 1}, \tag{5.5}$$

where

$$\bar{\mathbf{h}}_{k,g} = \left[1, e^{-j\ell d \sin\theta^{\text{UG}}_{k,g} \cos\varphi^{\text{UG}}_{k,g}}, \ldots, e^{-j(W-1)\ell d \sin\theta^{\text{UG}}_{k,g} \cos\varphi^{\text{UG}}_{k,g}}\right]^{\mathsf{T}} \otimes \left[1, e^{-j\ell d \sin\theta^{\text{UG}}_{k,g} \sin\varphi^{\text{UG}}_{k,g}}, \ldots, e^{-j(L-1)\ell d \sin\theta^{\text{UG}}_{k,g} \sin\varphi^{\text{UG}}_{k,g}}\right]^{\mathsf{T}},$$

is the LoS deterministic component, which describes the large-scale fading phenomena, and $\tilde{\mathbf{h}}_{k,g} \sim \mathcal{CN}(\mathbf{0}, \mathbf{I}_S)$ is the NLoS stochastic fluctuation due to multi-path propagation. Moreover, d is the distance between each element of the UAV's UPA, $\ell = \frac{2\pi}{c} f^{\text{UG}}$, c is the speed of light, and f^{UG} the carrier frequency. Given the channel model description, the gain between the UAV and each GN can be expressed as:

$$\gamma_{k,g} = \left| \sqrt{\beta \left(d^{\text{UG}}_{k,g}\right)^{-2}} \mathbf{w}_k^{\mathsf{H}} \mathbf{h}_{k,g} \right|^2, \tag{5.6}$$

where β denotes the channel power gain at the reference distance of 1 m, and $\mathbf{w}_k \in \mathbb{C}^{S\times 1}$ is the beam-forming vector.

The energy harvested by each g-th GN from the UAV can be non-linearly modeled [217], [220] as:

$$E_{k,g} = \frac{\alpha_0 P \delta \gamma_{k,g}}{\alpha_1 P \gamma_{k,g} + \alpha_1^2}, \tag{5.7}$$

where P is the transmission power of the UAV, and $\alpha_0 = 0.399$, $\alpha_1 = 0.826$ are positive constants determined in [217], [223]. Note that the adopted non-linear model is preferred with respect to a linear one, since it improves the overall accuracy and better estimates the time required to recharge each GN.

5.4 Satellite Model

This Section discusses the model adopted to describe the uplink communication between the GNs and the LEO CubeSat, to derive an expression of the link budget, which is then employed to obtain the reciprocal visibility time, and hence the mission duration. Among the possible channel models available in the scientific literature [224], the proposed one aligns with the specifications outlined in 3GPP TR 38.811 [90]. It is worth mentioning that, since the locations of GNs and the trajectory of the satellite are known, a compensation of the frequency shift introduced by the Doppler effect can be always performed, and hence it is not taken into account. Moreover, the considered uplink channel is typically characterized by a large elevation angle of the LEO CubeSat with respect to GNs [225], thus leading to a communication link dominated by a strong LoS component and hence a negligible slow fading. Besides, the satellite is distant several hundred kilometers from the nodes, and hence the channel is subject to a significant pathloss which makes the multi-path effect negligible [226].

To avoid interference among different nodes, the communication system has been designed in a TDMA fashion, such that at most one node per timeslot can communicate with the LEO CubeSat. This comes with the advantage, differently from Frequency Division Multiple Access (FDMA), that the GNs can effectively exploit all the available bandwidth. Each GN employs a COTS horizontally-oriented monopole antenna, assumed to be lossless, with linear polarization that operates at frequency f^{SG} in the S-band [166]. In particular, the

antenna gain [166] can be expressed solely as function of the elevation angle $\vartheta_{n,g}^{\mathrm{SG}}$:

$$G_{n,g}^{\mathrm{G}} = 4\,\frac{\cos^2\left(\frac{\pi}{2}\cos\vartheta_{n,g}^{\mathrm{SG}}\right)}{\sin^2\vartheta_{n,g}^{\mathrm{SG}}\int_0^{\pi}\frac{\cos^2\left(\frac{\pi}{2}\cos\vartheta\right)}{\sin\vartheta}d\vartheta}. \tag{5.8}$$

Likewise, the LEO CubeSat is equipped with a lossless circular patch antenna, whose gain [166] can be expressed as:

$$G_{n,g}^{\mathrm{S}} = 4\,\frac{\cos^2\varphi_{n,g}^{\mathrm{SG}}J_{02}'^2 + \cos^2\theta_{n,g}^{\mathrm{SG}}\sin^2\varphi_{n,g}^{\mathrm{SG}}J_{02}^2}{\int_0^{\pi/2}(J_{02}'^2 + \cos^2\theta J_{02}^2)\sin\theta d\theta}. \tag{5.9}$$

Specifically, J_{02}' and J_{02} read:

$$J_{02}' = J_0(\zeta\varrho\sin\theta_{n,g}^{\mathrm{SG}}) - J_2(\zeta\varrho\sin\theta_{n,g}^{\mathrm{SG}}), \tag{5.10}$$

$$J_{02} = J_0(\zeta\varrho\sin\theta_{n,g}^{\mathrm{SG}}) + J_2(\zeta\varrho\sin\theta_{n,g}^{\mathrm{SG}}), \tag{5.11}$$

with ζ being the free space phase constant and ϱ the effective radius.

Furthermore, the channel is characterized by different impairments [167] which can be modeled as follows:

$$L_{n,g}^{\mathrm{I}} = L_{n,g}^{\mathrm{A}}\,L_{n,g}^{\mathrm{R}}\,L_{n,g}^{\mathrm{Sc}}\,L^{\mathrm{P}}. \tag{5.12}$$

In particular, $L_{n,g}^{\mathrm{I}}$ is estimated by taking into account the air attenuation and the atmospheric gas absorption $L_{n,g}^{\mathrm{A}}$ [168], [171], [172], the rainfall droplet $L_{n,g}^{\mathrm{R}}$ [169], [170], the scintillation attenuation $L_{n,g}^{\mathrm{Sc}}$ [166], and the polarization attenuation L^{P} [166]. The transmitted signal of each GN undergoes polarization rotation during the propagation in the ionosphere. It means that the signal may be polarized differently than intended on the satellite side. This phenomenon can be mitigated by using a circular-polarized signal, causing a maximum misalignment of $\pi/4$, which leads to $L^{\mathrm{P}} = 2$. Therefore, the combination of (5.8), (5.9), and (5.12) leads to the definition of the link budget [167]:

$$\chi_{n,g}^{\mathrm{SG}} = \frac{\overline{P}\,G_{n,g}^{\mathrm{S}}\,G_{n,g}^{\mathrm{G}}}{L_{n,g}^{\mathrm{FS}}\,L_{n,g}^{\mathrm{I}}}, \tag{5.13}$$

where $\overline{P}$ defines the transmission signal power of the GN. Further, $L_{n,g}^{\mathrm{FS}}$ [90] describes the free space propagation loss, which depends on the carrier frequency* f^{SG} and the GN-CubeSat distance $d_{n,g}^{\mathrm{SG}}$.

Moreover, the receiver sensitivity [167] represents the noise power of the link and is defined as

$$\Upsilon_{n,g}^{\mathrm{SG}} = k_B\,\eta_{n,g}^{\mathrm{SG}}\,B, \tag{5.14}$$

with k_B being the Boltzmann constant, B the channel bandwidth, and η^{SG} describing the equivalent system noise temperature for both antenna and receiver noise.

Once the link budget and the receiver sensitivity are defined, it is possible to obtain the SNR as:

$$\Gamma_{n,g}^{\mathrm{SG}} = \frac{\chi_{n,g}^{\mathrm{SG}}}{\Upsilon_{n,g}^{\mathrm{SG}}}. \tag{5.15}$$

To evaluate the coverage of a radio access technology, the 3GPP introduced the MCL [227], which expresses the maximum loss in conducted power level, that a system may tolerate to

*It is assumed that f^{UG} and f^{SG} are different carriers defined in the S-band, such that the GN can employ the same monopole antenna for both information transmission and energy harvesting without interference.

properly establish a connection:

$$MCL = \frac{\overline{P}}{\hat{P}}, \tag{5.16}$$

where $\hat{P}$ is the minimum power required by the CubeSat to correctly decode the received signal. Therefore, it is possible to express the current uplink coupling loss for the g-th GN in the n-th timeslot as:

$$\Delta_{n,g}^{\text{SG}} = \frac{\overline{P}}{\chi_{n,g}^{\text{SG}}}. \tag{5.17}$$

Specifically, the GN is able to communicate with the CubeSat if and only if

$$\Delta_{n,g}^{\text{SG}} \leq MCL. \tag{5.18}$$

It is worth noting that $\Delta_{n,g}^{\text{SG}}$ is inversely proportional to $d_{n,g}^{\text{SG}}$, and hence to the elevation angle $\vartheta_{n,g}^{\text{SG}}$. The minimum elevation angle able to satisfy (5.18) is denoted as $\vartheta_{\text{MIN}}^{\text{SG}}$ and the period during $\vartheta_{\text{MIN}}^{\text{SG}} \leq \vartheta_{n,g}^{\text{SG}}$ is called reciprocal visibility time. Although the function of the coupling loss is dependent on non-invertible components [168]–[172], $\vartheta_{\text{MIN}}^{\text{SG}}$ can be obtained by intersecting the coupling loss curve with the MCL thresholds defined by the standard, also called coverage classes, shown in Figure 5.2.

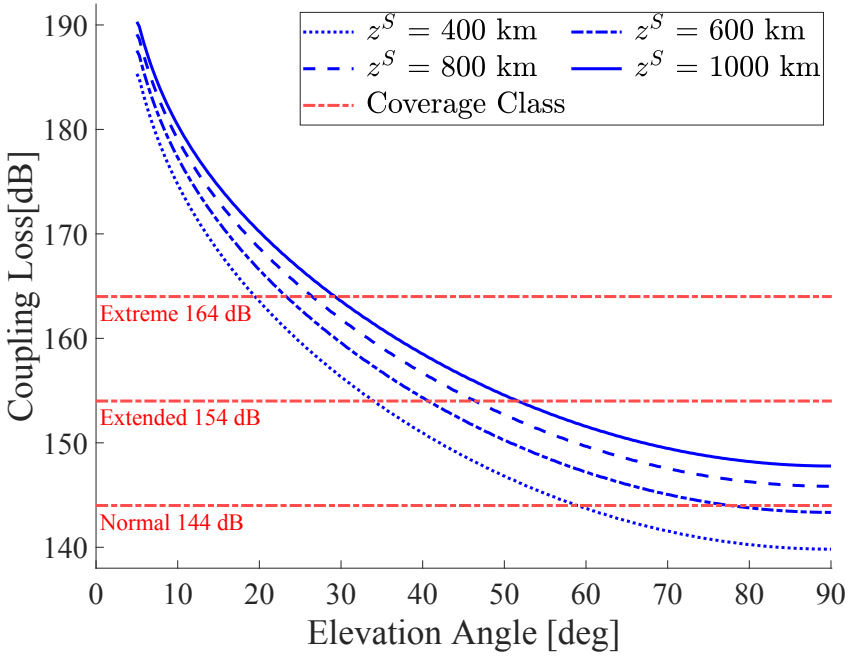

FIGURE 5.2: Maximum Coupling Loss thresholds of the coverage classes for different CubeSat's altitudes [163].

Proposition 1. *Without loss of generality, if the diameter of the area of interest is much smaller than the footprint of the CubeSat, its distance from each GN, defined in* (5.4)*, is approximately the same and can be expressed as* d_n^{SG}.

As a consequence of Proposition 1, it is considered the same reciprocal visibility period for each GN, which in turn defines the total duration of the second phase δN, as derived hereby.

The orbital period T^{S} of the CubeSat is denoted by the following equation:

$$T^{\text{S}} = 2\pi\sqrt{\frac{(r + z^{\text{S}})^3}{G^{\text{E}}\, M^{\text{E}}}}, \tag{5.19}$$

where M^{E} and G^{E} denote the mass and the gravitational constant of the Earth, respectively. Furthermore, the orbital speed v^{S} of an Earth's satellite is:

$$v^{\mathrm{S}} = \sqrt{\frac{G^{\mathrm{E}}\, M^{\mathrm{E}}}{(r + z^{\mathrm{S}})}} = \frac{2\pi(r + z^{\mathrm{S}})}{T^{\mathrm{S}}}. \tag{5.20}$$

Once defined the orbital speed v^{S}, it is necessary to compute the speed v^{F} of the covered area at the Earth side, namely footprint, as follows:

$$v^{\mathrm{F}} = v^{\mathrm{S}} - 2\pi\frac{z^{\mathrm{S}}}{T^{\mathrm{S}}} = 2\pi\frac{r}{T^{\mathrm{S}}}. \tag{5.21}$$

Moreover, the footprint diameter F^S can be expressed by:

$$F^{\mathrm{S}} = 2\, z^{\mathrm{S}}\, \tan(\theta^{\mathrm{SG}}_{\mathrm{MIN}}). \tag{5.22}$$

with $\theta^{\mathrm{SG}}_{\mathrm{MIN}} = \frac{\pi}{2} - \vartheta^{\mathrm{SG}}_{\mathrm{MIN}}$. Therefore, the duration δN, which corresponds to the visibility time T^{V} can be obtained as:

$$T^{\mathrm{V}} \triangleq \delta N = \frac{F^{\mathrm{S}}}{v^{\mathrm{F}}} = \frac{2\, z^{\mathrm{S}}\, \tan(\theta^{\mathrm{SG}}_{\mathrm{MIN}})}{r}\sqrt{\frac{(r + z^{\mathrm{S}})^3}{G^{\mathrm{E}}\, M^{\mathrm{E}}}}. \tag{5.23}$$

Finally, as a further consequence of Proposition 1, it is also possible to consider the same channel condition for each GN, and hence approximate Equation 5.15 as follows:

$$\Gamma^{\mathrm{SG}}_{n} \simeq \Gamma^{\mathrm{SG}}_{n,g} \forall g. \tag{5.24}$$

Consequently, recalling the well-known Shannon formula [228], the maximum achievable data rate of a CubeSat-GN link is

$$R^{\mathrm{SG}}_{n} = B \log_2(1 + \Gamma^{\mathrm{SG}}_{n}). \tag{5.25}$$

5.5 Wireless Power Transfer Optimization

Define $\mathbf{Q} = \{\mathbf{q}^{\mathrm{U}}_k\}_{k=1}^K$, $\mathbf{V} = \{\mathbf{v}^{\mathrm{U}}_k\}_{k=1}^K$, and $\mathbf{W} = \{\mathbf{w}_k\}_{k=1}^K$. The first phase concerning the kinematics of the drone and the node battery charging can be optimized by solving the following problem:

$$\max_{\eta_1, \mathbf{W}, \mathbf{Q}, \mathbf{V}} \eta_1 \quad \textbf{s.t.} \tag{5.26a}$$

$$\eta_1 \leq \sum_{k=1}^{K} E_{k,g}, \quad \forall g : 1, \ldots, G, \tag{5.26b}$$

$$\mathbf{q}^{\mathrm{U}}_{k+1} = \mathbf{q}^{\mathrm{U}}_k + \delta \mathbf{v}^{\mathrm{U}}_k, \quad \forall k : 1, \ldots, (K-1), \tag{5.26c}$$

$$\mathbf{q}^{\mathrm{U}}_1 = \mathbf{q}^{\mathrm{U}}_K = \mathbf{q}^{\mathrm{U}}_0, \tag{5.26d}$$

$$\mathbf{v}_1 = \mathbf{v}_K = \mathbf{0}, \tag{5.26e}$$

$$\|\mathbf{v}_k\| \leq v_{\mathrm{MAX}}, \quad \forall k : 1, \ldots, K, \tag{5.26f}$$

$$\|\mathbf{v}_{k+1} - \mathbf{v}_k\| \leq a_{\mathrm{MAX}}\delta, \quad \forall k : 1, \ldots, (K-1). \tag{5.26g}$$

Problem (5.26) aims at fairly maximizing the battery charge of all the nodes through constraint (5.26b). Equation (5.26c) describes the kinematics of the drone, with the given initial and final point of the trajectory $\mathbf{q}_0^{\mathrm{U}}$ and the correspondent speed imposed by (5.26d) and (5.26e), respectively. Moreover, (5.26f) and (5.26g) limit the maximum speed and acceleration of the flight by v_{MAX} and a_{MAX}, respectively. However, (5.26) is a MINLP problem, and hence intractable in the present form. In particular, the stochastic formulation of the channel gain requires a dedicated strategy to derive an optimal solution. Therefore, the original problem is divided in two sub-problems, which are then alternately solved until convergence to a quasi-optimal solution is achieved.

5.5.1 Sub-Problem 1: Charge Plan Optimization

The first sub-problem aims at optimizing the beamforming vectors $\mathbf{W}$, such that the amount of energy harvested by the GNs is maximized in a fairly manner, as follows:

$$\max_{\eta_1, \mathbf{W}} \eta_1 \quad \textbf{s.t.} \quad (5.26b). \tag{5.27}$$

Still, (5.27) is non-convex in $\mathbf{W}$ due to constraint (5.26b), which is affected by the stochastic nature of the energy term $E_{k,g}$. To tackle this issue, the Maximum Ratio Combining [228] approach is adopted as beamforming strategy, which is indeed the optimal solution to maximize the energy harvested by a single GN:

$$\mathbf{w}_k = \frac{\mathbf{h}_{k,g}}{\|\mathbf{h}_{k,g}\|}. \tag{5.28}$$

Therefore, it is necessary to define a charging plan $\mathbf{\Omega} = (\omega_{k,g}) \in \{0,1\}^{K \times G}$ describing which node is charged in each timeslot[†]. Hence, when a GN is selected, i.e., $\omega_{k,g} = 1$, the energy term $E_{k,g}$ can be rearranged combining (5.7) and (5.28) as

$$\widetilde{E}_{k,g} = \frac{\alpha_0 P \delta \beta \|\mathbf{h}_{k,g}\|^2}{\alpha_1 P \beta \|\mathbf{h}_{k,g}\|^2 + \alpha_1^2 \left(d_{k,g}^{\mathrm{UG}}\right)^2}, \tag{5.29}$$

which, however, maintains a stochastic nature. Given an Out-of-Service probability ε, the minimum guaranteed energy $\overline{E}_{k,g}$ harvested by a GN, i.e, $\omega_{k,g} = 1$, can be obtained as follows:

$$\begin{aligned} \mathbb{P}\left(\widetilde{E}_{k,g} < \overline{E}_{k,g}\right) &= \mathbb{P}\left(\|\mathbf{h}_{k,g}\|^2 < \frac{\alpha_1^2 \left(d_{k,g}^{\mathrm{UG}}\right)^2 \overline{E}_{k,g}}{P\beta\left(\alpha_0 \delta - \alpha_1 \overline{E}_{k,g}\right)}\right) \\ &= F\left(\frac{\alpha_1^2 \left(d_{k,g}^{\mathrm{UG}}\right)^2 \overline{E}_{k,g}}{P\beta\left(\alpha_0 \delta - \alpha_1 \overline{E}_{k,g}\right)}\right) \leq \varepsilon, \end{aligned} \tag{5.30}$$

with $F(\cdot)$ describing the Cumulative Distribution Function (CDF) of the stochastic energy expression $\widetilde{E}_{k,g}$ in (5.29). It is worth noting that the latter follows a non-central chi-squared distribution, and the correspondent CDF is

$$F(u) = 1 - Q_S\left(\sqrt{2S\kappa}, \sqrt{2(\kappa+1)u}\right), \tag{5.31}$$

[†]In this work, the side lobes that can eventually point to/illuminate other GNs are not considered, since their contribution is negligible.

where $Q_S(\cdot)$ is the Marcum Q-function of order S. Considering the worst-case scenario, in

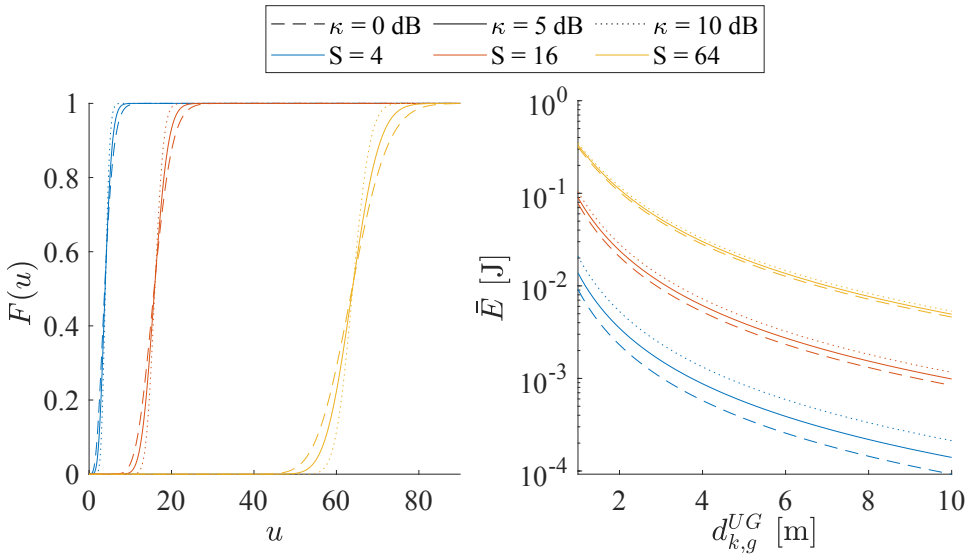

FIGURE 5.3: The CDF of the stochastic harvested energy $\widetilde{E}_{k,g}$ (left) and the minimum harvested energy $\overline{E}_{k,g}$ (right) with $\varepsilon = 0.01$ and $P = 49\,\mathrm{dBm}$, for different number of antenna elements S and K-factor κ.

which (5.30) holds with equality, the final energy term $\overline{E}_{k,g}$ can be derived as

$$\overline{E}_{k,g} = \frac{\alpha_0 P \delta \beta \overline{Q}_S^2}{\alpha_1 P \beta \overline{Q}_S^2 + 2\alpha_1^2 \left(d_{k,g}^{\mathrm{UG}}\right)^2 (\kappa + 1)}, \tag{5.32}$$

$$\overline{Q}_S \triangleq Q_S^{-1}\left(\sqrt{2S\kappa}, 1 - \varepsilon\right), \tag{5.33}$$

where $Q_S^{-1}(\cdot)$ is the inverse Marcum Q-function, which can be computed numerically or via analytical approximation. Figure 5.3 shows the CDF of $\widetilde{E}_{k,g}$ (left) defined in (5.31) and the derived energy term of $\overline{E}_{k,g}$ (right) obtained in (5.32).

Therefore, problem (5.27) can be rearranged as

$$\max_{\eta_1, \mathbf{\Omega}} \eta_1 \quad \textbf{s.t.} \tag{5.34a}$$

$$\mathbf{\Omega} \in \{0,1\}^{K \times G} \tag{5.34b}$$

$$\eta_1 \leq \sum_{k=1}^{K} \omega_{k,g} \overline{E}_{k,g}, \quad \forall g : 1, \ldots, G, \tag{5.34c}$$

$$\sum_{g=1}^{G} \omega_{k,g} \leq 1, \quad \forall k : 1, \ldots, K, , \tag{5.34d}$$

where $E_{k,g}$ in (5.26b) has been substituted with (5.32). Moreover, constraints (5.34b) and (5.34d) impose that the drone can only recharge one sensor per timeslot. Still, (5.34) is non-convex due to the presence of the binary charging plan $\mathbf{\Omega}$. To cope with this issue, several works in the scientific literature employ only the relaxation of the integer constraint followed by a rounding procedure of the obtained values, which often results to be infeasible or far from optimal in the best case. To avoid such a scenario and to derive a quasi-integer solution, it is jointly employed (i) the relaxation of (5.34b), and (ii) an additional term in the objective

function which encourages the adoption of a binary solution:

$$\max_{\eta_1,\mathbf{\Omega}} \eta_1 + \rho_1 \sum_{k=1}^{K}\sum_{g=1}^{G}\left(\omega_{k,g} - \frac{1}{2}\right)^2 \quad \textbf{s.t.} \tag{5.35a}$$

$$0 \leq \omega_{k,g} \leq 1, \quad \forall k : 1,\dots,(K-1), \forall g : 1,\dots,G, \tag{5.35b}$$

$$(5.34c), (5.34d).$$

In the above formulation, $\rho_1 \in \mathbb{R}^+$ acts as a weight that, if too low makes the additional term ineffective, otherwise if too high causes η_1 to become irrelevant. In the next Section, an empirical rule for the problem scaling, including ρ_1, will be discussed. Still, the objective function is non-convex with respect to $\mathbf{\Omega}$. To cope with this issue, the SCA technique is employed. Recalling that the first-order Taylor expansion is a global understimator for convex functions, it is possible to lower-bound the objective function for the local point $\overline{\omega}_{k,g}$, thus leading to the final formulation:

$$\max_{\eta_1,\mathbf{\Omega}} \eta_1 + \rho_1 \sum_{k=1}^{K}\sum_{g=1}^{G}\omega_{k,g}(2\overline{\omega}_{k,g} - 1) \quad \textbf{s.t.} \tag{5.36}$$

$$(5.34c), (5.34d), (5.35b).$$

It can be verified that (5.36) is convex. The scheduling plan is obtained by updating the value of the local point with the solution of the previous iteration, until convergence to a prescribed accuracy ξ is achieved.

Finally, since $\mathbf{\Omega} \in [0,1]^{K\times G}$, a round operation is performed. In particular, for each timeslot k, only the $\omega_{k,g}$ that has the maximum value is set to 1, while the others to 0. Therefore, constraints (5.34b) and (5.34d) are satisfied.

5.5.2 Sub-Problem 2: Drone Kinematics Optimization

Given the charging plan $\mathbf{\Omega}$ and the other results derived above, the trajectory-related parameters and the transmission plan are hereby optimized. Note that η_1 is re-optimized to derive a fair solution from the energy-harvesting perspective. The second sub-problem reads:

$$\max_{\eta_1,\mathbf{Q},\mathbf{V}} \eta_1 \quad \textbf{s.t.} \tag{5.37}$$

$$(5.34c), (5.26c) - (5.26g),$$

which however is non-convex due to the presence of the squared distance term $d_{k,g}^{\text{UG}}$ at the denominator of $\overline{E}_{k,g}$ in constraints (5.34c). To tackle this issue, it is first necessary to introduce a set of slack variables $\mathbf{B} = \{b_{k,g} \geq 0\}$. Then, recalling the definition of the distance in (5.2), the slack variables are lower-bounded such that

$$\left(d_{k,g}^{\text{UG}}\right)^2 \leq b_{k,g}. \tag{5.38}$$

Similarly to the previous sub-problem, the SCA technique is employed which leads to the following inequality chain

$$\begin{aligned}\overline{\overline{E}}_{k,g} &= \frac{\alpha_2}{\alpha_3+\alpha_4\bar{b}_{k,g}} - \frac{\alpha_2\alpha_4}{\left(\alpha_3+\alpha_4\bar{b}_{k,g}\right)^2}(b_{k,g}-\bar{b}_{k,g}) \\ &\overset{(a)}{\leq} \frac{\alpha_2}{\alpha_3+\alpha_4 b_{k,g}} \overset{(b)}{\leq} \overline{E}_{k,g},\end{aligned} \tag{5.39}$$

where (a) is due to the first order Taylor expansion, (b) follows from (5.38), $\alpha_2 \triangleq \alpha_0 P\delta\beta\overline{Q}_S^2$, $\alpha_3 \triangleq \alpha_1 P\beta\overline{Q}_S^2$, and $\alpha_4 \triangleq 2\alpha_1^2(\kappa+1)$. Hence, problem (5.37) is equivalent to

$$\max_{\eta_1,\mathbf{Q},\mathbf{V},\mathbf{B}} \eta_1 \quad \textbf{s.t.} \tag{5.40a}$$

$$\eta_1 \leq \sum_{k=1}^{K} \omega_{k,g}\overline{\overline{E}}_{k,g}, \quad \forall g:1,\ldots,G, \tag{5.40b}$$

$$(5.26c)-(5.26g),$$

because in order to maximize the objective function it is necessary to maximize the new energy term in (5.39) and hence minimize $b_{k,g}$, until (5.38) holds with equality. Therefore, problem (5.40) is convex with respect to $\mathbf{Q}$, $\mathbf{V}$, and $\mathbf{B}$ and it is iteratively solved until a prescribed accuracy ξ is achieved.

5.5.3 Overall Optimization Procedure

A quasi-optimal solution for the original problem (5.26) is derived by iteratively solving the two discussed sub-problems. It is worth specifying that, to avoid a waste of irradiated power, at the end of the entire procedure, the recharging plan $\mathbf{\Omega}$ is further improved by setting to zero the entries which do not satisfy a minimum harvested energy threshold ν, which typically takes place when the drone is too far from a specific node (as can be seen in Figure 5.3). For what concern the time complexity, the first sub-problem is in the order of $\mathcal{O}\left(I_1(KG+1)^{3.5})\right)$, where I_1 is the number of iterations required by SCA. Similarly, the second sub-problem has a complexity of $\mathcal{O}\left(I_2(4K+KG+1)^{3.5}\right)$. Therefore, the joint complexity is given by $\mathcal{O}\left(M_1(I_1(KG+1)^{3.5}+\ I_2(4K+KG+1)^{3.5})\right)$, where M_1 is denotes the number of iterations required to converge. More details can be found in Algorithm 1.

Algorithm 1 Optimization procedure.

Set $\mathbf{q}_g^{\mathrm{G}}$ and $\mathbf{q}_k^{\mathrm{S}}$ Compute R_k^{SG} and $\overline{Q}_S$ Initialize $\bar{b}_{k,g}$, $\bar{\omega}_{k,g}$ **for** $m:1,\ldots,M$ **do**
  for $i:1,\ldots,I$ **do**
    Solve (5.36) to obtain the objective function $s_{1,i}$, η_1, and $\mathbf{\Omega}$ $\bar{\omega}_{k,g} \leftarrow \omega_{k,g}\ \forall k,g$ **if** $i>1$ **and** $|s_{1,i}-s_{1,i-1}|/|s_{1,i}|<\xi$ **then**
      $s_{1,m}^* \leftarrow s_{1,i}$; **break**
  end
  Round the optimized $\mathbf{\Omega}$ **for** $i:1,\ldots,I$ **do**
    Solve (5.40) to obtain the objective function $s_{2,i}$, η_1, $\mathbf{Q}$, and $\mathbf{V}$ $\bar{b}_{k,g} \leftarrow b_{k,g}\ \forall k,g$ **if** $i>1$ **and** $|s_{2,i}-s_{2,i-1}|/|s_{2,i}|<\xi$ **then**
      $s_{2,m}^* \leftarrow s_{2,i}$; **break**
  end
  if $m>1$ **and** $|s_{1,m}^*-s_{1,m-1}^*|/|s_{1,m}^*|<\xi$ **and** $|s_{2,m}^*-s_{2,m-1}^*|/|s_{2,m}^*|<\xi$ **then**
    break
  Round and process the optimized $\mathbf{\Omega}$
end

Algorithm 2 Transmission Optimization.

Set $\mathbf{q}_g^{\mathrm{G}}$ and $\mathbf{q}_k^{\mathrm{S}}$ Compute R_k^{SG} and $\overline{Q}_S$ Initialize $\overline{\lambda}_{k,g}$ **for** $i : 1, \ldots, I$ **do**
  Solve (5.42) to obtain the objective function $s_{3,i}$, η_2, and $\mathbf{\Lambda}$ $\overline{\lambda}_{n,g} \leftarrow \lambda_{n,g}\ \forall n, g$ **if** $i > 1$ **and** $|s_{3,i} - s_{3,i-1}|/|s_{3,i}| < \xi$ **then**
    $s_3^* \leftarrow s_{3,i}$; **break**
end
Rectify the optimized $\mathbf{\Lambda}$

5.6 Ground Nodes-Satellite Transmission Optimization

Leveraging the results obtained in the previous optimized phase, i.e., the energy $E_{k,g}$ harvested by the GNs, the second phase encompassing the GNs' transmission scheduling can be optimized by deriving the optimal solution of the following problem:

$$\max_{\eta_2, \mathbf{\Lambda}} \quad \eta_2 \quad \textbf{s.t.} \tag{5.41a}$$

$$\mathbf{\Lambda} \in \{0,1\}^{K \times G} \tag{5.41b}$$

$$\eta_2 \leq \sum_{n=1}^{N} \lambda_{n,g} R_n^{\mathrm{SG}} \quad \forall g : 1, \ldots, G, \tag{5.41c}$$

$$\delta \overline{P} \sum_{n=1}^{N} \lambda_{n,g} \leq \sum_{k=1}^{K} E_{k,g}, \quad \forall g : 1, \ldots, G, \tag{5.41d}$$

$$\sum_{g=1}^{G} \lambda_{n,g} \leq 1, \quad \forall k : 1, \ldots, K. \tag{5.41e}$$

Problem (5.41) focuses on fairly maximizing the sum-rate of all CubeSat-GN links through constraint (5.41c). Moreover, (5.41d) states that a GN can transmit only if enough energy has been harvested. Constraints (5.41b) and (5.41e) impose that only a GN can transmit in each timeslot. However, also (5.41) is a MINLP problem and hence non-convex due to (5.41b), which describes the binary nature of the transmission plan $\mathbf{\Lambda}$. Following the same rationale adopted to convexify problem (5.34), the binary constraint (5.41b) is relaxed and a new constraint is added to the formulation. Again, to encourage the adoption of an integer solution, one more addendum is introduced in the objective function employing the SCA technique, thus leading to:

$$\max_{\eta_2, \mathbf{\Lambda}} \eta_2 + \rho_2 \sum_{n=1}^{N} \sum_{g=1}^{G} \lambda_{n,g} (2\overline{\lambda}_{n,g} - 1) \quad \textbf{s.t.} \tag{5.42a}$$

$$0 \leq \lambda_{n,g} \leq 1, \quad \forall n : 1, \ldots, N, \forall g : 1, \ldots, G, \tag{5.42b}$$

$$(5.41\text{c}) - (5.41\text{e}).$$

The above formulation is convex and it is iteratively solved until a prescribed accuracy ξ is achieved. Similarly to (5.36), $\mathbf{\Lambda}$ needs to be rectified to satisfy (5.41b). However, in this case, $\lambda_{k,g}$ is rounded to 1 only if the value is ≥ 0.99, otherwise it is set to zero. This operation guarantees that the transmission takes place only if the scheduled GN has sufficient energy.

The time complexity associated with the reference problem is in the order of $\mathcal{O}\left(I_3(KG+1)^{3.5})\right)$, where I_3 is the number of iterations required by SCA. More details of the overall proposed algorithm can be found in Algorithm 2.

Parameter	Value	Parameter	Value
K	$\{30, 60\}$ [#]	N	250 [#]
G	$\{5, 10, 15\}$ [#]	B	180 [kHz]
L, W	$\{15, 20\}$ [#]	δ	1 [s]
$\mathbf{q}_0^{\mathrm{U}}$	$[0, -15]$ [m]	$\mathbf{q}_0^{\mathrm{S}}$	$[-795, 0]$ [km]
z^{U}	1 [m]	z^{S}	1000 [km]
v_{MAX}	15 [m/s]	$\mathbf{v}^{\mathrm{S}}$	[6353, 0] [m/s]
a_{MAX}	3 [m/s^2]	$\vartheta_{\mathrm{MIN}}^{\mathrm{SG}}$	52 [deg]
f^{UG}	2.4 [GHz]	f^{SG}	1995 [MHz]
ζ	0.42 [#]	ϱ	3.05 [cm]
η^{SG}	615 [K]	ν	0.005 [#]
ρ_1	0.01[#]	ρ_2	2000 [#]
P	$\{46, 49\}$ [dBm]	$\overline{P}$	23 [dBm]
κ	10 [dB]	MCL	154 [dB]
ξ	10^{-3} [#]	ε	10^{-2} [#]

TABLE 5.2: Parameter settings.

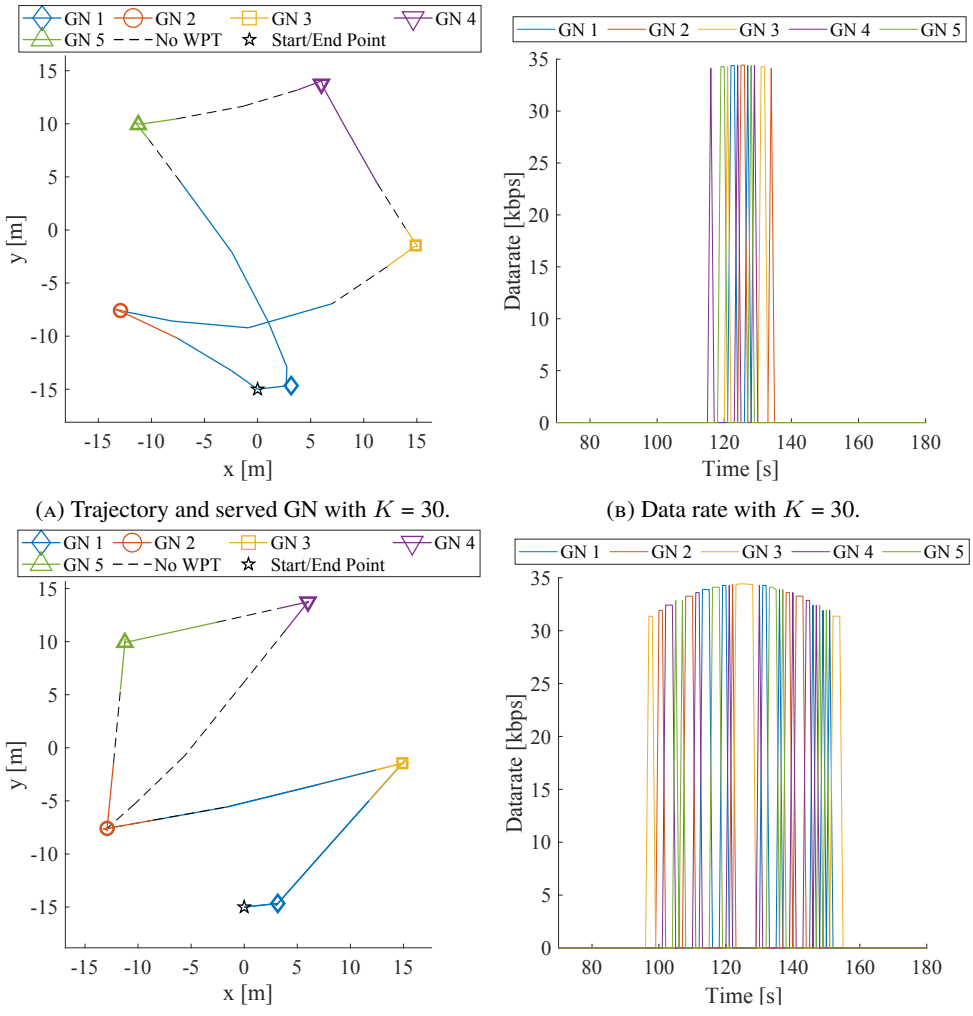

(A) Trajectory and served GN with $K = 30$.

(B) Data rate with $K = 30$.

(C) Trajectory and served GN with $K = 60$.

(D) Data rate with $K = 60$.

FIGURE 5.4: Analysis of the scenario with $G = 5$, $S = 225$, $P = 49\,\mathrm{dBm}$, and $\delta = 1\,\mathrm{s}$.

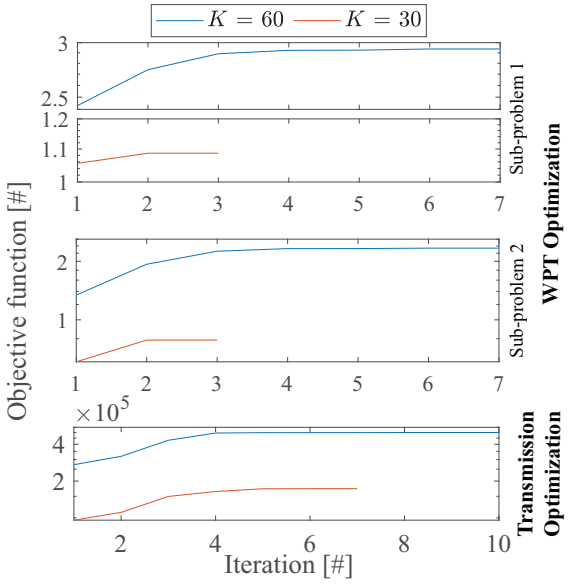

FIGURE 5.5: Convergence of the algorithms with $G = 5$, $S = 225$, $P = 49\,\mathrm{dBm}$, and $\delta = 1\,\mathrm{s}$.

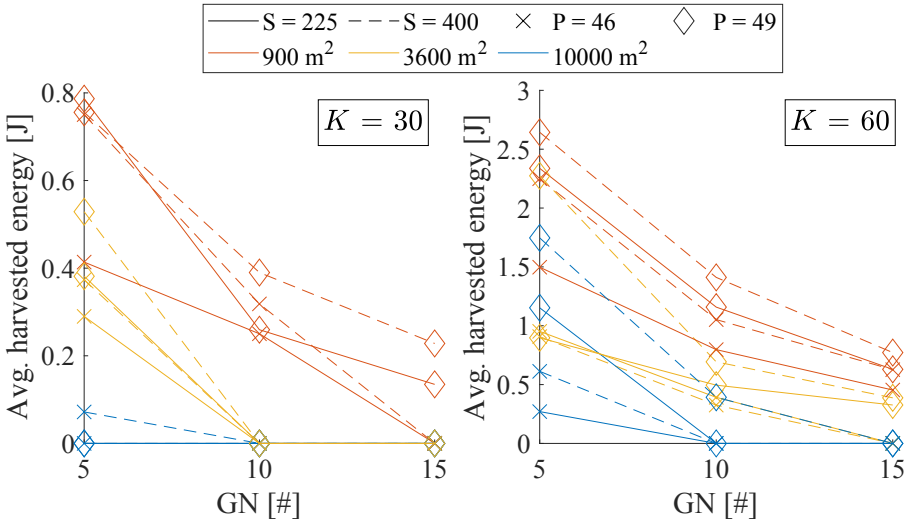

FIGURE 5.6: Average harvested energy for different parameters with $\delta = 1\,\mathrm{s}$.

5.7 Numerical results and Discussion

In this Section, a simulation campaign is carried out to assess the effectiveness of the proposed solution, which consists in sequentially executing Algorithm 1 and Algorithm 2.

The investigated scenarios involve different area sizes, i.e., 30x30 m^2, 60x60 m^2, and 100x100 m^2, in which $\{5,\ 10,\ 15\}$ GNs are uniformly deployed. The LEO CubeSat pursues a trajectory that follows a uniform linear motion, starting from position $\mathbf{q}_0^{\mathrm{S}}$ at velocity $\mathbf{v}^{\mathrm{S}}$. The parameters characterizing the CubeSat-GN link are set according to [193]. Furthermore, considering a noise figure of $5\,\mathrm{dB}$, the equivalent system noise temperature $\eta^{\mathrm{SG}} \simeq 615\,\mathrm{K}$ [166] is the sum of the antenna noise temperature and the receiver noise temperature, which correspond to $290\,\mathrm{K}$ and $150\,\mathrm{K}$, respectively. Moreover, the UAV is equipped with a squared UPA of $\{255,\ 400\}$ elements to wirelessly recharge each GN at $\{46,\ 49\}\,\mathrm{dBm}$.

The transmission power is set in compliance with the ITU-R M.2135-1 Report [229], [230] for a LTE macro-cell deployed in urban and rural areas. All the simulation parameters are summarized in Table 5.2.

A detailed discussion of the results, obtained by varying the aforementioned parameters, is followed by a comparison between the proposed solution and a baseline approach.

5.7.1 Objective function scaling

The normalization of the objective functions of both problems is deemed necessary, since their components have different orders of magnitude, which affect the optimization process, and hence the final solution. The possible values of η_1, given the involved parameters of problem (5.26), range from $\sim 10^{-1}$ to ~ 1, as can be verified by solving the relaxed problem (5.36), with $\rho_1 = 0$. Accordingly, to keep the fairness factor slightly above the additional term introduced to encourage integer solutions, the following $\rho_1 = 10^{-2}$ is adopted. The same rationale is applied for problem (5.42), thus leading to $\rho_2 = 2 \cdot 10^3$.

5.7.2 Analysis of the results

The first scenario considers $G = 5$ GNs recharged by a drone equipped with a UPA of $S = 225$ elements, with $P = 49\,\mathrm{dBm}$ and $K = \{30, 60\}$. Indeed, the goal is to highlight how the duration of the first phase affects the second one in terms of obtained GNs' data rate. In this regard, Figures 5.4a and 5.4c jointly depict (i) the trajectory followed by the drone, and (ii) the GN recharged during the flight, and (iii) the initial position of the UAV, which is coincident with its final one. As it can be seen, in both scenarios, the trajectory paths tend to be straight to save time, which is convenient to reduce the distance between the UAV and the served GN, thus maximizing the energy income. It is worth noting that, thanks to the procedure performed at the end of the recharging phase, the drone does not irradiate power when is too far from the served GN, thus saving energy that would be not efficiently harvested by the nodes.

Furthermore, Figures 5.4b and 5.4d represent the data rate of nodes-satellite communications. It can be observed that the data rates are subject to the pathloss which affects the satellite link. Indeed, the satellite trajectory is designed to firstly approach and then leave the reference area, thus leading to increasing and then decreasing data rates, that visually resemble a parabola. In both configurations, the latter is centered around the mid-point of the mission to maximize the overall sum-rate. However, for higher K, the effective transmission time of the second phase increases and, as a consequence, the shape of the parabola changes. This phenomenon is due to the fact that more energy is harvested in the recharging phase. Therefore, the maximum data rate of $\sim 35\,\mathrm{kbps}$ is achieved always at $\sim 125\,\mathrm{s}$, which corresponds to the instant where the distance is minimized, i.e., the satellite is almost orthogonal to the area. Instead, the minimum data rates achieved are $\sim 34\,\mathrm{kbps}$ for $K = 30$ and $\sim 31\,\mathrm{kbps}$ for $K = 60$. Moreover, according to the constraints (5.41b) and (5.41e) which model the TDMA protocol, the peaks of the curves never overlap.

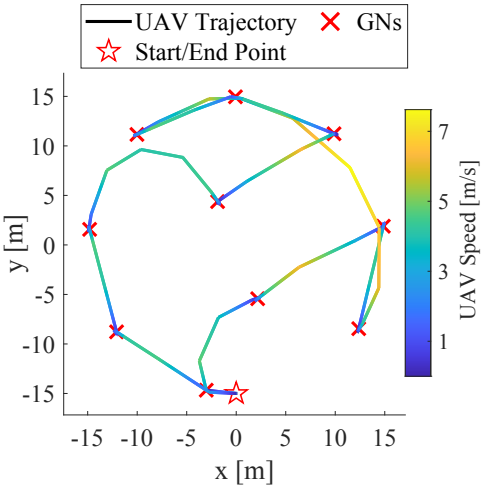

(A) Trajectory and speed. $G = 10$

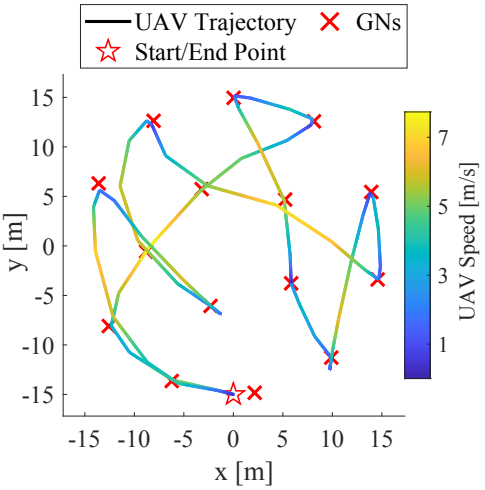

(B) Trajectory and speed. $G = 15$

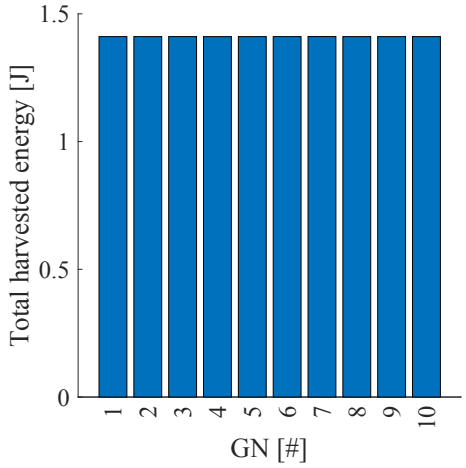

(C) Harvested energy. $G = 10$

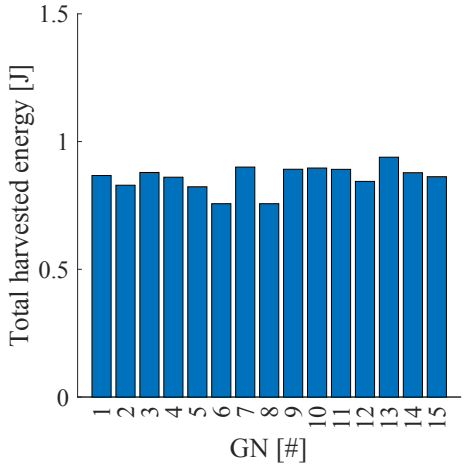

(D) Harvested energy. $G = 15$

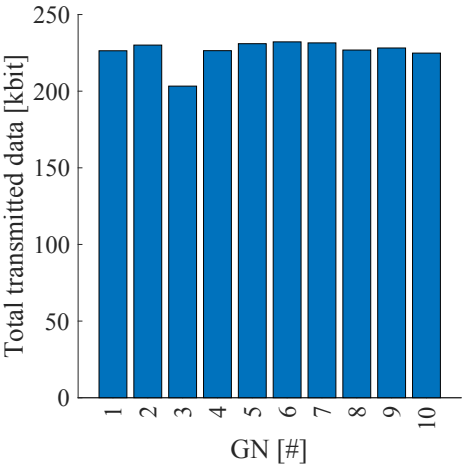

(E) Transmitted rate. $G = 10$

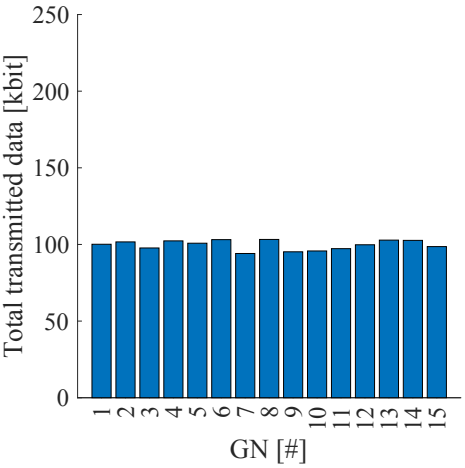

(F) Transmitted rate. $G = 15$

FIGURE 5.7: Analysis of the scenarios with $G = \{10, 15\}$, $S = 400$, $P = 49\,\text{dBm}$, $K = 60$, $\delta = 1\,\text{s}$.

For the sake of completeness, Figure 5.5 shows the convergence curves of the proposed optimization algorithms, specifically related to the first and second phases. It is noteworthy that in the two chosen configurations, Algorithm 1 achieves convergence after 7 iterations at most, while Algorithm 2 after 10 iterations, both with a prescribed accuracy of ξ.

To further investigate the impact on the harvested energy when the parameters involved in the scenario vary, Figure 5.6 shows the average amount collected by a GN. As expected, most of the unfeasible, i.e., no harvested energy, configurations involve a 100x100 m^2 area. Indeed, the speed and acceleration limits of the drone, together with the maximum duration of the second phase, play the most important role in the mission feasibility. Clearly, also the transmission power and the number of antenna elements are aspects that can also zero out the gathered energy, especially for a significant number of GNs. This result is of fundamental importance for the following analysis, since it provides a solid indication of which other configurations can be studied. It is worth mentioning that, across all the examined scenarios, the energy consumption of the UAV, which can be calculated with [231, Eq. 12], is significantly lower than the commonly used commercial drones.

To provide further insights, two more configurations are investigated with $G = \{10,\ 15\}$, $S = 400$, and $P = 49\,\mathrm{dBm}$. Figures 5.7a and 5.7b illustrate the trajectory and the speed of the drone. Clearly, in both setups, the UAV slows down and approaches the GNs as close as possible to increase the amount of harvestable energy. Indeed, the speed of the drone reaches a maximum of $\sim 8\,\mathrm{m/s}$.

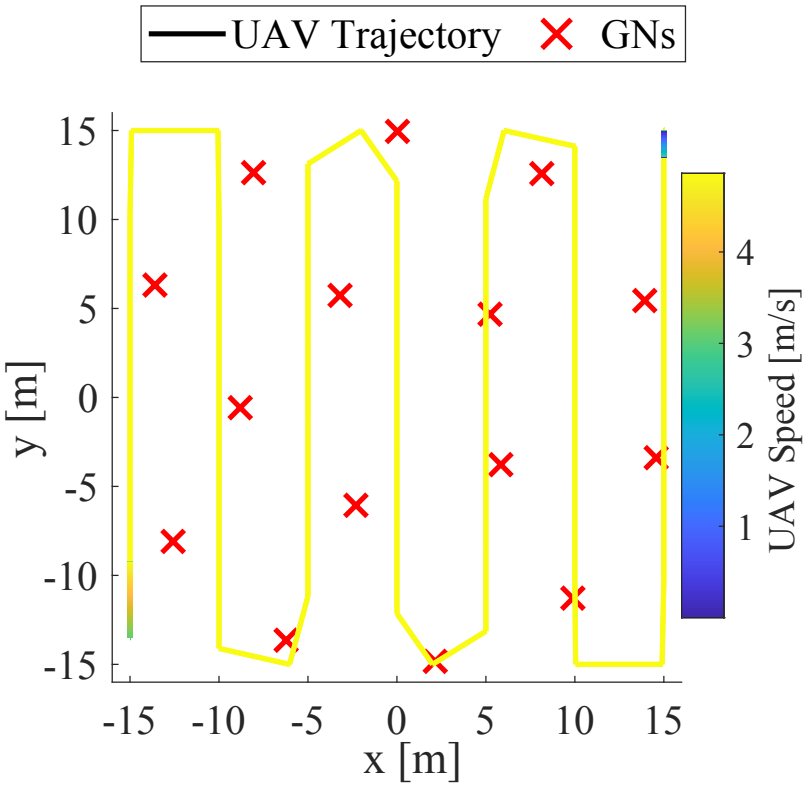

FIGURE 5.8: Example of the UAV trajectory and speed in the baseline scenario with $G = 15$ with K = 60, $\delta = 1\,\mathrm{s}$.

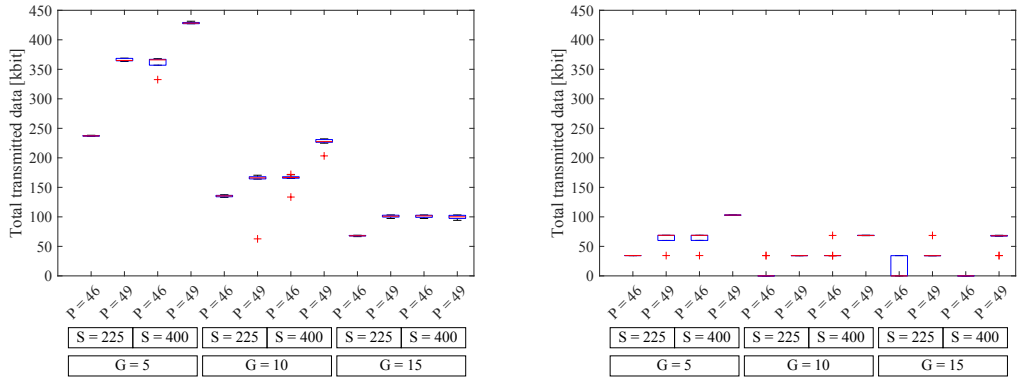

(A) Proposed algorithm.

(B) Baseline algorithm.

FIGURE 5.9: Comparison of the total transmitted data between the proposed solution and the baseline with $K = 60$, $\delta = 1\,\mathrm{s}$.

This behaviour is reflected in Figures 5.7c and 5.7d, where the total harvested energy per GN in both configurations is depicted. As a matter of fact, the proposed approach presents satisfactory results in terms of fairness. Moreover, it can be observed that the average amount of harvested energy decreases from $\sim 1.4\,\mathrm{J}$ with $G = 10$ to $\sim 0.9\,\mathrm{J}$ with $G = 15$. This in turn leads to a different amount of transmitted data (Figures 5.7e and 5.7f) with a mean of $\sim 225\,\mathrm{kbit}$ and $\sim 100\,\mathrm{kbit}$, with a coefficient of variation of 0.037 and 0.031, respectively.

In conclusion, to prove its effectiveness, the proposed solution is compared to a baseline approach across all previously investigated scenarios. Specifically, the baseline foresees the drone covering the interest area by following a sampled snake-like trajectory at the minimum possible speed which satisfies the mission duration. The drone periodically recharges the battery of the nearest node throughout the flight. Subsequently, the final state of charge for each GN serves as input for Algorithm 2, which will endeavor to fairly distribute the available transmission resources. An instance of the UAV trajectory and its speed is shown in Figure 5.8.

The results of the comparison between the proposed solution and the baseline, with $K = 60$ and $\delta = 1\,\mathrm{s}$, is illustrated in Figure 5.9. Each bar reports the distribution of the total transmitted data per each GN, for all the possible combinations of transmission power P, number of antenna elements S and number of GNs G. As it can be seen, the proposed solution achieves great performance when the number of GNs is small enough, i.e., $G = 5$, allowing the UAV to hover over each one as much as possible. Indeed, more energy harvested by each GN corresponds to a greater amount of data transmitted. The same holds true when P and S increase. Finally, the baseline does not always provide sufficient energy to the GNs for the transmission. Instead, the proposed method demonstrates a higher total transmitted data volume compared to the baseline approach, ranging from a minimum of 1.5 to a maximum of 7 times higher, due to its fairly optimized energy distribution.

Chapter 6

Boosting Service Provisioning in SIoT by Exploiting Trust and Capability Levels of Social Objects

The Social Internet of Things is gaining momentum thanks to its unique capability of i) autonomously building social relationships among smart objects and ii) supporting the novel services within the Social Network. During the service provisioning, the TMS is in charge of selecting suitable objects able to accomplish the requested services. In this context, available solutions present two relevant issues to be solved. First, they generally assume to select social objects that only achieve higher trustworthiness without considering their actual computing capabilities. Indeed, it would significantly compromise the Quality of Experience (QoE) in the Social Network of objects. Second, they assume to implement this task directly within constrained devices, becoming unpractical considering their limited computational and storage capabilities. To improve and speed up service provisioning, this work proposes a novel TMS scheme that fairly distributes service requests by jointly considering the trustworthiness and resource capabilities of available objects. This Trust Management System has been designed to exploit fog computing to efficiently handle the whole process of service provisioning in real-world deployments while relieving constrained devices from all processing and storage efforts. Its behavior is investigated through computer simulations. Obtained results demonstrated that the conceived approach outperforms baseline solutions in terms of latency, fairness in services distribution, and responsiveness in malicious nodes' detection.

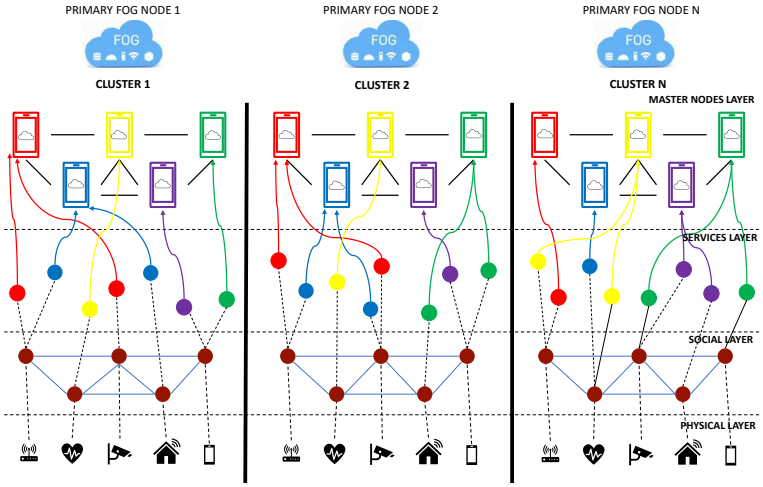

FIGURE 6.1: The proposed layered architecture.

6.1 Related works

At the time of this writing and to the best of the authors' knowledge, actual contributions only consider the design and the analysis of a TMS from a trustworthiness perspective, thus leaving some limitations on the implemented procedures concerning responsiveness, resource capability, efficiency, and scalability.

For example, the studies in [117] and [118] face the selection of the most suitable service provider in a TMS considering the energy constraints to evaluate the provider resources. The former proposes device trust dimension referred to the current energy status remaining unaware of device computational capabilities. The latter aims to increase the network lifetime, but it ignores the management of service requests and storage-saving procedures.

The paper [119] develops two algorithms for an efficient resource selection available through information sharing between social objects. Nevertheless, the described strategies do not implement a trust metric that jointly considers trustworthiness and resource efficiency aspects. The contribution in [120] proposes a distributed architecture based on a Blockchain for the secure provision of trust in an IoT system. It adopts a stochastic approach to detect and prevent malicious behaviors within a lightweight implementation. The results are obtained only for typical deployments operating with a limited number of nodes. So, the approach is not suitable for real-time systems, since it can only handle information generated at a quite low speed.

The authors in [121] investigate a TMS for the evaluation of service providers' past experiences and quality of service recommendations. The described self-adapted model dynamically fits changes in network context or type of demanded service. However, the presented model is entirely borne by the social objects. Consequently, it has the main limitation of the applicability to real-world scenarios with limited computation and storage capabilities of IoT devices.

Another work presented in [122] suggests a hybrid method to overcome the weakness of both centralized and decentralized approaches for trust management. Despite considering the evaluation of available resources, it mainly focuses on the user trust classification. In particular, it detects possible trust attacks via Machine Learning methods, without investigating the opportunity to distribute service requests to the most suitable service providers from the capability point of view.

Differently from the previously discussed studies, this work aims to solve the typical open issues regarding a TMS in SIoT environment, overcoming the limitations of the current state of the art. The strategy presented herein, in fact, investigates a novel resource capability-aware scheme that embraces several challenging aspects, such as responsiveness, resource capability, efficiency, and scalability in a SIoT environment to achieve trusted interactions in the service provisioning, supplying efficient resource management and quality of experience perceived by users.

6.2 The overall system architecture

This work considers a reference environment composed of several IoT nodes grouped in clusters (based on the geographical location) and managed in a distributed manner.

Fig.6.1 shows the resulting multi-layered SIoT architecture.

The lower layer is the Physical Layer, where the set of nodes is represented by the physical IoT devices. Each IoT device can act as a service requester or service provider. For the sake of generality, this work considers three different classes of IoT devices [232]:

- Class 0: devices are very constrained in terms of resources (i.e., sensors with tens or hundreds of kilobytes of RAM);

- Class 1: devices are constrained in terms of resources, but with some processing capabilities (i.e., Arduino, smart-cameras);
- Class 2: devices have enough resources and a lot of RAM to perform heavy computations (i.e., smartphones).

The second layer is the Social Layer. In this layer, IoT devices become social objects and, through their abstraction, they can represent the digital counterpart of the physical ones gaining the opportunity to expose their attributes useful to generate social relationships. In particular, a social object is identified by an ID, an owner and manufacturer identifier, and all the attributes specifying its performance abilities, such as power level and clock speed.

The third layer is the Service Layer. Here, each social object specifies the list of services it can provide. In such a virtualized service layer, a social object can join communities based on the same application context, facilitating network navigability.

Besides, the overall architecture embraces two levels leveraging fog computing technology. The first, namely the Master Node level, is formed by fog nodes with high computational capabilities to handle and distribute service requests. It hosts the TMS, which recommends the service provider to be selected during the service provisioning process. Each Master Node manages one or more service communities. Moreover, to support the decision for the most suitable service provider, it stores all the information related to past experiences and the whole set of attributes of registered social objects useful to generate a social-based virtual topology for each service community. The upper level, namely the Primary Fog level, is constituted by Primary Fog Nodes with high storage capacity that handles the set of information of a cluster of social objects. Specifically, a Primary Fog Node allows the proper synchronization between the distributed clusters structure through the interaction between other Primary Nodes.

6.3 Details on the conceived methodology

By joining the Social Network, a social object expresses its availability to provide a service. In this phase, through proper API, it communicates its attributes to Master Nodes, useful to reconstruct a virtual topology of the established social relationships. The social relationships calculation and storage are fully delegated to Master Nodes, enabling the applicability of the proposed strategy to a real-world scenario by offloading the social objects from this computational effort.

Whenever a node needs to retrieve a service, a request is sent to the Master Node that hosts the community providing that service. This approach simplifies the service discovery, thus limiting the selection to a subset of providers based on social relationships.

By handling a service request, each Master Node runs the TMS functionalities aiming to compute the most suitable service provider. Again, social objects are relieved of any computational load. This is a further advantage since the computation of the most suitable service provider could significantly impact storage and resources employed, being impractical for several IoT devices.

The two procedures implemented by the TMS for the management of service requests are summarized in the following steps.

Step 1 - Trust List Evaluation. For the incoming request, the Master Node verifies in its database the attendance of social objects displaying a social relationship with the requester. Consequently, it produces a Trust list of potential service providers. For each provider in the Trust list, the TMS evaluates the Trust value, which quantifies the level of trustworthiness of the service provider. It is computed as follows.

Considering the i-th social object requesting a service and the j-th social object as a possible provider, the Trust value $T_{i,j}$ is calculated through two main factors. Firstly, the

TABLE 6.1: Friendship ties rates.

Type of relationship	OOR	POR	C-LOR	C-WOR
S_{ij}	0.7	0.65	0.6	0.55

Sociality factor $S_{i,j}$ expresses the friendship ties between social objects. Table 6.1 describes the rates of the established relationship, classified in order of relevance (i.e., the Ownership Object Relationship (OOR) referred to the same owner is the stronger friendship tie, followed by Parental Object Relationship (POR), Co-Location Object Relationship (CLOR), and Co-Work Object Relationship (CWOR) referred to the same manufacturer, location, and working goal, respectively). Secondly, the Reputation factor $R_{i,j}$ is defined based on the history of the previous behavior of social objects, expressed through past received feedback. The Reputation factor is evaluated as follows:

$$R_{i,j} = \alpha\Delta_{i,j} + \beta\Theta_{i,j} + \gamma\Pi_{i,j}, \tag{6.1}$$

where:

- $\Delta_{i,j}$ represents the direct reputation and is calculated as the sum of positive feedback values divided by the total number of the feedbacks given by the i-th requester to the j-th provider;
- $\Theta_{i,j}$ represents the friend indirect reputation and is calculated as the sum of positive feedback values divided by the total number of the feedbacks given by friends of the i-th requester to the j-th provider;
- $\Pi_{i,j}$ represents the overall indirect reputation and is calculated as the sum of positive feedback values divided by the total number of the feedbacks given by the other non-friends of the i-th requester to the j-th providers;
- α, β, and γ are weights determining the relevance of each factor.

Finally, the Trust value is computed as reported in Eq.(6.2) (for details on the Trust model please refer to [109]):

$$T_{i,j} = S_{i,j} \cdot R_{i,j}. \tag{6.2}$$

Once the Trust value has been assigned to all potential providers in the Trust list, the procedure immediately discards any service provider with a Trust value lower than an empirically selected threshold. This feature prevents the possibility for misbehaved nodes to clean up their reputation and return to acting maliciously later.

Step 2 - Resource Capability Management. In order to increase the quality of the service provisioning experienced, the composed Trust list is double-sorted. Specifically, the first sorting parameter is the device class, whereas the second is the computed Trust value. This methodology represents a novel key aspect of the conceived scheme: this is a new ordering method aiming to ensure proper resource utilization, enabling the opportunity to satisfy delay-sensitive tasks demanding stringent performance and quality. The benefit of the trusted provider selection offering the right resources for the execution of the services will be motivated by the numerical results in the next Section.

Through the aforementioned strategy, the Master Node obtains a ranking based on social (Step 1) and performance (Step 2) perspectives. Besides, the proposed TMS performs

TABLE 6.2: Device parameters.

Social Object Class	Power Level	Clock Speed (Clk) [Megacyles/s]	QoE Class
Smartphone	0.8	2000	2
Smart Gateway	0.6	1000	1
Smart cam	0.4	1000	1
Sensors	0.2	40	0

TABLE 6.3: Services Requirements.

Service ID	1	2	3	4	5	6
Resource Consumption	0.3	0.2	0.1	0.2	0.1	0.3
Information Size (B) **[Mbit]**	1.4	1.0	0.6	1.0	0.6	1.4

a further assessment, considering the resource availability of suitable providers. Indeed, the resource management functionality monitors the resources of the recommended provider and verifies its availability to perform the service. If this check fails, the recommended provider is temporarily removed from the Trust list (it will be reconsidered in the list whenever it will have enough available resources). The system runs the same investigation on the updated ranking until an eligible provider is found.

The most suitable provider in the ranking, entertaining the needed resources, is selected for the service execution. Finally, the requester provides feedback about the executed service. The feedback communicates if the service accomplishment correctly matches with the requester's expectations. It is expressed with a binary value: 1 according to a service accomplished and 0 for a service not correctly completed. The received feedback is then stored in the proper Master Nodes, useful for Trust value updates in case of upcoming service requests.

6.4 Performance Evaluation

In this Section, the performance of the proposed methodology is evaluated through computer simulations. To this end, a C++ object-oriented and event-driven simulator has been developed from scratch to evaluate the average delay experienced in the service provisioning, the fairness in service distribution and the responsiveness offered by providers. The conceived scheme is compared with two other approaches. The first, which is the baseline approach, does not consider any knowledge of the quantity and the quality of the available resources in the network. The second, namely the resource availability aware approach (presented in [109]), takes into account resource availability but does not consider any resource capability management scheme for the selection of service providers in TMS.

6.4.1 Simulation parameters

Without loss of generality, the proposed scenario considers a cluster of social objects under the control of a single Primary Node. In this cluster, the TMS is performed by 5 Master Nodes. The number of social objects belonging to the cluster ranges from 100 to 300 (i.e., 100, 150, 200, and 300).

According to what is described in Section 6.2, each social object is characterized by a unique object ID, owner ID, manufacturer ID, geographical location, processor clock speed (expressed in megacycles/s), power level, and a list of offered services. Several types of devices (i.e., smartphones, smart gateway, smart cameras, and sensors) are generated within a

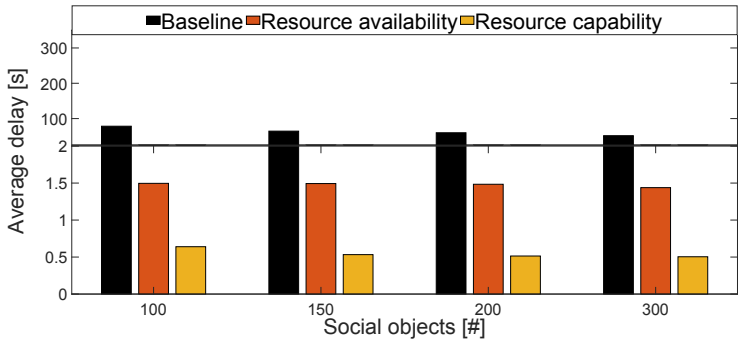

(A) λ = 4 requests/s.

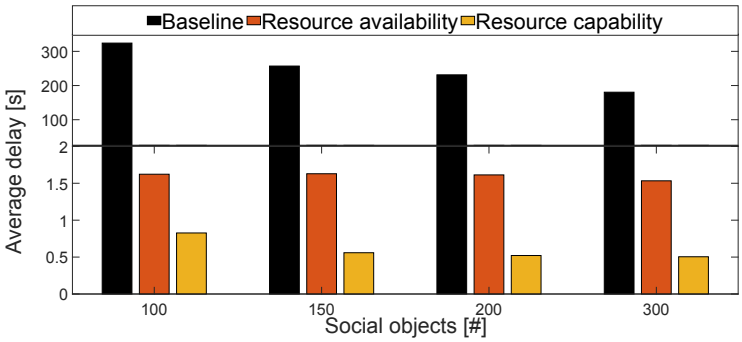

(B) λ = 10 requests/s.

FIGURE 6.2: Average delay.

uniform distribution across the cluster, whose computing capabilities are reported in Table 6.2. A social object can be classified into 3 different QoE classes (also reported in Table 6.2).

As expected for a common SIoT deployment, the conceived scheme assigns each generated social object to a Master Node. Then, the defined attributes, such as owner, manufacturer, and geographical position, allow to define social relationships. Specifically, this work considers OOR for objects owned by the same user, POR for devices produced by the same manufacturer, and CLOR for devices in the same location. Furthermore, the proposed scenario considers 6 different types of services, each one defined by a unique ID, a parameter addressing the requested resources for task completion (ranging from 0.1 to 0.3), and the bit size of the information to be processed as denoted in Table 6.3. According to this, the j-th social object can offer the service S by reserving part of its computing capabilities for an amount of time $t(j, S)$ equal to:

$$t(j, S) = \frac{X \cdot B(S)}{Clk(j)}, \tag{6.3}$$

where X is the number of CPU cycles needed to process a single bit, $B(S)$ describes the total number of bits to process to accomplish the service S, and $Clk(j)$ denotes the clock speed of the j-th social object in charge to process the service S expressed in cycles/s. According to [233], X has been set equal to 1000 $\frac{cycles}{bit}$.

To evaluate the network performance considering different traffic loads, service requests are generated accordingly to a Poisson distribution with an average rate λ ranging from 4 to 10 request/s and randomly selected from those described in Table 6.3. Moreover, for each considered scenario, results are obtained over 20 different seeds to account for several network topologies, services, and social relationship distributions.

TABLE 6.4: Processing time.

Scenario		Processing time [ms]
Social Objects	λ **[requests/s]**	
100	4	4.5
	10	3.6
150	4	1.3
	10	1.2
200	4	2.0
	10	1.7
300	4	4.2
	10	4.0

6.4.2 Average delay

The first KPI used to compare the conceived approach against the others is the average delay experienced in the service provisioning. It represents the average time taken by each requested service from its generation until the end of its execution. Results are reported in Fig. 6.2. More in detail, the baseline approach bases the provider selection only on the trustworthiness parameter while neglecting the availability of resources. As a result, it fosters the provider selection through the same small subset of nodes with high trustworthiness by overloading them with service requests. Therefore, even with low λ values, this approach experiences the highest average delay.

On the contrary, the resource availability approach experiences a lower average delay than the baseline thanks to its ability to spread service requests over the social objects owning enough free resources to accomplish it. This strategy significantly reduces the waiting time for an available provider. Delay results do not substantially vary even though the request rate increases.

Finally, the proposed resource capability-aware scheme always registers the lowest experienced delay. Indeed, considering providers with adequate resources and a higher QoE class during the provider selection boosts the performance for the fulfillment of the required tasks and drastically reduces latency in service provisioning. The efficiency of the proposed approach to accomplish requests by finding the best provider is confirmed in a large-scale scenario, ensuring better responsiveness and scalability for the network if compared with the others. In fact, in the case of 300 social objects and λ equal to 10 requests/s, the average delay reduces up to 67% with respect to the resource availability approach.

6.4.3 Processing Time

Table 6.4 shows the processing time of the conceived scheme to estimate the suitable service provider. The simulator runs on a computer equipped with a CPU i7-7700 and 16 GB of RAM. The processing time denotes the average time needed by a Master Node to perform the overall procedure executed in the TMS and described in Section 6.3. Each scheduled request is processed in a time range from 1.2 to 4.5 ms, which is very negligible if compared to the overall delay experienced in the service provisioning. Thus, the magnitude of the obtained processing times demonstrates the computational lightness and the scalability of the proposed scheme for different traffic loads and Social Network sizes.

6.4.4 QoE Fairness Index

To strengthen the obtained results, the well-known QoE Fairness Index (presented in [234]) is evaluated. The index estimation quantifies the fairness in service distribution by considering the QoE perceived by social objects. It is calculated as:

$$F = 1 - \frac{2\sigma}{H - L}, \tag{6.4}$$

where σ is the standard deviation providing a measure of the dispersion of QoE among social objects, while H and L are the upper and lower device classes, respectively. Fig. 6.3 depicts the QoE Fairness Index. On each box, the central mark denotes the median. The bottom and top edges, instead, indicate the 25^{th} and 75^{th} percentiles, respectively. Considering 100 social objects, the proposed approach experiences a QoE Fairness Index equal to 0.6, doubling if compared to the others. The efficiency also increases considering a larger Social Network size. In fact, the boost of the QoE Fairness Index triples in a large-scale scenario of 300 social objects, confirming the capability of the proposed approach to be scalable and fair in services distribution.

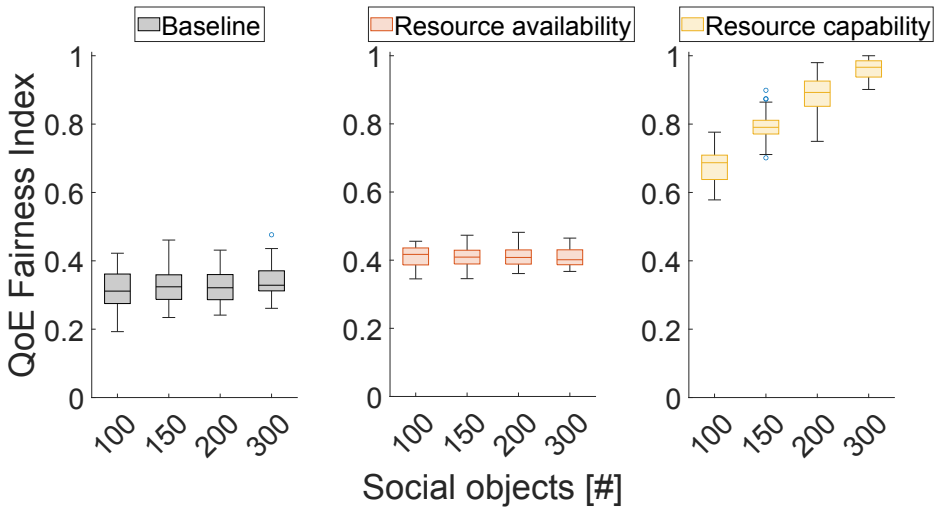

FIGURE 6.3: QoE Fairness Index.

6.4.5 Responsiveness in malicious nodes identification

This Section proposes further valuable considerations about the effectiveness of the conceived strategy in identifying malicious nodes. Fig.6.4 depicts the temporal evolution of the direct feedback received by the same provider averaged on the total number of feedback, called aggregated feedback. This aspect is evaluated in a Master Node for six social objects provisioning the same service. In this scenario, three selected nodes can act maliciously, providing poor services more frequently than others. Consequently, the assigned negative feedback impacts the overall reputation of the misbehaved provider. The obtained results show the ability of the proposed TMS to identify malicious nodes. Indeed, the misbehaved social objects are isolated from the service provisioning process and will never be contacted in the future, as testified by the red curves, truncated after about 1300 s. This result testifies that no further feedback will be provided anymore for the three malicious nodes that are banned from service provisioning. To provide further insight, Fig. 6.5 depicts the number of malicious nodes recognized by the TMS over time and averaged over 20 seeds for the three schemes chosen for

comparison. The considered scenario includes 100 social objects, and ten among them have a higher probability of acting maliciously. In this scenario, already after 500 seconds, the TMS designed in this work can identify a higher number of nodes to be excluded from the network if compared to the other solutions, testifying excellent responsiveness of the proposed approach to detect ambiguous behaviors during the service provisioning process.

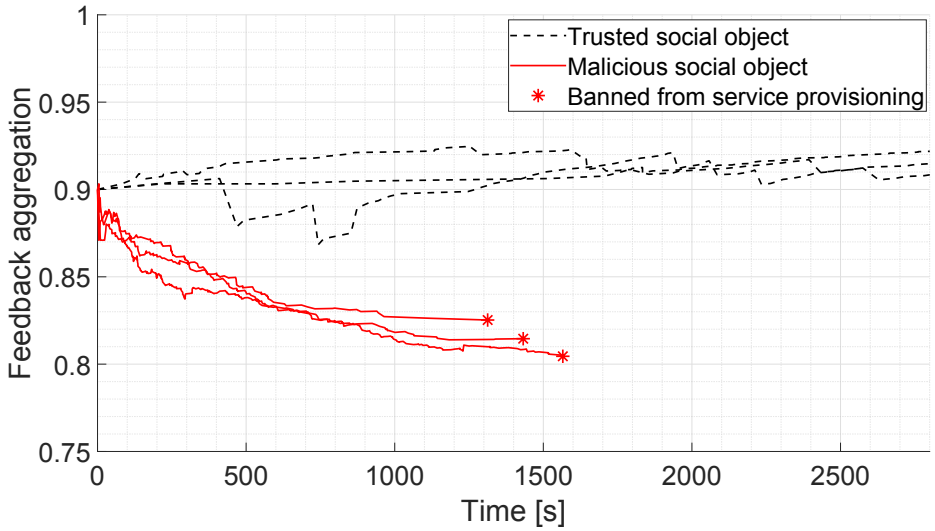

FIGURE 6.4: Temporal evolution of the aggregated feedback.

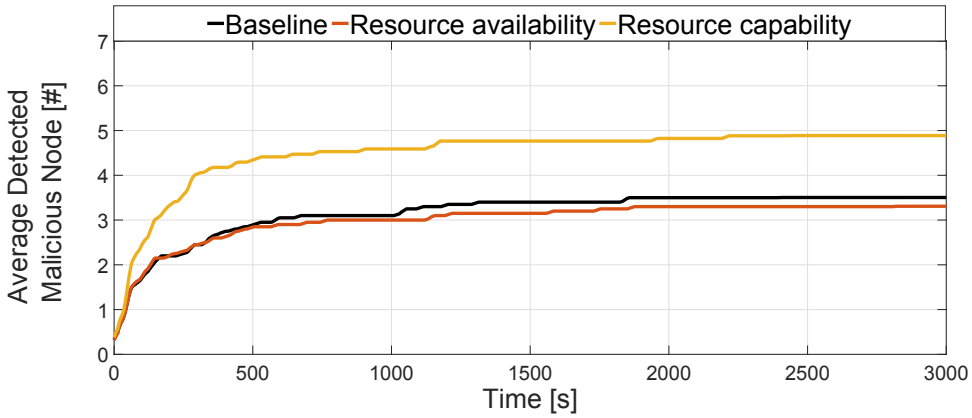

FIGURE 6.5: Responsiveness in malicious nodes identification.

Chapter 7

Light Fidelity for Internet of Things: A Survey

LiFi is quickly emerging as the next-generation communication technology thanks to its unique benefits, such as available spectrum, high data rates, low implementation costs, and inherent beamforming capabilities. As a consequence, it is endorsed by the scientific literature as an appealing innovation for disclosing disruptive services. The wavefront of LiFi technology is very wide: in this manuscript, we focus our attention on the interplay with the Internet of Things. Essentially, LiFi can assist the IoT in interconnecting a massive number of heterogeneous devices by addressing the current Radio Frequency spectrum bottleneck. Moreover, by investigating LiFi and IoT individually, several surveys and review papers testify to the noteworthiness of both technologies. However, to the best of the authors' knowledge, a comprehensive investigation of contributions where both of them interplay is missing. To fill this gap, this survey provides a thorough investigation of all the research areas in which LiFi key features might enhance the upcoming IoT networks. The evaluation of existing literature on LiFi adopted in the IoT domain can be valuable in identifying missing gaps arising from the interaction of these two technologies, as well as proficiently pinpointing future research directions.

7.1 The rationale of the proposed papers taxonomy on LiFi for IoT

The goal of this section is to explain the rationale at the basis of the classification of the papers that apply the multi-faceted aspects of the LiFi technology applied to the IoT environment. The classification approach proposed in this survey follows the taxonomy illustrated in Fig. 7.1. Specifically, papers are classified and discussed according to the following topics:

- **LiFi in IoT applications.** This section comprises all the works dealing with the implementation of the LiFi technology in a specific IoT application scenarios. There are some papers that provide only an overview of LiFi in different applications scenarios more suitable for the IoT market [235]–[237]. Other papers instead discuss a single IoT class of applications where LiFi can be fruitfully employed, like the e-health [238], telemedicine [239], mining environments [240], public transportation systems [241], smart factories [139], appliance automation [242], smart home [243], indoor positioning applications [244], [245], audio applications [246] and power grids [247].
- **Integration of heterogeneous communication technologies.** This section groups together all the papers that propose hybrid networks in which LiFi is integrated with other technologies like Wireless Fidelity (Wi-Fi) [236], [248]–[254] or last-generation cellular networks [139], [255], [256]. Different aspects of the integration are faced, starting from a review of the integration in some application scenarios (often discussing the

related advantages, limitations and challenges) [139], [235], [236], [255], [256] , to the implementation of QoS-aware strategies [250], [251], [254], proposals taking into account energy efficiency [248], [254], security aspects [249], or procedures at link layer [253].

- **Physical layer analysis.** Papers grouped in this section discuss several aspects related to the physical level of data transmission for LiFi systems in the IoT. Physical layer analysis is important to manage and improve several aspects of LiFi transmission, i.e., energy consumption [131], [132] and data rate [257] through Multiple-Input Multiple-Output (MIMO) techniques [132], [258] and modulation schemes [129], [235], [236], [252]. Also some security aspects related to LiFi can be analyzed at the physical layer [259].

- **Energy efficiency.** Papers belonging to this section analyze the energy consumption issue for the LiFi technology applied to IoT. The minimization of the energy consumption is achieved through different optimization strategies, ranging from the network design (i.e., the number of Access Points (APs)) [260], followed by the optimal selection of the LiFi AP that satisfies specific energy constraints [254], to the optimal allocation of the UL and/or DL transmission power [131], [254], the selection of the access scheme that minimizes energy consumption [129], [248], or exploiting MIMO transmission [132].

- **Design of communication schemes.** This section groups together all the contributions focused on the design and analysis of communication schemes and architectures that can be applied in the IoT context, and that implement the LiFi technology. In general, the architectural schemes discussed in this section describe the structure of the transmitter, the receiver, the components adopted to exchange data, and how they are interconnected. The architectural models related to the communication systems can be explicitly designed for specific application scenarios [129], [242], [247], [261], or to generic environments [244], [248], [262]–[265].

- **Positioning algorithms.** Papers that analyze this topic show how the LiFi technology can be effectively employed to estimate with high accuracy the position of IoT nodes in indoor environments. This task is accomplished through the proposal and implementation of algorithms that estimate the position of the IoT nodes by means of spatial coordinates [245] or time-based synchronization information [111], [266].

At the end of each section dedicated to a specific topic, a detailed analysis of the main findings is given, together with the related lessons learned.

Several papers analyze more than one topic among the ones described above. Thus, for ease of completeness, these papers have been analyzed in more sections of this survey, describing them from the point of view of the different topics they discuss.

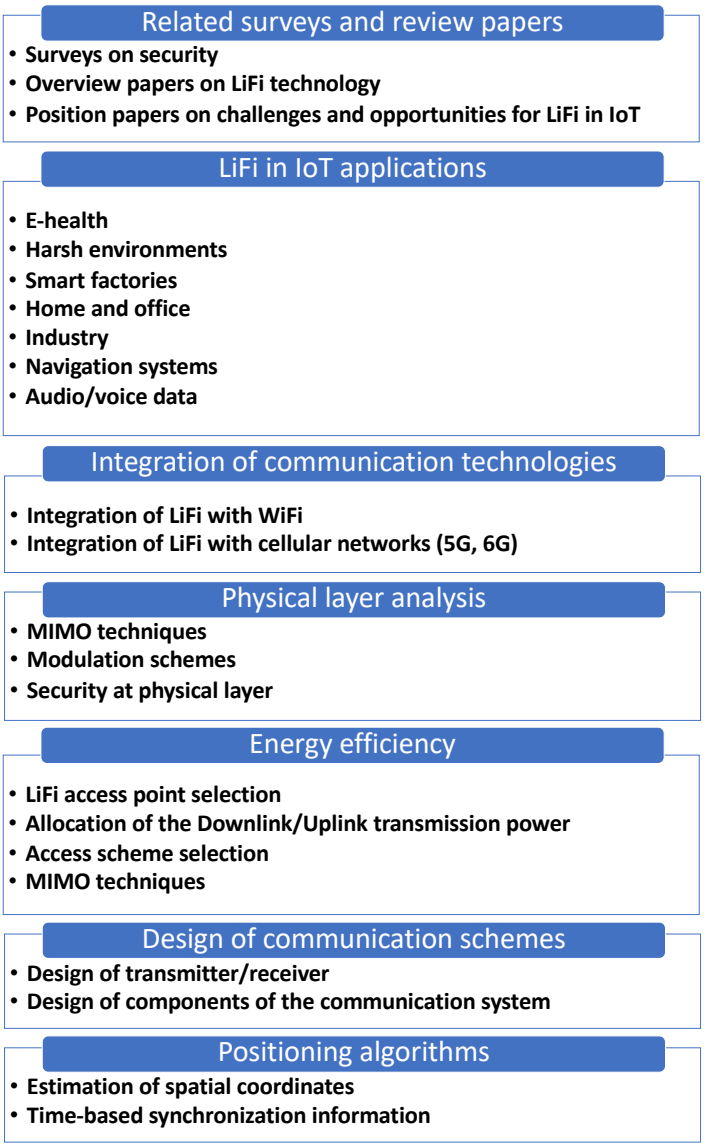

FIGURE 7.1: Paper taxonomy for LiFi in IoT environments

7.2 Related survey and review articles

The key articles related to the subject of this survey are briefly analyzed in this section, along with their main differences concerning the present contribution.

There are two survey papers dealing with LiFi networks [249], [259]. The contribution [249] surveys the state of the art related to authentication and handover protocols in hybrid LiFi/Wi-Fi networks. Specifically, the main security issues and the related solutions are addressed in this analysis. Also handover protocols for hybrid LiFi/Wi-Fi networks are discussed. Unfortunately, this survey is almost totally devoted to LiFi networks in general, without considering explicitly the IoT environment (it is only briefly mentioned in the Conclusions). The survey paper [259], instead, is mainly focused on the physical layer of VLC transmission. In this context, a security-related analysis is carried out, taking into account several factors like channel models, input distributions, network configurations, precoding/signaling

strategies, secrecy capacity, and information rates. A discussion of possible research directions related to security for VLC is also carried out. The main drawback of this contribution is that the LiFi technology is only superficially covered as a particularization of VLC and only in a specific scenario of hybrid LiFi/Wi-Fi networks. Furthermore, the IoT environment is not analyzed in detail. Rather, it is only mentioned in relation to the (high) number of connected devices.

Some contributions discuss several aspects of LiFi-based networks for the IoT [110], [235], [236], [239], [243], [255], [259], [267]–[269]. In all these works, the review of the state of the art literature on this theme is necessarily not thorough, being tailored to justify concepts and propose ideas, describe the implementation of ad-hoc systems, or clarify characteristics peculiar to LiFi. So, differently from the present contribution, they cannot be considered survey papers since the review work is partial and considers only some aspects of the integration of LiFi into IoT.

Papers [235], [236], [255] provide an overview of the LiFi technology, analyzing some technical aspects related to the physical layer (modulation techniques, channel capacity, adopted spectrum, etc.) and proposing application scenarios where LiFi can be employed. A discussion of the integration with other technologies like Wi-Fi [235], [236], [270], [271] or 5G [255] is also carried out. In all these contributions, being LiFi the central topic of both these works IoT is only cited and its description neglected. Another intriguing paper is [110], that highlights the main differences between VLC and LiFi. According to this, the IoT environment is neglected, and the review work is focused on the research topics relevant to LiFi, with reference to modulation techniques, physical components, multiplexed access in the channel, network models, interferences and models of integrated LiFi/Wi-Fi networks.

Papers [243], [267] are more related to the IoT world. They discuss the most relevant challenges and opportunities deriving from the integration of LiFi in IoT. In this context, the contribution [243] performs an exhaustive analysis of advantages and limitations of LiFi in IoT systems. A list of applications that support LiFi in IoT scenarios is also presented. Finally, an application example on smart home automation is designed, that integrates IoT and wireless communication. This paper exhaustively discusses the advantages and disadvantages of such integration, but it mainly presents the idea (as position paper), without analyzing the state of the art literature in support of it. The same topic is tackled in [267], where some solutions are discussed on the adoption of LiFi in IoT scenarios. The goal of this contribution is to evaluate the integration of LiFi and IoT into real-world applications and scenarios. Different aspects are discussed, ranging from use cases to algorithms at different layers of the protocol stack, mobility, standardization activities, and prototypes. The solutions discussed in this paper are developed in the framework of an innovation action project on LiFi, whose focus is on challenges and solutions that allow concretizing the research work on this topic into real-world applications. Like the work [243], this paper does not survey all the state of the art literature on LiFi for IoT.

The approach followed in [239], [268], [269] is to analyze some technological aspects of LiFi systems conceived for IoT applications. In [268], the main features needed to adapt LiFi systems to IoT applications are discussed, with a specific reference to the physical layer. In this layer, several features are analyzed, ranging from connectivity requirements (at different layers of the stack) to mobility support, implementation of integrated wireless/wired networks, and the management of interference. A broadband communication approach at the physical layer is also proposed, that integrates the LiFi technology with Plastic Optical Fiber (POF) links. The study is carried out in the framework of an EU H2020 project on the LiFi development for IoT.

The paper [269] analyzes the scientific contributions related to Optical Wireless Communication (OWC) technologies, including LiFi, devoted to IoT solutions. The review of the literature is more focused on OWC solutions than on LiFi, which is analyzed as part of the

OWC environment. The review of the contributions is tailored specifically for 5G and IoT scenarios.

The most significant open issues for LiFi systems as related to the 5G technology are also reviewed in [239]. The review work conducted in this paper touches different aspects ranging from link design to system requirements, challenges and techniques to mitigate the impairments. A prototype of a LiFi system is identified, with a detailed analysis of the structure of the transmitter and receiver. An implementation example based on telemedicine is also considered.

Papers [244], [272] provide an overview of some concepts of LiFi networks. Also in this case, the literature review is aimed at clarifying some conceptual aspects of LiFi technology, without conducting a wide-ranging and detailed description of its integration in the IoT paradigm, which instead is the goal of the present contribution.

The work [244] proposes a system in which LiFi serves IoT nodes. Indoor application scenarios are considered in this work, with a description of the LiFi Access Point (AP) and IoT devices. The proposed system is designed explicitly for LiFi-for-IoT scenarios, describing all the system parts and system architecture and performing feasibility analysis, with particular reference to positioning and power delivery aspects. Specifically, it suggests viable solutions for IoT nodes that only need to deliver data intermittently, such as On-Off Keying (OOK), Pulse Position Modulation (PPM), spatial PPM, and random number modulation by exploiting off-the-shelf LEDs as an enabler for the IoT environment Finally, the main research directions of LiFi for IoT are discussed.

A more general review of LiFi networks is carried out in [272], without any discussion of the integration with the IoT environment, which is relegated mainly to the application area. In this work, the main concepts of LiFi technology are discussed. They encompass LiFi networks, state of the art in standardization activities, and applications. The main features of terahertz communications are also presented for the integration of LiFi into future 5G&B scenarios.

7.3 Contribution of this survey and main differences with other surveys and review papers

To the best of the authors' knowledge, the present contribution is the only one providing a wide-ranging and integrated discussion of all the relevant aspects concerning the integration of LiFi in the IoT environment. From the analysis of the most recent literature on this theme, the following topics have been analyzed in this work:

- Coexistence of LiFi and IoT in a specific application scenarios (e.g. e-health, hazardous environments, public transportation systems, home automation, etc.);
- Integration of LiFi and IoT with other communication technologies (like Wi-Fi and optical fibers).
- Physical layer analysis, which extends the survey work made in [259] (that nonetheless mainly discusses security issues). The analysis at this level concerns mostly modulation and coding schema.
- Energy-efficient strategies, aiming to optimize the energy consumption of LiFi systems that can operate in the IoT context. In some contributions, energy efficiency is considered as a QoS requirement.
- Communication schemes, discussing in detail the system components and their interconnections for data transmission/reception in LiFi-based systems. In some works, this topic is related to the development of specific application scenarios.

TABLE 7.1: Review of other surveys/review papers and comparison with this survey.

Covered topics	[259]	[249]	[236]	[235]	[255]	[110]	[243]	[267]	[268]	[269]	[239]	[244]	[272]	This work
Application scenarios			✓	✓			✓	✓			✓	✓	✓	✓
Energy-efficient strategies														✓
Integration of different technologies		✓	✓	✓	✓	✓							✓	✓
Physical layer analysis	✓		✓	✓	✓				✓	✓			✓	✓
Communication schemes						✓			✓	✓	✓	✓		✓
Positioning evaluation strategies														✓

- Positioning strategies based on LiFi, aiming to detect the position of IoT devices as precisely as possible, and in real-time.

Starting from this schematization followed in this contribution, and comparing the topics listed above with the survey and review papers described in Section 7.2, the following important differences arise:

- The two survey papers [249], [259] are the only ones that carry out a thorough review of the literature on LiFi technology. Nevertheless, this analysis is not explicitly referred to its integration with the IoT environment. Furthermore, the survey works are mainly dedicated to LiFi security aspects [249], [259] and protocols [249], and on the integration of LiFi with Wi-Fi, neglecting several other relevant topics (i.e.: application scenarios, integration among different technologies, energy-efficient strategies, etc., as listed above).

- The contributions [110], [235], [236], [239], [243], [255], [267]–[269] cannot be properly considered as survey works, as specified above, since their review work is tailored to the investigation of specific aspects, or to better support the analysis and implementation of particularized schema, thus considers only some aspects of the integration of LiFi into IoT.

- Papers [244], [272] are even more general in their literature review, which is performed to overview some basic concepts of the LiFi technology and not always referred to its implementation in the IoT environment. Also in this case, the analysis of the state of the art literature does not take into account, point by point, all the most important aspects of the application of LiFi to the IoT.

For ease of completeness, Table 7.1 shows the main differences between this survey work and the other survey and review papers on the adoption of LiFi for the IoT found in literature, highlighting the missing topics of the latter that are covered in this contribution.

7.4 LiFi in IoT applications

This section describes all the papers that focus on specific IoT applications where the LiFi technology can be effectively adopted. According to the state of the art literature, the IoT applications scenarios chosen for the implementation of LiFi are mainly indoor (even if there are some exceptions to this, as shown in [235], [237], [241], [245]) and range from e-health [238], [239] to harsh environments [240], smart factories [139], home and office [237], [243], industry [237], [247], navigation systems [245] and transmission of audio/voice data [245], [246]. Many of these scenarios are briefly cited in the review paper [235], [236], which also mentions other interesting scenarios like underwater, aircraft, defense, disaster management and risky environments.

Several application scenarios are grouped, listed and briefly discussed in the review papers [235], [236]. The goal here is to better highlight the potential of the LiFi technology in

practical application examples, in a more general framework of a technological overview of LiFi and the description of its potential in several scenarios of interest. Many LiFi applications are also suitable for IoT networks, even if this technology is not explicitly described in these works.

The contribution [237] focuses on the integration of LiFi use cases in the IoT environment. Starting from the assumption that LiFi solutions are usually customized for their own ecosystem, the goal of this study is to propose and discuss a LiFi system concept and how it can satisfy the requirements imposed by IoT applications. The main LiFi use cases, with related requirements for IoT applications, are described pointing out the flexibility in the adoption and versatility of hardware and software components.

The integration of LiFi in IoT for the e-health scenario is analyzed in [238]. The integration between these two technologies is exploited for the enhancement of a health monitoring system, where a doctor can quickly update the health conditions of his/her patients in the cloud. The cloud is the IoT system while the LiFi network guarantees very fast and noninterfering connectivity. the doctor can thus analyze the patient's data and provide real-time feedback to the assisting person. The key-elements of the health monitoring system are precisely identified, and their interaction is described, also providing flow diagrams of the system.

LiFi is also used in mining environments, as described in [240]. This work focuses on critical environments where the management of emergency information is very difficult because of the poor coverage of Wi-Fi technology. Specifically, LiFi is used to monitor the critical conditions detected through IoT sensors. A decision-making system is also developed to detect abnormal conditions in the presence of hazardous gas. Performance analysis of the proposed system is evaluated in a real testbed, describing the hardware components adopted.

The LiFi technology is exploited in [241] for local advertising in the public transportation scenario. This paper focuses on the outdoor scenario (as shown in Fig. 7.2), where LiFi is used to transmit the local advertisement to devices close to LED sources, but the proposed model is claimed to be suitable also for indoor IoT communications, increasing their data reliability and solving bandwidth bottlenecks. Both transmitter and receiver sections are analyzed in detail for LiFi communication, providing a hardware-based implementation model and testing its performance in terms of signal attenuation and bit error rate.

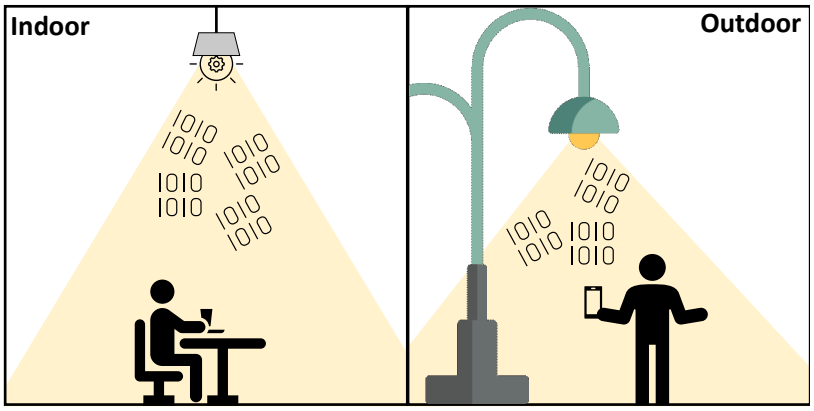

FIGURE 7.2: Figure on LiFi in indoor and outdoor environments.

LiFi is employed to support smart factories in combination with the 5G network in [139]. The main requirements for this use case are analyzed, in terms of coverage, throughput, network infrastructure, data reliability and delay. A factory demonstrator that considers the factory environmental conditions and the integration between LiFi (in the access network) and

5G (in the core network) components and protocol stacks is then implemented. Its goal is to demonstrate reliable communication between end IoT devices and application servers.

In the work [242], the LiFi technology is adopted to build an appliance automation model in combination with the Message Queue Telemetry Transport (MQTT) protocol, which is an application layer protocol typical of IoT environments. The proposed model is implemented in a hierarchical hybrid star-tree IoT network, with three levels of hierarchy. The leaf nodes lying at the third level of the hierarchy (the most peripheral one) are provided with LiFi technology and transmit data to a centralized server by using MQTT. The amount of data collected by LiFi nodes is analyzed by means of Machine Learning (ML) algorithms, to predict their temporal behaviour.

The main goal of the contributions [239], [243], [244] is to discuss the main challenges, opportunities [239], [243] and possible research directions [244] arising when LiFi is adopted to enhance the connectivity of IoT nodes. Nevertheless, in all these papers application examples are also presented, to provide a more clear discussion of the covered topics. Specifically, a home automation system integrating LiFi and IoT is discussed in [243]. The focus here is on the design and implementation of a home controlling and monitoring system. The main system functions are described, and a block diagram of the system is proposed, where all the components are identified and described also in terms of network connectivity. An android-based app for appliance control is also proposed, for the practical implementation of the home control system. In the review paper [239], telemedicine is adopted as an application example to address the challenges to be faced when LiFi is adopted in IoT networks. To this end, a LiFi architecture is proposed as a possible implementation scenario within hospitals. The application consists of a circuit transmitting information (an audio signal, in the example) via LiFi. All the components of the prototype are chosen and connected, and the signal is transmitted through LEDs with high illumination capabilities. The main challenges observed in the prototype implementation are also discussed. A more general indoor application scenario is proposed in [244], where LiFi serves IoT nodes. The proposed application scenario is suitable to provide some kind of services such as precise positioning, energy harvesting and security [244]. The system is described in detail, together with all its components, also providing a feasibility analysis in terms of power, energy efficiency, response time and data rate. A comparison with the adoption of LiFi with RF transmission is also carried out, highlighting the main limitations and challenges brought by LiFi. Finally, the main research directions to enable the LiFi/IoT integration are addressed.

A prototype of a LiFi system transmitting an analog audio signal is also discussed in [246] for IoT applications. The audio signal comes from a mobile phone. It is modulated and converted into light emitted by blinking LEDs. A solar cell receives the light signal and forwards it to a speaker. The system is implemented with real HW components, testing its effectiveness and addressing the main advantages in the adoption of LiFi for applications in IoT.

Location-based applications are discussed in [245], that employ LiFi as integrated with Wi-Fi for indoor scenarios where GPS-based systems obtain poor coverage performance. In addition, a voice-based input system is implemented, that generates voice alerts in presence of hurdles for visually impaired people.

Integration of LiFi in power grids, which is a typical IoT application, is the topic of [247]. The paper discusses the so-called Optical Internet-of-things (OIoT), which is the IoT that adopts optical wireless connections. This concept is translated into power grid environments. This paper analyzes the optical theory on the basis of OIoT. It is then exploited to develop an analytical method for the OIoT performance evaluation, and design the block-based diagram of an optical wireless communication system for the power grid. Finally, different application scenarios in the power grid domain are described, where OIoT can be effectively exploited.

The papers analyzed in this section testify that the LiFi technology can be effectively adopted in a wide variety of application scenarios peculiar to the IoT world, where each application has its own traffic features [244]. In these contexts, LiFi can be very advantageous for different reasons: high energy efficiency [241], security [239], [241], [243], high precision in localization [244], huge available bandwidth [238], [243], low-cost components [238], robustness towards electromagnetic interference [237], [239], [241], [243] and capability to serve a huge amount of IoT nodes [241], [244]. Nevertheless, the abovementioned studies suggest that LiFi is still not mature to totally replace the Wi-Fi connections currently adopted in IoT, at least in the short term. Instead, it should be integrated and harmonized with existing technologies [239]. In fact, LiFi suffers from some limitations that can be relevant in some IoT environments. Just to cite some of them: the necessity of a LoS and a very short distance between two LiFi nodes, a constant light source to access the network, the high difficulty in implementing LiFi connections in outdoor scenarios due to other interfering light sources (like the sun) and varying weather conditions, and the time and expensiveness needed to set-up and install LiFi infrastructures [243]. As a consequence, LiFi will be worth being adopted in all that IoT applications, especially indoor, that need to be optimized for high throughput, high reliability, or low latency, at the same time optimizing costs [237]. From the analysis carried out in these papers, it is also noteworthy that most probably LiFi will be the best candidate technology for the future IoT [237], [244].

7.5 Integration of heterogeneous communication technologies

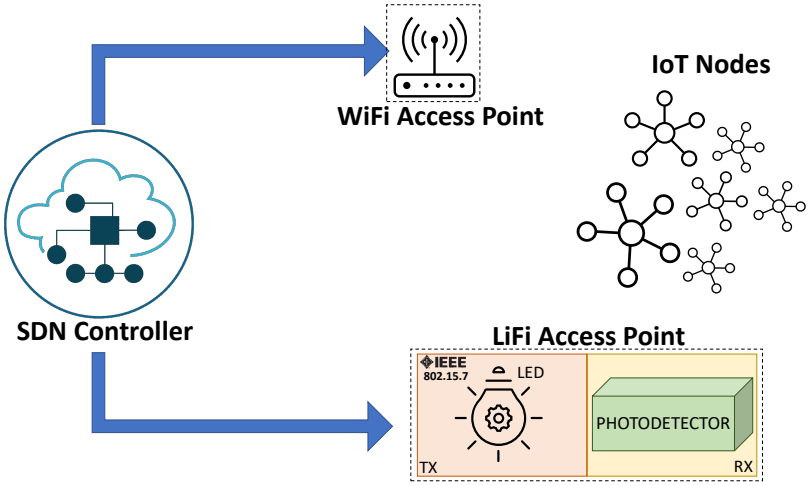

FIGURE 7.3: Example of Integration of heterogeneous communication technologies.

This section describes the proposals for the integration of different communication technologies that include the adoption of LiFi in IoT environments, as shown in Fig. 7.3. In particular, relying solely on traditional networks to accommodate the explosive growth in bandwidth demand from the burgeoning number of IoT devices is no longer sufficient. In fact, LiFi systems have drawbacks due to the blockages of the light path that limit the received signal due to opaque objects and obstacles. Consequently, combining LiFi and RF can be an easier way to fulfill future IoT requirements. The most widely discussed kind of integration is between LiFi and Wi-Fi communication technologies, as testified by several papers found on this topic [235], [236], [248]–[251], [253], [254].

The contribution [248] proposes a technique for energy harvesting, in a scenario that combines both Wi-Fi and LiFi. The goal of the proposal is to achieve higher data rates by integrating both technologies rather than using them separately. The analysis is carried out by designing a model that accounts for the capability of the energy-harvesting sensor to transfer the harvested energy to the sensor node or storage charge and to manage the output of sensors. The performance comparison, in terms of data rate and BER, is conducted for LiFi only, Wi-Fi only, and hybrid scenarios considering bidirectional communication.

Papers [235], [236], [249] discuss the integration between LiFi and Wi-Fi. In these papers, an explicit description of the IoT environment is missing. Nevertheless, there are some aspects detailed that are suitable for IoT-related networks (e.g., some application scenarios, some system specifications, etc.). Specifically, the study [249] attempts to highlight potential security issues when employing LiFi solely and during the handover protocols between Wi-Fi and LiFi technologies. It explores a wide range of LiFi and handover LiFi/Wi-Fi protocols by disclosing security flaws that might lead to severe attacks. It describes some methodologies to increase security, like the adoption of beamforming methods that reduce the SNR of unauthorized entities in VLC networks to zero, or channel matrices for precoded signals that are invertible only for authorized users. Channel security during the handover process is improved by avoiding the share of the same passwords.

Papers [235], [236] basically adopt the same approach to provide an overview of the main features, developments, advantages and challenges of LiFi. More in detail, the contribution [235] proposes an analysis of the LiFi technology, its main developments, its advantages and limitations. The combination of LiFi and Wi-Fi is discussed, with a focus on the advantages of the resulting hybrid network, especially in terms of security, data rate, coverage and precise positioning in indoor environments. Different possibilities of combination are also presented. Another contribution that provides an overview of the implementation of LiFi over Wi-Fi is found in [236]. Starting from the description of the evolution of the VLC technology into LiFi, a technical comparison between LiFi and Wi-Fi is performed. Some specific aspects are mentioned, i.e., IEEE standardization, the implemented topologies of LiFi and Wi-Fi networks, the operation bands, the coverage and the data rate. Also in this paper, these topics are summarized without going into deep detail.

Also the works [250], [251], [254] deal with hybrid LiFi/Wi-Fi IoT networks. In this scenario, the contributions [250], [251] define the optimization problem of the selection of the most suitable AP based on client-specific QoS constraints in the indoor LiFi/Wi-Fi environment. According to the QoS provisioning mechanism, the IoT nodes can select a LiFi or a Wi-Fi AP, given specific QoS constraints. More specifically, the work in [250] presents an innovative access device selection strategy that attempts to optimize the channel quality (i.e., throughput, energy consumption, and delay) while allowing each IoT node to define its subset of QoS requirements. The goal is the reduction of the average delay experienced by each IoT node while satisfying all the QoS constraints. This methodology is implemented in a Mininet-based indoor hybrid LiFi/Wi-Fi network.

The study carried out in [250] has then been extended in [251] by presenting an enhanced algorithm of access device selection that is solved with a game-theory approach. This paper analyses in-depth the LiFi channel while assessing its data rate capacity by varying the angle of inclination of the APs with regard to IoT nodes. It reduces the average delay and increases the average throughput of the network while meeting the QoS requirements of the IoT nodes. The performance of the proposed algorithm is evaluated by emulating a real-world scenario.

In the paper [254], the integration between LiFi and Wi-Fi translates into modeling differently the LiFi and Wi-Fi channels and integrating these two models for the formulation of the optimization algorithm that allows to select the most suitable AP that maximizes energy efficiency, thus respecting specific QoS guarantees. The proposed methodology is also compared with Wi-Fi-only and LiFi-only scenarios.

The LiFi/Wi-Fi combination is analyzed in [253] at the single interface level. This work considers a virtual interface, composed of the aggregation of two physical interfaces, one based on LiFi and the second on Wi-Fi, obtained by means of a bonding driver at the data link layer. Some performance results are presented, focused on the evaluation of the connectivity downtime occurring during the switching from one physical interface to the other, due to different reasons (signal loss, interface failure, load balancing, etc.)

Other works present an overview of an hybrid LiFi/Wi-Fi network able to overcome the shortcomings of both standalone technologies by combining the fast data transfer capabilities of LiFi with the wide coverage of Wi-Fi, without focusing on the IoT domain. Specifically, [270] presents an overview of LiFi technology, practical concepts for implementing LiFi-based indoor networks, and criteria for measuring network performance. It also discusses how to design and set up a LiFi-based indoor network as standalone LiFi or hybrid LiFi/Wi-Fi network. Furthermore, [271] presents network architectures, cell deployments, multiple access and modulation schemes, illumination requirements, and backhaul. Moreover, key performance metrics are then reviewed to demonstrate the superiority of hybrid LiFi/Wi-Fi network against standalone networks. Then, the challenges are elaborated on key research topics including user behavior modeling, interference management, handover, and load balancing. It also examines the potential benefits of LiFi/Wi-Fi network for application services, such as indoor positioning and physical layer security.

Another topic on this theme debated in the modern literature consist of the integration of LiFi with 3GPP-based last-generation cellular networks like 5G&B, which are suitable for IoT support. This aspect is emphasized in [139], [255], [256].

In this context, in [139] LiFi is integrated in the 5G network. The focus of this work is to exploit the LiFi technology in the access network while using the 5G technology in the core network. Since, differently from 5G, LiFi is a non-3GPP technology, the effort of this study is devoted to the integration of the LiFi and 5G components and the related protocol stacks. A demonstrator is also developed, that shows the reliability of the communication between IoT devices and application servers.

The integration between LiFi and 5G is discussed in [255]. Even though this paper does not propose any novel methodology, it carries out a comparison between the main LiFi performance parameters with the correspondent 5G ones, to evaluate the possibility of implementation of LiFi-based cellular networks. Accordingly, the main aspects of LiFi technology are discussed exhaustively, also briefly mentioning the integration of LiFi with Wi-Fi.

More tailored to the integration of LiFi into future 5G&B network is the work [256], which recommends the further integration of 5G&B in a LiFi/Wi-Fi network to provide high coverage also on subways, aircraft, and trains. Specifically, 5G&B would ensure connectivity to the public network, LiFi would achieve a reasonable indoor data rate, and Wi-Fi would compensate for LiFi shortcomings (e.g., penetrating walls).

The analysis of the literature on this topic suggests that the integration process of the LiFi technology with other existing and consolidated technologies like Wi-Fi or 5G is a central topic in the framework of the LiFi technology. In fact, when a new promising technology (like LiFi is) arises, it needs a more or less long period of integration and coexistence with the other existing ones, that have already been implemented in existing network infrastructures. So, it is not surprising that there is a consistent amount of research work that tackles the integration between LiFi and Wi-Fi, which is widely adopted in IoT scenarios. Also the integration with 5G&B systems is a promising line of research, since the last-generation cellular networks are standardized also taking into account the IoT environment. As a consequence of this, a relevant effort should be spent on the interoperability among the different standards, developed for architectures, devices, and protocols that characterize Wi-Fi, 5G, 5G&B, and LiFi systems.

In the context of this integration, efforts have been devoted to designing communication

schemes satisfying specific QoS guarantees. The fulfillment of this goal for LiFi-based networks helps improve the LiFi network performance in terms of different metrics like energy consumption, data rate, and network throughput. On the contrary, this is not a trivial task. Indeed, strategies in this direction always translate into finding the solution to a constrained optimization problem, which is usually a complex and computationally intensive task, not suitable for IoT devices that usually are resource-constrained. The task becomes even more complex when the QoS guarantees are heterogeneous, depending on the features of the IoT nodes.

7.6 Physical layer analysis

In this section, the strategies related to the physical layer of LiFi transmission in IoT are discussed in detail.

Physical layer aspects can be found in the framework of energy efficiency strategies, as testified by [131], [132]. More specifically, in [131] the enhancement in energy efficiency performance in a LiFi environment for IoT is studied by modeling a Non-Orthogonal Multiple Access (NOMA) channel. This channel is modeled with an optimal power allocation method to achieve greater performance than a standard Orthogonal Multiple Access (OMA) channel while still meeting all of the QoS requirements of a IoT node. Also in paper [132], the energy efficiency of a VLC communication is boosted by leveraging an adaptive MIMO strategy. This paper investigates the effectiveness of various MIMO approaches by identifying the most energy-efficient method while fulfilling an acceptable error rate.

Related to MIMO techniques is also the work [258]. It proposes a MIMO technique for a OOK modulation suited for the VLC. Even though the strategy is presented for only one transmitter and one receiver (being not suitable for IoT scenarios with high numbers of nodes), the proposed methodology can improve the LiFi communication if compared to conventional schemes, in terms of data rate and communication range.

Many papers discuss modulation schemes for LiFi [129], [130], [235], [236], [252]. In [130], the main modulation schemes are grouped into two different categories, such as single carrier modulated transmission and multiple carriers modulated transmission. The former includes both Pulse-Based Modulation (PBM) (i.e., OOK, Pulse Amplitude Modulation (PAM), Pulse Width Modulation (PWM), PPM [273]) and Continuous Wave Modulation (CWM). In detail, a PBM imposes that the signal is composed of a periodic pulse (AC current) that is added to the illumination (DC current) by modulating the amplitude of the light. On the contrary, the CWM modulates the light intensity with a sinusoidal carrier signal. Herein, the information can be coded either by amplitude (ASK), phase (PSK) or frequency (FSK) shift keying. Finally, if the signal is modulated both in amplitude and phase is called Quadrature Amplitude Modulation (QAM) [123]. The latter uses many carriers to convey information. Specifically, the main method is the OFDM which maps bits with a given modulation scheme (e.g., QAM) by exploiting orthogonal subcarriers. Then, the output is obtained using the Fourier transform [274]. Nevertheless, OFDM signals should be shaped for LiFi systems to allow for LED source intensity modulation. Hence, a positive limitation is essential for an optical modulation system to cut off noise and ensure the accuracy of the modulated signal. Indeed, to counteract the bipolar nature of the OFDM signal, the DC-biased optical OFDM (DCO-OFDM) is commonly employed. Alternatively, the asymmetrically clipped optical OFDM (ACO-OFDM) only transfers data on the odd subcarriers. The resulting bipolar signal at the output of the IFFT is clipped at zero to give a non-negative signal. However, it sacrifices some spectral performance to ensure that no data is lost. Finally, even though the DCO-OFDM attain higher spectral efficiency and data rates [270], [271], ACO-OFDM is employed in more energy-efficient applications [271], [275], [276].

Modulation schemes for LiFi are reviewed also in papers [236], [252]. Both these contributions describe the modulation techniques adopted for LiFi, subdividing them into two main groups: modulation schemes in common with radio wave communications, further classified into single carrier and multicarrier modulations, and modulations techniques that are exclusively adopted in LiFi transmission since they exploit features peculiar of light signals. In [129] the coexistence issues among low-power IoT nodes with low data rates and LiFi nodes that can easily manage high data rates and high reliability is faced at the physical layer. In fact, this work evaluates the suitable modulation techniques such as QAM, PAM, Color-Shift Keying (CSK), Discrete Hartley Transform (DHT), DCO-OFDM, interleaved subcarrier mapping, modified data sequence and multi-access techniques such as Wavelength Division Multiplexing (WDM) and Orthogonal Frequency Division Multiple Access (OFDMA). In addition, the performance of each technique is evaluated in terms of Peak to Average Power Ratio (PAPR), delay and throughput. Also the contribution [235] evaluates the performance of alternative modulation schemes, including OFDM, Filter Bank Multi-Carrier (FBMC), and Universal Filtered Multi-Carrier (UFMC) in a LiFi environment using MATLAB simulations. More in detail, this work emphasizes the benefits of using UFMC with respect to OFDM in terms of BER, PAPR, spectral density, and spectral efficiency while at the same time guaranteeing a lower implementation complexity.

Different physical layer aspects are tackled in [259]. This contribution highlights the security challenges that might arise while using VLC communication technology by examining several configurations for data transmission such as Single-Input Single-Output (SISO), MISO, MIMO, and hybrid LiFi/Wi-Fi systems. To cope with this issue, this paper reviews different channel models, user mobility, and KPIs capable of monitoring the safety of this technology. Moreover, security approaches at the physical layer are investigated for boosting VLC channel security, also analyzing the impact of factors like input signaling, the number of eavesdroppers, and Channel State Information (CSI) availability at transmitting nodes on the security performance of the system.

Another contribution is found in [257], that deals with the parallel transmission of data in a LiFi network. This work considers an area covered by several LiFi APs simultaneously connected to an IoT node. In this scenario, an optimal resource allocation algorithm is proposed, that aims to maximize the achievable data rate of the LiFi network. Several factors are taken into account in the resulting optimization problem: the channel model, the node mobility, and the light-path blockage modeled by analytical functions.

This section explores papers that discuss the implementation of traditional RF modulation schemes in the optical domain, including the modifications and adaptations needed to make them suitable for use in a LiFi network (such as adding a DC-bias). However, it is not yet proven whether all of these approaches adopted for the RF domain can be effectively implemented in their current form also in LiFi networks, without introducing penalties like a reduction in spectral efficiency and data rate. Furthermore, a recurring theme in these works is the possibility to consider a LiFi/Wi-Fi network, which still allows for the use of traditional RF approaches by trying to fit the well-known results into the optical domain. Unfortunately, none of the current state of the art approaches precisely focuses on the IoT environment whenever addressing these considerations.

Papers dealing with this topic reveal that the almost totality of the physical layer aspects are well-known concepts, related to modulation schema and multi-antenna transmission techniques. The most relevant aspect is the description of features of the physical signal that are peculiar to LiFi transmission since they exploit the characteristics of the light signal. Results testify that some schemes can outperform the modulation schemes adopted in Wi-Fi networks in some network configurations. Another issue is the coexistence at the physical layer between classical Wi-Fi nodes, which typically are low-power and low-rate nodes, and LiFi nodes that

can manage very high data rates. This is another aspect, strictly related to the LiFi/Wi-Fi integration discussed in Section 7.5, that requires further research efforts.

There are also some security aspects discussed at the physical layer. The starting assumption is that the LiFi signal is, by its own nature, open and broadcast, and this surely poses important security issues also for LiFi networks. Security is faced from the point of view of the physical signal, involving aspects like beamforming, MIMO techniques, modulation and precoding schemes, and CSI.

7.7 Energy efficiency

This section analyzes all the research papers proposing solutions for energy efficiency suitable for LiFi in IoT scenarios [129], [131], [132], [248], [254], [260]. In all the analyzed papers, energy efficiency may be achieved by:

- selecting the optimal number of APs [260];
- electing the optimal LiFi AP [254];
- properly allocating transmission power in UL and/or DL directions [131], [254];
- choosing the most appropriate multiple access scheme [129], [248];
- designing antenna arrays in MIMO transmission techniques [132].

As testified in [129], at the physical layer an energy-efficient transmission in LiFi networks is influenced by the modulation scheme. Several modulation schemes can be adopted in LiFi systems, as highlighted in Section 7.6. Nevertheless, the choice of the modulation technique in IoT scenarios, where nodes are power- and resource-constrained, must be decided carefully. Indeed, multi-carrier modulation techniques like OFDM and its variants can provide higher spectral efficiency and throughput; nevertheless, they typically suffer from high computational complexity and energy consumption [244], [277], [278]. So, these techniques are not recommended for IoT nodes. From this point of view, single-carrier and pulse-based modulation techniques like OOK, PAM and CSK could be more effective. Such modulation schemes optimize the optical power utilization, also simplifying the design of the transmitter, where energy saving can be obtained by exploiting OOK. More specifically, higher energy efficiency can be reached if the OOK is implemented with switching transmitters where the power consumed is mainly due to the LED energy consumption [135]. In fact, by properly setting the amplitudes of the on and off states in the OOK-modulated signal, the dissipated energy in the optical transmitter can be made very negligible [135].

One of the main strengths of LiFi technology is its ability to provide both connectivity and illumination, indeed, [260] proposes a trade-off between the number of APs and energy consumption, using constraints that impose a threshold regarding the minimum level of illumination of the environment, by maximizing network performance in terms of the achieved data rate per user. More APs installed in the network mean a greater data rate experienced by each user (but the generated inter-AP interference will also increase). Conversely, the fewer the number of APs, the less energy is consumed (but the average level of illumination will also decrease). The decisive choice is made by the network designer, who selects the most essential metric from network performance and energy usage.

The contribution provided in [254] aims at decreasing the energy of IoT nodes in a hybrid LiFi/Wi-Fi network. Specifically, it designs a Mixed-Integer Linear Programming (MILP) problem that finds the optimum AP while satisfying all QoS constraints, the maximum number of simultaneously connected IoT nodes to each AP, and taking into account the upper bound of each IoT node transmission power. More in detail, the goal is to maximize the energy

efficiency of every IoT node, by setting the minimum transmission power able to meet the throughput constraints related to energy consumption. Performance results are compared with Wi-Fi-only or LiFi-only network scenarios.

In the context of multiple access schemes, a promising technique is given by NOMA. Differently from orthogonal multiple access schemes (like OFDM previously discussed) where users are allocated into orthogonal time and frequency resources, in NOMA all the users share simultaneously the whole time and frequency resources, since they are multiplexed in the power domain and demultiplexed by means of Successive Interference Cancellation (SIC) techniques [131], [279]. Some works in literature have proven the effectiveness of this scheme in multi-user IoT scenarios for 5G systems [279]–[281]. The same contribution [279] also testifies the suitability of NOMA schemes also for VLC networks. It is noteworthy that the adoption of NOMA schemes overcomes the inherent limitations of techniques like the above-mentioned OOK. Indeed, even if OOK is one of the simplest modulation techniques adopted in optical communications, it is not always suitable for high-rate transmission due to its low spectral efficiency. Conversely, also NOMA schemes can be made energy-efficient in LiFi systems by designing ad-hoc power allocation schemes that optimize the power allocated by users, at the same time improving the error performance of the system [279].

Given the considerations reported above, another low-complexity power adaptation strategy is proposed in [131] to improve the energy efficiency in a LiFi transmission for IoT environments. The proposal consists of a NOMA scheme that optimally adapts transmission power to maximize the energy efficiency in both DL and UL channels, achieving QoS guarantees for bidirectional communication. To this end, it proposes a closed-form solution with a low-complexity power allocation scheme suitable for LiFi bidirectional channel (i.e., visible light for the DL, infrared for the UL). The network energy efficiency is improved by reducing the likelihood of user outage while meeting all the QoS guarantees.

The lack of transmission methods capable of spatially multiplexing numerous devices without requiring a recurrent fee payment (e.g., NB-IoT) is critical in IoT scenarios. The contribution [129] addresses this issue by providing an innovative energy-efficient communication strategy based on optical OFDM in LiFi environment, that achieves interference-free communication. In the proposed system, LiFi users coexist with IoT devices under a common LiFi AP. This scheme is useful for taking the most appropriate decision on the combination of multiple access and modulation techniques in both the DL and UL channels, to save energy. Delay and throughput performance are also evaluated.

The work [248] provides a model based on the integration of an energy-harvesting wireless sensor network with hybrid LiFi/Wi-Fi communication techniques. This study presents a model that allows for multiple channel accesses while reducing interference. It accounts for the capability of the energy harvesting sensor to transfer the harvested energy to the sensor node or storage charge and to manage the output of sensors. In this context, the single-carrier modulation schemes (e.g., PPM, OOK, PAM) are analyzed for LiFi, also addressing dimming performance for the OOK for visible light systems [248] or in hybrid visible light/infrared communication systems [134]. Multicarrier modulation techniques, like OFDM, are also mentioned as more effective for high data-rate transmission, or in presence of signal distortion and frequency selectivity in the optical channel [248]. It is well known in fact that OFDM presents higher spectral efficiency and robustness against dispersion and varying channel conditions [135]. This contribution also analyzes the CSK as a LiFi-specific modulation. Finally, the simulation results show that a bidirectional multiaccess/multiuser hybrid LiFi/Wi-Fi communication scheme can be effectively utilized due to its ability to provide interoperability for multiple devices/users at a high data throughput rate of 25 Mb/s.

As remarked in [282], MIMO can be effectively adopted in IoT environments due to its capability of serving simultaneously a large amount of IoT nodes, at the same time improving energy and spectral efficiency and increasing the overall system capacity. This holds true

especially when a large number of antennas is deployed at the base station side [282]. Several other contributions also highlight the effectiveness of the MIMO adoption in different frequency bands, including millimeter wave (mmWave), terahertz (THz) and optical wireless bands, thus guaranteeing reliable and energy efficient communication in several IoT scenarios [283], [284].

Indeed, different MIMO transmission techniques are proposed in [132] for an indoor LiFi system based on VLC and employed in IoT scenarios. In detail, an adaptive method is proposed to enhance the energy efficiency of MIMO for VLC. Specifically, by varying the channel conditions, the desired spectral efficiency, and a target error rate, the MIMO technique is selected from three options: repetition coding, spatial multiplexing, and a modified version of spatial modulation. Finally, MIMO technique with the lowest energy requirement is chosen based on the user's location, thus reducing energy consumption, by also considering the desired spectral efficiency and target BER. This adaptive method can be particularly useful in IoT applications where energy consumption is a critical concern.

Since MIMO is based on spatial diversity for signal transmission, its performance is influenced by the position of the LiFi network elements (light sources and photo-detectors), and by the channel conditions [285]. The analysis carried out in this paper shows that this diversity factor impacts the main parameters that contribute to energy consumption, i.e., the optical power needed to reach a target BER. So, the optimization of the energy consumption depends on the chosen MIMO technique as related to the specific IoT scenario (more details on this can be found in [132]).

The works analyzed in this section suggest that the minimization of energy consumption is of paramount importance in LiFi networks serving IoT systems. Indeed, IoT nodes are usually battery-powered and batteries should last for a very long time. This issue is exacerbated for LiFi access networks, thought to achieve very high data rates that require a higher power consumption at the node side to meet this requirement. Efforts in this direction have been made mostly by analyzing data transmission at the physical layer, considering LiFi channel models, energy-efficient modulation schemes, the adoption of MIMO strategies and the optimization of the transmission power for the LiFi nodes.

7.8 Design of communication schemes

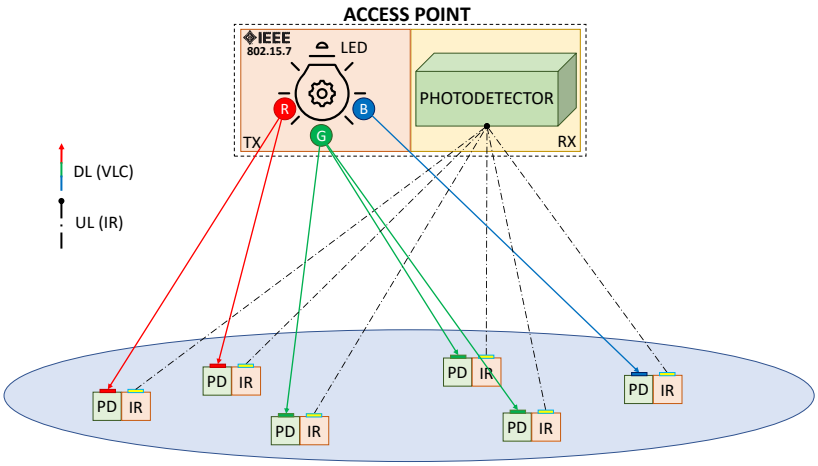

Figure 7.4: Example of design of communication scheme.

This section identifies and discusses the contributions that analyze communication schemes applicable to IoT environments adopting the LiFi technology, as shown in Fig. 7.4.

In this framework, a basic approach is proposed in [264]. In this work, the system is made up of a smartphone and a LED that implements a LiFi bidirectional channel. The former is outfitted with a flashlight as a transmitter and a camera that serves as a receiver. The initial stage in acquiring information is a picture captured by the camera, which extracts the brightness component of the image. The LED position is then detected. The signal is decoded after equalization and quantization. Finally, the information can be successfully collected following the error-checking procedure. Furthermore, the LED can act both as a transmitter and a receiver. Specifically, variations in incoming light intensity can be detected by charging a reversed biased LED and measuring its electric tension after a short time interval [264]. Specific efforts have been made in the design of communication schemes for outdoor scenarios, which are critical for LiFi networks [262], [263]. The authors in [262] propose use cases suitable for a disaster scenario by exploiting the VLC over a lighthouse to communicate with fishermen in an emergency situation. The outdoor LiFi communication scheme is implemented following the DMX512-A standard that enables the unidirectional data transmission for VLC. Specifically, the device block diagram includes a power supply, a serial interface linked directly to a laptop and a microcontroller that manages the light-based transmitter or receiver. Another contribution in [263] designs a SDN-enabled LiFi attocellular network virtualization able to share the infrastructure over multiple Mobile Virtual Network Operators (MVNOs). This is possible thanks to a resource slicing application offered by the northbound of the SDN controller that is also able to handle the on-demand creation of a LiFi DL channel. Under heterogeneous bursty traffic conditions, the proposed approach aims to maximize the data rate and optimize the allocated resources of each MVNO infrastructure, while minimizing the fees incurred by the providers. To this end, a heuristic matching game method is exploited to properly address the resulting optimization strategy.

Differently from the previous works, communication schemes for indoor scenarios are proposed in [129], [242], [247], [261]. The authors of [129] propose a novel architecture for LiFi-based indoor networking for IoT users. In detail, the work designs a LiFi AP with a transmitter that can operate on three distinct wavelengths (i.e. red, blue, and green) to communicate with different receivers at the same time, and a receiver consisting of a photodetector capable of gathering IoT node signals. Furthermore, it proposes equipping IoT nodes with one element capable of sending in the infrared band and the other component capable of receiving by filtering the system's different wavelengths. Once the communication equipment has been described, the block diagram of the various forms of modulation employed in the DL channel is defined, beginning from modulation and moving through the DAC and ADC until the signal demodulation. The work in [242] envisions the deployment of a one-way LiFi hotspot that is engaged for DL communication only. It transmits the data stream to the end user by generating it via LED. First, the data stream is encoded by the transmitter, enabling an asynchronous communication based on MQTT and with frames as small as 11 bits (one start bit, two stop bits, and eight ASCII characters). Finally, the receiver may decode the broadcast signal into alphanumeric characters by analyzing the received frame with the help of a solar panel that detects tiny changes in light. The benefits of adopting LiFi in high interference conditions due to high voltage and strong magnetic fields are shown in [247]. First, this contribution introduces a novel concept called the Internet of Light, in which lights are assigned an IPV6 address and are considered network nodes. In detail, a sensor is inserted inside a High Voltage Direct Current converter to provide constant feedback on its functioning state. Finally, the voltage is detected by the sensor, which sends the signal created by a modulator to the light source, which is received by an optical antenna of the receiver and demodulated before passing to the signal processing phase. According to the authors of [261], a LiFi network is used to achieve device-to-device (D2D) communication in an ultra-dense Industrial Internet of Things (IIoT) environment, by adopting a scenario drawn from the IEEE 802.11bb standard for VLC communication.

The choice of such a standard is particularly suitable for the analysis of realistic IIoT scenarios, like the one described in detail in [286], especially for what concerns the channel model. Furthermore, as remarked in [287], if compared to the other optical wireless communications standards like IEEE 802.15.7, IEEE 802.15.13, or the ITU-T G.9991, IEEE 802.11bb introduces only slight modifications to the MAC layer of the IEEE 802.11 standard adopted by for Wi-Fi, thus easing the LiFi/Wi-Fi coexistence which is an important aspect in an IoT environment [248], [254], [271].

In this scenario, the network is split into clusters identifiable by a given LiFi AP, and each of these AP covers a variable number of mobile devices that act as relying upon the AP for the gathered data from the IIoT nodes. Specifically, the IIoT nodes use the measured received optical intensity to choose the optimal mobile device suitable for the D2D. Finally, the network performance is quantified by evaluating different mobile device speeds, transmitter heights from the ground, and room sizes.

Unlike the previous contributions, papers [244], [248] focus on energy harvesting strategies. The work in [244] introduces IoT nodes that are self-sustaining in terms of energy and conducts a feasibility analysis using the existing technology. It specifically provides three alternative setups that employ an AP outfitted with a LED for transmission, a photodetector, and a CMOS camera for data reception. In the first configuration, an IoT node is equipped with a solar panel that can perform both energy harvesting and data reception in DL, while for transmission a liquid crystal shutter is employed, which can perform both backscattering and UL communication in VLC. The second configuration employs a solar panel that is also responsible for waking up the IoT node to allow communication in the UL channel exploiting the infrared technology. The third configuration presents a hybrid node that uses both LiFi and RF, with the DL channel acting as a control channel to efficiently employ the RF, interrupting the sleep state. This study also illustrates three potential autonomous setups from the standpoint of energy, which is a crucial requirement for the IoT.

Another contribution analyzes a typical indoor IoT environment for smart housing and smart industries using a hybrid LiFi/Wi-Fi network [248]. The proposed system includes an EH-sensor node that can manage energy harvesting and communicates utilizing the frame structure defined in the 802.15.7 standard. When smart devices want to connect with EH-sensor, they transmit data to the frame creator block. Then, the output is sent to the encoder block. Once encoded, the data frame is sent from the modulation block to the LED driver, which produces blue light to interact with the EH-sensor. Indeed, it has an optical color filter to filter the blue-colored LED light and receive the data frame with the help of the photodetector. Furthermore, it keeps the received data in the buffer after demodulating and decoding the data frames. When EH-sensors wish to connect with smart devices opposite approach is taken utilizing a green LED light to avoid interference.

Finally, the contribution [265] proposes a solution for data storage in a secure LiFi environment for the IoT. Specifically, it describes a LiFi-IoT environment in which the sensors are coupled to a microcontroller capable of driving an array of LiFi transmitters, as shown in Fig. 7.5. Consequently, another array of photodetectors serves as an AP through the proposed system, which also includes a Advanced Encryption Standard (AES) algorithm adopting 128-bit symmetric keys and a Role-Based Access Control (RBAC) authentication and authorization mechanism. As a result, a method to securely store the sensed data is implemented.

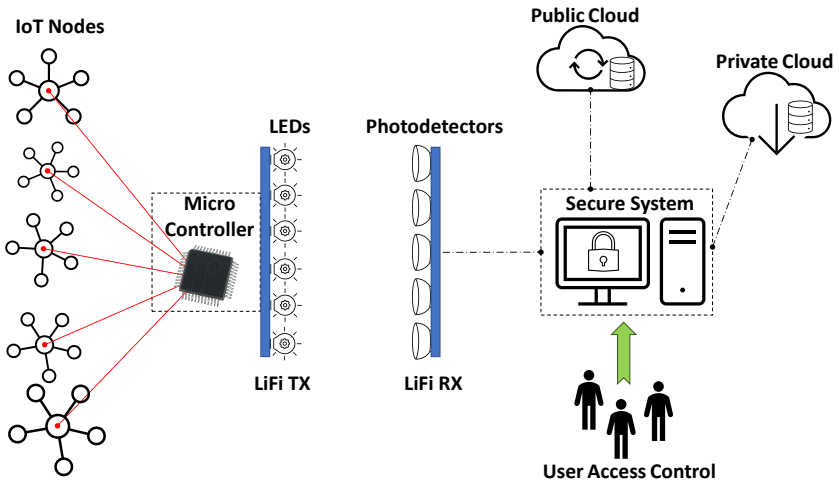

FIGURE 7.5: Example of a security system.

The communication schemes proposed in the analyzed works often investigate in depth the components of the communication systems and relate them to specific use case scenarios. An important aspect covered in these contributions is the proposal of communication schemes for outdoor scenarios, that are more critical for LiFi-based communication. In this context, the optimal selection of available resources to maximize the network data rate seems to be an interesting topic, bringing encouraging performance results. Unfortunately, finding the solution to this kind of optimization problem is time- and resource-consuming, making it difficult to meet the real-time requirements that are instead important in some IoT scenarios. Also, some standardization aspects and the coexistence among different modulation schemes at the physical layer are discussed, thus making the proposed schemes suitable for implementation into real testbeds.

It can be noted anyway that the proposed schemes are quite simple, in most cases being made of a single transmitter and a single receiver. More complex, multi-node scenarios, that are much closer to the IoT reality, are almost totally neglected or are evaluated theoretically, or their performance analysis is carried out through simulations. Also, a compliance analysis of the different standards adopted, wherever implemented simultaneously in the proposal, would be beneficial for practical implementations and performance evaluation in real-world scenarios, especially when LiFi is integrated with Wi-Fi technology. Another important lesson learned is that almost all the proposed communication schemes are described at the physical layer. To strengthen the analysis and provide a more exhaustive description of the schemes, an analysis of the schemes at higher layers (e.g., network layer, application layer, etc.) with the related standardized protocols adopted, would be beneficial.

Some security aspects are also tackled in the context of communication schemes. Nevertheless, security protocols for LiFi is still a work in progress that requires more investigation. Actually, the solutions proposed focus mainly on cryptographic mechanisms. Nevertheless, they must be chosen accurately, to meet the resource-constrained nature of IoT nodes, at the same time being fully compliant with the ongoing standardization efforts in the LiFi environment.

7.9 Positioning algorithms

This section describes the positioning algorithms proposed in LiFi networks for IoT applications. The proposed algorithms allow the localization of IoT nodes, also in hybrid indoor and outdoor environments, as shown in Fig. 7.6.

The work [245] provides an integration of the outdoor navigation system (e.g., Global Positioning System) with an indoor navigation system (e.g., LiFi technology). It designs a technique for indoor localization, which is primarily used to store a series of points that represent the latitude and longitude while it proposes a triangulation method for outdoor locating systems.

According to [111], [266], the implementation of LiFi positioning algorithms is a promising solution for indoor applications [111] and industrial environments [266]. In both these contributions, an indoor standard-compliant positioning system based on the so-called time-of-flight approach is implemented. It makes use of the frame structure of LiFi transmission, as stated in the International Telecommunication Union (ITU) Telecommunications Sector G.9991 recommendation [288]. Based on the information contained in the LiFi frame, two kinds of time information are derived: coarse time information (obtained by using the frame synchronization preamble) and fine time information (derived from the channel estimation preamble), to estimate the relative distance between each LiFi AP and the IoT node with high precision.

Real-world tests have been used to validate the proposed system.

Positioning algorithms can be useful to estimate the position of IoT nodes with high accuracy, thus being of great importance in some industrial environments or indoor scenarios where the position of an IoT node must be derived precisely. The main drawback of such techniques resides in the complexity of the LiFi network, which must be composed of a high number of APs to combine the information on the node position coming from the different APs, and the short coverage range of the LiFi signal that is negatively influenced by attenuations and obstacles. Another issue is that the positioning algorithms proposed in the state of the art literature could be energy-consuming, especially in scenarios with high mobility of IoT nodes, since their position needs to be continuously updated as they move in the reference area. So, their implementation should be carefully evaluated in such scenarios, when energy saving becomes a relevant issue.

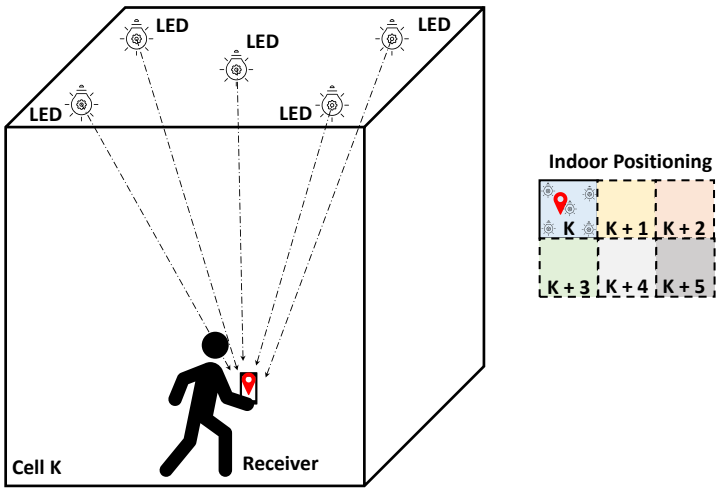

FIGURE 7.6: Example of indoor positioning approach.

7.10 Challenges and future research directions

This section aims at addressing the main challenges of LiFi adoption in IoT scenarios as derived from the analysis of the current literature, to find the related missing gaps. Based on this, possible research directions can be drawn to suggest what kind of themes deserve to be further investigated by future research work.

According to the analysis of the current literature, LiFi technology can fulfill the majority of the requirements of future systems put forward in the IoT field, including 5G, 5G&B, and others. Sharing LiFi and IoT technologies can be a highly effective solution to many of the challenges that take place in Wi-Fi access networks, particularly in terms of data rates, energy consumption, and scalability. This validates the potential of LiFi in a wide variety of IoT scenarios. However, it should be noted that most of the LiFi-based technology is still under investigation. Therefore, in the authors' opinion, it is necessary to pay attention to the obligation to examine crucial theoretical issues.

The first issue is that building LiFi networks to serve IoT systems requires the use of a small cell architecture, which leads to a dense deployment of LEDs. As highlighted in the analyzed papers, this raises the problem of managing inter-cell optical interference, in the framework of light transmission which is different from RF signal transmission. Additional research is needed in this direction. In this case, it is desirable to conduct full-scale experiments using models of real network sections. This aspect is another interesting research direction that can be further explored to provide innovative and effective theoretical models for the LiFi part of the network in IoT scenarios. Another problem that needs further research efforts is the management of the handover of IoT nodes in indoor scenarios with multiple APs and mobile devices. This aspect is important, especially in dense scenarios with real-time data exchange, to minimize service interruptions and maximize system efficiency.

The second issue is related to the thorough evaluation of the throughput performance of IoT systems when using strategies of interference management like MIMO. Some works coping with this issue propose the adoption of MIMO techniques to increase the system throughput and energy efficiency. Nevertheless, the effectiveness of such adoption is considered as for RF systems. Also in this case, a thorough evaluation of the real performance of MIMO together with its effectiveness in terms of throughput and quality of service would be beneficial in future research works, especially in real testbeds.

Another interesting research field is related to the challenging issue of the proposal and adoption of analytical models for LiFi explicitly tailored for the IoT domain. In fact, many papers in the scientific literature focus on the analytical models for the LiFi network ([125], [289]–[294]). Nevertheless, all the models proposed in the abovementioned papers refer only to LiFi systems, totally neglecting their integration with the IoT environment. Furthermore, there is still a lack of a reliable channel model for these systems [126]. For instance, unrealistic assumptions are made about the receiver's placement, such as presuming that the LiFi receiver is vertically upward or randomly located within the communication range of the transmitter [126].

Consequently, it is challenging to adapt these models to an environment full of constraints such as the IoT is. Indeed, there is a need to comprehend, design and validate the models produced for LiFi networks in the IoT context. At the same time, mathematical expressions and formulas taken from monographs are used, which do not fully take into account the parameters of modern transmitters and receivers of light signals in the IoT domain. Thus, it would be interesting to create a layout of the minimum configuration of the LiFi system, take measurements and validate the model as accurately as possible by comparing the measurement results with the outputs of the analytical model. This aspect has currently not been properly addressed by the current literature and requires a relevant effort, to properly align analytical results with experimental ones in integrated LiFi/IoT scenarios, and iteratively refine the proposed models accordingly, to solve LiFi network design problems in the IoT domain.

As a result of the conducted survey work, it is evident that much effort in the field of LiFi technology has been devoted to the analysis of the physical layer of light signal propagation between the transmitter (LED) and the photodetector. There are no exhaustive studies of LiFi systems that would analyze the processes of information from the source to the recipient at all levels: physical, channel, network, and above, even by adopting cross-layer approaches. The

key challenge is that each level has its own methods and procedures of data flow management, and there are opportunities to improve the efficiency of the system by analyzing the way(s) data is packetized and packets are managed at the different layers of the stack. In this context, also security assumes relevancy. More specifically, the management of authentication and authorization procedures is actually a challenge and needs further research to find the best trade-off among conflicting requirements, such as the implementation of lightweight security procedures to save the computational resources of IoT nodes, the layer(s) of the stack at which these procedures should e implemented, and the maintenance of the security guarantees when handover among different APs occurs. From this point of view, centralized or distributed security procedures could be implemented; nevertheless, they should take into account the specific IoT application scenario and the system architecture. In any case, by using recent achievements in solving the problems of information transfer at each level, it is feasible to identify new potential directions for the development of even more efficient LiFi systems.

Chapter 8

A Primer on Visible Light Indoor Positioning System via Intelligent Metasurface Reflectors

This Chapter introduces a novel IPS which jointly employs VLC and IMR. Starting from the channel gain and noise characterization, a RSS-based IMR-assisted Trilateration methodology is discussed. Specifically, the positioning error is modeled as a function of different parameters such as number of collected samples, bandwidth, and optical transmission power. A simulation campaign is carried out to assess the performance of the proposal under several configuration settings. Numerical results show the promising potential of this algorithm in terms of positioning accuracy.

8.1 System Model

This work considers a scenario that involves an indoor environment characterized by (i) a ceiling-mounted LED, (ii) N IMRs [143] installed on the walls of the room, and (iii) a PhotoDetector (PD) placed on the ground in an unknown location, as illustrated in Figure 8.1.

In particular, the LED emits incoherent light and is located at a fixed position $\mathbf{q} = [q^{\mathrm{x}}, q^{\mathrm{y}}, q^{z}]^{\mathsf{T}} \in \mathbb{R}^3$. Moreover, the IMRs are deployed at $\mathbf{w}_n = [w_{\mathrm{n}}^{\mathrm{x}}, w_{\mathrm{n}}^{\mathrm{y}}, w_{\mathrm{n}}^{z}]^{\mathsf{T}} \in \mathbb{R}^3$ and can operate in two modes, denoted by $a_n \in \{0, 1\}$ with $n = 1, \ldots, N$, which are (i) total absorption (i.e., $a_n = 0$) and (ii) specular reflection (i.e., $a_n = 1$). Finally, the PD is located at $\mathbf{u} = [u^{\mathrm{x}}, u^{\mathrm{y}}, 0]^{\mathsf{T}} \in \mathbb{R}^3$ and is characterized by a light detector area A. In this scenario, it is essential to take into account that the dimensions of the light source of the LED are deemed irrelevant when compared to the distances between the IMR and the light source. As a result, any point of observation on the surface of the reflector will perceive all points of the source to be at the exact same location, allowing us to regard the source as a single point, known as point source assumption.

8.1.1 Visible Light Channel Gain Model

The LoS channel gain [143] characterizing a VLC system is defined as follows

$$h_0 = \begin{cases} \frac{(m+1)A}{2\pi d_0^2} G \cos^m(\Theta) \cos(\theta), & 0 \leq \theta \leq \psi, \\ 0, & \text{otherwise}, \end{cases} \tag{8.1}$$

where Θ and θ are the angles of irradiance and incidence between the LED and PD. Moreover, ψ denotes the Field of View (FoV) of the PD, $d_0 = \|\mathbf{q} - \mathbf{u}\|$ is the LED-PD distance, and G

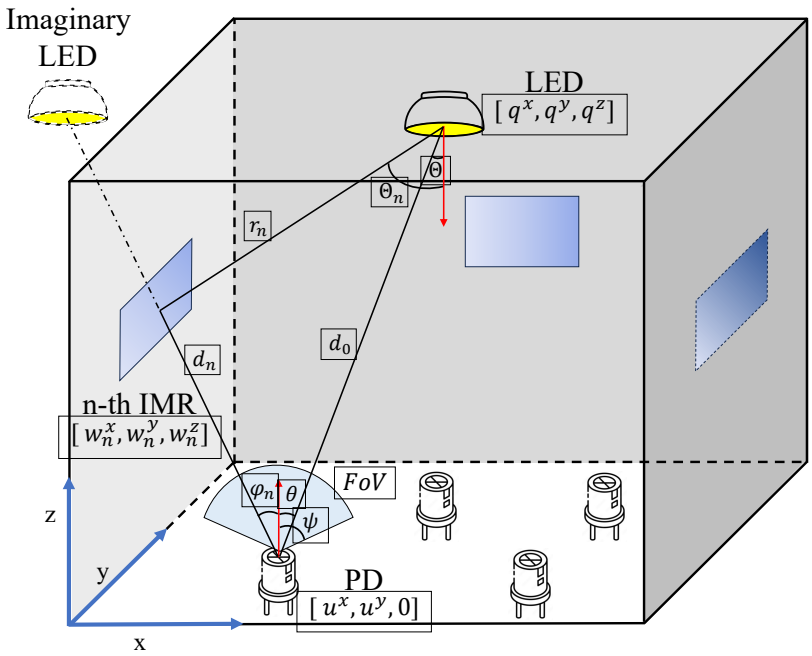

FIGURE 8.1: System Model.

describes the non-imaging concentrator. It can be represented as follows,

$$G = \begin{cases} T\frac{f^2}{\sin^2\psi}, & 0 \leq \theta \leq \psi, \\ 0, & \text{otherwise}, \end{cases} \tag{8.2}$$

where T is the gain of the optical filter, and f being the refractive index, and the Lambertian index is $m = -\frac{1}{\log_2 \cos(\Theta_{1/2})}$ with $\Theta_{1/2}$ is equal to the half-intensity radiation angle.

Generally, when indoor scenarios are considered, a wide range of NLoS phenomena affect the communication, including reflection, diffraction, scattering, and penetration paths. Nevertheless, due to the significant loss characterizing the VLC communication systems, penetration and diffuse reflection paths are commonly disregarded. Further, the diffraction can be neglected, given the extremely small wavelength scale [295]. As a result, only the specular reflection emerges as the prominent NLoS component within the context of IMR-assisted environments. The evaluation of this contribution, originating from the LED, undergoing reflection from the n-th IMR, and detected by the PD, can be model as in Eq. (8.1) but considering a longer path [296]. The latter encompasses both the LED-IMR and IMR-PD links, as

$$h_n = \begin{cases} \rho\frac{(m+1)A}{2\pi(r_n+d_n)^2} G \cos^m(\Theta_n)\cos(\varphi_n), & 0 \leq \varphi_n \leq \psi, \\ 0, & \text{otherwise}, \end{cases} \tag{8.3}$$

with ρ representing the reflection factor of all IMRs, Θ_n denoting the angle of irradiance between the LED and the n-th IMR, and φ_n representing the angle of incidence between the n-th IMR and the PD. Additionally, $d_n = \|\mathbf{w}_n - \mathbf{u}\|$ denotes the distance between the n-th IMR and the PD, while $r_n = \|\mathbf{q} - \mathbf{w}_n\|$ represents the distance between the LED and the n-th IMR. It is worth mentioning that, in the context of VLC, the wavelength is the order of the nanoscale. Hence, the near field assumption holds true since the signal propagation distance is smaller than $\frac{2D^2}{\lambda}$, where D represents the maximum size of the IMR and λ is the wavelength. As a consequence, the path loss follows the additive model [296]. Finally, by combining Eq. (8.1) and Eq. (8.3) the total received power at the PD side [144] can be

expressed as, $P = p\left(h_0 + \sum_{n=1}^{N} a_n h_n\right)$, where p is the transmitted power.

8.1.2 Visible Light Channel Noise Model

To achieve a precise estimation of the PD position, it is imperative to acknowledge the influence of noise affecting the channel. Indeed, due to the substantial attenuation of the VLC link, the magnitude of the noise could be comparable or even higher with respect to the one of the original signal. This contribution can be modeled according to a Gaussian distribution

$$\eta \sim \mathcal{N}(0, \sigma^2), \tag{8.4}$$

having zero mean and σ^2 as the variance. The latter primarily accounts for the impact of two distinct noise sources.

The first is known as shot noise, which is a random variation in signal intensity due to the discrete nature of particle interactions, such as photons striking a sensor, causing fluctuations especially at low signal levels.

This phenomenon can be mathematically expressed by means of its variance [9] as:

$$\sigma_{\text{S}}^2 = 2qRPB + 2qI_1B, \tag{8.5}$$

where q is the electron charge, R represents the responsivity of the PD, B is the equivalent noise bandwidth, I_1 is the current due to the background light.

The second source of noise is represented by the thermal noise, which causes shifts in current induced by the thermal agitation of electrons in the receiver circuit [9]. Specifically, its variance can be modeled as follows [297]:

$$\sigma_{\text{T}}^2 = \frac{8\pi\kappa\tau}{G_0}\nu A I_2 B^2 + \frac{16\pi^2\kappa\tau\zeta}{g}\nu^2 A^2 I_3 B^3, \tag{8.6}$$

where κ is the Boltzmann's constant, τ is the absolute temperature, G_0 is the open-loop voltage gain, and ν is the fixed capacitance of PD. Furthermore, ζ is the channel noise factor, g the transconductance, I_2 and I_3 are the noise bandwidth factors [298]. Finally, the total noise variance is denoted by $\sigma^2 = \sigma_{\text{S}}^2 + \sigma_{\text{T}}^2$.

8.1.3 Received Signal

Given the FoV constraint satisfied, it is assumed that the LED and the PD has the same orientation, i.e., $\cos\Theta = \cos\theta = q^z/d_0$, and hence the direct channel in (8.1) reads

$$h_0 = \frac{AG(m+1)(q^z)^{m+1}}{2\pi(d_0)^{m+3}}. \tag{8.7}$$

Similarly to the LoS case, it is possible to rearrange the IMR contribution in (8.3) as

$$h_n = \rho\frac{AG(m+1)}{2\pi(r_n + d_n)^2 d_n}U_n w_n^z, \tag{8.8}$$

since the position of LED and IMR are fixed, $\cos^m(\Theta_n) = U_n$ and $\cos(\varphi_n) = w_n^z/d_n$. Finally, leveraging the results above, the electric current signal received by the PD is

$$\mu = RP + \eta. \tag{8.9}$$

8.2 RSS-based IMR-assisted Trilateration

This work proposes an IPS relying on a multi-stage process, namely RSS-based IMR-assisted Trilateration. In the first step, $K_0 \in \mathbb{N}$ samples of the non-coherent light emitted by the LED are collected. Then, the average of this set is computed to reduce the noise and to obtain a more accurate representation of the underlying signal. The same procedure is also adopted for each IMR by gathering $K_n \in \mathbb{N}$ samples, where only one known IMR is set as reflective at a time. Therefore, recalling the definition in (8.9), the estimated current at receiver side is

$$\hat{\mu}_n = \frac{1}{K_n}\sum_{k=1}^{K_n} \mu_k = Rp\left(h_0 + a_n h_n\right) + \frac{1}{K_n}\sum_{k=1}^{K_n} \eta_{n,k} \triangleq \mu_n + \overline{\eta}_n, \tag{8.10}$$

where $\eta_{n,k} \sim \mathcal{N}(0, \sigma_n^2)$ denotes the k-th independent noise realization when n-th IMR is active, modeled according to (8.4). This contribution can be specialized in LoS and NLoS cases.

8.2.1 Line-of-Sight Link

Initially, the PD starts to detect the light received directly from the LED. The incoming signal μ_0 denotes the particular case where all the IMR are set in the absorptive status, by satisfying $\sum_{n=1}^{N} a_n = 0$. Furthermore, it is composed by solely the average of K_0 samples of the LED that generate an amount of current related to the LoS link equal to

$$\hat{\mu}_0 = Rph_0 + \frac{1}{K_0}\sum_{k=1}^{K_0} \eta_{0,k} \triangleq \mu_0 + \overline{\eta}_0, \tag{8.11}$$

with $\eta_{n,k} \sim \mathcal{N}(0, \sigma_0^2)$. Nevertheless, the estimated distance between the LED and the PD, denoted with $\hat{d}_0 \in \mathbb{R}$, is obtained by inverting the average received current in (8.11). To this aim, it is mandatory to leverage the noiseless model in order to avoid dealing with the intractable reciprocal Gaussian distribution. Therefore, it is possible to directly estimate the distance between the LED and the PD as follows,

$$\hat{d}_0 = \sqrt[m+3]{\frac{RAGp(m+1)(q^z)^{m+1}}{2\pi\hat{\mu}_0}} \triangleq \sqrt[m+3]{\frac{\beta_0}{\hat{\mu}_0}}. \tag{8.12}$$

8.2.2 Non-Line-of-Sight Link

When the n-th IMR is enabled, the total measured current can be estimated using the general expression (8.10). Hence, by subtracting the previous estimated LED contribution in (8.11) as

$$\hat{\Delta}_n = \hat{\mu}_n - \hat{\mu}_0, \tag{8.13}$$

it is possible to evaluate solely the IMRs contribution.

Therefore, the estimated distance $\hat{d}_n$ between the PD and the active IMR is derived by solving the following

$$(r_n + \hat{d}_n)^2 \hat{d}_n = \rho \frac{RAGp(m+1)}{2\pi\hat{\Delta}_n} U_n w_n^z \triangleq \frac{\beta_n}{\hat{\Delta}_n} \triangleq \alpha_n, \tag{8.14}$$

which has three different solutions. Nevertheless, only one of them is real and reads

$$\hat{d}_n = \frac{1}{3\tau_n}(r_n - \tau_n)^2, \tau_n = \sqrt[3]{\sqrt{27 r_n^3 \alpha_n + \frac{729}{4}\alpha_n^2} + r_n^3 + \frac{27}{2}\alpha_n}. \tag{8.15}$$

8.2.3 Linear Least Square Method

Once the PD has accumulated all the contributions from the IMRs, it proceeds to estimate its position employing LLS Trilateration method [9]. First, a system of $N+1$ equations is defined, with N averaged non-zero IMR contributions for each anchor. Specifically, the system links the estimated distance between each entity with the horizontal position of the PD, denoted as $\hat{\mathbf{u}} = [\hat{u}^{\mathrm{x}}, \hat{u}^{\mathrm{y}}]^T$, to derive as follows

$$\begin{cases} \hat{d}_0^2 = (\hat{u}^{\mathrm{x}} - q^{\mathrm{x}})^2 + (\hat{u}^{\mathrm{y}} - q^{\mathrm{y}})^2 + (0 - q^{\mathrm{z}})^2, \\ \hat{d}_1^2 = (\hat{u}^{\mathrm{x}} - w_1^{\mathrm{x}})^2 + (\hat{u}^{\mathrm{y}} - w_1^{\mathrm{y}})^2 + (0 - w_1^{\mathrm{z}})^2, \\ \qquad\qquad \vdots \\ \hat{d}_N^2 = (\hat{u}^{\mathrm{x}} - w_N^{\mathrm{x}})^2 + (\hat{u}^{\mathrm{y}} - w_N^{\mathrm{y}})^2 + (0 - w_N^{\mathrm{z}})^2. \end{cases} \tag{8.16}$$

It is possible to represent (8.16) in a linearized form by selecting an anchor equation as the reference and subtracting the others from it, as $\mathbf{A}\hat{\mathbf{u}} = \hat{\mathbf{y}}$ where

$$\mathbf{A} = \begin{bmatrix} w_1^{\mathrm{x}} - q^{\mathrm{x}} & w_1^{\mathrm{y}} - q^{\mathrm{y}} \\ \vdots & \vdots \\ w_N^{\mathrm{x}} - q^{\mathrm{x}} & w_N^{\mathrm{y}} - q^{\mathrm{y}} \end{bmatrix}, \hat{\mathbf{y}} = \frac{1}{2}\begin{bmatrix} \hat{d}_0^2 - \hat{d}_1^2 - \|\mathbf{q}\|^2 + \|\mathbf{w}_1\|^2 \\ \vdots \\ \hat{d}_0^2 - \hat{d}_N^2 - \|\mathbf{q}\|^2 + \|\mathbf{w}_N\|^2 \end{bmatrix}.$$

It is important to note that, a minimum of three non-zero contributions (corresponding to $N \geq 2$ IMRs), are required to make the system feasible. Finally, by leveraging the least square method, the estimated horizontal PD position is

$$\hat{\mathbf{u}} = (\mathbf{A}^T\mathbf{A})^{-1}\mathbf{A}^T\hat{\mathbf{y}}. \tag{8.17}$$

8.3 Positioning Error

In this Section, the analysis on the positioning error is conducted in order to derive the number of samples required to achieve a prescribed accuracy. The goal is to guarantee that the absolute error between the actual signal and the estimated one is lower than a certain threshold δ_0 with a probability greater than $1-\varepsilon$, such that

$$\mathbb{P}(|\hat{\mu}_0 - \mu_0| \leq \delta_0) = \mathbb{P}\big(|\overline{\eta}_{0,k}| \leq \delta_0\big) = \mathbb{P}\left(\frac{\sigma_0}{\sqrt{K_0}}\big|\mathcal{N}(0,1)\big| \leq \delta_0\right) =$$
$$\mathbb{P}\left(\mathcal{HN}\left(\frac{\sigma_0}{\sqrt{K_0}}\right) \leq \delta_0\right) = \operatorname{erf}\left(\sqrt{\frac{\delta_0^2 K_0}{2\sigma_0^2}}\right) \geq 1 - \varepsilon. \tag{8.18}$$

Imposing the minimum tolerable error probability with strict equality, the number of samples required is obtained as

$$K_0 = 2\sigma_0^2\delta_0^{-2}\operatorname{erf}^{-1}(1-\varepsilon)^2. \tag{8.19}$$

The above rationale can be applied also to the IMR case, while considering the error brought by $\hat{\mu}_0$ in (8.13) as

$$\mathbb{P}\left(|\hat{\Delta}_n - \Delta_n| \leq \delta_n\right) = \mathbb{P}\left(\left|\mathcal{N}\left(0, \frac{\sigma_0^2}{K_0}\right) - \mathcal{N}\left(0, \frac{\sigma_n^2}{K_n}\right)\right| \leq \delta_n\right) = \mathbb{P}\left(\mathcal{HN}\left(\sqrt{K}\right) \leq \delta_n\right) = \operatorname{erf}\left(\delta_n (2K)^{-\frac{1}{2}}\right) \geq 1 - \varepsilon, \tag{8.20}$$

where $K = \frac{\sigma_0^2 K_n + \sigma_n^2 K_0}{K_0 K_n}$ and $\Delta_n = \mu_n - \mu_0$. After some mathematical manipulations, the number of required samples is

$$K_n = \frac{2\sigma_n^2 K_0}{\delta_n^2 K_0 \operatorname{erf}^2(1-\varepsilon) - 2\sigma_0^2} = \frac{2\left(\sigma_n \operatorname{erf}^{-1}(1-\varepsilon)\right)^2}{\delta_n^2 - \delta_0^2}, \tag{8.21}$$

which demonstrates that the IMR contribution cannot be more precise than the LED one, i.e., $\delta_n > \delta_0$. Further, for $\varepsilon \to 0$, the absolute errors ϵ_0 and ϵ_n between the distance and its estimate, in the two cases, can be expressed starting from the absolute errors on the current $\delta_0 = \mu_0 - \hat{\mu}_0$ and $\delta_n = \Delta_n - \hat{\Delta}_n$. Therefore, starting from the definition of β_0 and β_n in (8.12) and (8.14), it results that

$$\begin{aligned}
&\delta_0 = \frac{\beta_0}{d_0^{m+3}} - \frac{\beta_0}{(d_0+\epsilon_0)^{m+3}} \Rightarrow \epsilon_0 = d_0\left(\sqrt[m+3]{\frac{\mu_0}{\mu_0 - \delta_0}} - 1\right),\\
&\delta_n = \beta_n\left(\frac{1}{(r_n+d_n)^2 d_n} - \frac{1}{(r_n+d_n+\epsilon_n)^2(d_n+\epsilon_n)}\right)\\
&\quad\Rightarrow (r_n+d_n+\epsilon_n)^2(d_n+\epsilon_n) = \frac{(r_n+d_n)^2 d_n \beta_n}{\beta_n - \delta_n (r_n+d_n)^2 d_n} \triangleq \gamma_n\\
&\quad\Rightarrow \epsilon_n = \hat{d}_n\big|_{\alpha_n = \gamma_n} - d_n,
\end{aligned}$$

where $\hat{d}_n$ is defined in (8.15). Finally, by rearranging the estimated position in (8.17) as $\hat{\mathbf{u}} = (\mathbf{A}^T\mathbf{A})^{-1}\mathbf{A}^T(\mathbf{y} + \tilde{\mathbf{y}})$, the error positioning vector $\mathbf{e} = [e^x, e^y]^T = (\mathbf{A}^T\mathbf{A})^{-1}\mathbf{A}^T\tilde{\mathbf{y}}$, where

$$\tilde{\mathbf{y}} = \frac{1}{2}\begin{bmatrix} \epsilon_0(\epsilon_0 + 2d_0) - \epsilon_1(\epsilon_1 + 2d_1) \\ \vdots \\ \epsilon_0(\epsilon_0 + 2d_0) - \epsilon_N(\epsilon_N + 2d_N) \end{bmatrix}.$$

The above chain of equations provide a analytical tool to assess the performance of IRS-assisted VLC systems.

8.4 Numerical Results

A simulation campaign is conducted hereby to provide useful results on the channel model and on the proposed RSS-based IPS. All the simulations, if not otherwise specified, adopt the following parameters [297], [298]: $\psi = \Theta_{1/2} = 70°$, $f = 1.5$, $\rho = 0.95$, $A = 0.2\,\mathrm{cm}^2$, $R = 0.54\,\mathrm{A/W}$, $T = 1$, $I_1 = 5\,\mathrm{pA}$, $I_2 = 0.562$, $I_3 = 0.0868$, $\tau = 295\,\mathrm{K}$, $G_0 = 10$, $\zeta = 1.5$, $g = 30\,\mathrm{mS}$, $\nu = 112\,\mathrm{pF/cm}^2$. For the sake of the analysis, in Fig. 8.2, the IMR contribution is analyzed imposing $d_0 = r_n = K_0 = K_n = 1$. Specifically, Fig. 8.2a depicts the signals (μ_0 and Δ_n) and the noise average power as a function of the distance, with a transmission power $p = 1000\,\mathrm{lumen}$ ($683\,\mathrm{lumen} = 1\,\mathrm{W}$). As expected, all curves diminish as the related distance increases, even if for higher bandwidth values this trend is less evident due to the dominance of the thermal noise over the shot one. Indeed, the former does not

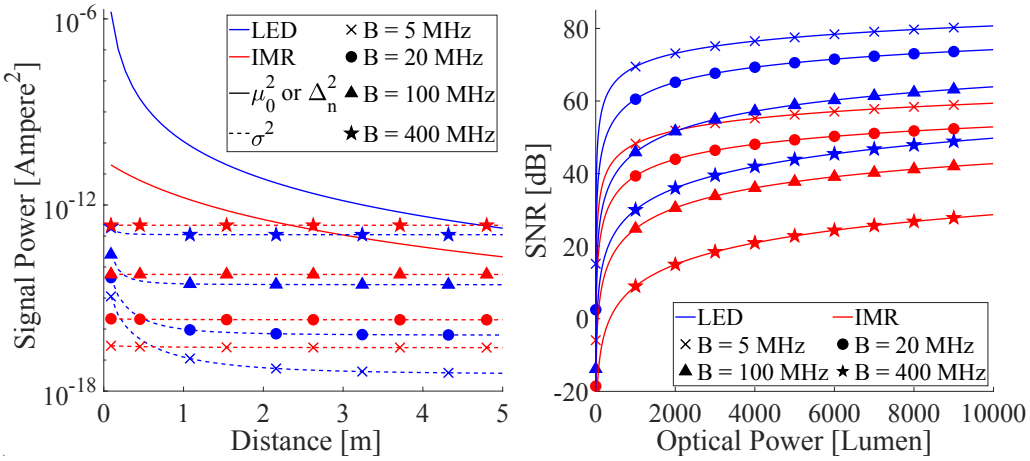

(A) Signal Power (B) SNR

FIGURE 8.2: Signal power and SNR for different bandwidths.

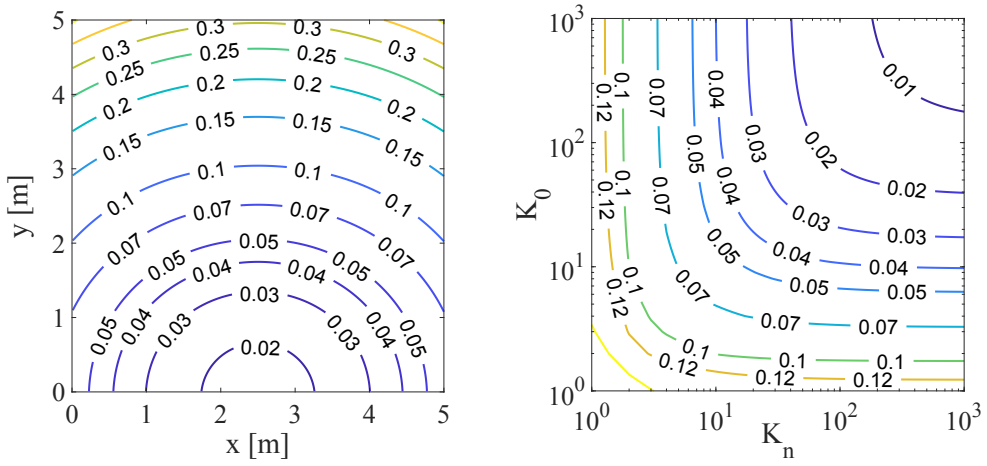

(A) $K_0 = 5$ and $K_n = 10$ (B) PD placed in the room center

FIGURE 8.3: Absolute error ϵ_n for different PD position and number of samples.

depend on the received power and hence the related curves do not decay with the distance. These results are further confirmed by Fig. 8.2b, where the SNR is reported as a function of the optical power. Clearly, under the selected parameter set, even with a low transmission power is always possible to obtain a satisfactory SNR also for the reflected signal (denoted by the red lines). However, this is not necessary true for all distances and hence a sufficient number of samples is required to obtain a target accuracy.

In this regard, it is considered a room of 5x5x3 m with a LED located at $\mathbf{q} = [2.5, 2.5, 3]^\mathsf{T}$, $N = 4$ IMRs mounted on the walls at $\mathbf{w}_1 = [2.5, 0, 2]^\mathsf{T}$, $\mathbf{w}_2 = [0, 2.5, 2]^\mathsf{T}$, $\mathbf{w}_3 = [5, 2.5, 2]^\mathsf{T}$, and $\mathbf{w}_4 = [2.5, 5, 2]^\mathsf{T}$, $B = 5\,\text{MHz}$, $\varepsilon = 10^{-3}$. Fig. 8.3 illustrates the absolute error ϵ_n when (i) the position of the PD changes and (ii) the number of samples K_0 and K_n varies with the PD fixed in the center of the room. Remarkably, $\epsilon_n \sim 7\,\text{cm}$ can be achieved with few samples and a low transmission power at the considered distance, i.e, $\sim 3\,\text{m}$. It is worth specifying that these results are valid for all the IMRs, which are symmetrically deployed, and are upper-bounds for ϵ_0.

Finally, adopting the same room configuration, Fig. 8.4 shows the RMSE, i.e., $\|\mathbf{e}\|$, for $N = 2$ and $N = 4$ IMRs by imposing $K_0 = 50$ and $K_n = 100$. The first setup provides

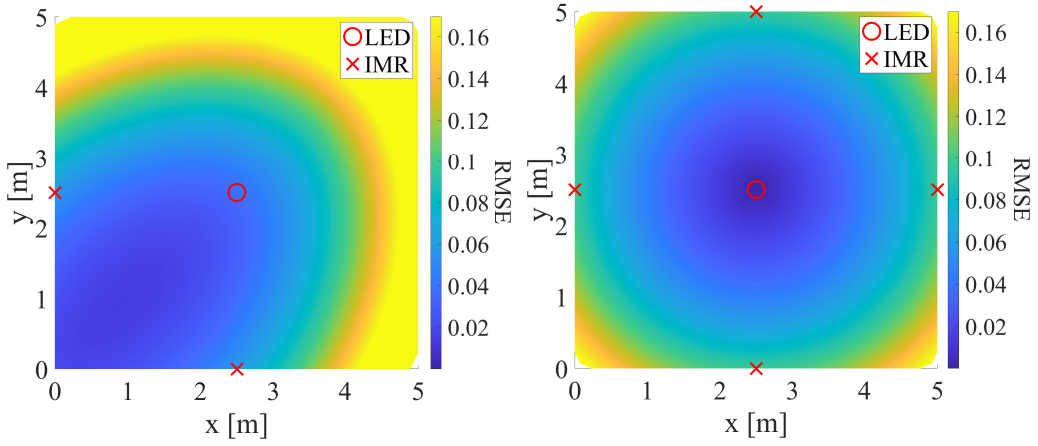

(A) $N = 2$ (B) $N = 4$

FIGURE 8.4: RMSE for different number of IMR.

the maximum accuracy in the area encompassed by the three entities, expressed with a pattern slightly deformed towards the center of mass weighted on the received power. On the contrary, the symmetrical deployment of the IMRs in the second configuration leads to a uniform coverage in terms of accuracy emerging as a pattern centered around the LED projected position.

Conclusions and Future Works

This work investigates the critical necessity of integrating NTN technologies into terrestrial networks to meet the evolving worldwide demands of the last decade for seamless connectivity. To this aim, Chapter 1 outlines the necessary steps to bridge this gap, thus effectively mitigating the digital divide. In particular, while 5G technology has undeniably advanced our communication capabilities, the proliferation of IoT smart devices, even in areas that are challenging to reach via terrestrial infrastructure, necessitate the development of the next-generation network (i.e., 5G&B). Bridging the digital divide in remote areas remains a significant challenge, and innovative solutions such as NTN, with their extensive coverage, are essential. Furthermore, the rise of the deployment of LEO CubeSats in the space-segment, driven by standardization and cost reductions, exemplifies the potential for space-based technology integration to enable ubiquitous connectivity. Nevertheless, 5G&B-based network requires more than just NTN solutions, terrestrial network advancements are equally important. Indeed, resource virtualization and VLC, standardized by IEEE 802.11bb and commonly referred to as LiFi, play pivotal roles in the evolution of the 5G&B networks in the IoT domain. On one hand, resource virtualization, as laid out by the rise of the Digital Twin, is a crucial component of network progress, blurring the line between the physical and digital realms. It offers novel avenues for human-machine interaction and allows for the integration of intelligent services into everyday activities. On the other hand, LiFi, in particular, offers high-speed data transmission through LED technology, leveraging existing lighting infrastructure to reduce deployment costs, enhance energy efficiency, and provide immunity to interference. In this rapidly evolving landscape, the synergy between space-based and terrestrial technologies will continue to drive innovation and shape the future of communication and connectivity, ensuring a more inclusive, efficient, and resilient digital future.

In particular, Chapter 2 presented a robust NB-IoT architecture for satellite communication, with a specific focus on its applicability in agriculture. The chapter delved into link-level considerations, including antenna selection and the fine-tuning of critical parameters, ensuring the reliability of the communication link. The crucial innovation is the assumption of deploying the entire protocol stack onboard the satellite, a departure from the conventional approach. Technical adaptations for the radio interface were explored to enable seamless connections between NTN terminals and remote satellites. Rigorous system-level simulations were conducted, validating the architecture's adherence to NB-IoT specifications and demonstrating its feasibility. Future research will broaden the scope to diverse applications, employing an experimental testbed to elevate technology readiness.

Chapter 3 introduced an extension of the open-source 5G-air-simulator, which models a satellite-based architecture for Narrowband Internet of Things (NB-IoT). This extension incorporates several crucial features, including blind repetitions management, the Layer-2 Satellite (L2S) model, cell selection procedures, and a satellite mobility model. This tool holds the promise of supporting research on satellite-based NB-IoT communication systems. Additionally, to demonstrate its effectiveness, the chapter presents a set of preliminary performance metrics derived from a monitored scenario. These results shed light on the significant impact of constellation configuration on latency and service reliability. Notably, the simulation tool underscores the importance of proper constellation dimensioning, showing that more satellites per orbit result in moderate NPRACH preamble collisions, leading to lower packet

delays and higher average delivery ratios for NTN terminals. Future work may expand upon this system-level investigation by assessing the effects of constellation configuration on more complex network topologies, examining multi-tone uplink and downlink channel configurations, and analyzing energy consumption patterns.

Chapter 4 proposed a novel 5G&B-oriented architecture with advanced orchestration capabilities of security services into the Non-Terrestrial segment. Specifically, it provides these main scientific contributions: i) a definition of network architecture and protocol stack enabling the interaction among terrestrial and space network entities, ii) a definition of a system model describing the network configuration and the delays associated with the deployment of specific security services, and iii) formulation of optimization problem willing to dynamically allocate security VNFs among satellites over a looking-ahead horizon. Three alternative heuristic methods for the aforementioned optimization problem have been investigated through computer simulation to assess the overall performance of the proposed approach. Obtained results demonstrated the ability of the conceived approach to deploying the requested services within a strict deadline. Specifically, the SA-based solution demonstrates to outperform the other approaches in terms of service deployment delays, resource consumption, and processing time. Future research activities will investigate more complex scenarios envisaging a deep integration of terrestrial and NTN, embracing other space network elements (such as drones). Moreover, they will also evaluate the effectiveness of the proposed solution through real experimental testbeds.

Chapter 5 presented a Satellite-IoT network powered by a UAV via WPT. Starting from the system model, two MINLP problems have been formulated to fairly maximize the harvested energy of the GNs and the total transmitted data towards a LEO CubeSat. This requires a joint optimization approach that encompasses recharge and transmission scheduling plans while accounting for drone kinematics. To handle the non-convexity of both problems, the former has been decomposed into two sub-problems and then reformulated by also applying SCA technique. Meanwhile, the latter is tackled by employing the same two aforementioned techniques. A simulation campaign has been conducted in order to evaluate the algorithm performance over different (i) number of GNs, (ii) number of antenna elements of the UAV, (iii) WPT transmission power levels, (iv) area sizes, and (v) mission duration. Finally, the proposed solution is compared with a reference baseline approach, demonstrating a substantial performance improvement, ranging from 1.5 to 7 times, in terms of the total amount of transmitted data. In the future, the research efforts will be focused on the following directions (i) extend the algorithm to multiple drones for a thoroughly integrated NTN cooperative network. (ii) investigate inductive and capacitive WPT models to improve the overall efficiency. (iii) employ 3D antenna arrays for a more flexible beam-steering and -forming strategies. (iv) expand the trajectory optimization and GN placement considering different heights to address different terrain conditions. (v) consider the presence of a IRS that can enhance the energy harvested by GNs. Finally, the proposal will lay the groundwork for the realization of a testbed that will be used for experimentation and measurements in the context of 5G&B technologies.

Chapter 6 proposed a novel resource capability-aware TMS scheme in the service provisioning for a SIoT environment. The proposed strategy aims to grant trusted services with a high QoE, overcoming some fundamental limitations in this research field, such as responsiveness, resource capability, efficiency, and scalability. Then, the performance of the proposed approach has been compared to baseline solutions. Obtained results highlight that the proposed scheme can process service requests in real-time, experiencing low latency within a fair resource distribution and relieving the IoT devices from any computational load. Furthermore, it allows a responsive identification of malicious nodes, preventing them from acting as providers for forthcoming service requests. Future research activities will further examine the multi-clustered structure by investigating the synchronization procedure between Primary Nodes. Furthermore, a security service will be set for real-time propagation of the malicious

nodes identification along the clusters.

Chapter 7 provided a thorough overview of the research activities on the LiFi technology applied to the IoT scenario. After a detailed description of the novel aspects of this work and the main differences from the other surveys and review papers, the surveyed papers have been classified based on the different topics, that range from the adoption of LiFi in IoT applications to integrated communication technologies, the solution to optimization problems, QoS provisioning, energy efficiency, physical layer analysis, positioning strategies, security and proposals of communication schemes. From the analysis of the surveyed literature, some important conclusions can be drawn. First, there are some topics that attract much interest, like the adoption of LiFi technology in different application scenarios and the integration or coexistence of LiFi with other technologies like Wi-Fi or cellular networks. This is testified by the number of works on these topics. Second, the QoS provisioning is mostly related to the solution to optimization problems, that sometimes is hard to find due to the complexity of the problem itself and not always suitable for IoT devices, which usually have reduced computational resources. Third, the energy saving issue is crucial in IoT environments, where nodes are battery-powered. Nevertheless, for the sake of feasibility in IoT environments, the proposed strategies must keep a low complexity and a high transmission efficiency. Fourth, it is very important to focus the research efforts on the coexistence of LiFi with other communication technologies (Wi-Fi or cellular networks), preventing communication systems and network architectures to be designed from scratch. The main difficulty related to this topic is the integration and interaction among different protocols, developed by different standardization bodies, and at different layers of the stack. Additional efforts have thus to be spent in this direction.

Chapter 8 investigated the performance of the RSS-based IMR-assisted Trilateration, starting from the mathematical model of the VLC channel and the related noise contribution. The impact of the number of samples collected, the distance of the PD, and the bandwidth on the overall accuracy has been evaluated through an analytical study and corroborated by numerical results. The derived findings can be employed for the design and assessment of such IPS. Future works include the optimization of the position of LED and IMRs, as well as the investigation of the PD tilting angle and different multiplexing techniques.

In conclusion, the integration of terrestrial and non-terrestrial technologies in the IoT network represents a pivotal aspect, as extensively discussed in this work. This integration necessitates adaptations ranging from the physical and link levels to the application level, with a crucial focus on resource virtualization and optimization. Hence, it is imperative for terrestrial networks to facilitate the continuous development, even among the challenges posed by the scarcity of available spectrum in the radio frequency domain. Indeed, this work also includes preliminary investigations into the performance of the innovative LiFi technology.

Bibliography

[1] M. M. Azari, S. Solanki, S. Chatzinotas, *et al.*, "Evolution of non-terrestrial networks from 5G to 6G: A survey," *IEEE communications surveys & tutorials*, 2022.

[2] O. Kodelhi, A. Guidotti, and A. Vanelli-Coralli, "Integration of Satellites in 5G through LEO Constellations," in *IEEE Global Communications Conference (GLOBECOM 2017)*, 2017, pp. 1–6. DOI: 10.1109/GLOCOM.2017.8255103.

[3] F. Rinaldi, H. .-. Maattanen, J. Torsner, *et al.*, "Non-Terrestrial Networks in 5G Beyond: A Survey," *IEEE Access*, vol. 8, pp. 165 178–165 200, 2020. DOI: 10.1109/ACCESS.2020.3022981.

[4] A. Vanelli-Coralli, A. Guidotti, T. Foggi, G. Colavolpe, and G. Montorsi, "5G and Beyond 5G Non-Terrestrial Networks: trends and research challenges," in *2020 IEEE 3rd 5G World Forum (5GWF)*, IEEE, 2020, pp. 163–169.

[5] 3gpp, "Study on Narrow-Band Internet of Things (NB-IoT) / enhanced Machine Type Communication (eMTC) support for Non-Terrestrial Networks (NTN)," 3rd Generation Partnership Project, Technical Report (TR) 36.763, 2021.

[6] Z. Xiao, J. Yang, T. Mao, *et al.*, "LEO Satellite Access Network (LEO-SAN) towards 6G: Challenges and Approaches," *IEEE Wireless Communications*, pp. 1–8, 2022. DOI: 10.1109/MWC.011.2200310.

[7] L. Atzori, A. Iera, G. Morabito, and M. Nitti, "The Social Internet of Things (SIoT) – When social networks meet the Internet of Things: Concept, architecture and network characterization," *Computer Networks*, vol. 56, Nov. 2012. DOI: 10.1016/j.comnet.2012.07.010.

[8] IEEE, "IEEE Approved Draft Standard for Information Technology–Telecommunications and Information Exchange Between Systems Local and Metropolitan Area Networks–Specific Requirements - Part 11: Wireless LAN Medium Access Control (MAC) and Physical Layer (PHY) Specifications Amendment 7: Light Communications," *IEEE P802.11bb/D7.0, March 2023*, pp. 1–29, 2023.

[9] Y. Zhuang, L. Hua, L. Qi, *et al.*, "A survey of positioning systems using visible LED lights," *IEEE Communications Surveys & Tutorials*, vol. 20, no. 3, pp. 1963–1988, 2018.

[10] 3gpp, "Study on architecture aspects for using satellite access in 5G," 3rd Generation Partnership Project, Technical Report (TR) 23.737, 2019.

[11] G. Araniti, A. Iera, S. Pizzi, and F. Rinaldi, "Toward 6G Non-Terrestrial Networks," *IEEE Network*, vol. 36, no. 1, pp. 113–120, 2022. DOI: 10.1109/mnet.011.2100191.

[12] O. Kodheli, E. Lagunas, N. Maturo, *et al.*, "Satellite Communications in the New Space Era: A Survey and Future Challenges," *IEEE Communications Surveys Tutorials*, vol. 23, no. 1, pp. 1–1, 2020. DOI: 10.1109/COMST.2020.3028247.

[13] X. Zhu and C. Jiang, "Creating Efficient Integrated Satellite-Terrestrial Networks in the 6G Era," *IEEE Wireless Communications*, 2022.

[14] 3GPP, "E-UTRA and E-UTRAN; LTE Physical Layer, General Description," 3rd Generation Partnership Project (3GPP), Technical Specification (TS) 36.201, 2018, Release 15.

[15] 3GPP, "E-UTRA and E-UTRAN; LTE Physical Layer, Overall Description," 3rd Generation Partnership Project (3GPP), Technical Specification (TS) 36.300, 2018, Release 15.

[16] X. Lin, A. Adhikary, and Y. .-. Eric Wang, "Random Access Preamble Design and Detection for 3GPP Narrowband IoT Systems," *IEEE Wireless Communications Letters*, vol. 5, no. 6, pp. 640–643, 2016. DOI: 10.1109/LWC.2016.2609914.

[17] K. Mekki, E. Bajic, F. Chaxel, and F. Meyer, "A comparative study of LPWAN technologies for large-scale IoT deployment," *ICT Express*, vol. 5, no. 1, pp. 1–7, 2019, ISSN: 2405-9595. DOI: https://doi.org/10.1016/j.icte.2017.12.005. [Online]. Available: http://www.sciencedirect.com/science/article/pii/S2405959517302953.

[18] O. Kodheli, N. Maturo, S. Andrenacci, S. Chatzinotas, and F. Zimmer, "Link budget analysis for satellite-based narrowband IoT systems," in *International Conference on Ad-Hoc Networks and Wireless*, Springer, 2019, pp. 259–271.

[19] G. Charbit, D. Lin, K. Medles, L. Li, and I. Fu, "Space-Terrestrial Radio Network Integration for IoT," in *Proc. of IEEE 6G Wireless Summit (6G SUMMIT)*, 2020, pp. 1–5. DOI: 10.1109/6GSUMMIT49458.2020.9083854.

[20] K. O'Hara and G. Skidmore, "Providing Narrowband IoT Coverage with Low Earth Orbit Satellites," *Microwave Journal*, vol. 62, no. 12, pp. 74–84, 2019.

[21] Z. Qu, G. Zhang, H. Cao, and J. Xie, "LEO Satellite Constellation for Internet of Things," *IEEE Access*, vol. 5, pp. 18 391–18 401, 2017. DOI: 10.1109/ACCESS.2017.2735988.

[22] S. Cluzel, L. Franck, J. Radzik, *et al.*, "3GPP NB-IOT Coverage Extension Using LEO Satellites," in *Proc. of IEEE Vehicular Technology Conference (VTC Spring)*, 2018, pp. 1–5. DOI: 10.1109/VTCSpring.2018.8417723.

[23] A. K. Dwivedi, S. Praneeth Chokkarapu, S. Chaudhari, and N. Varshney, "Performance Analysis of Novel Direct Access Schemes for LEO Satellites Based IoT Network," in *Proc. of IEEE Annual International Symposium on Personal, Indoor and Mobile Radio Communications*, 2020, pp. 1–6. DOI: 10.1109/PIMRC48278.2020.9217207.

[24] O. Kodheli, S. Andrenacci, N. Maturo, S. Chatzinotas, and F. Zimmer, "An Uplink UE Group-Based Scheduling Technique for 5G mMTC Systems Over LEO Satellite," *IEEE Access*, vol. 7, pp. 67 413–67 427, 2019. DOI: 10.1109/ACCESS.2019.2918581.

[25] M. Conti, S. Andrenacci, N. Maturo, S. Chatzinotas, and A. Vanelli-Coralli, "Doppler Impact Analysis for NB-IoT and Satellite Systems Integration," in *Proc. of IEEE International Conference on Communications (ICC)*, 2020, pp. 1–7. DOI: 10.1109/ICC40277.2020.9149140.

[26] O. Kodheli, N. Maturo, S. Chatzinotas, S. Andrenacci, and F. Zimmer, "On the Random Access Procedure of NB-IoT Non-Terrestrial Networks," in *Proc. of IEEE Advanced Satellite Multimedia Systems Conference (ASMS) and 16th Signal Processing for Space Communications Workshop (SPSC)*, IEEE Virtual Conference, 2020.

[27] A. Guidotti, A. Vanelli-Coralli, M. Conti, *et al.*, "Architectures and Key Technical Challenges for 5G Systems Incorporating Satellites," *IEEE Transactions on Vehicular Technology*, vol. 68, no. 3, pp. 2624–2639, 2019. DOI: 10.1109/TVT.2019.2895263.

[28] 3GPP, "Solutions for NR to support Non-Terrestrial Networks (NTN)," 3rd Generation Partnership Project (3GPP), Technical report (TR) 38.821, 2019, Release 16.

[29] 3GPP, "[IoT-NTN] Applicability of TR 38.821 (MediaTek)," 3rd Generation Partnership Project (3GPP), Discussion, Decision R2-2011275, Nov. 2020, RAN WG2 112e.

[30] ITU, "IMT Vision – Framework and overall objectives of the future development of IMT for 2020 and beyond," International Telecommunication Union (ITU), Recommendation 2083-0, 2015, ITU-R M.2083-0.

[31] S. Narayanan, D. Tsolkas, N. Passas, and L. Merakos, "NB-IoT: A Candidate Technology for Massive IoT in the 5G Era," in *Proc. of IEEE International Workshop on Computer Aided Modeling and Design of Communication Links and Networks (CAMAD)*, 2018, pp. 1–6. DOI: 10.1109/CAMAD.2018.8514963.

[32] M. Gineste, T. Deleu, M. Cohen, *et al.*, "Narrowband IoT Service Provision to 5G User Equipment via a Satellite Component," in *Proc. of IEEE Globecom Workshops (GC Wkshps)*, 2017, pp. 1–4. DOI: 10.1109/GLOCOMW.2017.8269209.

[33] O. Liberg, S. E. Löwenmark, S. Euler, *et al.*, "Narrowband Internet of Things for Non-terrestrial Networks," *arXiv preprint arXiv:2010.04906*, 2020.

[34] J. Doré and V. Berg, "Turbo-FSK: A 5G NB-IoT Evolution for LEO Satellite Networks," in *Proc. of IEEE Global Conference on Signal and Information Processing (GlobalSIP)*, 2018, pp. 1040–1044. DOI: 10.1109/GlobalSIP.2018.8646371.

[35] O. Kodheli, S. Andrenacci, N. Maturo, S. Chatzinotas, and F. Zimmer, "Resource Allocation Approach for Differential Doppler Reduction in NB-IoT over LEO Satellite," in *Proc. of IEEE Advanced Satellite Multimedia Systems Conference and the 15th Signal Processing for Space Communications Workshop (ASMS/SPSC)*, 2018, pp. 1–8. DOI: 10.1109/ASMS-SPSC.2018.8510724.

[36] S. Cluzel, M. Dervin, J. Radzik, S. Cazalens, C. Baudoin, and D. Dragomirescu, "PHYSICAL LAYER ABSTRACTION FOR PERFORMANCE EVALUATION OF LEO SATELLITE SYSTEMS FOR IOT USING TIME-FREQUENCY ALOHA SCHEME," in *Proc. of IEEE Global Conference on Signal and Information Processing (GlobalSIP)*, 2018, pp. 1076–1080. DOI: 10.1109/GlobalSIP.2018.8646372.

[37] 3gpp, "System architecture for the 5G System (5GS) - 3GPP TS 23.501 version 17.4.0 Release 17," 3rd Generation Partnership Project, Technical Specification (TS) 36.331, May 2022, Version 17.4.0.

[38] M. Cui, Y. Fei, and Y. Liu, "A Survey on Secure Deployment of Mobile Services in Edge Computing," *Security and Communication Networks*, vol. 2021, 2021.

[39] P. Ranaweera, A. D. Jurcut, and M. Liyanage, "Survey on Multi-Access Edge Computing Security and Privacy," *IEEE Communications Surveys Tutorials*, pp. 1–1, 2021. DOI: 10.1109/COMST.2021.3062546.

[40] M. Giordani and M. Zorzi, "Non-Terrestrial Networks in the 6G Era: Challenges and Opportunities," *IEEE Network*, vol. 35, no. 2, pp. 244–251, 2021. DOI: 10.1109/MNET.011.2000493.

[41] E. Yaacoub and M.-S. Alouini, "A Key 6G Challenge and Opportunity—Connecting the Base of the Pyramid: A Survey on Rural Connectivity," *Proceedings of the IEEE*, vol. 108, no. 4, pp. 533–582, 2020. DOI: 10.1109/jproc.2020.2976703.

[42] H. Cui, J. Zhang, Y. Geng, *et al.*, "Space-air-ground integrated network (SAGIN) for 6G: Requirements, architecture and challenges," *China Communications*, vol. 19, no. 2, pp. 90–108, 2022. DOI: 10.23919/jcc.2022.02.008.

[43] R. Doriguzzi-Corin, S. Scott-Hayward, D. Siracusa, M. Savi, and E. Salvadori, "Dynamic and Application-Aware Provisioning of Chained Virtual Security Network Functions," *IEEE Transactions on Network and Service Management*, vol. 17, no. 1, pp. 294–307, Mar. 2020, ISSN: 1932-4537. DOI: 10.1109/tnsm.2019.2941128.

[44] Q.-V. Pham, R. Ruby, F. Fang, *et al.*, "Aerial Computing: A New Computing Paradigm, Applications, and Challenges," *IEEE Internet of Things Journal*, pp. 1–1, 2022. DOI: 10.1109/jiot.2022.3160691.

[45] A. Chaoub, M. Giordani, B. Lall, *et al.*, "6G for Bridging the Digital Divide: Wireless Connectivity to Remote Areas," *IEEE Wireless Communications*, vol. 29, no. 1, pp. 1–9, 2021. DOI: 10.1109/MWC.001.2100137.

[46] M. Jia, L. Zhang, J. Wu, S. Meng, and Q. Guo, "Collaborative Satellite-Terrestrial Edge Computing Network for Everyone-Centric Customized Services," *IEEE Network*, pp. 1–21, 2022. DOI: 10.1109/mnet.131.2200375.

[47] Z. Zhang, W. Zhang, and F.-H. Tseng, "Satellite Mobile Edge Computing: Improving QoS of High-Speed Satellite-Terrestrial Networks Using Edge Computing Techniques," *IEEE Network*, vol. 33, no. 1, pp. 70–76, 2019. DOI: 10.1109/MNET.2018.1800172.

[48] W. Sun, H. Zhang, R. Wang, and Y. Zhang, "Reducing Offloading Latency for Digital Twin Edge Networks in 6G," *IEEE Transactions on Vehicular Technology*, vol. 69, no. 10, pp. 12 240–12 251, 2020. DOI: 10.1109/TVT.2020.3018817.

[49] H. A. Almashhadani, X. Deng, S. N. A. Latif, M. M. Ibrahim, and A. H. Alshammari, "An Edge-Computing Based Task-Unloading Technique with Privacy Protection for Internet of Connected Vehicles," *Wireless Personal Communications*, pp. 1–22, 2021.

[50] ZhenQin, Y. Liao, and D. Shen, "Multi-MEC server multi-user resource allocation in heterogeneous network," *Journal of Physics: Conference Series*, vol. 1792, p. 012 005, Feb. 2021. DOI: 10.1088/1742-6596/1792/1/012005.

[51] J. Plachy, Z. Becvar, E. C. Strinati, and N. d. Pietro, "Dynamic Allocation of Computing and Communication Resources in Multi-Access Edge Computing for Mobile Users," *IEEE Transactions on Network and Service Management*, vol. 18, no. 2, pp. 2089–2106, 2021. DOI: 10.1109/TNSM.2021.3072433.

[52] Y. Deng, Z. Chen, X. Chen, and Y. Fang, "Throughput Maximization for Multi-edge Multi-user Edge Computing Systems," *IEEE Internet of Things Journal*, pp. 1–1, 2021. DOI: 10.1109/JIOT.2021.3084509.

[53] S. Yuan, M. Peng, Y. Sun, and X. Liu, "Software defined intelligent satellite-terrestrial integrated networks: Insights and challenges," *Digital Communications and Networks*, 2022, ISSN: 2352-8648. DOI: https://doi.org/10.1016/j.dcan.2022.06.009.

[54] M. Pattaranantakul, R. He, Z. Zhang, A. Meddahi, and P. Wang, "Leveraging Network Functions Virtualization Orchestrators to Achieve Software-Defined Access Control in the Clouds," *IEEE Transactions on Dependable and Secure Computing*, vol. 18, no. 1, pp. 372–383, 2021. DOI: 10.1109/tdsc.2018.2889709.

[55] V. Eramo, E. Miucci, M. Ammar, and F. G. Lavacca, "An Approach for Service Function Chain Routing and Virtual Function Network Instance Migration in Network Function Virtualization Architectures," *IEEE/ACM Transactions on Networking*, vol. 25, no. 4, pp. 2008–2025, 2017. DOI: 10.1109/tnet.2017.2668470.

[56] S. Sahhaf, W. Tavernier, M. Rost, *et al.*, "Network service chaining with optimized network function embedding supporting service decompositions," *Computer Networks*, vol. 93, pp. 492–505, 2015, Cloud Networking and Communications II, ISSN: 1389-1286. DOI: https://doi.org/10.1016/j.comnet.2015.09.035.

[57] Y. T. Woldeyohannes, A. Mohammadkhan, K. K. Ramakrishnan, and Y. Jiang, "ClusPR: Balancing Multiple Objectives at Scale for NFV Resource Allocation," *IEEE Transactions on Network and Service Management*, vol. 15, no. 4, pp. 1307–1321, 2018. DOI: 10.1109/tnsm.2018.2870733.

[58] H. Hawilo, M. Jammal, and A. Shami, "Network Function Virtualization-Aware Orchestrator for Service Function Chaining Placement in the Cloud," *IEEE Journal on Selected Areas in Communications*, vol. 37, no. 3, pp. 643–655, 2019. DOI: 10.1109/jsac.2019.2895226.

[59] R. Ponmagal, S. Karthick, B. Dhiyanesh, S. Balakrishnan, and K. Venkatachalam, "Optimized virtual network function provisioning technique for mobile edge cloud computing," *Journal of Ambient Intelligence and Humanized Computing*, vol. 12, no. 6, pp. 5807–5815, 2021.

[60] N. Moradi, A. Shameli-Sendi, and A. Khajouei, "A Scalable Stateful Approach for Virtual Security Functions Orchestration," *IEEE Transactions on Parallel and Distributed Systems*, vol. 32, no. 6, pp. 1383–1394, 2021. DOI: 10.1109/tpds.2021.3049804.

[61] A. Shameli-Sendi, Y. Jarraya, M. Pourzandi, and M. Cheriet, "Efficient Provisioning of Security Service Function Chaining Using Network Security Defense Patterns," *IEEE Transactions on Services Computing*, vol. 12, no. 4, pp. 534–549, 2019. DOI: 10.1109/tsc.2016.2616867.

[62] Y. Liu, Y. Lu, W. Qiao, and X. Chen, "A Dynamic Composition Mechanism of Security Service Chaining Oriented to SDN/NFV-Enabled Networks," *IEEE Access*, vol. 6, pp. 53 918–53 929, 2018. DOI: 10.1109/access.2018.2870601.

[63] S. Demirci, S. Sagiroglu, and M. Demirci, "Energy-efficient virtual security function placement in NFV-enabled networks," *Sustainable Computing: Informatics and Systems*, vol. 30, p. 100 494, 2021, ISSN: 2210-5379. DOI: https://doi.org/10.1016/j.suscom.2020.100494.

[64] F. Wang, D. Jiang, S. Qi, C. Qiao, and H. Song, "Fine-Grained Resource Management for Edge Computing Satellite Networks," in *2019 IEEE Global Communications Conference (GLOBECOM)*, 2019, pp. 1–6. DOI: 10.1109/globecom38437.2019.9013467.

[65] Y. Yin, C. Huang, D.-F. Wu, *et al.*, "Deep Reinforcement Learning-Based Joint Satellite Scheduling and Resource Allocation in Satellite-Terrestrial Integrated Networks," *Wireless Communications and Mobile Computing*, vol. 2022, 2022.

[66] C. Wang, L. Liu, C. Jiang, S. Wang, P. Zhang, and S. Shen, "Incorporating Distributed DRL into Storage Resource Optimization of Space-Air-Ground Integrated Wireless Communication Network," *IEEE Journal of Selected Topics in Signal Processing*, pp. 1–1, 2021. DOI: 10.1109/jstsp.2021.3136027.

[67] G. Cui, X. Li, L. Xu, and W. Wang, "Latency and Energy Optimization for MEC Enhanced SAT-IoT Networks," *IEEE Access*, vol. 8, pp. 55 915–55 926, 2020. DOI: 10.1109/ACCESS.2020.2982356.

[68] Y. Hao, Z. Song, Z. Zheng, Q. Zhang, and Z. Miao, "Joint Communication, Computing, and Caching Resource Allocation in LEO Satellite MEC Networks," *IEEE Access*, vol. 11, pp. 6708–6716, 2023. DOI: 10.1109/ACCESS.2023.3237701.

[69] S. Pan, S. Cao, L. Yan, and H. Wang, "A Dynamic Predictive VM Resource Scaling Strategy in Satellite-Ground Computing Networks," in *The 5th International Conference on Computer Science and Application Engineering*, ser. Csae 2021, Sanya, China: Association for Computing Machinery, 2021, ISBN: 9781450389853. DOI: 10.1145/3487075.3487145.

[70] M. Tong, X. Wang, S. Li, and L. Peng, "Joint Offloading Decision and Resource Allocation in Mobile Edge Computing-Enabled Satellite-Terrestrial Network," *Symmetry*, vol. 14, no. 3, 2022, ISSN: 2073-8994. DOI: 10.3390/sym14030564.

[71] Z. Jia, M. Sheng, J. Li, Y. Zhu, W. Bai, and Z. Han, "Virtual Network Functions Orchestration in Software Defined LEO Small Satellite Networks," in *ICC 2020 - 2020 IEEE International Conference on Communications (ICC)*, 2020, pp. 1–6. DOI: 10.1109/icc40277.2020.9148906.

[72] Z. Jia, M. Sheng, J. Li, *et al.*, "Joint Optimization of VNF Deployment and Routing in Software Defined Satellite Networks," in *2018 IEEE 88th Vehicular Technology Conference (VTC-Fall)*, 2018, pp. 1–5. DOI: 10.1109/VTCFall.2018.8690972.

[73] Z. Jia, M. Sheng, J. Li, D. Zhou, and Z. Han, "VNF-Based Service Provision in Software Defined LEO Satellite Networks," *IEEE Transactions on Wireless Communications*, vol. 20, no. 9, pp. 6139–6153, 2021. DOI: 10.1109/twc.2021.3072155.

[74] I. Maity, T. X. Vu, S. Chatzinotas, and M. Minardi, "D-ViNE: Dynamic Virtual Network Embedding in Non-Terrestrial Networks," in *2022 IEEE Wireless Communications and Networking Conference (WCNC)*, Ieee, 2022, pp. 166–171.

[75] X. Gao, R. Liu, and A. Kaushik, "Virtual Network Function Placement in Satellite Edge Computing with a Potential Game Approach," *IEEE Transactions on Network and Service Management*, pp. 1–1, 2022. DOI: 10.1109/tnsm.2022.3141165.

[76] G. Wang, S. Zhou, S. Zhang, Z. Niu, and X. Shen, "SFC-based service provisioning for reconfigurable space-air-ground integrated networks," *IEEE Journal on Selected Areas in Communications*, vol. 38, no. 7, pp. 1478–1489, 2020.

[77] H. Yang, W. Liu, X. Wang, and J. Li, "Group Sparse Space Information Network with Joint Virtual Network Function Deployment and Maximum Flow Routing Strategy," *IEEE Transactions on Wireless Communications*, pp. 1–1, 2023. DOI: 10.1109/TWC.2022.3233067.

[78] X. Gao, R. Liu, and A. Kaushik, "Service Chaining Placement Based on Satellite Mission Planning in Ground Station Networks," *IEEE Transactions on Network and Service Management*, vol. 18, no. 3, pp. 3049–3063, 2021. DOI: 10.1109/tnsm.2020.3045432.

[79] W. Qiao, X. Ni, Y. Lu, X. Li, D. Zhao, and Y. Liu, "A Service Function Chain Deployment Scheme of the Software Defined Satellite Network," *Mobile Information Systems*, vol. 2022, 2022.

[80] X. Gao, R. Liu, A. Kaushik, and H. Zhang, "Dynamic Resource Allocation for Virtual Network Function Placement in Satellite Edge Clouds," *IEEE Transactions on Network Science and Engineering*, pp. 1–1, 2022. DOI: 10.1109/tnse.2022.3159796.

[81] X. Qin, T. Ma, Z. Tang, X. Zhang, H. Zhou, and L. Zhao, "Service-Aware Resource Orchestration in Ultra-Dense LEO Satellite-Terrestrial Integrated 6G: A Service Function Chain Approach," *IEEE Transactions on Wireless Communications*, pp. 1–1, 2023. DOI: 10.1109/TWC.2023.3239080.

[82] A. Petrosino, G. Piro, L. A. Grieco, and G. Boggia, "An Optimal Allocation Framework of Security Virtual Network Functions in 6G Satellite Deployments," in *2022 IEEE 19th Annual Consumer Communications & Networking Conference (CCNC)*, 2022.

[83] F. Glover, "Tabu search: A tutorial," *Interfaces*, vol. 20, no. 4, pp. 74–94, 1990.

[84] D. Bertsimas and J. Tsitsiklis, "Simulated annealing," *Statistical science*, vol. 8, no. 1, pp. 10–15, 1993.

[85] B. Freisleben and P. Merz, "A genetic local search algorithm for solving symmetric and asymmetric traveling salesman problems," in *Proceedings of IEEE International Conference on Evolutionary Computation*, 1996, pp. 616–621. DOI: 10.1109/icec.1996.542671.

[86] "IMT Vision–Framework and overall objectives of the future development of IMT for 2020 and beyond," *Recommendation ITU*, vol. 2083, no. 0, 2015.

[87] H. Tataria, M. Shafi, M. Dohler, and S. Sun, "Six Critical Challenges for 6G Wireless Systems: A Summary and Some Solutions," *IEEE Vehicular Technology Magazine*, vol. 17, no. 1, pp. 16–26, 2022. DOI: 10.1109/MVT.2021.3136506.

[88] M. Giordani, M. Polese, M. Mezzavilla, S. Rangan, and M. Zorzi, "Toward 6G Networks: Use Cases and Technologies," *IEEE Communications Magazine*, vol. 58, no. 3, pp. 55–61, 2020. DOI: 10.1109/MCOM.001.1900411.

[89] J. Liu, Y. Shi, Z. M. Fadlullah, and N. Kato, "Space-Air-Ground Integrated Network: A Survey," *IEEE Communications Surveys & Tutorials*, vol. 20, no. 4, pp. 2714–2741, 2018. DOI: 10.1109/COMST.2018.2841996.

[90] 3GPP, "Study on New Radio (NR) to support non-terrestrial networks (NTNs)," 3rd Generation Partnership Project (3GPP), Technical Specification (TS) 38.811, 2020, Version 15.2.0, Release 15.

[91] 3GPP, "Non-terrestrial networks (NTN) related RF and co-existence aspects," 3GPP, Technical Report (TR) 38.863, 2022, Release 17.

[92] 3GPP, "Study on requirements and use cases for network verified UE location for Non-Terrestrial-Networks (NTN) in NR," 3GPP, Technical Report (TR) 38.882, 2022, Release 18.

[93] M. M. Azari, S. Solanki, S. Chatzinotas, *et al.*, "Evolution of Non-Terrestrial Networks From 5G to 6G: A Survey," *IEEE Communications Surveys & Tutorials*, vol. 24, no. 4, pp. 2633–2672, 2022.

[94] M. Mozaffari, X. Lin, and S. Hayes, "Toward 6G with Connected Sky: UAVs and Beyond," *IEEE Communications Magazine*, vol. 59, no. 12, pp. 74–80, 2021.

[95] P. Boccadoro, D. Striccoli, and L. A. Grieco, "An Extensive Survey on the Internet of Drones," *Ad Hoc Netw.*, vol. 122, p. 102 600, 2021, ISSN: 1570-8705. arXiv: 2007.12611.

[96] D. C. Nguyen, M. Ding, P. N. Pathirana, *et al.*, "6G Internet of Things: A Comprehensive Survey," *IEEE Internet of Things Journal*, vol. 9, no. 1, pp. 359–383, 2022. DOI: 10.1109/JIOT.2021.3103320.

[97] X. Lu, P. Wang, D. Niyato, D. I. Kim, and Z. Han, "Wireless Charging Technologies: Fundamentals, Standards, and Network Applications," *IEEE Communications Surveys & Tutorials*, vol. 18, no. 2, pp. 1413–1452, 2016. DOI: 10.1109/COMST.2015.2499783.

[98] S. Zhang, W. Liu, and N. Ansari, "Joint Wireless Charging and Data Collection for UAV-Enabled Internet of Things Network," *IEEE Internet of Things Journal*, vol. 9, no. 23, pp. 23 852–23 859, 2022.

[99] J. Mu and Z. Sun, "Trajectory Design for Multi-UAV-Aided Wireless Power Transfer toward Future Wireless Systems," *Sensors*, vol. 22, no. 18, p. 6859, 2022.

[100] Y. Liu, K. Xiong, Y. Lu, Q. Ni, P. Fan, and K. B. Letaief, "UAV-aided wireless power transfer and data collection in Rician fading," *IEEE Journal on Selected Areas in Communications*, vol. 39, no. 10, pp. 3097–3113, 2021.

[101] Y. Hu, X. Yuan, G. Zhang, and A. Schmeink, "Sustainable wireless sensor networks with UAV-enabled wireless power transfer," *IEEE Transactions on Vehicular Technology*, vol. 70, no. 8, pp. 8050–8064, 2021.

[102] X. Mo, Y. Huang, and J. Xu, "Radio-map-based robust positioning optimization for UAV-enabled wireless power transfer," *IEEE Wireless Communications Letters*, vol. 9, no. 2, pp. 179–183, 2019.

[103] K. K. Nguyen, A. Masaracchia, V. Sharma, H. V. Poor, and T. Q. Duong, "RIS-assisted UAV communications for IoT with wireless power transfer using deep reinforcement learning," *IEEE Journal of Selected Topics in Signal Processing*, 2022.

[104] X. Yuan, H. Jiang, Y. Hu, and A. Schmeink, "Joint Analog Beamforming and Trajectory Planning for Energy-Efficient UAV-Enabled Nonlinear Wireless Power Transfer," *IEEE Journal on Selected Areas in Communications*, vol. 40, no. 10, pp. 2914–2929, 2022.

[105] X. Yuan, Y. Hu, and A. Schmeink, "Joint design of UAV trajectory and directional antenna orientation in UAV-enabled wireless power transfer networks," *IEEE Journal on Selected Areas in Communications*, vol. 39, no. 10, pp. 3081–3096, 2021.

[106] Z. Liu, S. Zhao, Q. Wu, Y. Yang, and X. Guan, "Joint Trajectory Design and Resource Allocation for IRS-Assisted UAV Communications With Wireless Energy Harvesting," *IEEE Communications Letters*, vol. 26, no. 2, pp. 404–408, 2022. DOI: 10.1109/LCOMM.2021.3128545.

[107] H. Hu, K. Xiong, G. Qu, Q. Ni, P. Fan, and K. B. Letaief, "AoI-Minimal Trajectory Planning and Data Collection in UAV-Assisted Wireless Powered IoT Networks," *IEEE Internet of Things Journal*, vol. 8, no. 2, pp. 1211–1223, 2021. DOI: 10.1109/JIOT.2020.3012835.

[108] L. Atzori, A. Iera, and G. Morabito, "From "smart objects" to "social objects": The next evolutionary step of the internet of things," *IEEE Communications Magazine*, vol. 52, no. 1, pp. 97–105, 2014. DOI: 10.1109/MCOM.2014.6710070.

[109] G. Sciddurlo, I. Huso, D. Striccoli, G. Piro, and G. Boggia, "A Multi-tiered Social IoT Architecture for Scalable and Trusted Service Provisioning," in *2021 IEEE Global Communications Conference (GLOBECOM)*, 2021, pp. 1–6. DOI: 10.1109/GLOBECOM46510.2021.9685084.

[110] H. Haas, L. Yin, Y. Wang, and C. Chen, "What is LiFi?" In *2015 European Conference on Optical Communication (ECOC)*, 2016, pp. 1–3. DOI: 10.1109/ECOC.2015.7341879.

[111] S. M. Kouhini, Z. Ma, C. Kottke, S. M. Mana, R. Freund, and V. Jungnickel, "LiFi based Positioning for Indoor Scenarios," in *2021 17th International Symposium on Wireless Communication Systems (ISWCS)*, 2021, pp. 1–5. DOI: 10.1109/ISWCS49558.2021.9562207.

[112] X. Sun, Y. Zhuang, J. Huai, *et al.*, "RSS-Based Visible Light Positioning Using Nonlinear Optimization," *IEEE Internet of Things Journal*, vol. 9, no. 15, pp. 14 137–14 150, 2022. DOI: 10.1109/JIOT.2022.3156616.

[113] A. M. Esfahani, A. M. Rahmani, and A. Khademzadeh, "MSIoT: Mobile Social Internet of Things, A New Paradigm," in *2020 10th International Symposium onTelecommunications (IST)*, 2020, pp. 187–193. DOI: 10.1109/IST50524.2020.9345837.

[114] Z. Yang, K. Yang, L. Lei, K. Zheng, and V. C. M. Leung, "Blockchain-Based Decentralized Trust Management in Vehicular Networks," *IEEE Internet of Things Journal*, vol. 6, no. 2, pp. 1495–1505, 2019. DOI: 10.1109/JIOT.2018.2836144.

[115] H. Zhang, L. Zhu, H. Du, *et al.*, "Structural Balance of Social Internet of Things Networks with Ambiguous Relationships," *Wireless Communications and Mobile Computing*, vol. 2021, p. 7 964 409, Aug. 2021, ISSN: 1530-8669. DOI: 10.1155/2021/7964409.

[116] A. Tewari and B. Gupta, "Security, privacy and trust of different layers in Internet-of-Things (IoTs) framework," *Future Generation Computer Systems*, vol. 108, pp. 909–920, 2020, ISSN: 0167-739X. DOI: https://doi.org/10.1016/j.future.2018.04.027.

[117] Z. Chen, R. Ling, C.-M. Huang, and X. Zhu, "A scheme of access service recommendation for the Social Internet of Things," *International Journal of Communication Systems*, vol. 29, no. 4, pp. 694–706, 2016. DOI: https://doi.org/10.1002/dac.2930.

[118] A. Zannou, A. Boulaalam, and E. H. Nfaoui, "SIoT: A New Strategy to Improve the Network Lifetime with an Efficient Search Process," *Future Internet*, vol. 13, no. 1, 2021, ISSN: 1999-5903. DOI: 10.3390/fi13010004.

[119] A. Metrouh, "Social Internet of Things: a novel selection approach for dynamic resources substitution," *Evolutionary Intelligence*, Jun. 2021. DOI: 10.1007/s12065-021-00580-3.

[120] B. Bordel and R. Alcarria, "Distributed Trust and Reputation Services in Pervasive Internet-of-Things Deployments," in *International Symposium on Mobile Internet Security*, Springer, 2021, pp. 16–29.

[121] R. Abidi and N. B. Azzouna, "Self-adaptive trust management model for social IoT services," in *2021 International Symposium on Networks, Computers and Communications (ISNCC)*, 2021, pp. 1–7. DOI: 10.1109/ISNCC52172.2021.9615856.

[122] W. Abdelghani, I. Amous, C. A. Zayani, F. Sèdes, and G. Roman-Jimenez, "Dynamic and scalable multi-level trust management model for Social Internet of Things," *The Journal of Supercomputing*, Jan. 2022, ISSN: 1573-0484. DOI: 10.1007/s11227-021-04205-5.

[123] M. S. Islim and H. Haas, "Modulation techniques for li-fi," *ZTE communications*, vol. 14, no. 2, pp. 29–40, 2019.

[124] E. Ramadhani and G. Mahardika, "The technology of lifi: A brief introduction," in *IOP conference series: materials science and engineering*, IOP Publishing, vol. 325, 2018, p. 012 013.

[125] M. D. Soltani, M. A. Arfaoui, I. Tavakkolnia, *et al.*, "Bidirectional Optical Spatial Modulation for Mobile Users: Toward a Practical Design for LiFi Systems," *IEEE Journal on Selected Areas in Communications*, vol. 37, no. 9, pp. 2069–2086, 2019. DOI: 10.1109/JSAC.2019.2929381.

[126] M. A. Arfaoui, M. D. Soltani, I. Tavakkolnia, *et al.*, "Measurements-Based Channel Models for Indoor LiFi Systems," *IEEE Transactions on Wireless Communications*, vol. 20, no. 2, pp. 827–842, 2021. DOI: 10.1109/TWC.2020.3028456.

[127] D. Ramananda, A. M. Sequeira, S. R. Raikar, and C. K. Shanbhag, "Design and Implementation of LiFi Communication system," in *IOP Conference Series: Materials Science and Engineering*, IOP Publishing, vol. 594, 2019, p. 012 041.

[128] R. Sharma, D. S. Gurjar, E. Rahman, A. Raghav, P. Shukla, and V. Mishra, "LiFi Technology: A Breakthrough for Massive Data Rates in Indoor Applications," in *Intelligent Systems for Social Good: Theory and Practice*. Singapore: Springer Nature Singapore, 2022, ch. 11 June 2022, pp. 63–79, ISBN: 978-981-19-0770-8. DOI: 10.1007/978-981-19-0770-8_6.

[129] D. N. Anwar, R. Ahmad, and A. Srivastava, "Energy-Efficient Coexistence of LiFi Users and Light Enabled IoT Devices," *IEEE Transactions on Green Communications and Networking*, vol. 6, no. 2, pp. 930–950, 2022. DOI: 10.1109/TGCN.2021.3116267.

[130] A. M. Damerdash, D. Abdelhameed, M. Aly, E. M. Ahmed, and M. A. Ahmed, "Energy efficiency assessment of power electronic drivers and LED lamps in Li-Fi communication systems," *Energy Reports*, vol. 7, pp. 7648–7662, 2021, ISSN: 2352-4847. DOI: https://doi.org/10.1016/j.egyr.2021.10.112.

[131] C. Chen, S. Fu, X. Jian, M. Liu, X. Deng, and Z. Ding, "NOMA for Energy-Efficient LiFi-Enabled Bidirectional IoT Communication," *IEEE Transactions on Communications*, vol. 69, no. 3, pp. 1693–1706, 2021. DOI: 10.1109/TCOMM.2021.3051912.

[132] I. Tavakkolnia, C. Chen, R. Bian, and H. Haas, "Energy-Efficient Adaptive MIMO-VLC Technique for Indoor LiFi Applications," in *2018 25th International Conference on Telecommunications (ICT)*, 2018, pp. 331–335. DOI: 10.1109/ICT.2018.8464933.

[133] "IEEE Draft Standard for Local and metropolitan area networks - Part 15.7: Short-Range Optical Wireless Communications," *IEEE P802.15.7/D3, August 2018*, pp. 1–412, 2018.

[134] X. You, J. Chen, Y. Zhong, S. Chen, and C. Yu, "Efficient Dimming Control with Time Domain Hybrid Modulation in Indoor Hybrid Visible Light/Infrared Communication Systems," in *2019 24th OptoElectronics and Communications Conference (OECC) and 2019 International Conference on Photonics in Switching and Computing (PSC)*, 2019, pp. 1–3. DOI: 10.23919/PS.2019.8817648.

[135] M. Hinrichs, P. Berenguer, J. Hilt, *et al.*, "A Physical Layer for Low Power Optical Wireless Communications," *IEEE Transactions on Green Communications and Networking*, vol. 5, no. 1, pp. 4–17, 2021. DOI: 10.1109/TGCN.2020.3038692.

[136] H. Jmila, G. Blanc, M. R. Shahid, and M. Lazrag, "A Survey of Smart Home IoT Device Classification Using Machine Learning-Based Network Traffic Analysis," *IEEE Access*, vol. 10, pp. 97 117–97 141, 2022. DOI: 10.1109/ACCESS.2022.3205023.

[137] K. Lueth, M. Hasan, S. Sinha, *et al.*, "State of IoT-spring," Spring, East Lansing, Michigan, Tech. Rep., May 2022. [Online]. Available: https://iot-analytics.com/number-connected-iot-devices/.

[138] A. S. Abohamama, A. El-Ghamry, and E. Hamouda, "Real-Time Task Scheduling Algorithm for IoT-Based Applications in the Cloud–Fog Environment," *Journal of Network and Systems Management*, vol. 30, no. 4, 2022. DOI: 10.1007/s10922-022-09664-6.

[139] M. Müller, M. Emmelmann, D. Behnke, *et al.*, "LiFi with 5G for the Smart Factory," in *2022 IEEE Wireless Communications and Networking Conference (WCNC)*, 2022, pp. 2310–2315. DOI: 10.1109/WCNC51071.2022.9771969.

[140] D. Bozanis, N. G. Evgenidis, V. K. Papanikolaou, *et al.*, "Indoor 3D Visible Light Positioning Analysis with Channel Estimation Errors," in *2023 30th International Conference on Systems, Signals and Image Processing (IWSSIP)*, 2023, pp. 1–4. DOI: 10.1109/IWSSIP58668.2023.10180234.

[141] S. Ma, B. Li, G. Zhang, *et al.*, "Centimeter-Level 3D Mobile Online Visible Light Positioning System With Single LED-Lamp," *IEEE Internet of Things Journal*, pp. 1–1, 2023. DOI: 10.1109/JIOT.2023.3285556.

[142] R. Liu, Z. Liang, K. Yang, and W. Li, "Machine Learning Based Visible Light Indoor Positioning With Single-LED and Single Rotatable Photo Detector," *IEEE Photonics Journal*, vol. 14, no. 3, pp. 1–11, 2022. DOI: 10.1109/JPHOT.2022.3163415.

[143] S. Aboagye, A. R. Ndjiongue, T. M. N. Ngatched, O. A. Dobre, and H. V. Poor, "RIS-Assisted Visible Light Communication Systems: A Tutorial," *IEEE Communications Surveys & Tutorials*, vol. 25, no. 1, pp. 251–288, 2023. DOI: 10.1109/COMST.2022.3225859.

[144] S. Ibne Mushfique, A. Alsharoa, and M. Yuksel, "MirrorVLC: Optimal Mirror Placement for Multielement VLC Networks," *IEEE Transactions on Wireless Communications*, vol. 21, no. 11, pp. 10 050–10 064, 2022. DOI: 10.1109/TWC.2022.3182013.

[145] A. M. Abdelhady, A. K. S. Salem, O. Amin, B. Shihada, and M.-S. Alouini, "Visible Light Communications via Intelligent Reflecting Surfaces: Metasurfaces vs Mirror Arrays," *IEEE Open Journal of the Communications Society*, vol. 2, pp. 1–20, 2021. DOI: 10.1109/OJCOMS.2020.3041930.

[146] A. Guidotti, A. Vanelli-Coralli, T. Foggi, *et al.*, "LTE-based Satellite Communications in LEO Mega-Constellations," *International Journal of Satellite Communications and Networking*, 2017.

[147] C. B. Mwakwata, H. Malik, M. Mahtab Alam, Y. Le Moullec, S. Parand, and S. Mumtaz, "Narrowband Internet of Things (NB-IoT): From physical (PHY) and media access control (MAC) layers perspectives," *Sensors*, vol. 19, no. 11, p. 2613, 2019.

[148] T. Ojha, S. Misra, and N. Raghuwanshi, "Wireless sensor networks for agriculture: The state-of-the-art in practice and future challenges," *Comput. Electron. Agric.*, vol. 118, pp. 66–84, 2015.

[149] K. Goel and A. K. Bindal, "Wireless Sensor Network in Precision Agriculture: A Survey Report," in *2018 Fifth International Conference on Parallel, Distributed and Grid Computing (PDGC)*, 2018, pp. 176–181. DOI: 10.1109/PDGC.2018.8745854.

[150] G. Castellanos, M. Deruyck, L. Martens, and W. Joseph, "System Assessment of WUSN Using NB-IoT UAV-Aided Networks in Potato Crops," *IEEE Access*, vol. 8, pp. 56 823–56 836, 2020. DOI: 10.1109/ACCESS.2020.2982086.

[151] *Satellite technologies for IoT applications*, https://iotuk.org.uk/wp-content/uploads/2017/04/Satellite-Applications.pdf, Accessed: 2019-01-29.

[152] *Development guide for agriculture using NB-IoT*, https://www.gsma.com/iot/resources/guide2-nbiot-agriculture, Accessed: 2018-10-05.

[153] H. Jawad, R. Nordin, S. Gharghan, A. Jawad, and M. Ismail, "Energy-Efficient Wireless Sensor Networks for Precision Agriculture: A Review," *Sensors*, vol. 17, no. 8, 2017, ISSN: 1424-8220. DOI: 10.3390/s17081781. [Online]. Available: https://www.mdpi.com/1424-8220/17/8/1781.

[154] D. Brunelli, A. Albanese, D. d'Acunto, and M. Nardello, "Energy Neutral Machine Learning Based IoT Device for Pest Detection in Precision Agriculture," *IEEE Internet of Things Magazine*, vol. 2, no. 4, pp. 10–13, 2019. DOI: 10.1109/IOTM.0001.1900037.

[155] M. M. Islam, M. S. Hossain, R. K. Reza, and A. Nath, "IoT Based Automated Solar Irrigation System Using MQTT Protocol In Charandeep Chakaria," in *2019 1st International Conference on Advances in Science, Engineering and Robotics Technology (ICASERT)*, 2019, pp. 1–6. DOI: 10.1109/ICASERT.2019.8934504.

[156] R. Maheswari, H. Azath, P. Sharmila, and S. Sheeba Rani Gnanamalar, "Smart Village: Solar Based Smart Agriculture with IoT Enabled for Climatic Change and Fertilization of Soil," in *2019 IEEE 5th International Conference on Mechatronics System and Robots (ICMSR)*, 2019, pp. 102–105. DOI: 10.1109/ICMSR.2019.8835454.

[157] J. P. Shanmuga Sundaram, W. Du, and Z. Zhao, "A Survey on LoRa Networking: Research Problems, Current Solutions, and Open Issues," *IEEE Communications Surveys Tutorials*, vol. 22, no. 1, pp. 371–388, 2020. DOI: 10.1109/COMST.2019.2949598.

[158] GSMA, "NB-IoT deployment guide to basic feature set requirements," GSM Association et al., Tech. Rep., 2019. [Online]. Available: https://www.gsma.com/iot/wp-content/uploads/2019/07/201906-GSMA-NB-IoT-Deployment-Guide-v3.pdf.

[159] 3GPP, "General Packet Radio Service (GPRS) enhancements for Evolved Universal Terrestrial Radio Access Network (E-UTRAN) access," 3rd Generation Partnership Project (3GPP), Technical Specification (TS) 23.401, 2020, Release 16.

[160] Z. Shelby, K. Hartke, and C. Bormann, *The Constrained Application Protocol (CoAP)*, RFC 7252, Jun. 2014. DOI: 10.17487/RFC7252. [Online]. Available: https://rfc-editor.org/rfc/rfc7252.txt.

[161] 3GPP, "Evolved Universal Terrestrial Radio Access (E-UTRA); Packet Data Convergence Protocol (PDCP) specification," 3rd Generation Partnership Project (3GPP), Technical Report (TS) 36.323, 2020, Release 16.

[162] 3GPP, "Evolved Universal Terrestrial Radio Access (E-UTRA); Radio Link Control (RLC) protocol specification," 3rd Generation Partnership Project (3GPP), Technical Report (TS) 36.322, 2020, Release 16.

[163] 3GPP, "Evolved Universal Terrestrial Radio Access (E-UTRA) Medium Access Control (MAC) protocol specification," 3rd Generation Partnership Project (3GPP), Technical Report (TS) 36.321, Jan. 2020, Release 16.

[164] 3GPP, "LTE; Evolved Universal Terrestrial Radio Access (E-UTRA); Physical layer procedures," 3rd Generation Partnership Project (3GPP), Technical Report (TR) 36.213, 2020, Release 14.

[165] 3GPP, "FL Summary on enhancements on UL time and frequency synchronization for NR NTN," 3rd Generation Partnership Project (3GPP), Discussion, Decision R1-2009748, Nov. 2020, RAN WG1 103e.

[166] C. A. Balanis, *Antenna Theory: Analysis and Design, 2nd Edition*. Wiley, 1996.

[167] L. J.Ippolito, *Satellite Communications Systems Engineering: Atmospheric Effects, Satellite Link Design and System Performance*, 2nd. Wiley Publishing, 2017, ISBN: 1119259371.

[168] ITU, "Attenuation by atmospheric gases and related effects," International Telecommunication Union (ITU), Recommendation, 2019, ITU-R P.676-12.

[169] ITU, "Propagation data and prediction methods required for the design of Earth-space telecommunication systems," International Telecommunication Union (ITU), Recommendation, 2017, ITU-R P.618-13.

[170] ITU, "Characteristics of precipitation for propagation modelling," International Telecommunication Union (ITU), Recommendation, 2021, ITU-R P.837-7.

[171] ITU, "Attenuation due to clouds and fog," International Telecommunication Union (ITU), Recommendation, 2019, ITU-R P.840-8.

[172] ITU, "Propagation data and prediction methods required for the design of Earth-space telecommunication systems," International Telecommunication Union, Recommendation, 2015, Recommendations Radiowave Propag. ITU-R 618-12.

[173] N. Grody, "Antenna temperature for a scanning microwave radiometer," *IEEE Transactions on Antennas and Propagation*, vol. 23, no. 1, pp. 141–144, 1975. DOI: 10.1109/TAP.1975.1141020.

[174] *Payload Specification for 3U, 6U, 12U and 27U*, http://www.planetarysystemscorp.com/web/wp-content/uploads/2017/08/2002367E-Payload-Spec-for-3U-6U-12U-27U.pdf, Accessed: 2020-12-10.

[175] *Satellite Design and Operations*, https://www.agi.com/missions/satellite-missions-design, Accessed: 2020-12-10.

[176] S. Martiradonna, A. Grassi, G. Piro, and G. Boggia, "5G-air-simulator: An open-source tool modeling the 5G air interface," *Computer Networks*, vol. 173, no. 107151, p. 107 151, 2020, ISSN: 1389-1286. DOI: 10.1016/j.comnet.2020.107151.

[177] S. Martiradonna, A. Grassi, G. Piro, and G. Boggia, "Understanding the 5G-Air-simulator: a tutorial on design criteria, technical components, and reference use cases," *Computer Networks*, vol. 177, p. 107 314, 2020, ISSN: 1389-1286. DOI: https://doi.org/10.1016/j.comnet.2020.107314.

[178] S. Martiradonna, G. Piro, and G. Boggia, "On the evaluation of the NB-IoT random access procedure in monitoring infrastructures," *Sensors*, vol. 19, no. 14, p. 3237, 2019, ISSN: 1424-8220. DOI: 10.3390/s19143237.

[179] A. Petrosino, G. Sciddurlo, S. Martiradonna, D. Striccoli, G. Piro, and G. Boggia, "WIP: An Open-Source Tool for Evaluating System-Level Performance of NB-IoT Non-Terrestrial Networks," in *2021 IEEE 22nd International Symposium on a World of Wireless, Mobile and Multimedia Networks (WoWMoM)*, 2021, pp. 236–239. DOI: 10.1109/WoWMoM51794.2021.00042.

[180] ITU, "Topography for Earth-to-space propagation modelling," International Telecommunication Union (ITU), Recommendation, 2019, ITU-R P.1511.

[181] M. De Sanctis, E. Cianca, G. Araniti, I. Bisio, and R. Prasad, "Satellite Communications Supporting Internet of Remote Things," *IEEE Internet of Things Journal*, vol. 3, no. 1, pp. 113–123, 2016. DOI: 10.1109/JIOT.2015.2487046.

[182] R. Birkeland and D. Palma, "An assessment of IoT via satellite: Technologies, Services and Possibilities," in *International Astronautical Congress, Washington D.C*, Oct. 2019.

[183] G. Aiyetoro and P. Owolawi, "Spectrum Management Schemes for Internet of Remote Things (IoRT) Devices in 5G Networks via GEO Satellite," *Future Internet*, vol. 11, no. 12, p. 257, 2019.

[184] G. Aiyetoro and P. Owolawi, "Dynamic Packet Scheduling for Internet of Remote Things (IoRT) devices in 5G Satellite Networks," in *Proc. of IEEE International Conference on Advances in Computing and Communication Engineering (ICACCE)*, 2020, pp. 1–6. DOI: 10.1109/ICACCE49060.2020.9154993.

[185] I. F. Akyildiz and A. Kak, "The Internet of Space Things/CubeSats," *IEEE Network*, vol. 33, no. 5, pp. 212–218, 2019. DOI: 10.1109/MNET.2019.1800445.

[186] A. Mahmood and S. Zafar, "Performance Analysis of Narrowband Internet of Things (NB-IoT) Deployment Modes," in *Proc. of IEEE International Multitopic Conference (INMIC)*, 2019, pp. 1–8. DOI: 10.1109/INMIC48123.2019.9022748.

[187] 3GPP, "Cellular system support for ultra-low complexity and low throughput Internet of Things (CIoT)," 3rd Generation Partnership Project (3GPP), Technical report (TR) 45.820, 2015, Release 13.

[188] 3GPP, "Study on RAN Improvements for Machine-Type Communications," 3rd Generation Partnership Project (3GPP), Technical Report TR 37.868, 2011.

[189] S. Martiradonna, A. Grassi, G. Piro, L. A. Grieco, and G. Boggia, "An Open Source Platform for Exploring NB-IoT System Performance," in *European Wireless Conference*, 2018, pp. 1–6.

[190] Y. Hao, L. Zhang, L. Zheng, Z. Zhao, and Z. Li, "An Efficient VNF Deployment Scheme for Reliable Service Chain in Software Defined Satellite Networks," in *2022 37th Youth Academic Annual Conference of Chinese Association of Automation (YAC)*, 2022, pp. 1363–1366. DOI: 10.1109/YAC57282.2022.10023572.

[191] A. Guidotti, A. Vanelli-Coralli, V. Schena, *et al.*, "The path to 5G-Advanced and 6G non-terrestrial network systems," in *2022 11th Advanced Satellite Multimedia Systems Conference and the 17th Signal Processing for Space Communications Workshop (ASMS/SPSC)*, IEEE, 2022, pp. 1–8.

[192] T. Villela, C. A. Costa, A. M. Brandão, F. T. Bueno, and R. Leonardi, "Towards the thousandth CubeSat: A statistical overview," *International Journal of Aerospace Engineering*, vol. 2019, 2019.

[193] G. Sciddurlo, A. Petrosino, M. Quadrini, *et al.*, "Looking at NB-IoT over LEO satellite systems: Design and evaluation of a service-oriented solution," *IEEE Internet of Things Journal*, vol. 9, no. 16, pp. 14 952–14 964, 2021.

[194] N. Hyodo, T. Sato, R. Shinkuma, and E. Oki, "Virtual Network Function Placement for Service Chaining by Relaxing Visit Order and Non-Loop Constraints," *IEEE Access*, vol. 7, pp. 165 399–165 410, 2019. DOI: 10.1109/access.2019.2934725.

[195] S. J. Ling, J. Sanny, and W. Moebs, *University Physics, Volume 1 (OpenStax)*, 2016.

[196] 3gpp, "Study on New Radio (NR) to support non-terrestrial networks," 3rd Generation Partnership Project, Technical Report (TR) 38.811, 2017.

[197] 3gpp, "Study on management and orchestration aspects of integrated satellite components in a 5G network," 3rd Generation Partnership Project, Technical Report (TR) 28.808, 2021.

[198] X. Lin, S. Rommer, S. Euler, E. A. Yavuz, and R. S. Karlsson, "5G from Space: An Overview of 3GPP Non-Terrestrial Networks," *IEEE Communications Standards Magazine*, vol. 5, no. 4, pp. 147–153, 2021. DOI: 10.1109/MCOMSTD.011.2100038.

[199] Z. Lai, H. Li, Q. Wu, *et al.*, "Futuristic 6G Pervasive On-Demand Services: Integrating Space Edge Computing With Terrestrial Networks," *IEEE Vehicular Technology Magazine*, pp. 2–11, 2022. DOI: 10.1109/MVT.2022.3221391.

[200] I. Ahmad, J. Suomalainen, P. Porambage, A. Gurtov, J. Huusko, and M. Höyhtyä, "Security of Satellite-Terrestrial Communications: Challenges and Potential Solutions," *IEEE Access*, vol. 10, pp. 96 038–96 052, 2022. DOI: 10.1109/access.2022.3205426.

[201] S. P. E. Corporation. "Fourth Quarter 2021." (2021), [Online]. Available: https://www.spec.org/power_ssj2008/results/res2021q4/ (visited on 10/20/2021).

[202] FortiGate. "Virtual Appliances." (2021), [Online]. Available: https://www.fortinet.com/content/dam/fortinet/assets/data-sheets/fortigate-vm.pdf (visited on 10/20/2021).

[203] Cisco. "Virtual Appliance." (2021), [Online]. Available: https://www.cisco.com/c/en/us/products/collateral/security/adaptive-security-virtual-appliance-asav/adapt-security-virtual-appliance-ds.html (visited on 10/20/2021).

[204] Juniper. "Virtual Appliance." (2021), [Online]. Available: https://www.juniper.net/content/dam/www/assets/datasheets/us/en/security/vsrx-virtual-firewall-datasheet.pdf (visited on 10/20/2021).

[205] S. A. R. Shah and B. Issac, "Performance comparison of intrusion detection systems and application of machine learning to Snort system," *Future Generation Computer Systems*, vol. 80, pp. 157–170, 2018, ISSN: 0167-739x. DOI: https://doi.org/10.1016/j.future.2017.10.016.

[206] D. Lacković and M. Tomić, "Performance analysis of virtualized VPN endpoints," in *2017 40th International Convention on Information and Communication Technology, Electronics and Microelectronics (MIPRO)*, 2017, pp. 466–471. DOI: 10.23919/mipro.2017.7973470.

[207] H. Malik, H. Pervaiz, M. Mahtab Alam, Y. Le Moullec, A. Kuusik, and M. Ali Imran, "Radio Resource Management Scheme in NB-IoT Systems," *IEEE Access*, vol. 6, pp. 15 051–15 064, 2018. DOI: 10.1109/ACCESS.2018.2812299.

[208] H. Chelle, M. Crosnier, R. Dhaou, and A.-L. Beylot, "Adaptive Load Control for IoT Based on Satellite Communications," in *2018 IEEE International Conference on Communications (ICC)*, 2018, pp. 1–7. DOI: 10.1109/ICC.2018.8422804.

[209] Z. Gao, A. Liu, C. Han, and X. Liang, "Non-Orthogonal Multiple Access-Based Average Age of Information Minimization in LEO Satellite-Terrestrial Integrated Networks," *IEEE Transactions on Green Communications and Networking*, vol. 6, no. 3, pp. 1793–1805, 2022. DOI: 10.1109/TGCN.2022.3159559.

[210] C. Zhan, H. Hu, X. Sui, Z. Liu, J. Wang, and H. Wang, "Joint Resource Allocation and 3D Aerial Trajectory Design for Video Streaming in UAV Communication Systems," *IEEE Transactions on Circuits and Systems for Video Technology*, vol. 31, no. 8, pp. 3227–3241, 2021. DOI: 10.1109/TCSVT.2020.3035618.

[211] S. Mirbolouk, M. Valizadeh, M. C. Amirani, and S. Ali, "Relay Selection and Power Allocation for Energy Efficiency Maximization in Hybrid Satellite-UAV Networks With CoMP-NOMA Transmission," *IEEE Transactions on Vehicular Technology*, vol. 71, no. 5, pp. 5087–5100, 2022. DOI: 10.1109/TVT.2022.3152048.

[212] Y. Wang, Z. Li, Y. Chen, *et al.*, "Joint Resource Allocation and UAV Trajectory Optimization for Space–Air–Ground Internet of Remote Things Networks," *IEEE Systems Journal*, vol. 15, no. 4, pp. 4745–4755, 2021. DOI: 10.1109/JSYST.2020.3019463.

[213] N. Wang, F. Li, D. Chen, L. Liu, and Z. Bao, "NOMA-Based Energy-Efficiency Optimization for UAV Enabled Space-Air-Ground Integrated Relay Networks," *IEEE Transactions on Vehicular Technology*, vol. 71, no. 4, pp. 4129–4141, 2022. DOI: 10.1109/TVT.2022.3151369.

[214] C. R. Valenta and G. D. Durgin, "Harvesting Wireless Power: Survey of Energy-Harvester Conversion Efficiency in Far-Field, Wireless Power Transfer Systems," *IEEE Microwave Magazine*, vol. 15, no. 4, pp. 108–120, 2014. DOI: 10.1109/MMM.2014.2309499.

[215] T. Terauchi, K. Suto, and M. Wakaiki, "Harvest-Then-Transmit-Based TDMA Protocol with Statistical Channel State Information for Wireless Powered Sensor Networks," in *2021 IEEE 93rd Vehicular Technology Conference (VTC2021-Spring)*, 2021, pp. 1–5. DOI: 10.1109/VTC2021-Spring51267.2021.9449083.

[216] C. Pan, H. Ren, K. Wang, *et al.*, "Reconfigurable Intelligent Surfaces for 6G Systems: Principles, Applications, and Research Directions," *IEEE Communications Magazine*, vol. 59, no. 6, pp. 14–20, 2021. DOI: 10.1109/MCOM.001.2001076.

[217] Z. Chu, P. Xiao, D. Mi, *et al.*, "Wireless Powered Intelligent Radio Environment with Non-Linear Energy Harvesting," *IEEE Internet of Things Journal*, pp. 1–1, 2022. DOI: 10.1109/JIOT.2022.3162761.

[218] D. Zhang, Q. Wu, M. Cui, G. Zhang, and D. Niyato, "Throughput Maximization for IRS-Assisted Wireless Powered Hybrid NOMA and TDMA," *IEEE Wireless Communications Letters*, vol. 10, no. 9, pp. 1944–1948, 2021. DOI: 10.1109/LWC.2021.3087495.

[219] M. Wu, L. Su, J. Chen, *et al.*, "Development and Prospect of Wireless Power Transfer Technology Used to Power Unmanned Aerial Vehicle," *Electronics*, vol. 11, no. 15, p. 2297, 2022.

[220] Z. Wang, T. Lv, J. Zeng, and W. Ni, "Placement and Resource Allocation of Wireless-Powered Multiantenna UAV for Energy-Efficient Multiuser NOMA," *IEEE Transactions on Wireless Communications*, pp. 1–1, 2022. DOI: 10.1109/TWC.2022.3169533.

[221] M.-G. Kim and H.-S. Jo, "Performance Analysis of NB-IoT Uplink in Low Earth Orbit Non-Terrestrial Networks," *Sensors*, vol. 22, no. 18, 2022, ISSN: 1424-8220. DOI: 10.3390/s22187097. [Online]. Available: https://www.mdpi.com/1424-8220/22/18/7097.

[222] M. M. Azari, F. Rosas, K.-C. Chen, and S. Pollin, "Ultra Reliable UAV Communication Using Altitude and Cooperation Diversity," *IEEE Trans. Commun.*, vol. 66, no. 1, pp. 330–344, 2017.

[223] Y. Chen, N. Zhao, and M.-S. Alouini, "Wireless Energy Harvesting Using Signals From Multiple Fading Channels," *IEEE Transactions on Communications*, vol. 65, no. 11, pp. 5027–5039, 2017. DOI: 10.1109/TCOMM.2017.2734665.

[224] V. M. Baeza, E. Lagunas, H. Al-Hraishawi, and S. Chatzinotas, "An Overview of Channel Models for NGSO Satellites," in *2022 IEEE 96th Vehicular Technology Conference (VTC2022-Fall)*, 2022, pp. 1–6. DOI: 10.1109/VTC2022-Fall57202.2022.10012693.

[225] N. Okati, T. Riihonen, D. Korpi, I. Angervuori, and R. Wichman, "Downlink Coverage and Rate Analysis of Low Earth Orbit Satellite Constellations Using Stochastic Geometry," *IEEE Transactions on Communications*, vol. 68, no. 8, pp. 5120–5134, 2020. DOI: 10.1109/TCOMM.2020.2990993.

[226] Q. Chen, Z. Wang, G. F. Pedersen, and M. Shen, "Joint Satellite-Transmitter and Ground-Receiver Digital Pre-Distortion for Active Phased Arrays in LEO Satellite Communications," *Remote Sensing*, vol. 14, no. 17, 2022, ISSN: 2072-4292.

[227] 3GPP, "Study on provision of low-cost Machine-Type Communications (MTC) User Equipments (UEs) based on LTE," 3rd Generation Partnership Project (3GPP), Tech. Rep. TR 36.888, Jun. 2013, Release 12.

[228] J. R. Barry, E. A. Lee, and D. G. Messerschmitt, *Digital communication*. Springer Science & Business Media, 2003.

[229] "Guidelines for evaluation of radio interface technologies for IMT-Advanced – Report ITU-R M.2135-1," International Telecommunication Union (ITU), Tech. Rep., 2009.

[230] Q. Zhang, G. Wang, J. Chen, G. B. Giannakis, and Q. Liu, "Mobile Energy Transfer in Internet of Things," *IEEE Internet of Things Journal*, vol. 6, no. 5, pp. 9012–9019, 2019. DOI: 10.1109/JIOT.2019.2926333.

[231] Y. Zeng, J. Xu, and R. Zhang, "Energy Minimization for Wireless Communication With Rotary-Wing UAV," *IEEE Trans. Wireless Commun.*, vol. 18, no. 4, pp. 2329–2345, Apr. 2019.

[232] M. O. Ojo, S. Giordano, G. Procissi, and I. N. Seitanidis, "A Review of Low-End, Middle-End, and High-End Iot Devices," *IEEE Access*, vol. 6, pp. 70 528–70 554, 2018. DOI: 10.1109/ACCESS.2018.2879615.

[233] G. Zhang, F. Shen, Y. Zhang, R. Yang, Y. Yang, and E. A. Jorswieck, "Delay Minimized Task Scheduling in Fog-Enabled IoT Networks," in *2018 10th International Conference on Wireless Communications and Signal Processing (WCSP)*, 2018, pp. 1–6. DOI: 10.1109/WCSP.2018.8555532.

[234] T. Hoßfeld, L. Skorin-Kapov, P. E. Heegaard, and M. Varela, "Definition of QoE fairness in shared systems," *IEEE Communications Letters*, vol. 21, no. 1, pp. 184–187, 2016.

[235] S. Alshami, "Performance Analysis of OFDMA, UFMC, and FBMC for Optical Wireless Communication," in *2021 1st International Conference on Emerging Smart Technologies and Applications (eSmarTA)*, 2021, pp. 1–4. DOI: 10.1109/eSmarTA52612.2021.9515739.

[236] K. T. Swami and A. A. Moghe, "A Review of LiFi Technology," in *2020 5th IEEE International Conference on Recent Advances and Innovations in Engineering (ICRAIE)*, 2020, pp. 1–5. DOI: 10.1109/ICRAIE51050.2020.9358340.

[237] K. L. Bober, V. Jungnickel, M. Emmelmann, *et al.*, "A Flexible System Concept for LiFi in the Internet of Things," in *IEEE 87th Vehicular Technology Conference (VTC Spring)*, 2020, pp. 1–4. DOI: 10.1109/ICTON51198.2020.9203185.

[238] J. Patel, P. Trivedi, and D. Patel, "A Performance Analysis of "Light Fidelity" and "Internet of Things" and It's Application," in *2017 International Conference on Transforming Engineering Education (ICTEE)*, 2017, pp. 1–4. DOI: 10.1109/ICTEED.2017.8585696.

[239] P. Lorenz and L. Hamada, "LiFi Towards 5G: Concepts Challenges Applications in Telemedecine," in *2020 Second International Conference on Embedded and Distributed Systems (EDiS)*, 2020, pp. 123–127. DOI: 10.1109/EDiS49545.2020.9296435.

[240] M. Mekala, P. Viswanathan, N. Srinivasu, and G. Varma, "Accurate Decision-making System for Mining Environment using Li-Fi 5G Technology over IoT Framework," in *2019 International Conference on contemporary Computing and Informatics (IC3I)*, 2019, pp. 74–79. DOI: 10.1109/IC3I46837.2019.9055546.

[241] J. Dinesh Kumar, K. Priyadharsini, K. Srinithi, R. Samprtiha, and C. Ganesh Babu, "An Experimental Analysis of Lifi and Deployment on Localization Based Services and Smart Building," in *2021 International Conference on Emerging Smart Computing and Informatics (ESCI)*, 2021, pp. 92–97. DOI: 10.1109/ESCI50559.2021.9396889.

[242] C. SaiSankeerth Reddy, G. SakethRam, C. SaiSumanth Reddy, B. Yasaswi, and P. Pandey, "Appliance Automation Using LiFi with MQTT in Hybrid Star and Tree Network Setup," in *2018 International Conference on Research in Intelligent and Computing in Engineering (RICE)*, 2018, pp. 1–6. DOI: 10.1109/RICE.2018.8509085.

[243] M. Sathiyanarayanan, V. Govindraj, and N. Jahagirdar, "Challenges and opportunities of integrating Internet of Things (IoT) and Light Fidelity (LiFi)," in *2017 3rd International Conference on Applied and Theoretical Computing and Communication Technology (iCATccT)*, 2017, pp. 137–142. DOI: 10.1109/ICATCCT.2017.8389121.

[244] I. Demirkol, D. Camps-Mur, J. Paradells, M. Combalia, W. Popoola, and H. Haas, "Powering the Internet of Things through Light Communication," *IEEE Communications Magazine*, vol. 57, no. 6, pp. 107–113, 2019. DOI: 10.1109/MCOM.2019.1800429.

[245] D. Manimaran, M. Anu, and C. Steffi.F, "Integration of Indoor and Outdoor Voice Based Navigation Detection using Light based Communication (Lifi) and IoT," in *2021 5th International Conference on Computing Methodologies and Communication (ICCMC)*, 2021, pp. 400–403. DOI: 10.1109/ICCMC51019.2021.9418379.

[246] R.A.A.Othman, D. ap Sagaran, M. Mokayef, and W.I.I.R.B.W.M.Nasir, "Effective LiFi communication for IoT applications," in *2018 IEEE 4th International Symposium in Robotics and Manufacturing Automation (ROMA)*, 2018, pp. 1–4. DOI: 10.1109/ROMA46407.2018.8986698.

[247] Z. Zhou, M. Kavehrad, W. Wang, and J. Jiang, "Research on Optical Internet-of-Things for Informalization Development of Modern Power Grids," in *2020 IEEE/IAS Industrial and Commercial Power System Asia (I&CPS Asia)*, 2020, pp. 1480–1485. DOI: 10.1109/ICPSAsia48933.2020.9208568.

[248] P. K. Sharma, Y.-S. Jeong, and J. H. Park, "EH-HL: Effective Communication Model by Integrated EH-WSN and Hybrid LiFi/WiFi for IoT," *IEEE Internet of Things Journal*, vol. 5, no. 3, pp. 1719–1726, 2018. DOI: 10.1109/JIOT.2018.2791999.

[249] I. Sulayman, R. He, M. Manka, A. Ning, and A. Ouda, "LiFi/WiFi Authentication and Handover Protocols: Survey, Evaluation, and Recommendation," in *2021 International Symposium on Networks, Computers and Communications (ISNCC)*, 2021, pp. 1–6. DOI: 10.1109/ISNCC52172.2021.9615853.

[250] M. Asad, S. Qaisar, and A. Basit, "Client Based Access Layer QoS Provisioning in Beyond 5G IoT Networks," in *2020 3rd International Conference on Advanced Communication Technologies and Networking (CommNet)*, 2020, pp. 1–8. DOI: 10.1109/CommNet49926.2020.9199612.

[251] M. Asad, S. Qaisar, and A. Basit, "Client-Centric Access Device Selection for Heterogeneous QoS Requirements in Beyond 5G IoT Networks," *IEEE Access*, vol. 8, pp. 219 820–219 836, 2020. DOI: 10.1109/ACCESS.2020.3042522.

[252] S. Alfattani, "Review of LiFi Technology and Its Future Applications," *Journal of Optical Communications*, vol. 42, no. 1, pp. 121–132, 2021. DOI: doi:10.1515/joc-2018-0025.

[253] L. Pescosolido, E. Ancillotti, and A. Passarella, "Performance Evaluation of Switching Between WiFi and LiFi under a Common Virtual Network Interface," in *2022 IEEE International Conference on Smart Computing (SMARTCOMP)*, 2022, pp. 275–280. DOI: 10.1109/SMARTCOMP55677.2022.00067.

[254] M. Asad and S. Qaisar, "Energy Efficient QoS-Based Access Point Selection in Hybrid WiFi and LiFi IoT Networks," *IEEE Transactions on Green Communications and Networking*, vol. 6, no. 2, pp. 897–906, 2022. DOI: 10.1109/TGCN.2021.3115729.

[255] H. Haas, "LiFi is a paradigm-shifting 5G technology," *Reviews in Physics*, vol. 3, pp. 26–31, 2018. DOI: https://doi.org/10.1016/j.revip.2017.10.001.

[256] C. Zeyu, "6G, LIFI and WIFI Wireless Systems: Challenges, Development and Prospects," in *2021 18th International Computer Conference on Wavelet Active Media Technology and Information Processing (ICCWAMTIP)*, 2021, pp. 322–325. DOI: 10.1109/ICCWAMTIP53232.2021.9674090.

[257] X. Wu and D. C. O'Brien, "Parallel Transmission LiFi," *IEEE Transactions on Wireless Communications*, vol. 19, no. 10, pp. 6268–6276, 2020. DOI: 10.1109/TWC.2020.3001983.

[258] H. Nguyen and Y. M. Jang, "Design of MIMO C-OOK using Matched filter for Optical Camera Communication System," in *2021 International Conference on Artificial Intelligence in Information and Communication (ICAIIC)*, 2021, pp. 474–476. DOI: 10.1109/ICAIIC51459.2021.9415204.

[259] M. Arfaoui, M. Soltani, I. Tavakkolnia, *et al.*, "Physical Layer Security for Visible Light Communication Systems: A Survey," *IEEE Communications Surveys & Tutorials*, vol. 22, no. 3, pp. 1887–1908, 2020. DOI: 10.1109/COMST.2020.2988615.

[260] M. Kafafy, Y. Fahmy, and M. Khairy, "Multi-cell VLC system design under illumination and communication constraints," *Optical Switching and Networking*, vol. 34, pp. 23–34, 2019, ISSN: 1573-4277. DOI: https://doi.org/10.1016/j.osn.2019.05.001.

[261] A. B. Ozyurt and W. O. Popoola, "LiFi-Based D2D Communication in Industrial IoT," *IEEE Systems Journal*, pp. 1–8, 2022. DOI: 10.1109/JSYST.2022.3179183.

[262] N. Partheeban, V. Nagaraju, N. J. Kumar, A. M. Ali, and B. R. T. Bapu, "An Improved Internet of Things enabled Wireless Data Transmission using Visible Light Communication," in *2022 International Conference on Advances in Computing, Communication and Applied Informatics (ACCAI)*, 2022, pp. 1–7. DOI: 10.1109/ACCAI53970.2022.9752518.

[263] H. Alshaer, H. Haas, and O. Y. Kolawole, "An Optimal Networked LiFi Access Point Slicing Scheme for Internet-of-Things," in *2021 IEEE International Conference on Communications Workshops (ICC Workshops)*, 2021, pp. 1–6. DOI: \\10.1109/ICCWorkshops50388.2021.9473868.

[264] A. Duquel, R. Stanica, H. Rivano, and A. Desportes, "Decoding methods in LED-to-smartphone bidirectional communication for the IoT," in *2018 Global LIFI Congress (GLC)*, 2018, pp. 1–6. DOI: 10.23919/GLC.2018.8319118.

[265] J. D. Bokefode, S. A. Ubale, and R. M. Gaikwad, "Retrieving Real Time Data Through IOT Devices and Storing Securely on Cloud Using Li-Fi," in *2018 3rd International Conference for Convergence in Technology (I2CT)*, 2018, pp. 1–5. DOI: 10.1109/I2CT.2018.8529393.

[266] S. M. Kouhini, C. Kottke, Z. Ma, *et al.*, "LiFi Positioning for Industry 4.0," *IEEE Journal of Selected Topics in Quantum Electronics*, vol. 27, no. 6, pp. 1–15, 2021. DOI: 10.1109/JSTQE.2021.3095364.

[267] V. Jungnickel, M. Hinrichs, K. Bober, *et al.*, "Enhance Lighting for the Internet of Things," in *2019 Global LIFI Congress (GLC)*, 2019, pp. 1–6. DOI: 10.1109/GLC.2019.8864126.

[268] J. Linnartz, C. Corrêa, T. Cunha, *et al.*, "ELIoT: New Features in LiFi for Next-Generation IoT," in *2021 Joint European Conference on Networks and Communications & 6G Summit (EuCNC/6G Summit)*, 2021, pp. 148–153. DOI: 10.1109/EuCNC/6GSummit51104.2021.9482478.

[269] M. Chowdhury, M. Hasan, M. Shahjalal, E. Shin, and Y. Jang, "Opportunities of Optical Spectrum for Future Wireless Communications," in *2019 International Conference on Artificial Intelligence in Information and Communication (ICAIIC)*, 2019, pp. 004–007. DOI: 10.1109/ICAIIC.2019.8668981.

[270] M. R. Ghaderi, "LiFi and Hybrid WiFi/LiFi indoor networking: From theory to practice," *Optical Switching and Networking*, vol. 47, p. 100 699, 2023, ISSN: 1573-4277. DOI: https://doi.org/10.1016/j.osn.2022.100699.

[271] X. Wu, M. D. Soltani, L. Zhou, M. Safari, and H. Haas, "Hybrid LiFi and WiFi Networks: A Survey," *IEEE Communications Surveys & Tutorials*, vol. 23, no. 2, pp. 1398–1420, 2021. DOI: 10.1109/COMST.2021.3058296.

[272] M. Popadić and E. Kočan, "LiFi Networks: Concept, Standardization Activities and Perspectives," in *2021 25th International Conference on Information Technology (IT)*, 2021, pp. 1–4. DOI: 10.1109/IT51528.2021.9390098.

[273] S. E. Nordholm and H.-J. Zepernick, "Modulation and Detection," *ELECTRICAL ENGINEERING - Vol. I*, 2005.

[274] A. F. Hussein, H. Elgala, and T. D. Little, "Evolution of Multi-Tier Transmission Towards 5G Li-Fi Networks," in *2018 IEEE Global Communications Conference (GLOBECOM)*, 2018, pp. 1–7. DOI: 10.1109/GLOCOM.2018.8647846.

[275] S. D. Dissanayake and J. Armstrong, "Comparison of ACO-OFDM, DCO-OFDM and ADO-OFDM in IM/DD Systems," *Journal of Lightwave Technology*, vol. 31, no. 7, pp. 1063–1072, 2013. DOI: 10.1109/JLT.2013.2241731.

[276] J. Armstrong and B. J. Schmidt, "Comparison of Asymmetrically Clipped Optical OFDM and DC-Biased Optical OFDM in AWGN," *IEEE Communications Letters*, vol. 12, no. 5, pp. 343–345, 2008. DOI: 10.1109/LCOMM.2008.080193.

[277] R. Iwasaki and K. Ohuchi, "PAPR Reduction in OFDM Signal by Combining Partial Transmit Sequences with Precoding Matrix," in *2018 12th International Conference on Signal Processing and Communication Systems (ICSPCS)*, 2018, pp. 1–6. DOI: 10.1109/ICSPCS.2018.8631723.

[278] M. Hinrichs, B. Poddig, M. Nölle, P. Hellwig, R. Freund, and V. Jungnickel, "Efficient Line Coding for Low-Power Optical Wireless Communications," in *2021 IEEE 94th Vehicular Technology Conference (VTC2021-Fall)*, 2021, pp. 1–7. DOI: 10.1109/VTC2021-Fall52928.2021.9625557.

[279] R. Raj and A. Dixit, "An Energy-Efficient Power Allocation Scheme for NOMA-Based IoT Sensor Networks in 6G," *IEEE Sensors Journal*, vol. 22, no. 7, pp. 7371–7384, 2022. DOI: 10.1109/JSEN.2022.3153314.

[280] Z. Ding, X. Lei, G. Karagiannidis, R. Schober, J. Yuan, and V. Bhargava, "A Survey on Non-Orthogonal Multiple Access for 5G Networks: Research Challenges and Future Trends," *IEEE Journal on Selected Areas in Communications*, vol. 35, no. 10, pp. 2181–2195, 2017. DOI: 10.1109/JSAC.2017.2725519.

[281] L. Chettri and R. Bera, "A Comprehensive Survey on Internet of Things (IoT) Toward 5G Wireless Systems," *IEEE Internet of Things Journal*, vol. 7, no. 1, pp. 16–32, 2020. DOI: 10.1109/JIOT.2019.2948888.

[282] R. Feng, C.-X. Wang, J. Huang, X. Gao, S. Salous, and H. Haas, "Classification and Comparison of Massive MIMO Propagation Channel Models," *IEEE Internet of Things Journal*, vol. 9, no. 23, pp. 23 452–23 471, 2022. DOI: 10.1109/JIOT.2022.3198690.

[283] E. Larsson, O. Edfors, F. Tufvesson, and T. Marzetta, "Massive MIMO for next generation wireless systems," *IEEE Communications Magazine*, vol. 52, no. 2, pp. 186–195, 2014. DOI: 10.1109/MCOM.2014.6736761.

[284] S. Gunnarsson, J. Flordelis, L. V. D. Perre, and F. Tufvesson, "Channel Hardening in Massive MIMO: Model Parameters and Experimental Assessment," *IEEE Open Journal of the Communications Society*, vol. 1, pp. 501–512, 2020. DOI: 10.1109/OJCOMS.2020.2987704.

[285] S. M. Kouhini, J. Hohmann, S. Mavanchery Mana, *et al.*, "All-Optical Distributed MIMO for LiFi: Spatial Diversity Versus Spatial Multiplexing," *IEEE Access*, vol. 10, pp. 102 646–102 658, 2022. DOI: 10.1109/ACCESS.2022.3207475.

[286] M. Uysal, F. Miramirkhani, T. Baykas, N. Serafimovski, and V. Jungnickel, "IEEE 802.11bb Reference Channel Models for Indoor Environments," IEEE, Istanbul, Turkey, Tech. Rep., Jul. 2018.

[287] A. A. Purwita and H. Haas, "Studies of Flatness of LiFi Channel for IEEE 802.11bb," in *2020 IEEE Wireless Communications and Networking Conference (WCNC)*, 2020, pp. 1–6. DOI: 10.1109/WCNC45663.2020.9120811.

[288] ITU, "High-speed indoor visible light communication transceiver – System architecture, physical layer and data link layer specification," ITU-T G.9991, Recommendation, Mar. 2019.

[289] H. B. Eldeeb, S. M. Mana, V. Jungnickel, P. Hellwig, J. Hilt, and M. Uysal, "Distributed MIMO for Li-Fi: Channel Measurements, Ray Tracing and Throughput Analysis," *IEEE Photonics Technology Letters*, vol. 33, no. 16, pp. 916–919, 2021. DOI: 10.1109/LPT.2021.3072254.

[290] S. M. Mana, K. G. K. Gabra, S. M. Kouhini, P. Hellwig, J. Hilt, and V. Jungnickel, "An Efficient Multi-Link Channel Model for LiFi," in *2021 IEEE 32nd Annual International Symposium on Personal, Indoor and Mobile Radio Communications (PIMRC)*, 2021, pp. 1–6. DOI: 10.1109/PIMRC50174.2021.9569661.

[291] S. M. Mana, K. G. K. Gabra, S. M. Kouhini, *et al.*, "LIDAR-Assisted Channel Modelling for LiFi," in *2022 Optical Fiber Communications Conference and Exhibition (OFC)*, 2022, pp. 1–3.

[292] M. Dehghani Soltani, A. A. Purwita, I. Tavakkolnia, H. Haas, and M. Safari, "Impact of Device Orientation on Error Performance of LiFi Systems," *IEEE Access*, vol. 7, pp. 41 690–41 701, 2019. DOI: 10.1109/ACCESS.2019.2907463.

[293] M. D. Soltani, Z. Zeng, I. Tavakkolnia, H. Haas, and M. Safari, "Random Receiver Orientation Effect on Channel Gain in LiFi Systems," in *2019 IEEE Wireless Communications and Networking Conference (WCNC)*, 2019, pp. 1–6. DOI: 10.1109/WCNC.2019.8886097.

[294] X. Wang, C. Gan, S. Wu, Y. Chen, and Y. Chen, "Founding AP's IVM and related IHM for subway LiFi network," *Optical Switching and Networking*, vol. 45, p. 100 676, 2022, ISSN: 1573-4277. DOI: https://doi.org/10.1016/j.osn.2022.100676.

[295] M. Obeed, A. M. Salhab, M.-S. Alouini, and S. A. Zummo, "On Optimizing VLC Networks for Downlink Multi-User Transmission: A Survey," *IEEE Communications Surveys & Tutorials*, vol. 21, no. 3, pp. 2947–2976, 2019. DOI: 10.1109/COMST.2019.2906225.

[296] S. Sun, F. Yang, J. Song, and Z. Han, "Joint Resource Management for Intelligent Reflecting Surface–Aided Visible Light Communications," *IEEE Transactions on Wireless Communications*, vol. 21, no. 8, pp. 6508–6522, 2022. DOI: 10.1109/TWC.2022.3150021.

[297] X. Zhang, J. Duan, Y. Fu, and A. Shi, "Theoretical Accuracy Analysis of Indoor Visible Light Communication Positioning System Based on Received Signal Strength Indicator," *Journal of Lightwave Technology*, vol. 32, no. 21, pp. 4180–4186, 2014. DOI: 10.1109/JLT.2014.2349530.

[298] T. Komine and M. Nakagawa, "Fundamental analysis for visible-light communication system using LED lights," *IEEE Transactions on Consumer Electronics*, vol. 50, no. 1, pp. 100–107, 2004. DOI: 10.1109/TCE.2004.1277847.